PEROVSKITE $ANbO_3$; A = K, Na NANOPARTICLES SYNTHESIZED BY MODIFIED SOLID STATE REACTION AND COMBUSTION METHODS

NOPSIRI CHAIYO

A THESIS SUBMITTED IN PARTIAL FULFILLMENT

OF THE REQUIREMENT FOR THE DEGREE OF

MASTER OF SCIENCE IN NANOSCIENCE AND NANOTECHNOLOGY

COLLEGE OF NANOTECHNOLOGY

KING MONGKUT'S INSTITUTE OF TECHNOLOGY LADKRABANG

2011

KMITL-2011-NT-M-001-006

Thesis Title	Perovskite $ANbO_3$; A = K, Na nanoparticles synthesized by modified solid state reaction and combustion methods
Student	Miss Nopsiri Chaiyo
Student ID	51064604
Degree	Master of Science
Program	Nanoscience and Nanotechnology
Year	2011
Thesis Advisor	Assist. Prof. Dr. Naratip Vittayakorn
Thesis Co advisor	Assist. Prof. Dr. Banjong Boonchom
Thesis Co advisor	Mr. Anucha Ruangphanit

ABSTRACT

Lead-free piezoelectric alkali niobate perovskite materials with the general formula, ABO_3 (A = K, Na; B = Nb), were synthesized through simple methods, namely "modified solid state reaction" and "combustion synthesis". The thermal behavior of the precursor was determined using thermo gravimetric analysis (TGA) and differential thermal analysis (DTA). The processing conditions, perovskite phase formation, influence of the fuel-to-oxidizer ratio, and crystal structure were characterized by the X-ray diffraction technique (XRD) and Fourier transform infrared (FTIR) spectroscopy. The morphology and particle size were investigated through a scanning electron microscope (SEM).

For the modified solid state reaction method, the perovskite phase of sodium niobate ($NaNbO_3$) and potassium niobate ($KNbO_3$) were synthesized using sodium oxalate ($Na_2C_2O_4$) and potassium oxalate monohydrate ($K_2C_2O_4 \cdot H_2O$) as starting materials, respectively. The conventional starting material such as carbonate compound was substituted by these oxalate compounds in order to avoid excessive reactivity with moisture. The perovskite phase was found to synthesize successfully at lower calcination temperatures than those used in the conventional solid state reaction method, which lie in the range of 800°C or more. $NaNbO_3$ was synthesized successfully at the low temperature of 475°C for 1 h, with an average crystallite size of 25.89 ±

5.64 nm (defined by XRD). In the case of $KNbO_3$ synthesis, fine $KNbO_3$ powder was synthesized at the calcination temperature of 550°C for 4 h. The powder obtained was found to be a uniform agglomerated particle that possessed an average crystallite size (defined by XRD) of between 33.67 ± 8.60 and 53.47 ± 12.03 nm. Furthermore, the increase in crystallinity of the perovskite phase was found to be affected by increasing dwell time and calcination temperature. This consequence may confirm that the dwell time and calcination temperature also play an important role in developing the pure phase creation.

For the combustion synthesis, $NaNbO_3$ was synthesized using sodium nitrate and glycine as starting material and fuel, respectively. The influence of the fuel-to-oxidizer ratio to perovskite phase formation was studied. The fuel-to-oxidizer molar ratio was found to affect the combustion reaction and character of the powder obtained. In the case of oxidant-rich condition, the combustion reaction cannot occur. In contrast, for stoichiometric and fuel-rich condition, the perovskite $NaNbO_3$ phase, with a mean crystalline size (calculated by X-ray line broadening) ranging from 47.01 ± 12.66 nm (ratio of 0.7) to 27.58 ± 14.45 nm (ratio of 2.0) was obtained. For increasing fuel content, combustion reaction can be raised easily, but high carboneous residual was found to be enhanced further.

Keywords : Lead-free piezoelectric, perovskite, combustion synthesis, alkali niobate

หัวข้อวิทยานิพนธ์	อนุภาคนาโนเพอรอฟสไกต์ A = K, Na สังเคราะห์โดยวิธีปฏิกิริยาสถานะของแข็งแบบดัดแปลงและวิธีแบบเผาไหม้
นักศึกษา	นางสาวนพศิริ ไชยโย
รหัสประจำตัว	51064604
ปริญญา	วิทยาศาสตรมหาบัณฑิต
สาขาวิชา	นาโนวิทยาและนาโนเทคโนโลยี
พ.ศ.	2554
อาจารย์ที่ปรึกษาวิทยานิพนธ์	ผศ.ดร.นราธิป วิทยากร
อาจารย์ที่ปรึกษาวิทยานิพนธ์ร่วม	ผศ.ดร.บรรจง บุญชม
อาจารย์ที่ปรึกษาวิทยานิพนธ์ร่วม	นายอนุชา เรืองพานิช

บทคัดย่อ

งานวิจัยนี้ศึกษาการสังเคราะห์โลหะอัลคาไลไนโอเบต ABO_3 (A = K, Na; B = Nb) ซึ่งเป็นวัสดุเพียโซอิเล็กทริกไร้สารตะกั่วที่มีโครงสร้างแบบเพอรอฟสไกต์ จากวิธีปฏิกิริยาสถานะของแข็งแบบดัดแปลงและวิธีแบบเผาไหม้ ซึ่งเป็นกระบวนการที่ไม่ซับซ้อน โดยทำการศึกษาพฤติกรรมทางความร้อนของสารตั้งต้น โดยใช้เทคนิคเทอร์โมกราวิเมทริกและดิฟเฟอเรนเชียลเทอร์มอลอะนาไลซิส (TG-DTA) จากนั้นทำการศึกษาการเกิดเฟสเพอรอฟสไกต์ อิทธิพลของสัดส่วนโดยโมลของสารเชื้อเพลิงต่อตัวออกซิไดส์และโครงสร้างผลึก โดยใช้เทคนิคการเลี้ยวเบนของรังสีเอกซ์ (XRD) และเทคนิคฟูเรียร์ทรานสฟอร์มอินฟราเรดสเปกโทรสโกปี (FT-IR) จากนั้นศึกษาสัณฐานวิทยาและขนาดอนุภาคด้วยกล้องจุลทรรศน์อิเล็กตรอนแบบส่องกราด (SEM)

สำหรับวิธีปฏิกิริยาสถานะของแข็งแบบดัดแปลง ผงผลึกโซเดียมไนโอเบต ($NaNbO_3$) และโพแทสเซียมไนโอเบต ($KNbO_3$) สามารถเตรียมได้โดยใช้โซเดียมออกซาเลต ($Na_2C_2O_4$) และโพแทสเซียมออกซาเลตโมโนไฮเดรต ($K_2C_2O_4 \cdot H_2O$) เป็นสารตั้งต้นแทนสารประกอบคาร์บอเนตเพื่อหลีกเลี่ยงปัญหาการดูดความชื้น ซึ่งพบว่าสามารถสังเคราะห์เฟสเพอรอฟสไกต์ได้ที่อุณหภูมิต่ำเมื่อเทียบกับวิธีปฏิกิริยาสถานะของแข็งแบบดั้งเดิมที่ใช้อุณหภูมิสูงมากกว่า 800 องศาเซลเซียส จากงานวิจัยพบว่าสามารถเตรียมผงผลึก $NaNbO_3$ ได้เมื่อผ่านการเผาแคลไซน์ที่อุณหภูมิ 475 องศาเซลเซียส เป็นเวลา 1 ชั่วโมง ผงผลึกมีขนาดผลึกเฉลี่ย 25.89 ± 5.64 นาโนเมตร ส่วนในกรณีการเตรียมผงผลึกโพแทสเซียมไนโอเบต ($KNbO_3$) พบว่าใช้อุณหภูมิในการเผาแคลไซน์เท่ากับ 550

องศาเซลเซียส เป็นเวลา 4 ชั่วโมง ผงผลึกมีการจับตัวกันและมีขนาดผลึกเฉลี่ยมีค่าระหว่าง 33.67 ± 8.60 ถึง53.47 ± 12.03 นาโนเมตร ทั้งนี้จากผลการวิจัยพบว่าอุณหภูมิและระยะเวลาในการเผาแคลไซน์ที่สูงขึ้นเป็นปัจจัยสำคัญที่มีผลต่อการเกิดเฟสและความเป็นผลึกที่สูงขึ้นด้วย

สำหรับวิธีการสังเคราะห์แบบเผาไหม้ เป็นการเตรียมผงผลึกโซเดียมไนโอเบต ($NaNbO_3$) ได้โดยใช้โซเดียมไนเตรทเป็นสารตั้งต้นและใช้ไกลซีนเป็นสารเชื้อเพลิง จากนั้นทำการศึกษาอิทธิพลของสัดส่วนโดยโมลของสารเชื้อเพลิงต่อตัวออกซิไดส์ที่มีผลต่อการเกิดเฟสเพอรอฟสไกต์ พบว่าสัดส่วนโดยโมลของสารเชื้อเพลิงต่อตัวออกซิไดส์มีผลต่อปฏิกิริยาการเผาไหม้และลักษณะเฉพาะของผงผลึก ไม่พบปฏิกิริยาการเผาไหม้เมื่อใช้สัดส่วนสารเชื้อเพลิงน้อยกว่าสมดุล แต่ในทางตรงกันข้าม เมื่อใช้สัดส่วนสารเชื้อเพลิงที่พอดีและมากเกินพอ พบว่าสามารถสังเคราะห์เฟสเพอรอฟสไกต์ $NaNbO_3$ ที่ขนาดผลึกเฉลี่ยมีค่าเท่ากับ 47.01 ± 12.66 นาโนเมตร และ 27.58 ± 14.45 นาโนเมตร เมื่อใช้สัดส่วนสารเชื้อเพลิงต่อตัวออกซิไดซ์เท่ากับ 0.7 และ 2.0 ตามลำดับ เมื่อเพิ่มปริมาณสารเชื้อเพลิงมากขึ้น พบว่าปฏิกิริยาการเผาไหม้สามารถเกิดขึ้นได้ดียิ่งขึ้นแต่พบสารประกอบคาร์บอนคงเหลือในปริมาณมากขึ้น

คำสำคัญ : วัสดุเพียโซอิเล็กทริกไร้สารตะกั่ว เพอรอฟสไกต์ วิธีการสังเคราะห์แบบเผาไหม้

ACKNOWLEDGMENTS

This thesis was accomplished in the Electroceramic Research Laboratory, College of Nanotechnology, King Mongkut's Institute of Technology Ladkrabang, Bangkok, Thailand.

I wish to acknowledge many people who have helped and assisted me, and shared my problems or just listened during the preparation of this thesis. First of all, I would like to thank, with deep appreciation, Assistant Professor Dr. Naratip Vittayakorn for his unending patience and invaluable suggestions, recommendations, inspirations and supports throughout my educational life, since being an undergraduate student. I would also like to thank Assistant Professor Dr. Banjong Boonchom and Mr. Anucha Ruangphanit for their kind advice, help and valuable information.

I would like to express my gratitude to Associate Professor Dr. Supon Ananta and Associate Professor Dr. Wisanu Pecharapa, for their helpful advice, useful comments and suggestions and devotion of their time to serve as members of the Examining Committee.

I am also grateful for all the help and support I received from the officers and technical staff at the Scientific Instruments Service Centre (SISC), Department of Chemistry, Faculty of Science, KMITL, for XRD and TGA analysis, and Mr. Apiruk Punkeaw of the Thai Microelectronics Center (TMEC), NECTEC, NSTDA, and Electron Microscopy Research and Service Center (EMRSc), Faculty of Science, Chiang Mai University for his SEM analysis.

I am indebted to the many people who influenced, helped and had fun in working with me when preparing this thesis, especially Miss Usa Sukkha, Miss Piyanut Charoonsuk, Mr. Sakulthai Kahatta, Mr. Aumpon Promsamlee and those too numerous to mention. My profound thanks are conveyed to members of the Electroceramic Research Laboratory who gave me so much assistance.

Special thanks go to my friends and the Chaba group, Mr. Chainarong Kongyai, Mr. Wuttinun Keawkanokvijit, Miss Praewpan Inpota, Miss Tritip Suwannapanon. Miss Wannisa Thanateboorapashup and Mr. Keattisak Lhanamwong, who relaxed, helped, cheered and encouraged me. Their advice and experience influenced and drove me to this point.

I wish to acknowledge the Thailand Graduate Institute of Science and Technology (TGIST), NSTDA for all its financial support.

Last but not least, I wish to dedicate this thesis to my parents, Mr. Nop Chaiyo and Mrs. Thanormsri Chaiyo, and Miss Sawitri Sriboonpeng, for their support, understanding and patience. Finally, this thesis would not have been possible without a good family, friends, co-workers and an excellent advisor.

NOPSIRI CHAIYO

TABLE OF CONTENTS

		Page
ABSTRACT (ENGLISH)		I
ABSTRACT (THAI)		III
ACKNOWLEDGMENT		V
LIST OF TABLES		IX
LIST OF FIGURES		X
ABBREVIATIONS AND SYMBOLS		XIV
CHAPTER 1	**INTRODUCTION**	1
	1.1 Overview	1
	1.2 Scope of this work	3
	1.3 Objectives of this work	4
CHAPTER 2	**LITERATURE REVIEW**	5
	2.1 Piezoelectric materials	5
	2.2 Lead zirconate titanate ($Pb(Zr, Ti)O_3$; PZT)	6
	2.3 Alkali niobate ceramics ABO_3 (A = K, Na; B = Nb)	11
	2.4 Solid state reaction method	31
	2.5 Combustion synthesis	34
CHAPTER 3	**EXPERIMENTAL PROCEDURES**	57
	3.1 Modified solid state reaction	59
	3.2 Combustion synthesis	61
	3.3 Characterization	64
CHAPTER 4	**RESULTS AND DISCUSSION**	66
	4.1 Solid state reaction synthesis of sodium niobate ($NaNbO_3$) powder at low temperature	66
	4.2 Synthesis of potassium niobate ($KNbO_3$) nano-powder by a modified solid state reaction	78

Page

4.3 Solution combustion synthesis and characterization of lead-free piezoelectric sodium niobate ($NaNbO_3$) powders 93

CHAPTER 5 CONCLUSIONS 106

5.1 Modified solid state reaction 106

5.2 Combustion synthesis 107

REFERENCES 108

APPENDIXS 122

VITA

LIST OF TABLES

Table		Page
2.1	Some materials produced by the combustion process.	37
2.2	List of metal carboxylate compounds and oxides formed by the CS method.	41
3.1	Specifications of the starting material powders used in this study.	58
4.1	Fraction of perovskite phase formed as a function of calcination temperature and dwell time.	75
4.2	Lattice parameters of the $KNbO_3$ powder calcined at various calcination temperatures for 4 h.	87
4.3	Mean crystalline size, *D*, of the $KNbO_3$ powder calcined at different temperatures for 4 h and different dwell time at 550°C.	88
4.4	Mean crystalline size, *D*, of $NaNbO_3$ powder obtained from various fuel-to-oxidant molar ratios.	102
5.1	The optimal calcination conditions for single perovskite phase and their characters.	107
1	Data of the preparation and the calculation of the amount of starting materials for combustion synthesis using the stoichiometric fuel-to-oxidizers molar ratio (0.56).	124

LIST OF FIGURES

Figure		Page
2.1	(a) The *direct* and (b) *converse* piezoelectric effect.	5
2.2	Versatile applications of piezoelectric ceramics in the commercial world.	6
2.3	The ideal perovskite structure with ABO_3 composition (a) and other ways of presenting the perovskite structure (b) and (c).	7
2.4	The binary phase diagram of lead zirconate-lead titanate.	9
2.5	Coupling coefficient, k_p and dielectric constant, ε_r values with different PZT compositional range.	9
2.6	Preliminary modification of the PZT phase diagram from Noheda *et al.*	10
2.7	Phase diagram of the $KNbO_3$-$NaNbO_3$ system.	12
2.8	Dielectric and piezoelectric properties as a compositional function of the $KNbO_3$-$NaNbO_3$ system.	14
2.9	SEM micrographs of $(1-x)KNbO_3$-$(x)NaNbO_3$ ceramics with various Na contents (x), (a) 0.2, (b) 0.3, (c) 0.4, (d) 0.5, (e) 0.6, (f) 0.7, and (g) 0.8.	15
2.10	Microstructure of the $K_{0.5}Na_{0.5}NbO_3$ ceramic spark plasma sintered at 920°C for 5 min before annealing at 900°C for 4 h. Micrograph by scanning electron microscopy (a) and micrographs of transmission by electron microscopy (b and c).	16
2.11	Comparison of the piezoelectric charge sensor constants at 25°C among developed $(K,Na)NbO_3$-$LiTaO_3$ ceramics (LF) and conventional PZT ceramics as a function of Curie temperature. PZT1: $Pb(Zr_{0.52}Ti_{0.48})O_3$. PZT2: $Pb_{0.988}(Zr_{0.48}Ti_{0.52})_{0.976}Nb_{0.024}O_3$. PZT3: commercially available PZT. PZT4: $\{(Pb_{0.85}Ba_{0.15})_{0.9925}La_{0.005}\}(Zr_{0.52}Ti_{0.48})O_3$.	17
2.12	Temperature dependence of electric-field-induced longitudinal strain for the textured (LF4T) and non-textured (LF4) ceramics of the $(K,Na)NbO_3$-$LiTaO_3$ system.	17

2.13	Polarized hysteresis loops of $[(Na_{0.535}K_{0.480})_{0.966}Li_{0.058}](Nb_{0.90}Ta_{0.10})O_3$ ceramics synthesized in a temperature range of 1,075-1,120°C.	20
2.14	Photographs of KLNNS2.5-5 ceramic membranes and buzzers.	21
2.15	Piezoelectric properties of (1-x)KNN-xBS ceramics at room temperature.	24
2.16	Values for d_{33}, k_p, $\varepsilon^T_3/\varepsilon_0$ and grain size of 0.95NKN-0.05BT ceramics sintered at various temperatures.	25
2.17	Micrographs from scanning electron microscopy of the thermally etched surface of (1-x)KNN-xBNT samples sintered at the optimum sintering temperature. (a) x = 50.01, (b) x = 50.02, (c) x = 50.03, (d) x = 50.04, (e) x = 50.05, and (f) x = 50.06.	26
2.18	Effect of 1 mol% oxide sintering additives on densification of $K_{0.5}Na_{0.5}NbO_3$ ceramics.	29
2.19	Microstructures of Na_2O excess in NKN-5LT samples sintered for 4 h in air at 900, 950, 1,000, 1,050 and 1,100°C, as a function of Na_2O content.	30
2.20	Polished and chemically etched surfaces of PZT ceramics sintered at 1,200°C for 2 h, as a function of the molar ratio of Pb/(Zr+Ti), observed by SEM.	32
2.21	X-ray pattern of calcined powder.	33
2.22	Fractured surface of a sintered KNN sample.	33
2.23	Schematic of the temperature-time curve during an exothermal reaction.	36
2.24	TEM micrographs showing typical morphology of as-prepared combustion synthesized powders: (a) ZnO and (b) ZBSCMK.	47
2.25	Combustion synthesis of Al_2O_3 in stoichiometric conditions at 600°C. The number in the bottom left-hand corner refers to the time that elapsed from when the dish was placed in the oven (expressed in minutes and seconds).	48
2.26	SEM photographs showing the powders produced by (a) solid-state reaction, (b) SHS–sample UB3, and (c) SHS–sample PB3.	50
2.27	Neutral and zwitterion structure of glycine.	50
2.28	Formation of voluminous zirconia (a) and TEM micrograph of ZrO_2 (b).	51
2.29	X-ray line broadening for ceria powder obtained through (a) the fuel-deficient, (b) the stochiometric, and (c) the fuel-rich precursor.	54

2.30	HRTEM micrographs of ceria powder obtained through (a) the fuel-deficient, and (b) the stoichiometric precursor.	55
2.31	TEM photograph of the synthesized Ni–Zn ferrite powders.	56
2.32	XRD patterns for products from different oxidant-to-fuel ratios.	56
3.1	Mixed and calcination processes (MCP) for powder preparation.	60
3.2	Schematic flow chart of the combustion synthesis process (CSP).	63
4.1	TG-DTA result of an uncalcined powder mixed in the stoichiometric proportion of $NaNbO_3$.	69
4.2	XRD patterns of $NaNbO_3$ powder calcined at various temperatures for 4 h with a heating/cooling rate of 20°C/min.	71
4.3	XRD patterns of $NaNbO_3$ powder calcined at the calcination temperature of 475°C for various dwell times with a heating/cooling rate of 20°C/min.	72
4.4	Johnson–Mehl–Avrami for the formation of perovskite phase in $NaNbO_3$ powders isothermally heat treated at 475°C.	76
4.5	SEM micrographs showing $NaNbO_3$ powders synthesized at 475°C for 60 min, with a heating/cooling rate of 20°C/min.	76
4.6	TG–DTA curves of an uncalcined powder mixed in the stoichiometric proportion of $KNbO_3$.	82
4.7	X-ray diffraction patterns of $KNbO_3$ powder calcined at various temperatures for 4 h with a heating/cooling rate of 20°C/min.	84
4.8	X-ray diffraction patterns of $KNbO_3$ powder calcined at the calcination temperature of 550°C for various dwell times with a heating/cooling rate of 20°C/min.	85
4.9	FT-IR spectra of an uncalcined powder mixed in the stoichiometric proportion of $KNbO_3$ and $KNbO_3$ particles calcined at 550°C.	90
4.10	SEM micrographs showing $KNbO_3$ powder synthesized at 550°C (a) and 700°C (b), for 4 h with a heating/cooling rate of 20°C/min.	91
4.11	TG-DTA curves of the precursor mixed in the stoichiometric proportion of $NaNbO_3$.	98

4.12 X-ray diffraction patterns of $NaNbO_3$ powder obtained from various fuel-to-oxidant molar ratios. 98

4.13 X-ray diffraction patterns of $NaNbO_3$ powder (obtained from the fuel-to-oxidant molar ratio of 1.0) calcined at various temperatures for 4 h with a heating/cooling rate of 20°C/min. 103

4.14 FT-IR spectra of the precursor mixed in the stoichiometric proportion of $NaNbO_3$ powder obtained from various fuel-to-oxidant molar ratios and after the calcination step. 104

4.15 SEM micrograph showing as-prepared $NaNbO_3$ powder synthesized using the fuel-to-oxidant molar ratio of 1.0 (a) and powder calcined at 400°C for 4 h (b). 105

ABBRAVIATIONS AND SYMBOLS

AN	silver niobate
AR	analytical Reagent
BNT	bismuth sodium tantalate
BT	barium titanate
CS	combustion synthesis
CSP	combustion synthesis process
DTA	differential thermal analysis
EEE	electrical and electronic equipment
ELV	end-of life vehicles
EU	European Union
FTIR	Fourier transform infrared
FWHM	full width at half maximum
HIP	hot isostatic pressing
HMT	hexamethyltetramine
HRTEM	high-resolution transmission electron microscope
JCPDS	the Joint Committee on Powder Diffraction Standards
JMA	Johnson–Mehl–Avrami
KAS	Kissinger-Akahira-Sunose
KN	potassium niobate
KNN	potassium sodium niobate
MCP	mixed and calcination processes
MPB	morphotropic phase boundary
NN	sodium niobate
PBDE	polybrominated diphenyl ethers
P-E loop	polarization hysteresis loop
PPTs	polymorphic phase transitions
PT	lead titanate
PZ	lead zirconate
PZT	lead zirconate titanate
RoHS	restrictions on the use of certain hazardous substances in electrical and electronic equipment

RTGG	relative template train growth technique
TEM	transmission electron microscope
SCS	smoldering combustion synthesis
SEM	scanning electron microscope
SPS	spark plasma sintering
SHS	self-propagating high temperature synthesis
SSC	solid state combustion
TGA	thermogravimetric analysis
VCS	volume combustion synthesis
WEEE	electrical and electronic equipment
XRD	X-ray diffraction technique
A	pre-exponential factor
d_{33}	longitudinal piezoelectric coefficient
d_{31}	transverse piezoelectric coefficient
d_{15}	shear piezoelectric coefficient
D	average crystallite size
e	Neper number (2.7183)
E	activation energy
E_c	coercive field
I_R	maximum intensity of residual starting component phase
$I_{Nb_2O_5}$	maximum intensity of Nb_2O_5 phase
I_{perov}	maximum intensity of perovskite phase
I_{pyro}	maximum intensity of pyrochlore phase
k	piezoelectric properties
k_B	Boltzmann constant
k_p	plana electromechanical coupling coefficient
k_t	thickness electromechanical coupling factor
P_r	remnant polarization
Q_m	mechanical quality factor
T_c	combustion temperature
T_C	Curie temperature

T_{ig}	ignition temperature
T_m	maximum temperature
$T_{T\text{-}O}$	orthorhombic-tetragonal phase transition
ε_r	dielectric constant
φ	elemental stoichiometric coefficient
λ	wavelength of X-ray radiation
ν_2	scissor bending mode
ν_3	asymmetric stretching mode
θ_B	diffraction angle
ρ	bulk densities
ρ_r	relative densities

CHAPTER 1

INTRODUCTION

1.1 Overview

Lead zirconate titanate ($Pb(Zr, Ti)O_3$; PZT) ceramics are well-known and widely used in piezoelectric applications, due to their superior piezoelectric properties near the morphotropic phase boundary (MPB) [1]. However, more than 60 wt % of the lead-based piezoelectric material contains poisonous lead, which is a major drawback. It has been reported that the use of lead-based ceramics causes serious environmental problems and numerous physical symptoms [2]. Furthermore, EU legislation will enforce draft directives for waste from electrical and electronic equipment (WEEE), and restrictions on the use of certain hazardous substances in electrical and electronic equipment (RoHS) and end-of life vehicles (ELV) [3, 4]. According to these issues, lead and other heavy metals should be phased out, and alternative lead-free piezoelectric materials are receiving considerable attentions.

Among various alternative families, perovskite-type alkali niobate ($ANbO_3$); A = K, Na ceramics have attracted much consideration. Potassium niobate ($KNbO_3$; KN) is a well-known perovskite oxide that possesses attractive physical and piezoelectric properties. Furthermore, the electromechanical coupling factor of the thickness extensional mode, k_t, was reported to reach as high as 0.69 for the 49.5°-rotated X-cut on the Y-axis [5]. This value of k_t is the highest among current lead-free piezoelectrics. Sodium niobate ($NaNbO_3$; NN) has been studied widely for its unusual structural transition series. It has a ferroelectric rhombohedral phase below -100°C, and is antiferroelectric with orthorhombic symmetry between -100°C and 640°C [6, 7]. Finally, it possesses cubic paraelectric above 640°C, and in addition, its antiferroelectric, perovskite-type nature can transform into a ferroelectric one by chemical doping, i.e. K^+ and Li^+ [8, 9]. In addition, potassium sodium niobate [$(K, Na)NbO_3$; KNN] is a solid solution of ferroelectric potassium niobate ($KNbO_3$; KN) and anti-ferroelectric sodium, niobate ($NaNbO_3$; NN) [10]. It possesses high properties for a composition near the morphotropic phase boundary (MPB), like the PZT-based system. KNN is considered to be a good lead-free candidate for the substitution of widely used commercial lead-based piezoelectric material [11, 12].

Generally, alkali niobate powders and ceramics are synthesized by conventional solid state reaction and ordinary air sintering methods, where alkali metal carbonate or oxide compound of starting materials are heated at high temperature (800°C or above) for a long duration [13, 14]. High calcination temperature can cause volatilization of alkali metal, thus causing this classical method difficulty in achieving a homogeneous mixture of the component [13-15]. Powder agglomeration can occur during heating, which could affect properties such as low surface area and low sinterability [15]. Thus, this method does not always allow for the production of dense, homogeneous single phase ceramics. The main hindrance regarding this alkali niobate based material lies in the difficulty of preparing dense and stoichiometric controlled ceramics. Therefore, development of alternative methods that can produce powder with high sinterability and controlled stoichiometric composition is necessary. In recent years, ultra fine ceramic powder, which is synthesized using mechanochemical synthesis [16], polymeric precursors [17], and hydrothermal and polymerized complex methods [18], has been described in the literature to enable production of desired compositions. However, most chemical synthesis routes require high purity reactants, which are more expensive and demand complicated procedures and specific apparatus. While synthesizing powder rapidly, with the desired composition, high porosity and high sinterability remains a challenge.

A modified solid state reaction method has been used to synthesize the $NaTaO_3$ perovskite-type material successfully, with reduced reaction temperature [19]. In this method, the carbonate compound was replaced by an oxalate one, and the addition of urea played an important role. The use of a relatively low reactivity, with moisture starting material, sodium oxalate ($Na_2C_2O_4$), has been described. This method was found to produce $NaTaO_3$ as a general route at the lower temperature of 500-600°C, when compared with conventional solid state reaction [19].

Combustion synthesis (CS) or self-propagating high temperature synthesis (SHS) is an effective, low-cost method for producing various industrially useful materials. It has been introduced as a quick, straightforward preparation process for producing homogeneous, very fine, crystalline and unagglomerated multicomponent oxide ceramic powders, without intermediate decomposition and/or calcination steps [20, 21]. The combustion synthesis technique begins with a mixture of easily oxidized reactants (such as nitrates) and a suitable organic fuel (such as urea [22], tartalic acid [23], alanine [24], glycine [25], etc.), which acts as a reducing agent. The mixture is then heated until it ignites, which is when the temperature of rapid exothermal

chemical reaction commences, and a self-sustaining combustion reaction starts. This highly exothermic reaction produces a high temperature and duration long enough for the synthesis to occur, even in the absence of an external heating source [26]. Ultrafine nano-sized powder also can be prepared by releasing a large amount of gas from the system. This process results in a dry, fluffy, crystalline, unagglomerated and fine oxide powder.

1.2 Scope of this work

The aim of this study was to produce lead-free piezoelectric alkali niobate perovskite ABO_3 (A=K, Na; B=Nb) powders through either of two simple methods: "modified solid state reaction" or "combustion synthesis". These powders are considered to be a good lead-free candidate for the substitution of widely used commercial lead-based piezoelectric material. In using the modified solid state reaction, potassium oxalate monohydrate ($K_2C_2O_4 \cdot H_2O$), sodium oxalate ($Na_2C_2O_4$) and niobium oxide (Nb_2O_5) were employed as the starting material. The influence of calcination temperatures and dwell times on the preparation of potassium niobate ($KNbO_3$; KN) and sodium niobate ($NaNbO_3$; NN) powders were investigated. For the combustion synthesis, potassium nitrate (KNO_3), sodium nitrate ($NaNO_3$) and niobiuim pentaoxide (Nb_2O_5) were used as starting reagents, and glycine (NH_2CN_2COOH) was applied as fuel. The influence of the fuel-to-oxidizer molar ratio, calcination temperatures and dwell times on the preparation of sodium niobate ($NaNbO_3$; NN) powders were examined. The thermal behavior of all precursors was determined using thermogravimetric analysis (TGA) and differential thermal analysis (DTA). The crystal structure, phase nucleation and influence of the fuel-to-oxidizer molar ratio, calcination temperature and dwell time of calcination to phase formation of as-synthesized and calcined powders were studied and characterized by the X-ray diffraction technique (XRD) and Fourier transform infrared (FTIR) spectroscopy. The morphology and particle size of the powders obtained were investigated through a scanning electron microscope (SEM).

1.3 Objectives of this work

This work focuses on the preparation of perovskite-type alkali niobate ($ANbO_3$); A = K, Na in order to fulfill the following objectives:

1.3.1 To prepare perovskite-type alkali niobate ($ANbO_3$); A = K, Na nanoparticles by two simple methods: "modified solid state reaction" and "combustion synthesis".

1.3.2 To investigate the influence of calcination temperatures and dwell times on the preparation of potassium niobate ($KNbO_3$; KN) and sodium niobate ($NaNbO_3$; NN) nanoparticles obtained by the modified solid state reaction method.

1.3.3 To determine the characteristics of potassium niobate ($KNbO_3$; KN) and sodium niobate ($NaNbO_3$; NN) nanoparticles obtained by obtained by the modified solid state reaction method.

1.3.4 To investigate the influence of the fuel-to-oxidizer molar ratio on the preparation of sodium niobate ($NaNbO_3$; NN) nanoparticles by the combustion method.

1.3.5 To investigate the influence of the calcination temperatures and dwell times on the phase formation of sodium niobate ($NaNbO_3$; NN) nanoparticles obtained by the combustion method.

1.3.6 To determine the characteristics of sodium niobate ($NaNbO_3$; NN) nanoparticles obtained by obtained by the combustion method.

CHAPTER 2

LITERATURE REVIEW

2.1 Piezoelectric materials [26]

'Piezoelectricity' is described as an interaction between electrical and mechanical systems. It is a direct result of the piezoelectric effect, which was instantaneously discovered in 1880 by Pierre and Jacques Curie, when the relation between pyroelectricity and crystal symmetry was studied. This word 'Piezoelectricity' was proposed by Hankel and it derived from the Greek word piezo or piezein, which means to squeeze or press, and electric or electron, which stands for amber – an ancient source of electric charge. Figure 2.1 shows schematics of (a) *direct* and (b) *converse* piezoelectric effect. The *direct* piezoelectric effect takes place when electric polarization is produced by mechanical stress; as force is applied to the piezoelectric material, an electric field is generated. On the other hand, the *converse* effect occurs when a crystal becomes strained as an electric field is applied. When a voltage is applied across a poled electroded piezoelectric device, the material expands in the direction of the field and contracts perpendicular to the field.

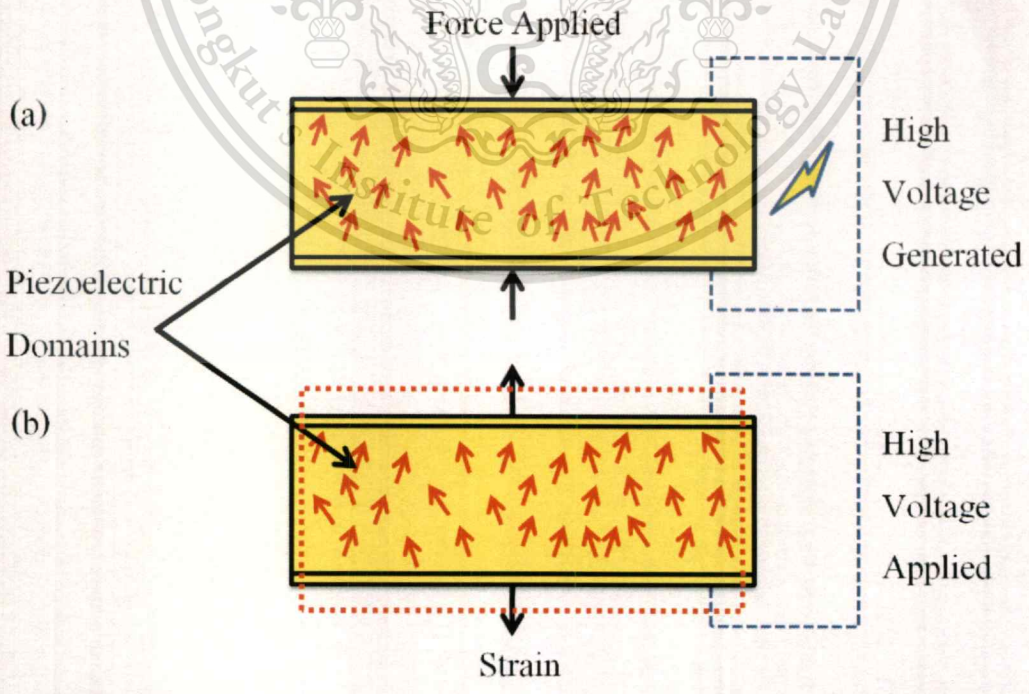

Figure 2.1 The *direct* (a) and *converse* (b) piezoelectric effect.

According to their properties, which can switch between mechanical force and an electrical energy, piezoelectric ceramics are widely used for versatile applications in electronic devices such as sensors, actuators, transducers, buzzers, etc., and other technological innovations and/or advanced electronic technology. Figure 2.2 shows versatile applications of piezoelectric ceramics in the commercial world and household goods, i.e. gas lighters, clocks, printers, shoes, automobiles, medical diagnostics, etc. Four main uses for these piezoceramics can be defined commonly as the generation of voltage, electromechanical actuation, frequency control and generation of acoustic and ultrasonic energy.

Figure 2.2 Versatile applications of piezoelectric ceramics in the commercial world.

2.2 Lead zirconate titanate ($Pb(Zr, Ti)O_3$; PZT) [27-30]

In the mid 1940's, near the end of World War II, barium titanate ($BaTiO_3$; BT) was the first piezoelectric ceramic material to be adopted and developed. However, the drawbacks of this material are twofolds: (1) it has a relatively low Curie temperature (T_C) of 120°C, which limits its use as a high-power transducer, and (2) it has a low electromechanical coupling factor of 0.35, which limits its operational output. By the late 1950s, the solid solution system of perovskite-structured lead zirconate titanate ($Pb(Zr, Ti)O_3$; PZT) had become a widespread piezoelectric ceramic material, since PZT exhibited more desirable characteristics such as higher electromechanical coupling coefficient, higher T_C value and a wide range of dielectric constants. Also, it could be poled easily and form solid-solution compositions with many constituents for wide achievable properties.

Lead zirconate titanate ($Pb(Zr, Ti)O_3$; PZT) is perovskite-type piezoelectric material, which maintains excellent piezoelectric properties across a wide temperature range, with good piezoelectric properties (k ~23-76%) and a high Curie temperature as great as 350°C. As an ideal case, ABX_3 is described schematically as belonging to perovskite. A and B are cations, whereas, X is found to be a possible anion such as O^{2-}, S^{2-}, F^-, Cl^{2-} and Br^-. Oxide is found to be the most abundant compound. Figure 2.3 (a) shows a simple arrangement of ions belonging to the ideal perovskite structure, with Figure 2.3 (b) and (c) illustrating ABO_3 composition presenting the perovskite structure in alternative ways. In Figure 2.3 (a), A cations (in blue) with larger atomic ratios are located at the center of the cube (A site), while B cations (in red) occupy the corners of the cube (B site). Oxygen (in green) is placed at the centers of twelve cube edges, giving corner-shared strings of BO_6 octahedra. Accordingly, the A cations occupy every hole created by 8 BO_6 octahedra, as seen clearly in Figure 2.3 (c), thus giving the A and B cation a 12- and 6-fold oxygen coordination, respectively. In the case of PZT, Pb atoms (in blue) occupy the A site, while Zr and Ti atoms (in red) reside in the B site.

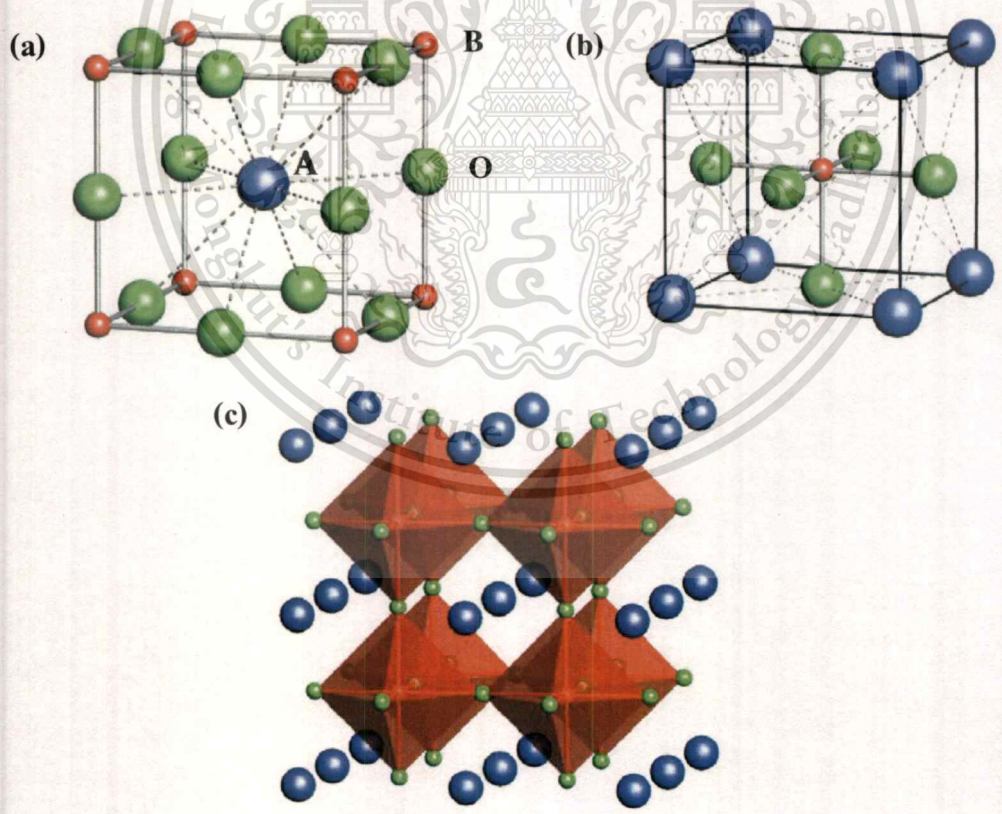

Figure 2.3 The ideal perovskite structure with ABO_3 composition (a), and other ways of presenting the perovskite structure (b) and (c) [31].

PZT is a solid solution of ferroelectric lead titanate ($PbTiO_3$; PT) and antiferroelectric lead zirconate ($PbZrO_3$; PZ). Lead titanate ($PbTiO_3$; PT) has a tetragonal structure, with its *c* axis approximately 6% longer than its *a* axis at room temperature, and it exhibits a Curie point at 495°C. Lead zirconate ($PbZrO_3$; PZ) possesses an orthorhombic structure, which exhibits a Curie point at 234°C. The binary phase diagram of the lead zirconate-lead titanate is illustrated in Figure 2.4. At a high temperature, PZT possesses a cubic paraelectric perovskite structure. As the temperature decreases, the material becomes ferroelectric with the symmetry of the tetragonal for Ti-rich compositions and rhombohedral for Zr-rich compositions. Accordingly, the morphotropic phase boundary (MPB) is defined as the composition at an abrupt structural change, with the composition being almost independent of temperature occurrence. Thus, the boundary between tetragonal and rhombohedral phases, at a composition close to $x = 0.48$, is supposed to be the MPB, which was found to be almost vertical in temperature scale. It has been reported that the best piezoelectric properties at room temperature, and their extraordinary behavior, can be obtained near the MPB composition of Zr:Ti = 52:48, which coexists between the tetragonal and rhombohedral perovskite (Figure 2.5). Figure 2.5 shows the coupling coefficient, (k_p), and dielectric constant, (ε_r), values with a different PZT compositional range. The k_p was found to increase dramatically when approaching a composition near 50% at the MPB. In addition, experiments have shown that maximum values of the dielectric constant, electromechnical coupling factors, and piezoelectric coefficients of PZT at room temperature constantly occur in composition along this phase boundary. Regarding PZT at this MPB, the piezoelectric coefficients, d_{33} ~400 pC/N, d_{31} ~-170 pC/N and d_{15} ~500 pC/N, were reported [28].

However, B. Noheda and J.A. Gonzalo (2000) [33] described a better understanding of the MPB of PZT. The MPB of PZT has been characterized on an extremely homogeneous ceramic sample by means of high resolution synchrotron X-ray powder diffraction measurement. It was found that an unexpected monoclinic phase could be seen to exist in between the well-known MPB of tetragonal and rhombohedral PZT phases. Figure 2.6 illustrates a modified PZT phase diagram from Noheda *et al.* When considering the phase diagram of two tetragonal and monoclinic phases, at room temperature, they were found to coexist over the range of $0.455 \leq x \leq 0.48$. It could be seen that enhanced piezoelectric activity of commercial composition is the result of relatively large ionic displacements associated with stress (electrical or mechanical) – induced rotation of the monoclinic polar axis.

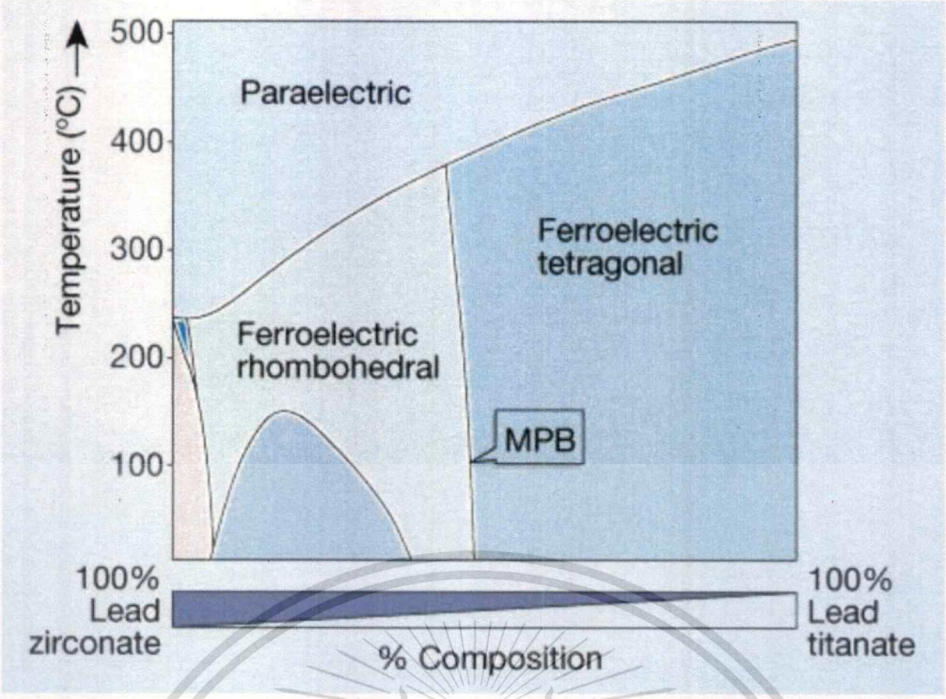

Figure 2.4 The binary phase diagram of lead zirconate-lead titanate [33].

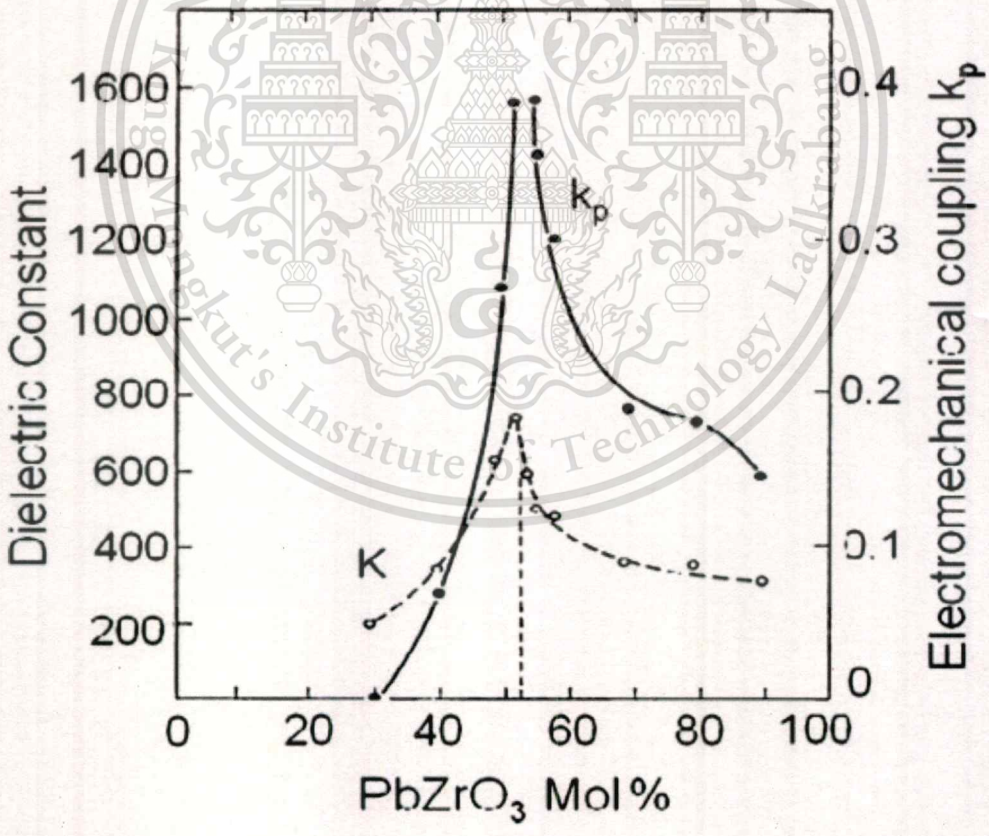

Figure 2.5 Coupling coefficient, k_p and dielectric constant, ε_r values with different PZT compositional ranges [29].

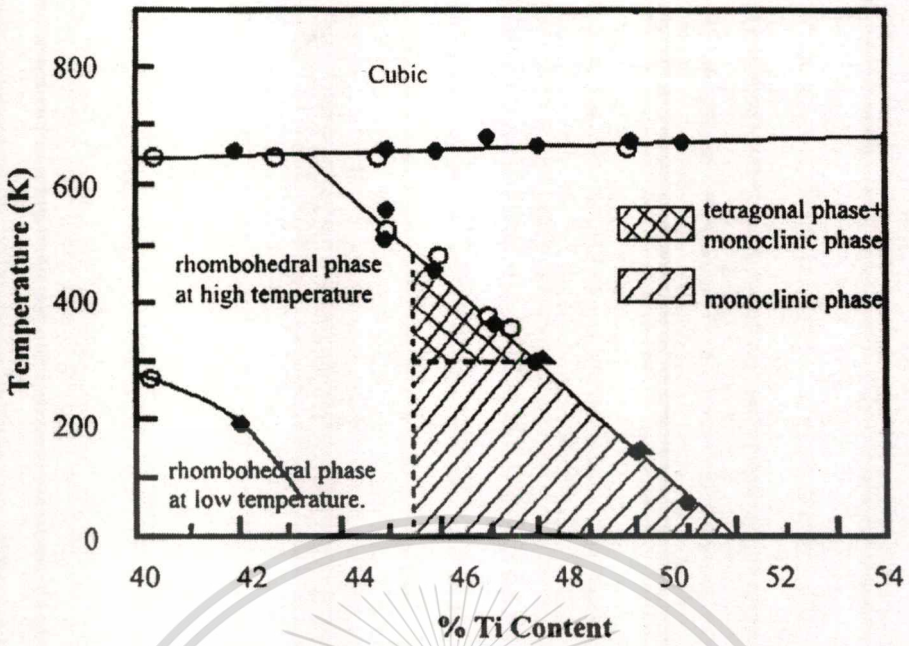

Figure 2.6 Preliminary modification of the PZT phase diagram from Noheda *et al.* [33].

Among new and useful piezoelectric ceramics that have appeared frequently, Pb(Zr, Ti)O_3 (PZT)-based ceramics are mostly used and attended to, due to their relatively high conversion efficiency, high Curie temperature and exceptional temperature stability. However, PZT-based ceramics possess excellent piezoelectric properties, although they contain more than 60 wt % lead. Lead is reported as a high toxic substance that can cause a variety of environmental problems and damage to the kidney, brain and nervous system as well as the intelligence status in children [34]. Also, numerous medical symptoms, i.e. headaches, constipation, nausea, anemia and reduced fertility have been reported [35]. In terms of legislation in the European Union (EU), two recent directives; 2002/95/EC "Directive on the restriction of the use of certain hazardous substances in electrical and electronic equipment" (hereafter RoHS Directive), and the 2002/96/EC "Directive on Waste Electrical and Electronic Equipment" (hereafter WEEE Directive), have put severe restrictions on the use of hazardous substances in electronic equipment [3-4]. The EU also looked for improvement in the environmental performance of all operators involved in the life cycle of electrical and electronic equipment, e.g. producers, distributors and consumers, and in particular, operators that are involved directly in the treatment of electrical and electronic solid waste. Actors in the product chain have to share responsibility for the life cycle of environmental impacts on the whole product system. The WEEE directive attempted to standardize the requirements for the collection and recycling of electronics in the

community, from small domestic appliances to medical equipment. Producers were required to finance the collection, sorting, recovery and environmentally sound disposal of WEEE. The RoHs directive banned the hazardous substances; Pb, Hg, Cd, Cr(VI), polybrominated biphenyls (PBB) and polybrominated diphenyl ethers (PBDE), in electrical and electronic equipment (EEE), which were being traded in the EU market. Thus, EU member states must ensure that all new electrical and electronic devices do not contain those toxic components and/or exceed certain maximum concentration values. Accordingly, lead and other heavy metals should have been phased out by 1st July, 2006 [3]. This initiative has had great influence on the current design process and manufacturing methods. In addition, the WEEE concept has been attended to by several industrialized countries such as China, Japan and the United States of America [36-37]. In response, lead-free and/or low-lead-content piezoelectric compositions have been studied intensively and developed for replacement of lead-based compositions in commercial applications.

2.3 Alkali niobate ceramics ABO_3 (A = K, Na; B = Nb) [9, 15]

It is known that alternative lead-free piezoelectric materials, which are considered thoroughly, could be separated according to their structure into three categories: Bismuth layer structured materials, tungsten bronze materials, and perovskite materials. Bismuth layer structured and tungsten bronze materials were found to possess a high Curie temperature (T_C), high mechanical quality factor (Q_m), large dielectric breakdown strength, and good aging characteristics. These properties have led two materials to ceramic filter and resonator applications. Unfortunately, their large crystal anisotropy can result in two-dimensional restriction on the permissions of spontaneous polarization, which causes low dielectric constant and poor piezoelectric properties. On the other hand, perovskite-type structure piezoelectric materials were found to possess superior piezoelectric properties, due to their spontaneous polarization to rotate along three-dimensional orientations (x, y, and z directions).

Alkali niobate ceramics, ABO_3 (A = K, Na; B = Nb), are considered to be a good lead-free candidate for the substitution of widely used commercial lead-based piezoelectric material. It has been reported that potassium niobate ($KNbO_3$; KN)-based ceramics – especially the solid solution of ferroelectric potassium niobate ($KNbO_3$; KN) and anti-ferroelectric sodium niobate ($NaNbO_3$; NN) – are attractive materials for the replacement of PZT, since they possess high

properties for composition near the morphotropic phase boundary (MPB), like the PZT-based system. Sodium potassium niobate, (K, Na)NbO_3, is a new piezoelectric perovskite ceramic, which was discovered in the 1950s. Its phase diagram was reported by G. Shirane *et al* [8]. Figure 2.7 shows the phase diagram for the solid solution (1-x)$KNbO_3$-(x)$NaNbO_3$ system. This system shows a relatively high degree of complexity, e.g. in comparison with the well-known PZT system. Several thermally induced phase transitions or polymorphic phase transitions (PPTs) have been reported. At room temperature, phase transitions lie at 17.5%, 32.5% and 47.5% NN content, with the latter commonly taken as 50/50 analogous to PZT. It should be noted that almost composition-independent PPT between ferroelectric phases (orthorhombic-tetragonal phase transition) at ~210°C ($T_{T\text{-}O}$) and ferroelectric and paraelectric phases (cubic-tetragonal phase transition) at ~420°C (T_C) have been shown. On the NN-rich side, only small substitutions of sodium by potassium can cause a transition to ferroelectric from pure antiferroelectric sodium niobate. The morphotrophic phase boundary near the 50% composition in (K, Na)NbO_3, which separates two orthorhombic ferroelectric phases, has been identified. Considering $K_{0.5}Na_{0.5}NbO_3$ ceramics sintered by the ordinary sintering method (air-fired) performed in 1959, the maximum value of electromechanical planar coupling coefficient (k_p) and piezoelectrical coefficient (d_{33}) was found to be 36% and 80 pC/N, respectively, with a dielectric constant of 290. Therefore, an intensive research effort has been focused on the (1-x)$KNbO_3$-$x$$NaNbO_3$ materials around this composition of MPB [39].

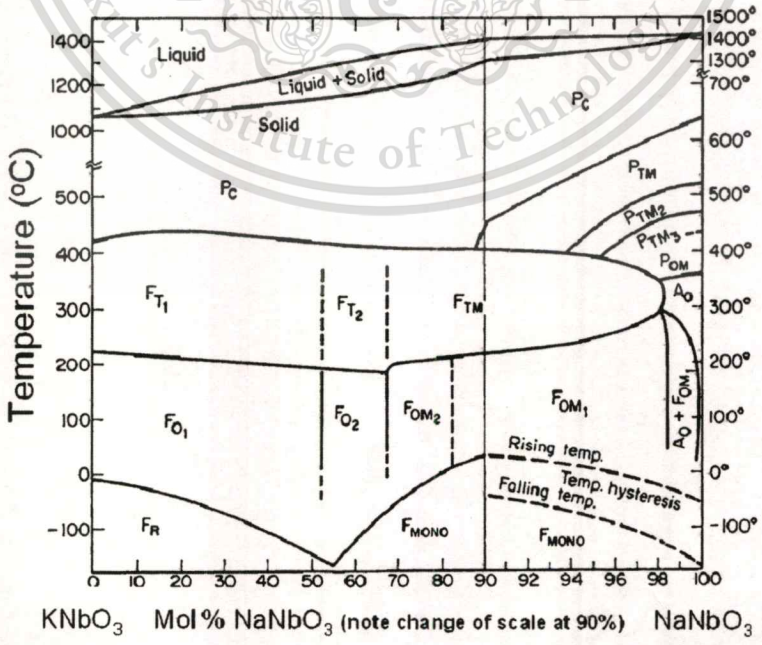

Figure 2.7 Phase diagram of the $KNbO_3$-$NaNbO_3$ system [29].

Unfortunately, one of the main obstacles for development of the KNN system as a commercial piezoceramic material was found to be difficulties in processing, especially densification. H. Birol *et al.* [40] reported on the preparation of the KNN ceramic by conventional processing. The sintering parameters were investigated and optimized to result in reproducible and high quality ceramics. KNN ceramics produced in their report exhibited theoretical density of over 95% and yielded superior piezoelectric properties (d_{33} ~100 pC/N and d_{31} ~43 pC/N). However, the preparation had to be performed carefully. The carbonate origins required extra care when taken against humidity and dried in an oven prior to mixing. The alumina crucible was heated before transferring the dried powder precursor in the calcination step. These processes were found to be more complicated and they needed extreme control over many parameters.

Regarding densification, it is difficult for the KNN solid solution system to reach full densities by natural sintering, due to high volatilization of potassium at high temperatures, and the phase stability of this material is limited to 1,140°C. Sintering at high temperatures is therefore impossible in the case of avoiding a stoichiometry controlled problem or formation of unexpected phases. The investigation of commercial compositions and optimum processing for obtaining reproducible properties has been widely studied. In terms of possible low temperature sintering, the aspects that are often considered can be divided as (1) pressure or electric field-assisted sintering, (2) addition of a small glass phase or different additions, (3) addition of some sintering aids, and (4) reduction in initial particle size, due to the driving force for sintering being inversely proportional to the particle size.

As early as 1962, undoped KNN with various K/Na ratios was prepared through the hot pressing method by R.E. Jaeger *et al* [41]. The relative density was increased from 94.2% to 98.9% by air sintering, with a high Curie temperature of ~420°C. Dielectric and piezoelectric properties, as a function of composition belonging to the $(1-x)KNbO_3$-$(x)NaNbO_3$ system, is given in Figure 2.8. A broad maximum in the planar electromechanical coupling coefficient was observed. Due to densification of the sample, dielectric constants and the planar electromechanical coupling coefficient were improved remarkably. The maximum, k_p at ~46%; highest remnant polarization, P_r, at ~33 μC/cm^2; lowest coercive field, E_c at ~4.7 kV/cm; and high piezoelectrical coefficient, d_{33}, at 127 pC/N with a dielectric constant of 490, were observed for x = 0.5 of the hot-pressed sample.

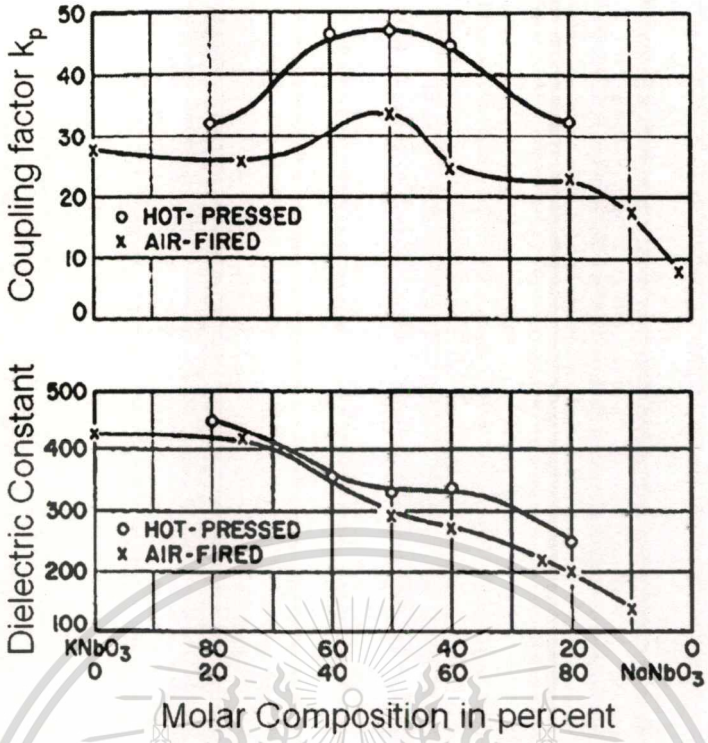

Figure 2.8 Dielectric and piezoelectric properties as a compositional function of the $KNbO_3$-$NaNbO_3$ system [41].

Hot isostatic pressing (HIP) and the spark plasma sintering (SPS) method have been used to achieve high densities, and relative densities above 99.5% were obtained by using HIP [42]. In 2004, high density $(1-x)KNbO_3$-$(x)NaNbO_3$ (x = 0.5, 0.6 and 0.7) ceramics were prepared successfully using the spark plasma sintering (SPS) method by R. Wang *et al.* [43]. A high temperature (up to ~1,700°C) and high pressure (up to ~0.6 GPa) were applied simultaneously during the sintering process. When compared to the hot press method, SPS possessed a character of super-high sintering speed. In $(1-x)KNbO_3$-$(x)NaNbO_3$ samples, SPS-sintered at 1,040-1,100°C was found to possess a higher room temperature dielectric constant, higher coercive fields, lower remnant polarizations and lower electromechanical coefficients than in hot-pressed $(1-x)KNbO_3$-$(x)NaNbO_3$ samples. The relative densities of the samples were estimated to be around 98%. Grain sizes showed a distribution of between ~2 and ~7 μm. The average grain size was relatively smaller than that of the hot-pressed samples, due to the short sintering duration and low annealing temperature halting growth of the grains.

After that, B.P. Zhang *et al.* fabricated $(1-x)KNbO_3$-$(x)NaNbO_3$ (x = 0.2-0.8) dense ceramics using the SPS method at a low temperature of 920°C [44]. Figure 2.9 illustrates the SEM micrographs of $(1-x)KNbO_3$-$(x)NaNbO_3$ ceramics at various compositions. The fractured surface showed that all the KNN samples were very dense, with almost no visible pores being found. An SPS temperature of >200°C, which was lower than the hot-pressing temperature, was used. The grain sizes were in the range of 200-500 nm. The piezoelectric constant (d_{33}) and planar electromechanical coupling coefficient (k_p) for $(1-x)KNbO_3$-$(x)NaNbO_3$ (x = 0.6), showed a maximum value of 148 pC/N and 38.9%, respectively. These maximum values were found to be strongly supported by the existing MPB-like region in this compositional area. However, J.F. Li *et al.* also reported the fabrication of $K_{0.5}Na_{0.5}NbO_3$ using the SPS method at the low temperature of 920°C [45]. It was found that the density of KNN ceramics was raised to 99% of the theoretical density at 4.47 g/cm^3. Figure 2.10 shows SEM and TEM micrographs of the SPS of $K_{0.5}Na_{0.5}NbO_3$ ceramics at 920°C for 5 min before annealing at 900°C for 4 h. The SEM micrograph of the fractured surface shows that the $K_{0.5}Na_{0.5}NbO_3$ ceramic was very dense. The TEM micrograph clearly shows that the grain sizes are in the range of 200-500 nm, which is much smaller than those reported elsewhere. J.F. Li *et al.* were the first to report production of this fine-grained microstructure, which was due to the powder densification process conducted by SPS at a low temperature and for a very short period.

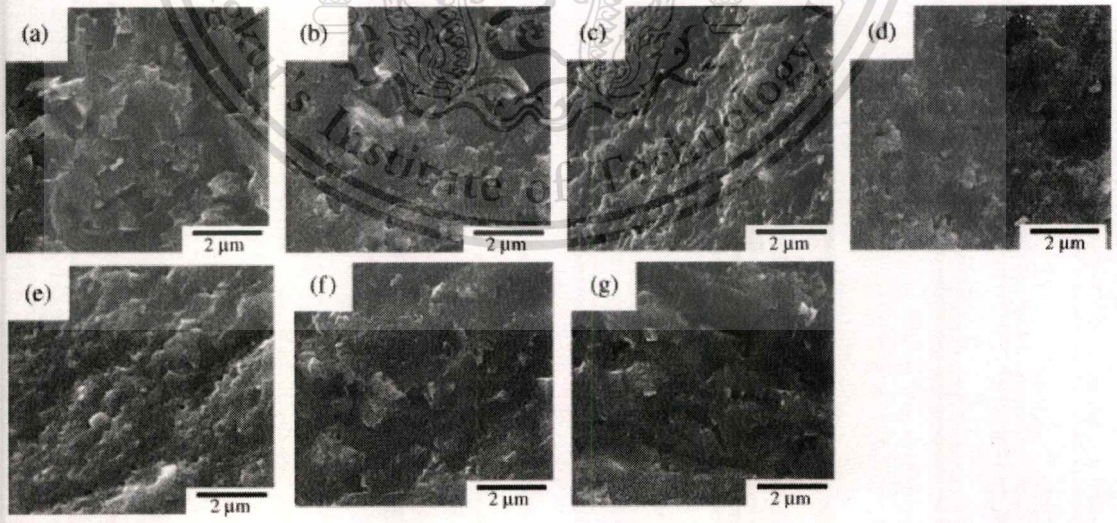

Figure 2.9 SEM micrographs of $(1-x)KNbO_3$-$(x)NaNbO_3$ ceramics with various Na contents (x), (a) 0.2, (b) 0.3, (c) 0.4, (d) 0.5, (e) 0.6, (f) 0.7, and (g) 0.8 [44].

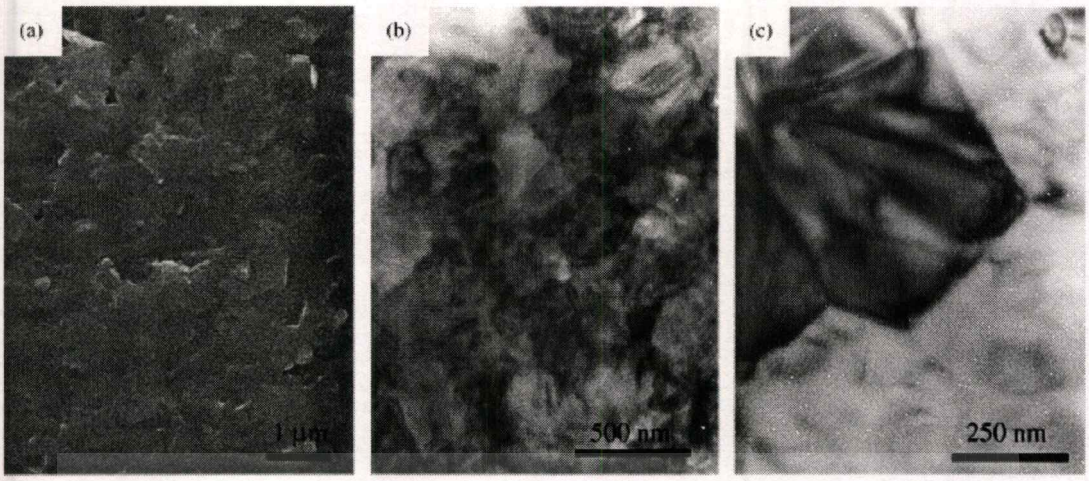

Figure 2.10 Microstructure of the $K_{0.5}Na_{0.5}NbO_3$ ceramic spark plasma sintered at 920°C for 5 min before annealing at 900°C for 4 h. Micrograph by scanning electron microscopy (a) and micrographs of transmission by electron microscopy (b and c) [45].

Unfortunately, the cost of HIP, SPS and this method are relative high and unsuitable for use in industrial production. Therefore, it is pertinent to further improve sintering of KNN ceramic under normal atmospheric conditions and ordinary processing. Doping to modify KNN ceramics was found to be an effective way to improve the sintering characteristic and electrical properties. In 2004, Y. Saito *et al.* reported that (K, Na)NbO_3-based perovskite solid solution was a compatible piezoelectric property to lead-based ceramics [46]. Since no effective alternative to PZT has yet been found, this work reported lead-free piezoelectric ceramic, with an electric-field-induced strain comparable to typical actuator-grade PZT, used the relative template train growth technique (RTGG). This research discussed a discovery of the MPB of solid solution in the (K, Na)NbO_3-$LiTaO_3$-$LiSbO_3$ pseudo-ternary system, which possessed a relatively high piezoelectric constant (d_{33}). The d_{33} constants and Curie temperatures (T_C) for the textured ceramics (LF3T and LF4T) are shown in Figure 2.11. The enhanced d_{33}constants were 373 and 416 pC/N for LF3T and LF4T, respectively, which were 1.8 and 1.6 times larger than those of the nontextured ceramics, LF3 and LF4, respectively. The temperature-independent characteristic of developed lead-free ceramics was found to be more prominent than conventional PZT ceramics (Figure 2.12). This could attract more attention and encourage researchers to develop further novel lead-free piezoelectric materials for replacing lead-based ones.

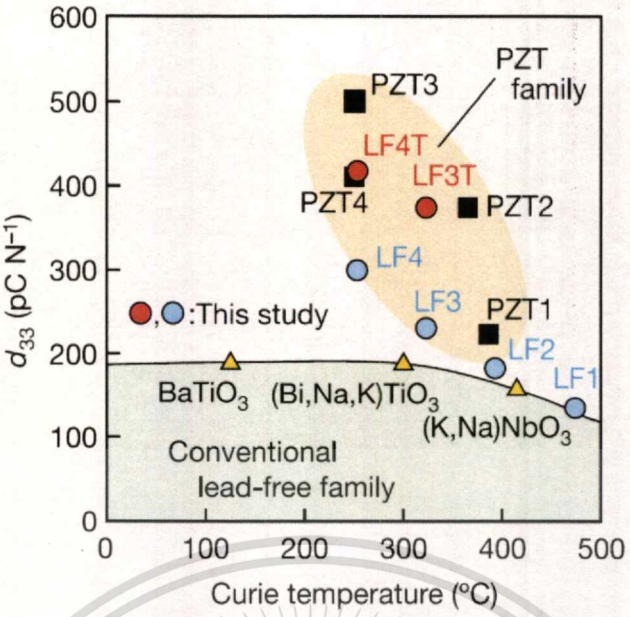

Figure 2.11 Comparison of the piezoelectric charge sensor constant at 25°C among developed (K, Na)NbO_3-$LiTaO_3$ ceramics (LF) and conventional PZT ceramics as a function of Curie temperature. PZT1: $Pb(Zr_{0.52}Ti_{0.48})O_3$. PZT2: $Pb_{0.988}(Zr_{0.48}Ti_{0.52})_{0.976}Nb_{0.024}O_3$. PZT3: commercially available PZT. PZT4: $\{(Pb_{0.85}Ba_{0.15})_{0.9925}La_{0.005}\}(Zr_{0.52}Ti_{0.48})O_3$ [46].

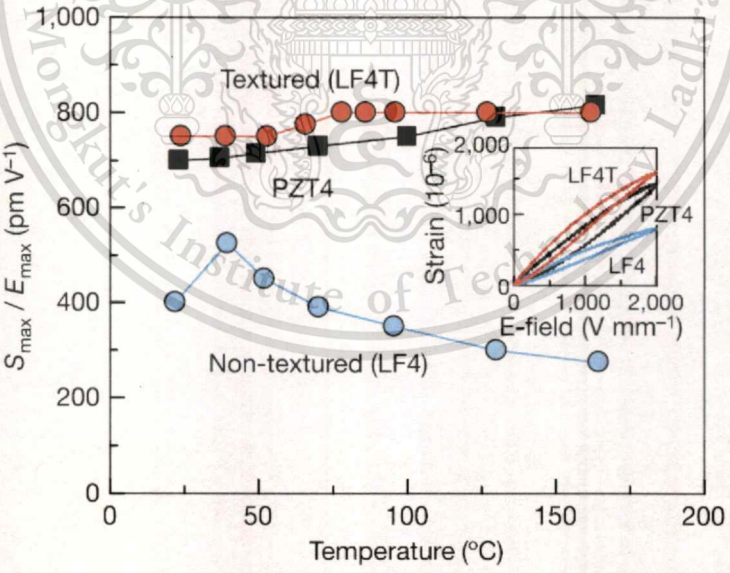

Figure 2.12 Temperature dependence of electric-field-induced longitudinal strain for the textured (LF4T) and non-textured (LF4) ceramics of the (K,Na)NbO_3-$LiTaO_3$ system [46].

Based on the concept of introducing cationic substitution in KNN to enhance its properties, several cations were concerned such as Li^+ and Sr^{5+} for the *A*-site substitution and Ta^{5+}, Sb^{5+} and Ti^{4+} for the *B*-site substitution. Li^+- and Ta^{5+}-modified KNN ceramics have been considered a good candidate and widely studied. Y. Gou *et al.* [47] prepared the $(1-x)K_{0.5}Na_{0.5}NbO_3$-$xLiTaO_3$ (x = 0.02-0.20) system. The cationic substitution effect of lithium for sodium and potassium in the *A*-sites, and tantalum for niobium in *B*-sites of the $(K_{0.5}Na_{0.5})NbO_3$ (KNN) perovskite lattice on symmetry and physical properties was investigated. A morphotropic phase boundary (MPB) between orthorhombic and tetragonal phases was found to appear at x = 0.5. A poled sample of MPB composition showed the largest values of dielectric constant = 570, planar electromechanical coupling coefficient k_p = 36%, and piezoelectric coefficients d_{33} = 200 pC/N. These extraordinary properties were described as a result of tetragonal-othorhombic (T_{T-O}) phase transition, which was shifted to room temperature. In 2005, potassium sodium niobate piezoelectric ceramics, substituted with lithium $(K_{0.5-x/2},Na_{0.5-x/2},Li)_xNbO_3$ (x = 0.05, 0.06, 0.065, 0.07) or lithium and tantalum $(K_{0.5-x/2},Na_{0.5-x/2},Li_x)Nb_{1-y},Ta_y)O_3$ [with (x,y) = (4,10) and (3,20)], were synthesized through traditional solid state sintering by E. Hollenstein *et al.* [48]. High densities and piezoelectric properties can be obtained in Li and Ta modified KNN ceramics by simple pressureless processing, without sintering aids, CIP or special powder handling. Resonance and converse piezoelectric (strain-field) measurements show the electromechanical thickness coupling coefficient (k_t) of 53% and converse piezoelectric coefficient (d_{33}) of around 200 pm/V for the Li-substituted ceramics, and a k_t of 52% and d_{33} of over 300 pm/V for the Li^+- and Ta-modified samples. When considering temperature dependence of the dielectric constant of Li^+-modified KNN, the Curie temperature is shifted to higher value, as the Li^+ content x is increased. T_{T-O} is moved to below room temperature for $x \geq 0.07$, indicating that the Li^+ addition stabilized the tetragonal phase. Li modified KNN ceramics are considered one of the most promising ways to obtain high properties of KNN-based ceramics. P. Zhao *et al.* prepared $[(Na_{0.535}K_{0.480})_{0.942+x}Li_{0.058}](Nb_{0.90}Ta_{0.10})O_3$ ceramics, compensated with Na and K at a fixed and optimized ratio of 0.535:0.480 [49]. A phase transition from tetragonal to orthorhombic symmetry was observed as x increased from 0.022 to 0.024, which resulted in enhancing increased piezoelectric coefficient and planar electromechanical coupling coefficient (k_p) from 216 and 38.1% to 268 pC/N and 46.2%, respectively. It is clear that d_{33}, k_p, and ε possess a peak value with an increasing compensatory amount of $Na_{0.535}K_{0.480}$. While the transition from tetragonal to orthorhombic phase is being completed in samples compensated with 2.4 at % $Na_{0.535}K_{0.480}$, either

d_{33} or k_p reaches its peak value. The optimized electrical performances in this study should be due to MPB behavior. Further $Na_{0.535}K_{0.480}$ compensation turned to decrease electrical properties. The reason for this lies in the fact that the composition of the ceramics may deviate from the ideal MPB composition, when the Na and K have been compensated sufficiently. Y. Chang *et al.* [50] studied the effects of Ta content on the phase transitional behavior, Raman spectrum, microstructure, and dielectric, piezoelectric and ferroelectric properties of $[(K_{0.458}Na_{0.542})_{0.96}Li_{0.04}](Nb_{1-x}Ta_x)O_3$ ceramics, prepared by the ordinary sintering technique. It was reported that Ta substitution for Nb led to disappearance of abnormal grain growth behavior, inhibition of grain growth, and improved density of ceramics. The proper substitution of Ta shifted the polymorphic phase transition (at T_{T-O}) to near room temperature, and coexistence of orthorhombic and tetragonal phases was formed, which led to significant enhancements of electrical properties. For ceramics with $x = 0.15$, electrical properties became the optimum, and were as follows: piezoelectric coefficient d_{33} = 298 pC/N, planar electromechanical coupling coefficient $k_p = 0.52$, dielectric constant $\varepsilon_r = 1195$, dielectric loss tan $\delta = 0.016$, $T_{T-O} = 35°C$, Curie temperature $T_C = 366°C$, remnant polarization $P_r = 28.68\ \mu C/cm^2$, and coercive field $E_c = 7.14$ kV/cm. P. Zhao *et al.* [51] prepared the Li/Ta-co-doped KNN ceramics with an optimal composition of $[(Na_{0.535}K_{0.480})_{0.966}Li_{0.058}](Nb_{0.90}Ta_{0.10})O_3$. The ferroelectric, piezoelectric and dielectric properties were investigated, with special emphasis on the influence of sintering temperatures (ranging from 1,075 to 1,120°C). Reports stated that when the sintering temperature was raised to 1,090°C, ε_r, d_{33} and k_p reached their maximum value of 720, 268 pC/N and 46.2%, respectively. The highest value of d_{33} should be attributed to MPB behavior of the ceramics. Figure 2.13 illustrates the polarization hysteresis loops of $[(Na_{0.535}K_{0.480})_{0.966}Li_{0.058}](Nb_{0.90}Ta_{0.10})O_3$ ceramics, synthesized at 1,075-1,120°C. The remnant polarization (P_r) of the sample, synthesized at 1,075°C, was 5.9 $\mu C/cm^2$; and when the sintering temperature was raised to 1,090°C, a well-saturated hysteresis loop was obtained and the P_r value reached as high as 11.5 $\mu C/cm^2$. Continuously increasing sintering temperature tended to decrease the P_r, because the seriously unbalanced relative ratios of individual samples were caused by the heavy losses of Na and K at a higher temperature.

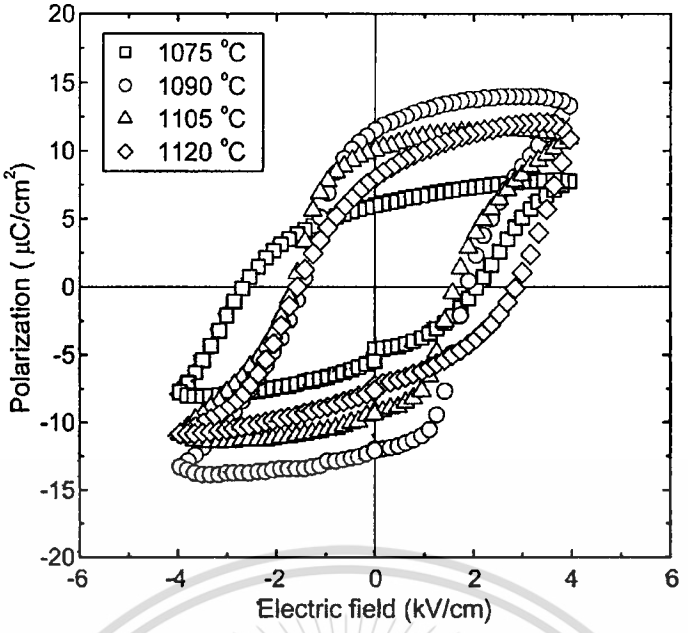

Figure 2.13 Polarization hysteresis loops of $[(Na_{0.535}K_{0.480})_{0.966}Li_{0.058}](Nb_{0.90}Ta_{0.10})O_3$ ceramics synthesized in a temperature range of 1,075-1,120°C [51].

N.M. Hagh *et al.* [52] reported the electromechanical properties of the $(K_{0.44}Na_{0.52}Li_{0.04})(Nb_{0.84}Ta_{0.10}Sb_{0.06})O_3$ (KNN-LT-LS) system. Higher electronegativities of Ta^{5+} and Sb^{5+} over Nb^{5+} resulted in formed bonds that were more covalent than ionic. Hence, the resultant Sp^3 hybridization of covalency over the ionic bond led to further improvement in piezoelectric properties of KNN-LT-LS. The oxygen flow rate was reported to be an effective factor in electromechanical properties of KNN-LT-LS ceramics. The highest electromechanical properties were achieved when ceramics are completely exposed to oxygen with a high flow rate. When sintering at 1,150°C for 1 h, with an oxygen flow rate of 180 cm^3/min, the KNN-LT-LS ceramics have $d_{33} \geq 300$ pC/N, $\varepsilon^T_{33} = 1865$, $\tan\delta = 0.02$, $k_{33} = 0.65$. In addition, it was noted that the KNN-$LiSbO_3$ system appeared more interesting as it revealed high piezoelectric properties at a relatively low cost. Although this kind of ceramic showed excellent electrical properties at room temperature, its temperature stability was relatively poor, and this may greatly limit its practical application. It has been reported also that Li^+ substitution for $(K_{0.5}Na_{0.5})^+$ in the KNN–$LiSbO_3$ system is more effective than Sb^{5+} substitution for Nb^{5+} in decreasing T_{T-O}. Further improvement of the sinterability and piezoelectric properties can be expected without decreasing T_{O-T} greatly by adding a proper amount of Li and Sb to KNN. Thus, good temperature stability at around room temperature can be achieved. L. Wu *et al.* [53] prepared $(K_{0.5-x}Li_x)Na_{0.5}(Nb_{1-y}Sb_y)O_3$ (KLNNS*x*-*y*,

x = 0-4 mol% and y = 0-8 mol%) ceramics by the conventional mixed oxide method. It was found that the sintering temperature decreased and the average grain size increased with increasing amounts of Li. A denser microstructure and better electrical properties of ceramics were obtained when compared to pure $K_{0.5}Na_{0.5}NbO_3$ ceramic. It was found that KLNNSx-y ceramics possessed a high density of more than 96% of theoretical values, which indicated that the addition of Li and Sb can assist the densification of KNN ceramics and improve ceramic sinterability. The experimental results showed that the KLNNS2.5-5 ceramic exhibits good electrical properties (k_p ~49%, k_{31} ~30% and $\varepsilon^T_{33}/\varepsilon_0$ ~543, tan δ ~0.019), and possesses good temperature stability in the temperature range of -40 to 85°C. Furthermore, buzzers based on KLNNS2.5–5 ceramic have been fabricated. Super-thin buzzers were prepared using KLNNS2.5–5 ceramic membranes, with diameters of 15-16 mm and thicknesses of 0.10-0.11 mm obtained by the roll forming process. Photographs of the KLNNS2.5–5 ceramic membranes and buzzers are shown in Figure 2.14. The electrical properties of the piezoceramic membranes were k_p = 0.44-0.45, ε_r = 450-550 (120 Hz), and tan δ = 0.020-0.035 (120 Hz).

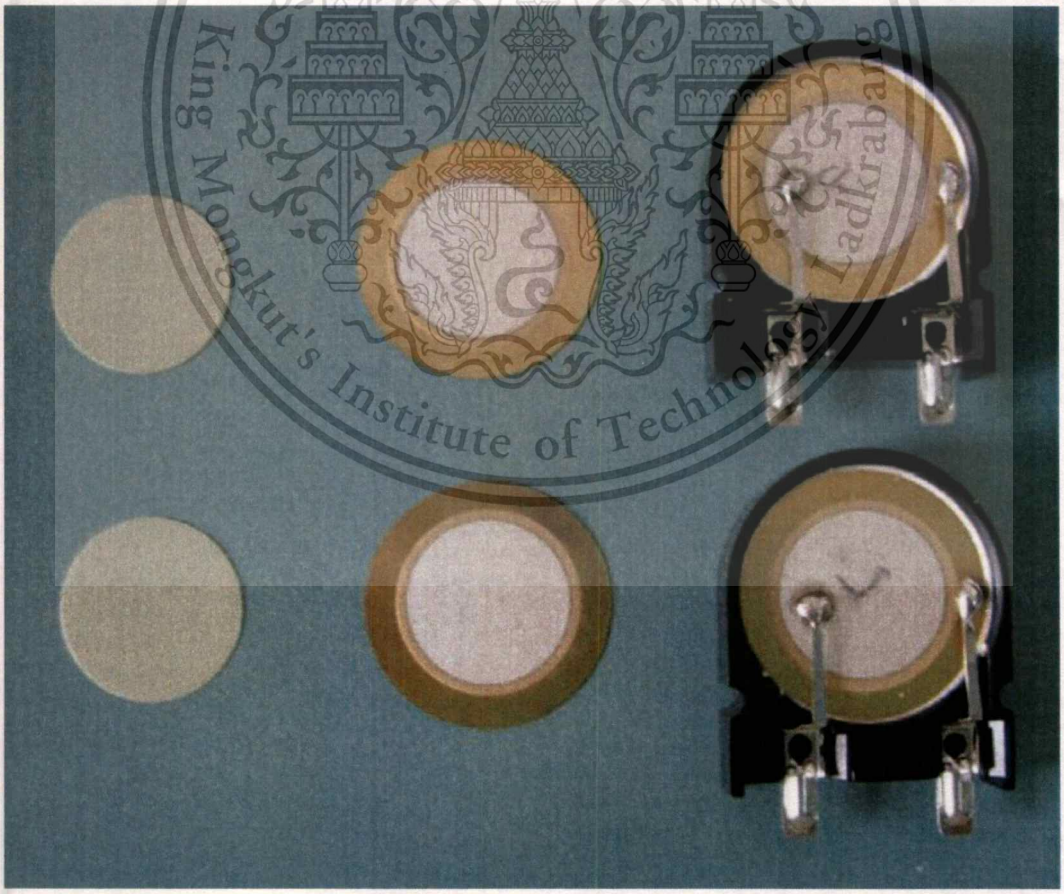

Figure 2.14 Photographs of KLNNS2.5-5 ceramic membranes and buzzers [53].

In 2006, T. Fu-sheng *et al.* [54] synthesized $(1\text{-}x)K_{0.5}Na_{0.5}NbO_3\text{-}xLiNbO_3$ (x = 0.04-0.07). The effect of Li on the sintering characteristic, phase structure and piezoelectric properties of ceramics was investigated. The sintering temperature of KNLN ceramics decreased with increasing Li content. However, these temperatures were found to be lower than that of pure KNN ceramics. The piezoelectric properties were enhanced greatly for compositions near MPB, and the values of all KNN-LN ceramics were exceeded by up to 180-200 pC/N. The electromechanical coupling coefficient (k_p) was 35-40%. The KNN-LN (x = 0.05, 0.06) was a promising high-temperature lead free piezoelectric ceramic.

As marked doping-enhanced piezoelectricity was found in Li and/or Ta-doped KNN solid solutions, strontium titanate ($SrTiO_3$) doping also was seen to enhance the piezoelectricity of KNN ceramics. $SrTiO_3$ possessed the same perovskite structure as KNN, and a complete solid solution could be performed. Y. Gou *et al.* prepared the $(1\text{-}x)K_{0.5}Na_{0.5}NbO_3\text{-}xSrTiO_3$ (KNN-ST; x = 0.005-0.100) ceramics [55]. The dependence of phase structure on the doping content of SrO and TiO_2 was determined, and the dielectric relaxor behavior was induced by doping SrO and TiO_2 into KNN. The sample in the composition of x = 0.005 to 0.020 exhibited excellent electrical properties, a piezoelectric constant (d_{33}) of 90-96 pC/N, electromechanical planar and thickness coupling coefficients of k_p = 26.6-32.5% and k_t = 39.8-43.8%. These results could attribute to the increase in sample density, which was a result of the cold-isostatic-pressing (CIP) process. Nevertheless, these $(1\text{-}x)K_{0.5}Na_{0.5}NbO_3\text{-}xSrTiO_3$ solid solutions were prepared with x = 0.0-0.30, using the conventionally mixed oxide method by R.C. Chang *et al.* [56]. It was reported that no KNN-ST specimens deliquesce when exposed to water for a long time. The bulk densities (ρ) of the doped ceramics reached up to 4.4-4.5 g/cm^3 (the theoretical density is 4.51 g/cm^3), which was equivalent to the relative densities (ρ_r) of 97-99%. KNN-ST ceramic, with x = 0.005, exhibited the maximum value of k_t and k_p which reached 42.2% and 36.1%, respectively. These values were relatively high when compared with PT-based (k_t = 0.36-0.57, k_p = 0.03-0.2) and PZT-based (k_t = 0.3-0.6, k_p = 0.5) ceramics. Furthermore, the addition of small amounts of $SrTiO_3$ yielded larger electromechanical coupling factors than those of pure KNN samples (k_t = 33.4%, k_p = 29.6%).

There was confirmation that high piezoelectric properties in Pb-based piezoelectric ceramics should be attributed to two main reasons, with the first being hybridization between the Pb 6*p* and O 2*p* orbits responsible for large piezoelectric responses. In the ABO_3 perovskite structure, the magnitude of π bonds between the *d* orbitals of B ions and 2*p* orbitals of O ions also

can result in the ferroelectricity magnitude of materials. Additionally, hybridization between *A*-site ions and O ions can increase the strength of π bonds, which affect higher ferroelectricity. Since Bi^{3+} is isoelectronic with Pb^{2+} and shows a valence electron configuration of $6s^2 6p^0$, it is an element preferred to replace Pb^{2+}. The second main reason is the formation of MPB, in which the polarization vector can rotate almost continuously under the external electric field. As it was reasonable to predict that introduction of Bi^{3+} into the *A*-sites of KNN ceramics can improve piezoelectric properties, owing to the above reason. S. Du *et al.* [57] prepared $(K_{0.5}Na_{0.5})_{1-3x}Bi_xNbO_3$ (KNBN) ceramics by conventional solid state sintering without cold-isostatic pressing. The phase structure, microstructure, and electrical properties of KNBN ceramics were studied. The addition of Bi^{3+} significantly improved electrical properties of $K_{0.5}Na_{0.5}NbO_3$ ceramics, while keeping the tetragonal-orthorhombic phase transition temperature ($T_{T\text{-}O}$) above 170°C. The KNBN (x = 0.01) ceramics showed the optimum electrical properties; d_{33} = 164 pC/N, k_p = 0.47, Q_m = 120, T_C = 403°C, $T_{O\text{-}T}$ = 174°C, P_r = 30.1 C/cm^2, and E_c = 6.18 kV/cm. Taking into account the electrical properties and polymorphic phase transition temperature ($T_{T\text{-}O}$), it can be concluded that the KNBN (x = 0.01) ceramic is a promising lead-free piezoelectric candidate material for practical application. The $(K_{0.5}Na_{0.5})NbO_3$-$BiMeO_3$ solid solution (where Me^{3+} = Sc, Al, Ga, Y, In, etc.) was a solid solution system predicted to possess high piezoelectric properties, due to formation of the MPB and hybridization between the Bi 6*p* and O 2*p* orbits [58]. The (1-x)$(K_{0.5}Na_{0.5})NbO_3$-$x$$BiScO_3$ (KNN-BS) solid solution was an example selected for studying the validity of this prediction. At room temperature, the polymorphic phase transition (PPT) from orthorhombic to tetragonal in (1-x)KNN-xBS ceramics is identified at x = 0.0175 by analyzing X-ray diffraction patterns and dielectric spectroscopy. Figure 2.15 shows the piezoelectric properties of (1-x)KNN-xBS ceramics at room temperature. At x = 0.0175, it can be seen clearly that the piezoelectric constant (d_{33}), planar electromechanical coupling coefficient (k_p), and thickness of electromechanical coupling coefficient (k_t) of (1-x)KNN-xBS ceramics reach their highest value, which is 253 pC/N, 0.48, and 0.49, respectively. In addition, it was also found that the piezoelectric properties of (1-x)KNN-xBS ceramics were sensitive to compositions when they readily decreased as the content of BNT deviated by 0.0175 mol. When compared to the other KNN-based and hard $Pb(Zr,Ti)O_3$ ceramics, it was concluded that the (1-x)KNN-xBS (x = 0.0175) ceramic was a promising candidate lead-free piezoelectric material.

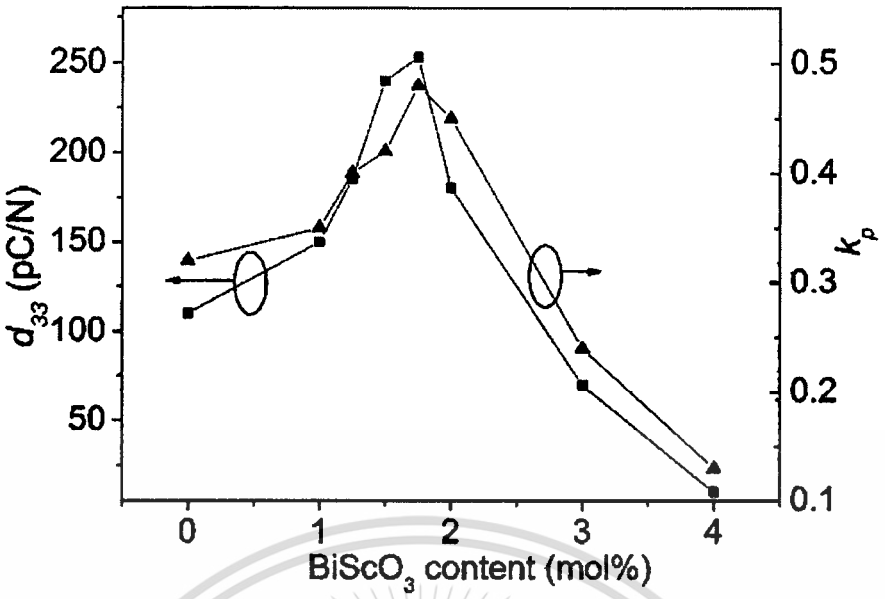

Figure 2.15 Piezoelectric properties of $(1-x)$KNN-xBS ceramics at room temperature [58].

A dense microstructure of the $0.95(Na_{0.5}K_{0.5})NbO_3$-$0.05BaTiO_3$ (0.95NKN-0.05BT) ceramics was prepared by C.W. Ahn *et al.* in 2007 [59]. The microstructure, formation process of the liquid phase, effect of Na_2O evaporation and resulting effect on the piezoelectric properties of ceramics were investigated. Grain growth was observed in the specimens sintered at 1,050-1,060°C, while a liquid phase was found in those sintered at above 1,050°C, which explained the increased sinterability and grain size. $KTiNbO_5$ and $Ba_6Ti_2Nb_8O_{30}$ secondary phases were also observed for specimens sintered at above 1,060°C. Evaporation of Na_2O was responsible for formation of the liquid phase, and $KTiNbO_5$ and $Ba_6Ti_2Nb_8O_{30}$ secondary phases. Figure 2.16 also illustrates the d_{33}, k_p, $\varepsilon^T_3/\varepsilon_0$ and grain size of the specimens muffled with 0.95NKN-0.05BT powders during sintering. The piezoelectric constant (d_{33}) and planar electromechanical coupling coefficient (k_p) values were increased significantly when compared to the non-muffling specimens, due to the enhanced poling efficiency resulting from increased resistivity of the specimens. Specimens sintered at 1,060°C for 2 h showed improved piezoelectric properties of d_{33} = 225 pC/N, k_p = 0.36 and $\varepsilon^T_3/\varepsilon_0$ = 1058.

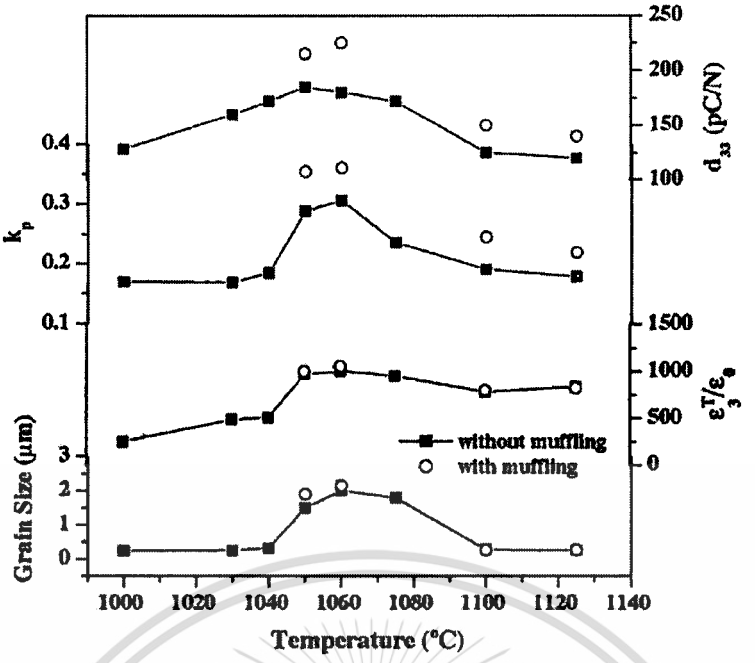

Figure 2.16 Values for d_{33}, k_p, $\varepsilon^T_3/\varepsilon_0$ and grain size of 0.95NKN-0.05BT ceramics sintered at various temperatures [59].

The $(Bi_{0.5}Na_{0.5})TiO_3$ (BNT) is considered to be a good candidate for lead-free piezoelectric ceramic, owing to its strong ferroelectricity at room temperature. However, BNT ceramics have two disadvantages: higher coercive field and lower phase transition temperature, which is called the depolarization temperature (from the ferroelectric to antiferroelectric phase). To decrease the coercive field and improve the piezoelectric properties of BNT ceramics, new solid solutions were formed. It is well known that the morphotropic phase boundary (MPB) plays a very important role in PZT ceramics because piezoelectric and dielectric properties are at maximum around the MPB that separates rhombohedral, tetragonal and/or monoclinic ferroelectric phases. BNT and KNN are a rhombohedral and orthorhombic ferroelectric, respectively, at room temperature. Therefore, H. Du *et al.* [60] reported reasonable anticipation that $(1\text{-}x)(K_{0.5}Na_{0.5})NbO_3\text{-}x(Bi_{0.5}Na_{0.5})TiO_3$ [$(1\text{-}x)$KNN-xBNT] solid solution possessed an MPB, owing to its different phase structures at room temperature; namely, $(1\text{-}x)$KNN-xBNT solid solution, which might possess high piezoelectric properties, due to MPB formation. The sintering temperature of $(1\text{-}x)$KNN-xBNT ($x > 0.02$) ceramics was found to be higher than its limit of 1,140°C, indicating that the addition of BNT improved phase stability of the KNN system. The

densities of (1-x)KNN-xBNT ceramics increased with increasing BNT, due to the increase of densification. Figure 2.17 illustrates SEM micrographs of the thermally etched surface of (1-x)KNN-xBNT samples, sintered at the optimum sintering temperature. It can be seen from Figures 2.17 (a)-(f) that the microstructure of (1-x)KNN-xBNT ceramics become increasingly homogeneous and uniform with increasing addition of BNT. The dielectric loss of the ceramics was found to decrease with increasing addition of BNT; low dielectric loss may be due to improvement of the bulk density. Furthermore, 0.94KNN-0.06BNT ceramics, possessed stable and lower dielectric loss (2%) at 10 kHz and high temperature (100-450°C), which was very important for high-temperature application of ceramics.

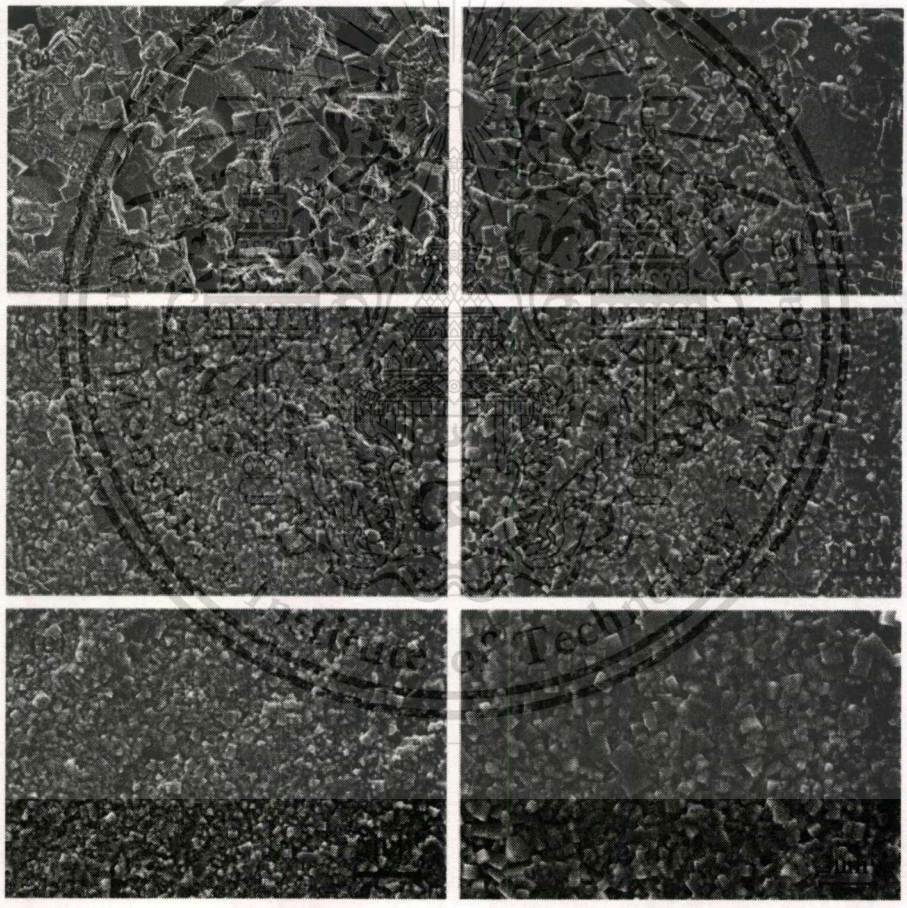

Figure 2.17 Micrographs from scanning electron microscopy of the thermally etched surface of (1-x)KNN-xBNT samples sintered at the optimum sintering temperature. (a) x = 50.01, (b) x = 50.02, (c) x = 50.03, (d) x = 50.04, (e) x = 50.05, and (f) x = 50.06 [60].

Silver niobate ($AgNbO_3$, AN) has attracted renewed interest, due to it being an antiferroelectric at room temperature and possessing extremely large polarization (52 $\mu C/m^2$) and electromechanical response, with a high T_C of 360°C. C. Xu *et al.* [61] fabricated a new lead-free solid solution $(1-x)(K_{0.5}Na_{0.5})NbO_3$-$xAgNbO_3$ (KNN-AN) using an ordinary ceramic technique. When considering the XRD patterns, ceramics possess a pure perovskite structure with orthorhombic symmetry (similar to a pure KNN) at $x \leq 0.20$. With the addition of Ag^+, the sintering temperature of the ceramics increases slightly and the grains become smaller and more uniform. Plots of variations between the remnant polarization (P_r) and coercive field (E_c), with x showing a P-E loop of ceramics with low Ag^+ concentration ($x = 0.16$), are well-saturated and square-like. With the increment of x, the P-E loop becomes flattened and slanted. It was shown that the ferroelectric properties of ceramics became weaker after addition of excess Ag^+. The ferroelectricity of the ceramics became weak at a high Ag^+ concentration. The ceramic with x = 0.10 possessed optimum electrical properties: d_{33}, = 135 pC/N, $k_p = 0.43$, $k_t = 0.46$, $\varepsilon_r = 470$, tan δ = 3.39%, and T_C = 394°C. C. L. Lei *et al.* [62] prepared (KNN-AN, with x = 0.00-0.36) in the form of ceramics by solid state reaction under an O_2 atmosphere. The crystal chemical study showed that Ag^+ ion diffused into KNN lattices formed a solid solution of perovskite structure with x up to 0.30. The substitution of Ag^+ ion for $(K_{0.5}Na_{0.5})^+$ ion resulted in a linear decrease in ferroelectric Curie temperature (T_C) from 420°C in KNN to 325°C in 0.70KNN-0.30AN, and the tetragonal to orthorhombic phase transition temperature (T_{T-O}) fell from 190°C to 150°C. The relative density of the KNN-AN ceramics reached 94% theoretically. The optimum piezoelectric properties were found in 0.82KNN-0.18AN ceramics, with a piezocoefficient d_{33} = 186 pC/N, an electromechanical coupling factor k_p = 42.5%, and a T_C = 355°C. For ceramics with x = 0.24, the remnant polarization reached a maximum value of P_r = 20 $\mu C/cm^2$, with a reduced coercive field of E_c = 6.4 kV/cm and T_C =340°C.

On the other hand, addition of a low melting point compound, which is also called "sintering aid", is expected to improve the sinterability of KNN-based ceramics without reducing piezoelectric properties. It was considered that sintering aids, which could be melted at low temperature, could form a liquid phase and promote the sintering process of the system. In 2004, M. Matsubara *et al.* reported that dense (K, Na)NbO_3 (KNN)-based ceramics were developed by optimization of sintering conditions with newly developed $K_4CuNb_8O_{23}$ (KCN) as a sintering aid [63]. The sinterability and electrical properties of KNN ceramics were investigated as a function

of KCN concentration. The density of KNN ceramics increased monotonically with increasing KCN contents, and reached its highest value of 4.40 g/cm^3 with the addition of 0.5 mol% KCN. This was explained by results from the liquid phase formation, which significantly promoted the densification of KNN ceramics. The Curie temperature of pure KNN ceramics was 420ºC and it decreased with increasing KCN content. KNN ceramics, with the addition of 0.5 mol% KCN, showed the planar mode electromechanical coupling factor (k_p) and mechanical quality factor (Q_m) reaching their highest value of 0.39 and 1,200, respectively. This KNN ceramic exhibited a large field-induced strain of 0.09% at 40 kV/cm and a piezoelectric constant d_{33} of 180 pm/V. Among several sintering aids, CuO was reported to be the most often-used. Those researchers reported that the addition of CuO greatly enhanced the sinterability of (K, Na)NbO_3 and (K, Na)(Nb, Ta)O_3. The density of $(K_{0.5}Na_{0.5})NbO_3$ ceramic was improved by up to 90% when adding 0.40 mol% of CuO. However, this research group also reported the effect of $K_4CuNb_8O_{23}$ (KCN) on the sinterability of those ceramics. At the stoichiometric composition of $(K_{0.5}Na_{0.5})NbO_3$, the addition of 0.2 mol% of CuO was not effective for densification, and the product revealed deliquescent properties. Conversely, KNN densified with 0.2 mol% of $K_4CuNb_8O_{23}$ (KCN), was found to yield compact density without deliquescence. The density of KNN ceramics increased with increasing KCN up to 0.5 mol% [64]. Incidentally, R. Zuo *et al.* [65] paid attention to the effect of oxide compounds as sintering aids for the sinterability and electrical performance of KNN ceramics. The addition of 1 mol% dopant, such as Zn, Cd, Sn, Sc, W, Ce and Y (in oxide form) was studied. Various kinds of oxide sintering additives have been used to improve the sintering of KNN. The effect of these oxides on densification is displayed in Figure 2.18. After sintering for 4 h, the densification was improved by adding 1 mol% oxides, such as ZnO, CdO, Sc_2O_3, and SnO_2; however, the addition of oxides, like CeO_2, Y_2O_3, and WO_3, severely inhibited sintering, as clearly seen from the curves. The addition of ZnO and SnO_2 was found to cause the most pronounced improvement. A high density of up to 97.5% TD can be achieved at 1,100ºC by using 1 mol% ZnO as a sintering aid. The following dielectric and piezoelectric properties were obtained: relative permittivity $\varepsilon^T_3/\varepsilon_0$ = 570-650, planar mode electromechanical coupling factor, k_p = 32%-44%, and piezoelectric strain constant, d_{33} = 92-117 pC/N.

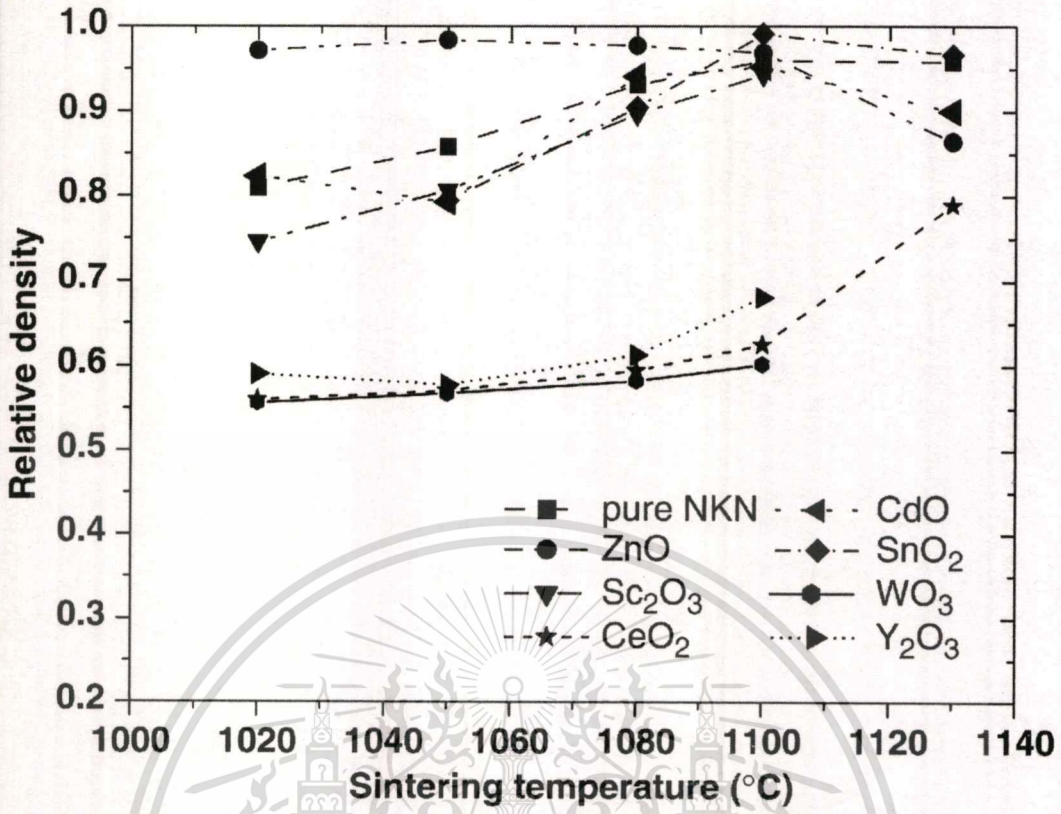

Figure 2.18 Effect of 1 mol% oxide sintering additives on densification of $K_{0.5}Na_{0.5}NbO_3$ ceramics [65].

Sodium oxide (Na_2O) is another sintering aid that has been studied. M.S. Kim *et al.* [66] developed Na_2O excess in $95(Na_{0.5}K_{0.5})NbO_3$-$5LiTaO_3$ (NKN-5LT) ceramics by the conventional sintering process. The effect of Na_2O additions on the microstructures and piezoelectric properties of NKN–5LT ceramics was investigated. It was reported that the sintering temperature was lowered by adding Na_2O. Figure 2.19 shows microstructures of the samples sintered at different temperatures for 4 h in air. Higher density of NKN-5LT ceramics was achieved by adding Na_2O and increasing heat-treatment temperature, as shown. In the 1 mol% Na_2O excess in NKN-5LT samples sintered at 1,050ºC for 4 h in air, the electromechanical coupling factor and piezoelectric constant of NKN–5LT ceramics were found to reach their highest value of 0.43 and 230 pC/N, respectively. Additionally, J. Hao *et al.* reported that addition of a small amount of MnO_2 promotes sintering KNN-based ceramics resulting in a significant improvement in densification [67]. The effect of a little MnO_2 (0.0-1.2 mol%) doping on the phase transition behavior, microstructure and electrical properties of $(K_{0.5}Na_{0.5})_{0.94}Li_{0.06}NbO_3$ (94KNN-6LN) ceramics has been investigated, and it was clearly found that the grains became distinctly smaller and more

uniform with increasing content of MnO_2. Introducing a small amount of MnO_2 could act as a grain growth inhibitor, thus resulting in grain size reduction. It could be noted that the addition of MnO_2 can improve the densification of 94KNN-6LN ceramics effectively. The mechanical quality factor, Q_m, of 94KNN-6LN ceramics was enhanced significantly, due to high densification. The Q_m in 1.2 mol% MnO_2-94KNN-6LN ceramics reached 301, which was four times more than the increase in 94KNN-6LN. The piezoelectric constant, d_{33}, and the planar electromechanical coefficient, k_p, still maintained relatively high values, which were about 141 pC/N and 32.0%, respectively.

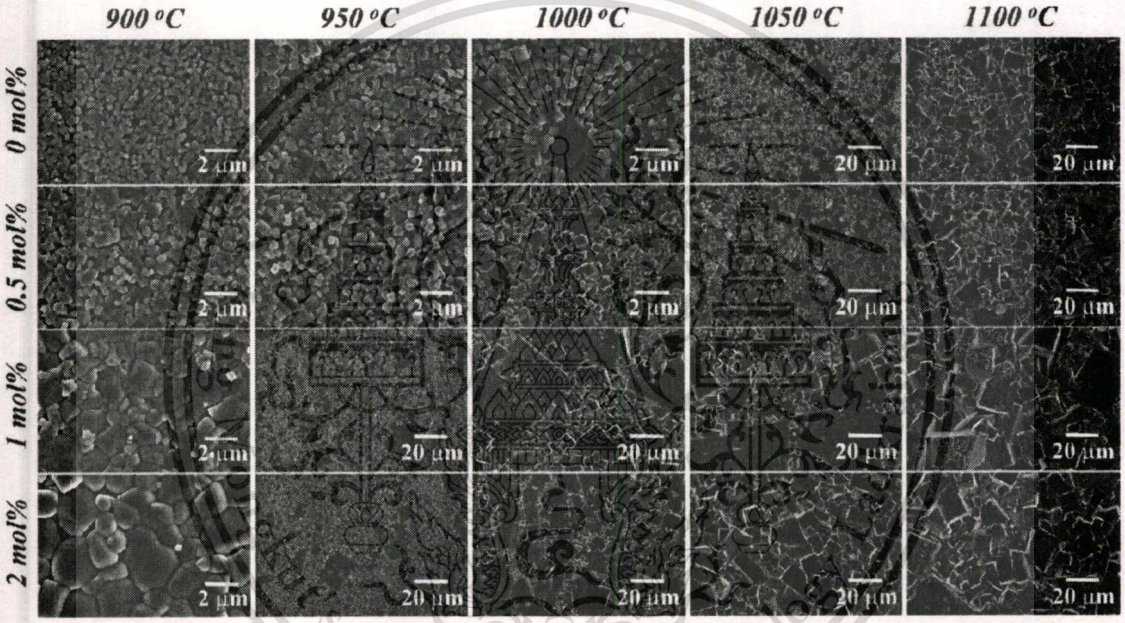

Figure 2.19 Microstructures of Na_2O excess in NKN-5LT samples sintered for 4 h in air at 900, 950, 1,000, 1,050 and 1,100°C, as a function of Na_2O content [66].

2.4 Solid state reaction method

In most interesting processes in ceramic technology, the solid state reaction method is the traditional and conventional one for producing oxide ceramics. It has been developed and modified in both scientific research and industrial mass production over many years and is probably one of the most fundamental and practical routine methods being used. In this solid state reaction method, the stoichiometric constituent of oxides and carbonate starting materials are mixed and then calcined in an air or oxygen atmosphere at a high temperature for an appropriate duration. Intermediate grinding is required to obtain phase-pure and homogeneous products. This method is found to be relatively simple, time-consuming and energy intensive and several advanced materials have been prepared with it. For the preparation of lead zirconate titanate (PZT) [68], powders of PbO, ZrO_2 and TiO_2 were used as raw materials, which were ball-milled in a polyethylene pot containing zirconia balls and ethanol. Dried mixtures were then calcined and ball-milled again before the production of PZT powders. Figure 2.20 shows the polished and chemically etched surfaces of sintered PZT ceramics using calcined powder produced by the solid state reaction method. In general, alkali niobate ceramics are synthesized by this conventional solid state reaction, where alkali metal carbonate or oxide compound of starting materials are used. For preparing potassium sodium niobate ($K_{1-x}Na_xNbO_3$) powders, K_2CO_3, Na_2CO_3 and Nb_2O_5 were used as raw materials [40, 47-50, 69]. The calcination temperatures were found to be in the range of 750°C to 950°C for 4 to 9 h. Figure 2.21 and 2.22 illustrate the X-ray pattern of calcined powders and SEM image of the fractured surface of a sinter KNN sample prepared by the solid state reaction method.

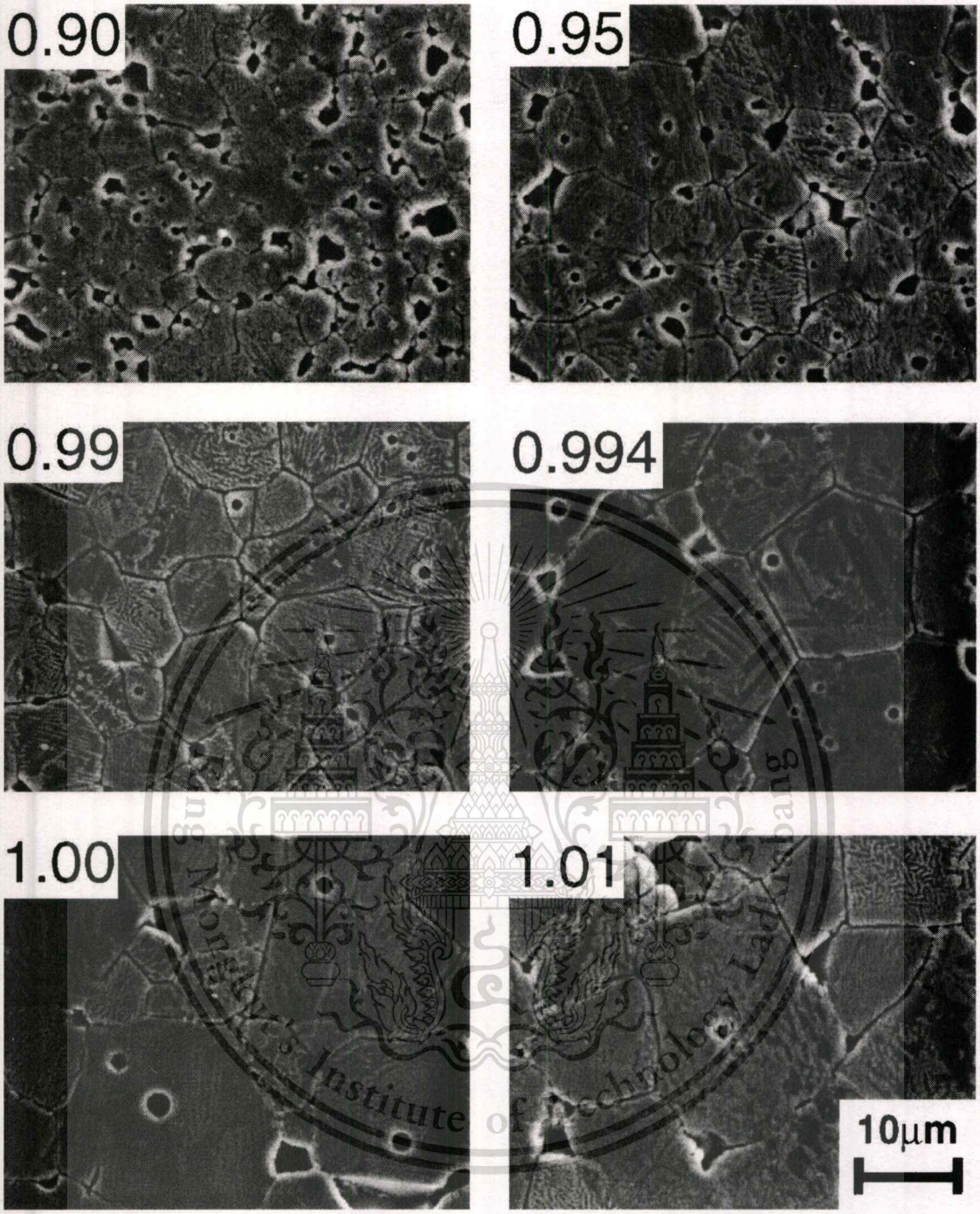

Figure 2.20 Polished and chemically etched surfaces of PZT ceramics sintered at 1,200°C for 2 h , as a function of the molar ratio of Pb/(Zr+Ti), observed by SEM [68].

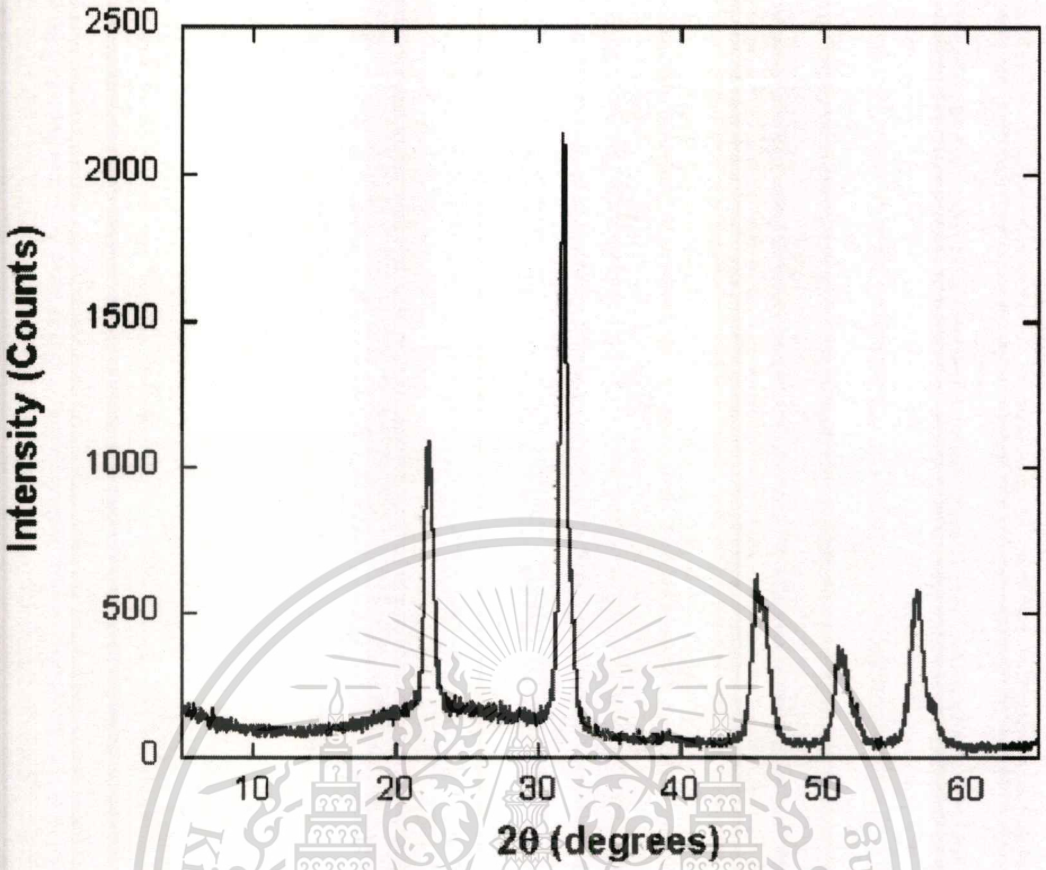

Figure 2.21 X-ray pattern of calcined powder [40].

Figure 2.22 Fractured surface of a sintered KNN sample [40].

2.5 Combustion synthesis

In general, alkali niobate powders are synthesized by conventional solid state reaction, where carbonate or oxide compound of starting materials is ground repeatedly and heated at high temperature (800°C or above) for a long duration to achieve the desired phase. The contamination from grinding is presented usually. Powder agglomeration can occur during heating, which could affect powder properties such as low surface area and low sinterability. High calcination and sintering temperature can cause deviation in the composition, due to volatilization of alkali metal. It is difficult to determine the appropriate conditions for reproducible preparation, due to this method sometimes allowing production of dense, homogeneous and single phase ceramics.

Combustion synthesis (CS) or self-propagating high temperature synthesis (SHS) is reported as a simple, rapid, effective, cheap and energetically economic method that yields high purity products for a range of industrially useful materials. This process is provided, based on the fundamentals of highly exothermic rodox chemical reaction, in which oxidation and reduced reaction take place simultaneously between easily oxidized reactants and reducing reagent. The energy released from the combustion reaction is high enough to heat the system and sustain it sufficiently to drive the occurring synthesis without an external source. Figure 2.23 demonstrates a schematic representation of the temperature-time curve during an exothermal redox reaction. The exothermic reaction is initiated at the ignition temperature (T_{ig}), and when the heat generated is apparent in a maximum or combustion temperature (T_c), it can volatilize low boiling point impurities that therefore result in purer products than those produced by more conventional techniques. After a self-sustaining and rather fast combustion reaction has taken place, a dry, fine and usually crystalline powder is obtained. Rapid evolution of gases produced in a large volume during chemical reaction can give this method capability of producing nano-size powder. Combustion synthesis (CS) has been used successfully in the preparation of a large number of technologically useful oxide (refractory oxides, magnetic, dielectric, semiconducting, insulator, catalysts, sensors, phosphors, etc.) and nonoxide (carbides, borides, silicides, nitrides, etc.) materials. This method was used in Russian commercial manufacturing. Some of these CS-produced materials from 1994 are listed in Table 2.1, and their applications can be classified as follows:

1. Abrasives, cutting tools and polishing powders, e.g. TIC, cemented carbides.

2. Resistive heating elements, e.g. $MoSi_2$.

3. Shape memory alloys (SMA), e.g. TiNi.

4. High temperature intermetallic compounds, e.g. nickel aluminides.

5. Steel processing additives, e.g. nitrided ferroalloys.

6. Electrodes for electrolysis of corrosive media, e.g. TIN, TiB_2.

7. Coatings for containment of liquid metals and corrosive media, e.g. products of aluminum and iron oxide thermite reactions.

8. Powders for further ceramic processing, e.g. Si_3N_4.

9. Thin films and coatings, e.g. $MoSi_2$, TiB_2.

10. Functionally-graded materials (FGM), e.g. TiC + Ni.

11. Composite materials, e.g. TiC + A_2O_3, TiC + Al_2O_3 + Al.

12. Materials with specific magnetic, electrical or physical properties, e.g. $BaTiO_3$, $YBa_2Cu_3O_{7-x}$.

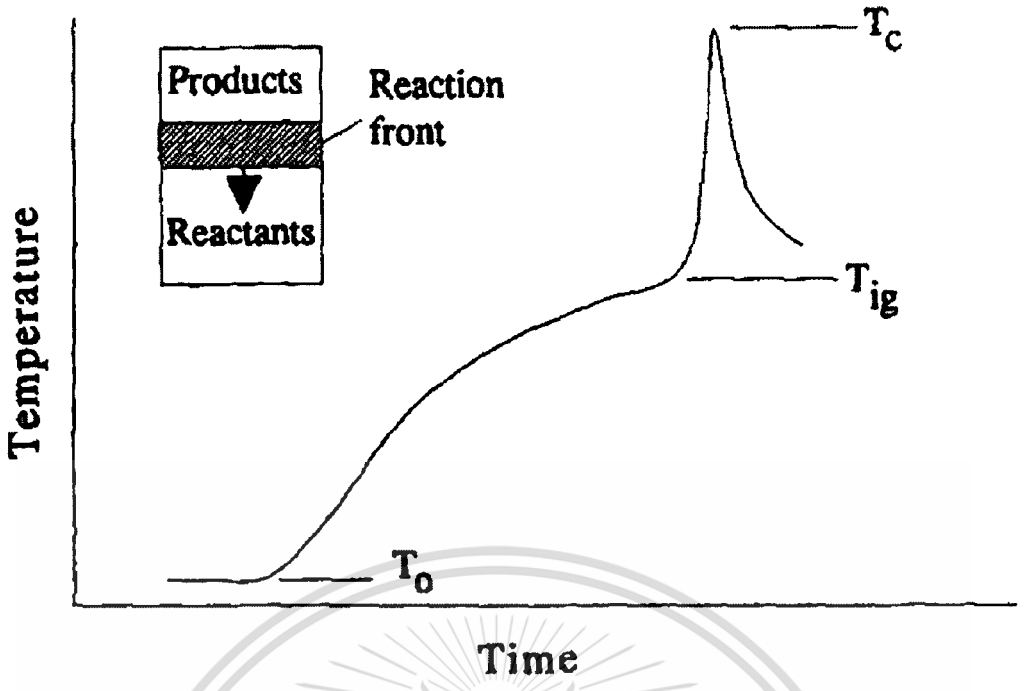

Figure 2.23 Schematic of the temperature-time curve during an exothermal reaction [70].

Table 2.1 Some materials produced by the combustion process [70].

Borides	CrB, HfB_2, NbB, NbB_2, TaB_2, TiB, TiB_2, LaB_6, MOB, MOB_2, MoB+Mo_2B, WB, W_2B_5, WB_4, ZrB_2, VB, V_3B_2, VB_2
Carbides	TiC, ZrC, HfC, NbC, SiC, Cr_3C_2, B_4C, WC, TaC, Ta_2C, VC, Al_4C, Mo_2C
Nitrides	Mg_3N_2, BN, AIN, SiN, Si_3N_4, TiN, ZrN, HfN, VN, NbN, Ta_2N, TaN (hexagonal and cubic)
Silicides	$TiSi_3$, Ti_5Si_3, ZrSi, Zr_5Si_3, $MoSi_2$, $TaSi_2$, Nb_5Si_3, $NbSi_2$, WSi_2, V_5Si_3,
Aluminides	NiAl, CoAl, $NbAl_3$
Hydrides	TiH_2, ZrH_2, NbH_2, CsH_2, PrH_2, IH_2
lntermetallics	NiAl, FeAl, NbGe, $NbGe_2$. TiNi, CoTi, CuAl
Carbonitrides	TiC-TiN, NbC-NbN, TdC-FeN, ZrC-ZrN
Cemented carbides	TiC-Ni, TiC-(Ni, MO), WC-Co, Cr_3C_2-(Ni, MO
Binary compounds	TiB_2-MoB_2, TiB_2-CrB_2, ZrB_2-CrB_2, TiC-WC, TiN-ZrN, MoS_2-NbS_2, WS_2-NbS_2
Chalcogenides	MgS, $NbSe_2$, $TaSe_2$, MoS_2, $MoSe_2$, WS_2, WSe_2
Composites	TiB_2-Al_2O_3, TiC-Al_2O_3, B_4C-Al_2O_3, TiN-Al_2O_3, TiC-TiB_2, $MoSi_2$-Al_2O_3, MoB-Al_2O_3, Cr_2O_3-Al_2O_3, 6VN-5Al_2O_3, ZrO_2-Al_2O_3-2Nb

When compared with conventional ceramic processing, the most obvious advantages of combustion synthesis are primarily: (1) generation of a high reaction temperature that can volatilize low boiling point impurities and, therefore, result in higher purity products; (2) simple exothermic nature of the reaction, which avoids the need for expensive processing facilities and equipment; (3) short exothermic reaction time that results in low operating and processing costs; (4) high thermal gradients and rapid cooling rates that can give rise to new non-equilibrium or metastable phases; (5) inorganic materials that, in one step, can be synthesized and consolidated into a final product by utilizing the chemical energy of the reactants; and (6) formation of virtually any size and shape of products. These advantages have fascinated researchers enough to become more active in investigating the combustion synthesis of new and improved materials, with specialized mechanical, electrical, optical and chemical properties.

From the historical perspective, Berzelius [71-72] found, as early as 1825, that zirconium oxide could be made by heating amorphous zirconium metal below redness, and the reaction could be ignited even below room temperature. This is probably the literature's earliest record on using combustion synthesis of a ceramic refractory material. At the end of the nineteenth century, and beginning of the twentieth, various nitrides of transition and rare-earth metals were prepared by this combustion synthesis. A more recent research, conducted on the combustion synthesis of advanced materials, began in 1967, guided by the Russian scientists, A.G. Merzhanov *et al.* [73], who created the term 'self-propagating high temperature synthesis' (SHS). This research group started a systematic investigation of combustion synthesis reactions. The potential of such a simple process was realized and the group began to investigate the synthesis of other high value and advanced ceramic materials. The synthesis of a large number of ceramics, composites and intermetallics, including carbides, borides, nitrides, beryllides, phosphides and rare-earth metal compounds was examined. Since the early 1980s, an increasing number of researchers, predominantly in Russia, the U.S.A. and Japan, have been investigating the application of combustion synthesis as an efficient and economical technique for the production of advanced materials and compounds.

2.5.1 The combustion synthesis using redox compounds and mixtures.

The preparation of fine particle oxide materials by the combustion of redox compounds is simple and attractive. Compounds that contain both oxidizing and reducing groups are applied as starting material. These redox compounds can be ignited properly and decomposed autocatalytically to yield voluminous products. K.C. Patil *et al.* [74] reported that $(NH_4)_2Cr_2O_7$, which contains both oxidizing ($Cr_2O_7^{2-}$) and reducing (NH_4^+) groups, can be ignited (using $KClO_3$-sucrose-H_2SO_4) and decomposed, resulting in voluminous green Cr_2O_3 (artificial volcano).

$$((NH_4)_2Cr_2O_{7(s)} \xrightarrow{\Delta} Cr_2O_3 + 2N_{2(g)} + 4H_2O_{(g)} \quad (2.1)$$

The exothermicity of the combustion reaction was explained, due to the oxidation of ammonium ion (NH_4^+) to N_2 and H_2O by the dichromate ion ($Cr_2O_7^{2-}$), which reduced itself to Cr^{3+}. The combustion was found to be a smoldering type (flameless) accompanied by evolution of gases, resulting in fine and voluminous Cr_2O_3 powder.

A new class of precursor containing a carboxylate anion, hydrazide, hydrazine or hydrazinium group, which can be ignited at low temperature (120-350°C) and decomposed autocatalytically to a yield fine particle and large surface area oxides, was then found accidentally. The high exothermicity (around 700°C) of combustion reaction was attributed to the oxidation of strong reducing agents such as COO^-, $N_2H_3^-$, N_2H_4 or $N_2H_5^+$ (present in the precursors) by atmospheric oxygen to CO_2, H_2O and N_2. K. C. Patil *et al.* reported the preparation, crystal structure and reactivity of various combustible precursors [75]. Table 2.2 gives a list of these compounds and the oxides formed through this combustion synthesis. The iron containing complexes, $Fe(N_2H_3COO)_2(N_2H_4)_2$ and $N_2H_5Fe(N_2H_3COO)_2 \cdot H_2O$, and their solid solutions were reported to be ignited at ~120°C (they can be ignited easily with a matchstick or candle flame) and combusted in the presence of atmospheric oxygen to yield nanosize Fe_2O_3 and ferrites. The smoldering-type combustion and evolution of large amounts of gaseous products (CO_2, H_2O, NH_3 etc.) resulted in the formation of fine oxide powder products. The surface area of these iron oxides ranged from 70 to 140 m^2g^{-1}. All the ferrites that were then pelletized and sintered at 1,000°C achieved a high density of ~98% theoretical density. Other nanosize oxides obtained by the combustible precursors were CeO_2, TiO_2 and Y_2O_3. Besides magnetic oxides, a few ferroelectric titanates also have been prepared by this process, i.e. $PbTiO_3$, $PbZrO_3$ and PZT. Although the preparation of fine particle oxide materials by the combustion of redox compounds

is simple and attractive, it has certain limitations. Firstly, preparation of the precursors requires a period as long as several days. Secondly, the yield is as low as 20% of the precursor. Finally, some of the metals cannot form complexes with the hydrazine carboxylate ligand and it is therefore impossible to use this method for preparing high-temperature oxides.

However, an alternative method found to avoid the redox compound limitation is using redox mixtures of the oxidizer and fuel similar to gun powder (which contains KNO_3+C+S) or solid propellant (which contains NH_4ClO_4+CTPB+Al). These redox mixtures can be ignited and undergo self-propagating combustion. The combustion synthesis using redox mixtures, which have been described and investigated widely, can be identified in two categories; (1) solid state combustion (SSC) and (2) solution combustion (SC).

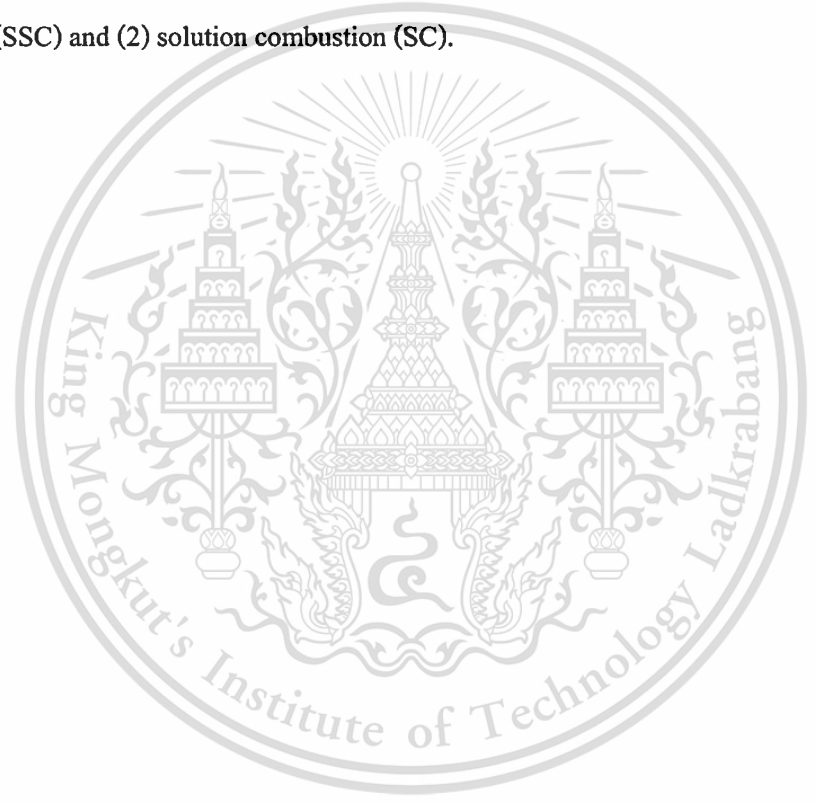

Table 2.2 List of metal carboxylate compounds and oxides formed by the CS method [75].

Metal carboxylate precursors to fine particle oxides			
Precursors	Oxides	Surface area (m^2/g)	Particle size (nm)
$Fe(N_2H_3COO)_2 \cdot (N_2H_4)_2$	γ-Fe_2O_3	68	17-23
$Zn(N_2H_3COO)_2 \cdot (N_2H_4)_2$	ZnO	67	
$Ce(N_2H_3COO)_2 \cdot 3H_2O$	CeO_2	90	
$Y(N_2H_3COO)_3 \cdot 3H_2O$	Y_2O_3	55	
$N_2H_5Fe(N_2H_3COO)_3 \cdot H_2O$	γ-Fe_2O_3	75	
$N_2H_5M_{1/3}Fe_{2/3}(N_2H_3COO) \cdot 3H_2O$			
M = Mg	$MgFe_2O_4$	114	10-25
M = Mn	$MnFe_2O_4$	140	
M = Co	$CoFe_2O_4$	116	
M = Zn	$ZnFe_2O_4$	108	
M = Cd	$CdFe_2O_4$	93	
$(N_2H_5)_3Ni_xZn_{1-x}Fe_2(N_2H_3COO)_9 \cdot 3H_2O$			
x = 0.2	$Ni_{0.2}Zn_{0.8}Fe_2O_4$	91	10-20
x = 0.4	$Ni_{0.4}Zn_{0.6}Fe_2O_4$	86	
x = 0.5	$Ni_{0.5}Zn_{0.5}Fe_2O_4$	90	
x = 0.6	$Ni_{0.6}Zn_{0.4}Fe_2O_4$	85	
x = 0.8	$Ni_{0.8}Zn_{0.2}Fe_2O_4$	91	
$N_2H_5M_{1/3}Co_{2/3}(N_2H_3COO)_3 \cdot H_2O$			
M = Mg	$MgCo_2O_4$	47	20
M = Mn	$MnCo_2O_4$	24	
M = Co	$FeCo_2O_4$	116	
M = Zn	$ZnCo_2O_4$	65	
$Mg_{1/3}Mn_{2/3}(N_2H_3COO)_2 \cdot 2H_2O$	$MgMg_2O_4$	28	
$Zn_{1/3}Mn_{2/3}(N_2H_3COO)_2 \cdot 2H_2O$	$ZnMg_2O_4$	61	
$N_2H_5Co_{1/3}Mn_{2/3}(N_2H_3COO)_3 \cdot H_2O$	$CoMg_2O_4$	76	35
$N_2H_5Ni_{1/3}Mn_{2/3}(N_2H_3COO)_3 \cdot H_2O$	$NiMg_2O_4$	20	
$TiO(N_2H_3COO)_2 \cdot 2H_2O$	TiO_2	114	20
$ZrTiO(OH)_2(N_2H_3COO)_4 \cdot 3H_2O$	$ZrTiO_4$	11	
$PbTiO(OH)_2(N_2H_3COO)_2 \cdot H_2O$	$PbTiO_3$	23	
$PbZrO(OH)_2(N_2H_3COO)_2 \cdot 4H_2O$	$PbZrO_3$	13	
$Pb(Zr_{0.53}Ti_{0.47})O(OH)_2(N_2H_3COO)_2 \cdot 4H_2O$	PZT	44	
$Pb_{0.92}La_{0.8}(Zr_{0.65}Ti_{0.35})O(OH)_2(N_2H_3COO)_2 \cdot 4H_2O$	PLZT	30	

2.5.2 Solid state combustion (SSC) [76-79]

In solid state combustion (SSC), initial reactants, intermediates and final products are all in the solid state. In this synthesis, the reactants are pressed into a pellet, which typically is cylindrical in shape, and then ignited by an exothermal source (e.g. tungsten coil, laser or microwave) from which an exothermic redox reaction can be initiated. Combustion of solid reactants can occur in two modes: (1) linear or self-propagating high temperature synthesis (SHS) and (2) bulk or volume combustion synthesis (VCS). After local initiation occurs in the SHS mode, a hot combustion wave passes through the heterogeneous mixture of reactants at 1,700-3,800°C and yields the condensed product desired. In VCS (thermal explosion) mode, the pellet is heated uniformly in a controlled manner until the reaction occurs simultaneously throughout the volume. This solid state combustion is reported to be the process used in the synthesis of a variety of advanced materials such as aluminides–AlNi (aerospace and turbine material); borides–TiB_2 (abrasives and cutting tool); carbides–SiC, TiC (abrasives and cutting tool); chalcogenides–MoS_2 (high temperature lubricant); hydrides–MgH_2 (hydrogen storage); nitrides–Si_3N_4 (ceramic engine parts); oxides–$La_{0.8}Sr_{0.2}CrO_3$ (fuel cell interconnect); phosphides–GaP (semiconductor), silicides–MoSi (high temperature heating element); and titanates–TiNi (shape memory alloy) [79]. A variety of catalysts, e.g. oxynitrides (honeycomb support for noble metals); complex cuprates, $LnMCu_{n-\delta}$, Ln = Y or La, M = Ca, Ba or Sr (ethylene synthesis); $LnCaB_6$ (oxidation of methane to ethylene); Fe–Al alloys (ammonia synthesis); modified spinel; and Fe–Cr oxides (pyrolysis of diesel fuel) have been prepared extensively by the SSC method [55-56]. Other technologically useful materials prepared by SSC are: solid oxide fuel cell materials: Sr and Ga doped LaFeO [79], $La_{0.84}Sr_{0.16}CrO_3$ [80], $La_{0.2}Sr_{0.8}Cr_{0.2}Fe_{0.8}O_{3-x}$ [81], $La_{1-x}Sr_xMnO_3$ [82]; the hydrogen storage alloy, Mg_2NiH_4 [83]; and porous NiTi (biomedical implant material) [84]. Unfortunately, it was found that using the SSC method was not easy in producing nanomaterials, due to the typical scale of heterogeneity for initial solid reactants being in the order of 10-100 μm.

2.5.3 Solution combustion (SC)

The solution combustion (SC) method of preparing oxide materials is a fairly recent development when compared to SSC or SHS techniques. Since J.J. Kingsley *et al.* [85] reported the serendipitous preparation of α-Al_2O_3 foam in 1988, by rapidly heating a solution of aluminium nitrate-urea mixture, a number of advanced materials have been prepared by this solution combustion process. Therefore, the SC method has been considered as a process that can prepare nanomaterial and be scaled up. Up until now, SC has been used all over the world for preparing oxide materials for a variety of applications. A wide range of technologically useful oxides (alumina to zirconia) have been prepared with interesting magnetic, dielectric, electrical, mechanical, catalytic, luminescent and optical properties. Base on the SC method, oxide compound can be prepared by rapidly heating aqueous solutions containing stoichiometric amounts of respective metal nitrate (oxidizer) and fuels (reducer). Several organic compounds have been applied as fuel such as urea, carbohydrazide, oxalyl dihydrazide, malonic acid, tartanic acid, citric acid, glycine, alanine, triethanoamine, hexamethyltetramine (HMT), etc. A saturated aqueous solution of the desired metal salts and suitable organic fuel is boiled until the mixture ignites and a self-sustaining and rather fast combustion reaction takes place, resulting in a dry, fine and usually crystalline oxide powder. Various fuels differ in reducing power and the amount of gas they generate, and all of them serve two purposes:

(1) A source of C and H, which on combustion, forms CO_2 and H_2O and liberates heat.

(2) To form complexes with metal ions facilitating homogeneous mixing of the cations in solution.

While redox reactions such as this are exothermic in nature and often lead to explosion if not controlled, the combustion of metal nitrates-urea mixtures usually occurs as a self-propagating and non-explosive exothermic reaction. The large amounts of gases formed can result in appearance of a flame, which may reach temperatures in excess of 1,000°C. In addition, metal nitrates are salts preferred for this solution combustion method, due to their water solubility (with good achievable homogenization in the solution) and the few hundred degrees needed to melt them. Hydrate salts are even more favored in this respect, as the water molecules do not affect the total valencies of the nitrate and are, therefore, irrelevant for the chemistry of the combustion.

By simple calcination, the metal nitrates can, of course, be decomposed into metal oxides when heating to or above the phase transformation temperature. A constant external heat supply is necessary. In this case, maintenance of the system at high temperature is required to accomplish the appropriate phase transformation. In the combustion synthesis, the energy released from the exothermic reaction between the metal nitrates and fuel usually ignites at a temperature much lower than that in the actual phase transformation, and can heat the system rapidly to a high temperature and sustain it long enough for the synthesis to occur, even in the absence of an external heat source. The basis of the combustion synthesis technique comes from the thermochemical concepts used in propellant chemistry [86]. The constitution of a fuel-oxidizer mixture is important in the field of propellants and explosives for various reasons, and the parameter used to express it must clearly indicate the closeness to the stoichiometry of the mixture, i.e., whether it is fuel-lean or fuel-rich stoichiometric. Jain *et al.* [86] introduced a simple method of calculating the oxidizing to reducing character of the mixture, irrespective of whether the elements are present in the oxidizer or fuel components of the mixture. Those authors also showed that, for a stoichiometric mixture, the magnitude of total composition of oxidizing and reducing elements is related closely to the heat of reaction (or difference summed up proportionately in bond energies of the products and reactants), and calculated thermodynamically from the formation temperatures of reactants and products. According to propellant chemistry, the usual products of the combustion reaction are CO_2, H_2O, and N_2. Therefore, the elements C and H are considered as reducing elements with the corresponding valencies of +4 and +1, oxygen is considered an oxidizing element with the valency of -2, and nitrogen is thought to have a valency of zero. The extrapolation from this concept of the combustion synthesis of ceramic oxides means that metals such as K, Na, Ca, Al, and Zr (or any

other metals) also are considered as reducing elements, with the corresponding valencies of +1, +1, +2, +3, and +4, respectively. The stoichiometric composition of the redox mixture for the combustion synthesis is calculated based on the total oxidizing and reducing valencies of the oxidizer and fuel, in order to release the maximum energy for the reaction. Additionally, in the case of multiple valence elements, the valence of the element in the product is used in the calculation. The elemental stoichiometric coefficient, ϕ, can be calculated in the following equation:

$$\phi = \mathrm{n}\frac{\text{total valaencies of fuel}}{\text{total valaencies of oxidizer}} \qquad (2.2)$$

where n is the mole of glycine. According to the propellant chemistry for stoichiometric redox reaction between fuel and an oxidizer, the ϕ ratio should be unified (stoichiometric). A $\phi < 1$ means oxidant-rich condition and $\phi > 1$ means fuel-rich condition. This ϕ ratio is referred to as a fuel-to-oxidizers ratio. It should be noted that this calculation is based on a theoretical reaction equation that neglects all secondary phenomena such as urea hydrolysis and thermal decomposition, as well as nitrate decomposition, which would alter the initial fuel-to-oxidizers ratio.

In 1996, D.A. Fumo *et al.* [21] reported the preparation of calcium aluminate cements for refraction by a straightforward combustion synthesis technique, using the corresponding metal nitrates-urea mixtures at low temperature and short reaction times. The effect of the oxidizer/fuel ratio in the redox mixture on the phase formation and characteristic of the powder produced were investigated. In this study, $Ca(NO_3)_2{\cdot}4H_2O$ and $Al(NO_3)_3{\cdot}9H_2O$ were used as cation sources, and urea $CO(NH_2)_2$ was used as fuel. The reactants were hand mixed in a wide-mouth vitreous silica basin (300 cm^3), and heated up to ~300°C on a hotplate inside a fume-cupboard under ventilation. After the thickened liquid began frothing and ignition took place, the reaction lasted for less than 1 minute, producing dry and very fragile foam. The as-prepared powders produced in the stoichiometric reactions showed that they consisted of very fine crystal agglomerates. The mixtures prepared with half the stoichiometric urea were found to fail in ignition and a wet gel remained after the water was drained. An X-ray diffraction pattern was obtained upon drying, and the only crystalline phases detected were the unhydrated metal nitrates. Calcination at 600°C resulted in a dried powder and successful nitrate decomposition, but the temperature was not enough to promote crystallization of the desired phase. Only when the calcination temperature

was increased to 900°C, could a sign of the crystalline aluminate be detected in the X-ray diffraction pattern. Although the combustion synthesis of fuel-lean mixtures was unsuccessful, the experiment validated the assumptions made in the theoretical calculation of the maximum temperature reached in the stoichiometric reaction. On the other hand, all fuel-rich mixtures were found to ignite easily. The high temperature was sustained longer and the combustion resulted in crystalline as-prepared powders. Calcination steps at higher temperatures only promoted the degree of crystallinity and grain growth.

In 1998, A.M. Segadães *et al.* [87] reported a combustion synthesis of aluminium titanate (Al_2TiO_5), using metal nitrate-urea mixtures at low temperature and short reaction times. Al_2TiO_5 was synthesized by using $Al(NO_3)_3 \cdot 9H_2O$ and liquid $Ti[O \cdot CH(CH_3)_2]_4$, as cation precursors, and urea $CO(NH_2)_2$ as fuel. NH_4NO_3 was used as a combustion aid. The appropriate amounts of reactants, with a little added water, were first melted in a wide-mouth vitreous silica basin (~200 cm^3) by rapid heating up to ~300°C on a hotplate inside a fume-cupboard under ventilation. Soon after the liquid thickened and began frothing, the basin was transferred to a muffle furnace, preheated to 500°C, where ignition took place. The reaction lasted for less than 1 minute and produced dry, white and very fragile foam, which crumbled easily into powder.

In 1999, V.C. Sousa *et al.* [88] described the combustion synthesis of zinc oxide (ZnO) and doped ZnO [e.g., ZnO-Bi_2O_3 (ZB), ZnO-Bi_2O_3-Sb_2O_3 (ZBS), ZnO-Bi_2O_3-Sb_2O_3-CoO-MnO (ZBSCM) and ZnO-Bi_2O_3-Sb_2O_3-CoO-Cr_2O_3 (ZBSCMK)] powder for varistor ceramics. $Zn(NO_3)_2 \cdot 6H_2O$, $Bi(NO_3)_3 \cdot 5H_2O$, $Co(NO_3)_2 \cdot 6H_2O$, $Mn(NO_3)_2 \cdot 5H_2O$, $Cr(NO_3)_3 \cdot 9H_2O$ were used as cation precursors and urea $CO(NH_2)_2$ as fuel for the combustion synthesis,. Firstly, the mixtures were heated up to ~300°C on a hotplate until they began to froth, then the basin was transferred to a box furnace, preheated to 500°C, where ignition took place. The powders obtained showed high specific surface areas and possessed particle sizes in the nanometer range. Figure 2.24 illustrates TEM photomicrographs of the as-prepared combustion synthesized powders, ZnO and ZBSCMK. Some particles were found to be crystallite agglomerates, according to the on-set of sintering during the fast combustion reaction.

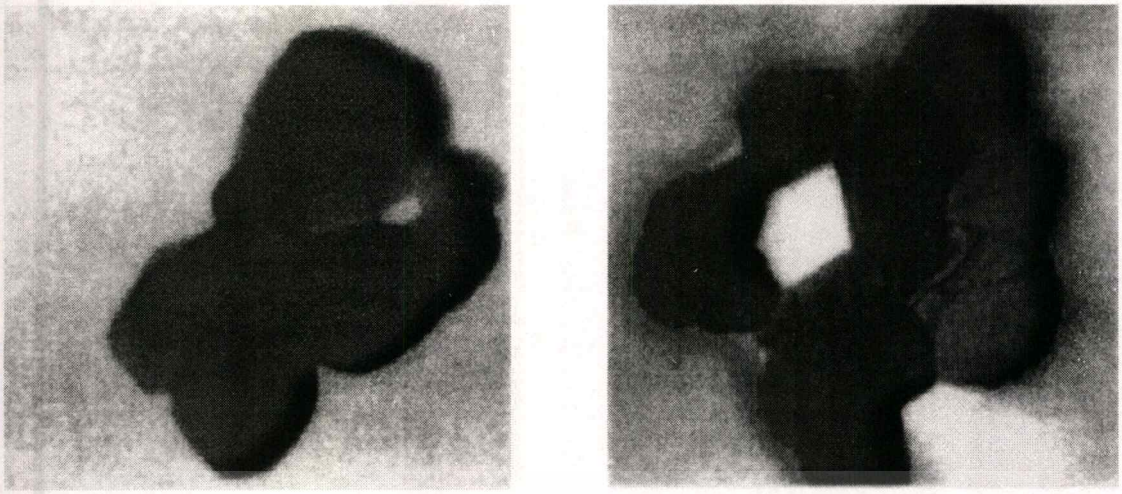

Figure 2.24 TEM micrographs showing typical morphology of as-prepared combustion synthesized powders: (a) ZnO and (b) ZBSCMK [88].

A. Civera *et al.* [89] applied combustion synthesis to produce $LaMnO_3$ perovskite-type catalysts for natural gas combustion. An aqueous solution containing metal precursors in the stoichiometric ratio was prepared from $La(NO_3)_3 \cdot 6H_2O$ and $Mg(NO_3)_2 \cdot 6H_2O$, whereas Mn metallic powder was used as a source of manganese, dissolved once with the addition of a suitable amount of HNO_3. Excess NO_3^- anions, introduced when dissolving Mn powder, were accounted for in calculation of the initial fuel-to-oxidizers ratio. Different amounts of $CO(NH_2)_2$, corresponding to various fuel-to-oxidizers ratios, were applied. After a few minutes stirring on a heating plate, to ensure proper homogeneity, the as-prepared solution was transferred to a ceramic dish, which was placed into a preheated oven and kept at a constant temperature in the range of 400-800°C. Different operating conditions affected the duration of the process as well as its intensity, and resulted in differences in the morphology of the products obtained: some had a foamy structure and crumbled easily to give a fine and volatile powder, whereas others were denser and needed proper grinding. A series of frames were extracted from a video recording of the process: the resulting images that depict the most relevant steps of the process, for the model case of alumina preparation, are shown in Figure 2.25. In this case, no visible reaction took place when employing the stoichiomatric ratio. A fuel-to-oxidizers ratio larger than 2 at an oven temperature of 600°C was found to be an optimum condition.

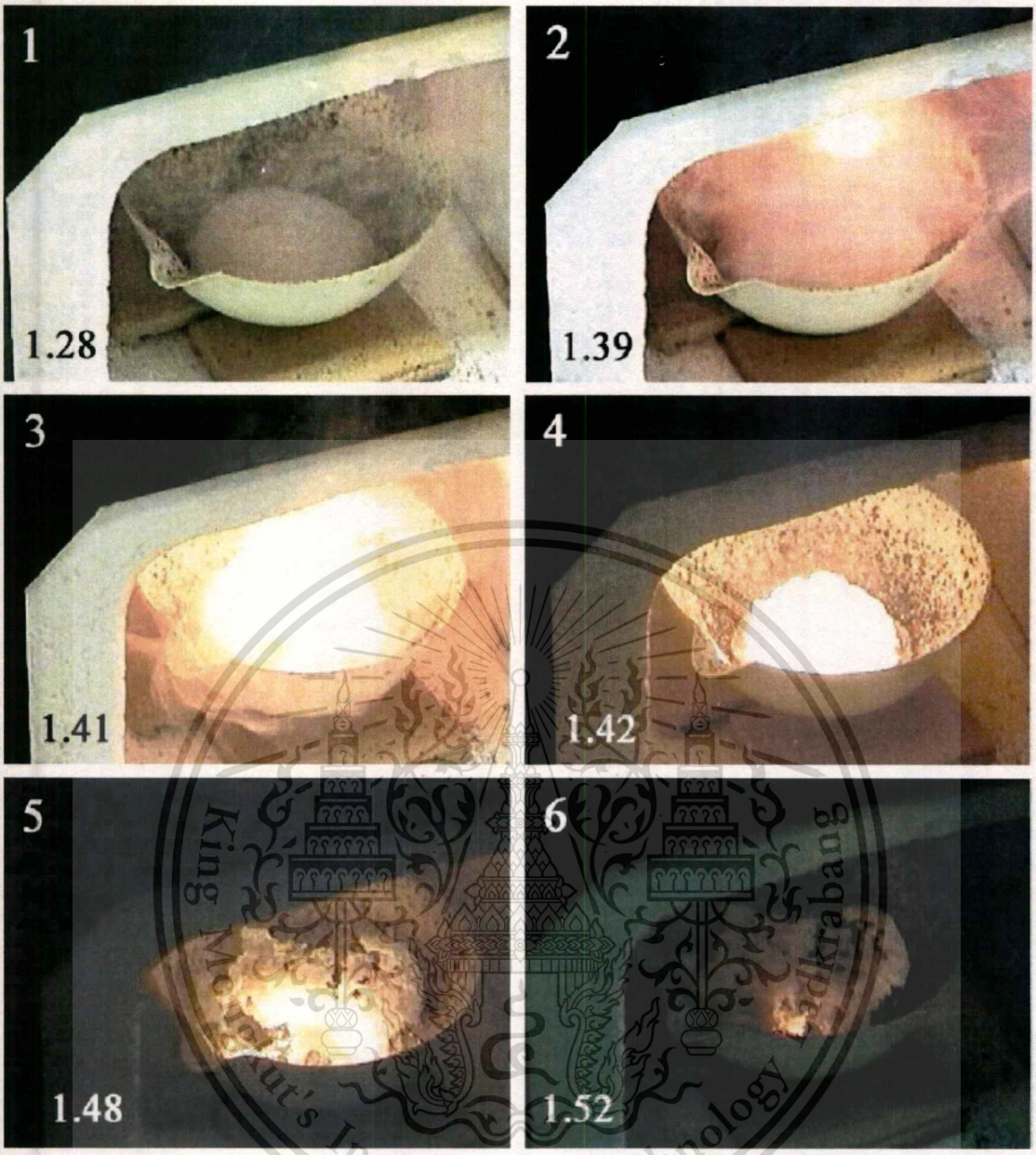

Figure 2.25 Combustion synthesis of Al_2O_3 in stoichiometric conditions at 600°C. The number in the bottom left-hand corner refers to the time that elapsed from when the dish was placed in the oven (expressed in minutes and seconds) [89].

In 2004, Z.S. Macedo *et al.* [90] performed a series of 20 experiments on powder production of the ferroelectric, $Bi_4Ti_3O_{12}$ (BIT), for exploring urea $[CO(NH_2)_2]$ and polysaccharide $[(C_6H_{10}O_5)_n]$ as fuel. An electric plate was used as a heating source to accelerate the ignition. Different experimental conditions such as annealing temperatures, stoichiometric ratios and the use of TiO_2 and $TiCl_2$ as titanium sources were investigated. The best results were achieved with a percentage weight of BIT higher than 93%. Samples un-annealed and annealed at 650ºC presented poor quality, but they resulted in powders with high BIT percentage when annealed between 800ºC and 1,000ºC for 30 min. The plate-like morphology of the BIT particles was observed in all the samples, as analyzed by SEM (Figure 1.26).

For nearly all of the previously described purposes, urea was found to be the most convenient fuel to use. It is not only commercially available and cheap, but it also generates the highest temperature, although fuel-rich mixtures might produce sintered particle agglomerates prematurely. However, glycine (NH_2CH_2COOH) was found to be an alternative fuel for the preparation of oxide powder by the combustion synthesis. Glycine is one of the cheapest amino acids known to act as a complexing agent for a number of metal ions, as it has a carboxylic acid group at one end and amino group at the other. This structure may change, thus transferring a proton from the COOH, carboxylic acid group, to the NH_2, amino group, leaving an ion with both a negative and positive charge. These results in a net neutral charge because the number of protonated ammonium groups with a positive charge is equal to that of deprotonated carboxylate groups with a negative charge. This ion is called a zwitterion (German for mongrel or hybrid ion), and such types are presented in Figure 2.27. The zwitterionic character of a glycine molecule can complex metal ions of varying ionic sizes effectively, which helps in preventing selective impulse to maintain compositional homogeneity among the constituents. On other hand, glycine also can serve as a fuel in the combustion reaction, when being oxidized by nitrate ions.

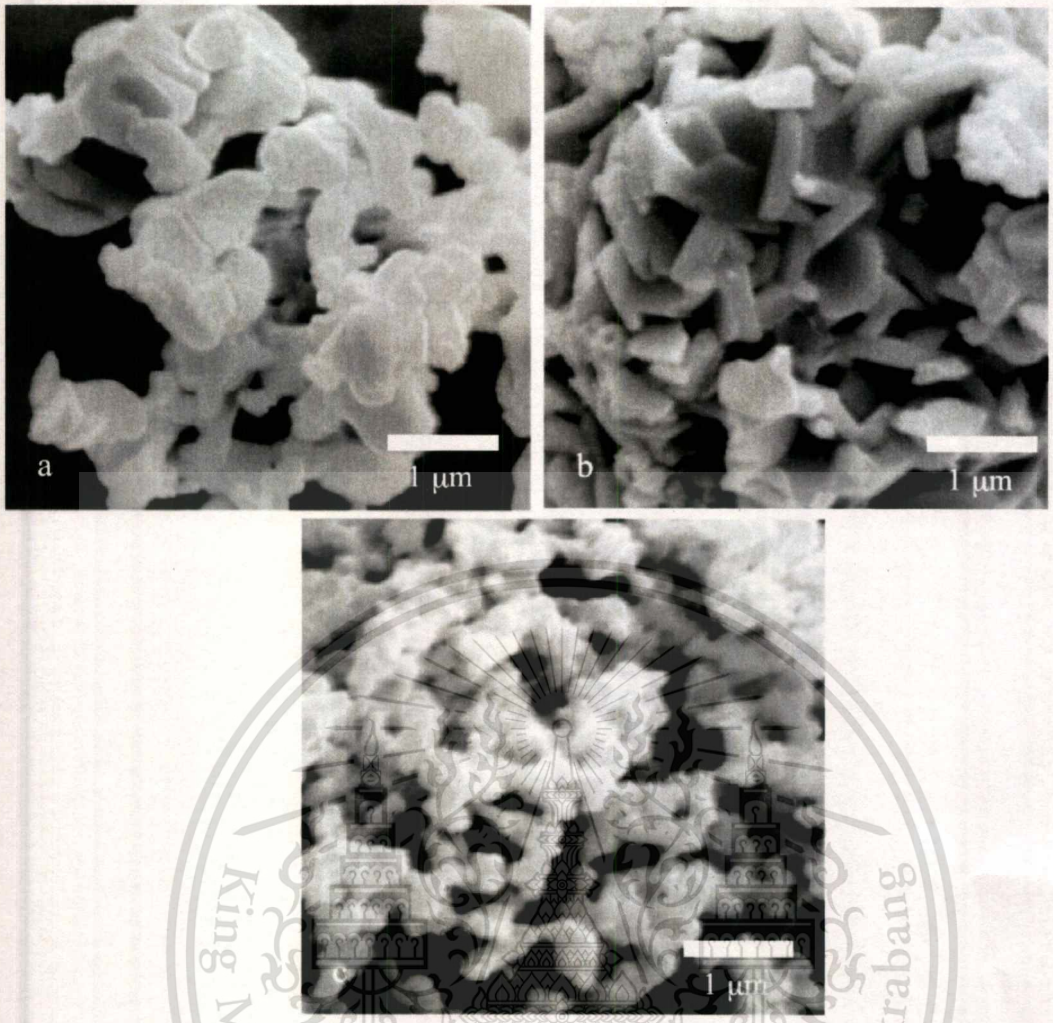

Figure 2.26 SEM photographs showing the powders produced by (a) solid-state reaction, (b) SHS–sample UB3, (c) SHS–sample PB3 [90].

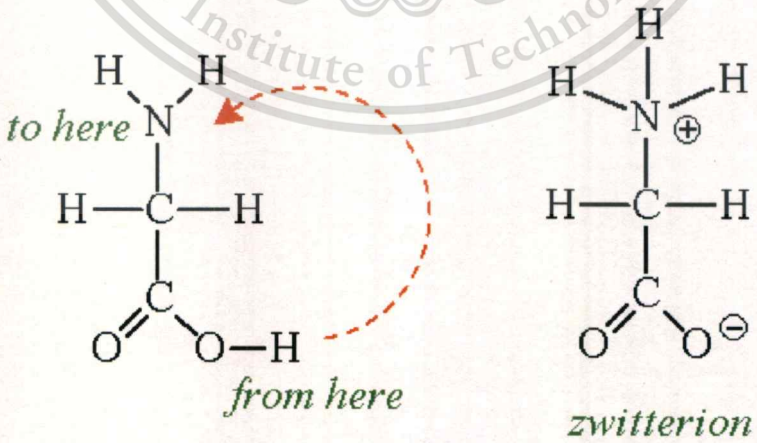

Figure 2.27 Neutral and zwitterion structure of glycine.

In 2001, T. Mimani *et al.* [91] prepared nanosize alumina, ceria, yttria, zirconia CeO_2-ZrO_2 (OSC), t-ZrO_2-Al_2O_3 (ZTA) and Y_2O_3-ZrO_2 (YSZ) by the combustion of aqueous solutions containing corresponding metal nitrate, ammonium nitrate and glycine redox mixtures. The aqueous solution, with redox mixture in a Pyrex container, was introduced in a preheated muffle furnace at 400°C for boiling, foaming and undergoing smoldering (flameless) combustion, and producing the corresponding oxides. The product remaining was voluminous and erupted like a volcano, as shown in Figure 2.28 (a). The TEM photograph of that zirconia powder shows a uniform and compact distribution of the particles [Figure 2.28 (b)], which were almost spherical to hexagonal geometry with a size of ≤ 20 nm. It appeared that the particles were dispersed with negligible agglomeration and they showed a higher surface area.

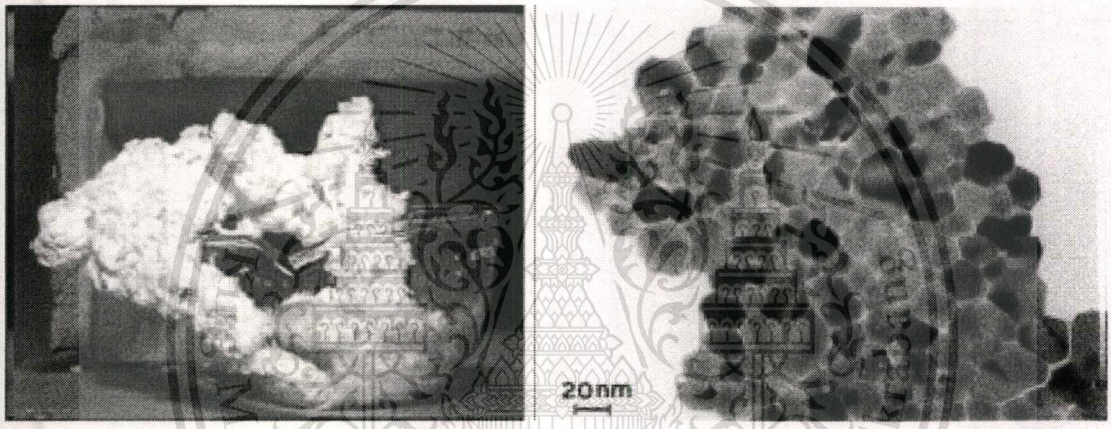

Figure 2.28 Formation of voluminous zirconia (a) and TEM micrograph of ZrO_2 (b) [91].

Barium titanate ($BaTiO_3$); a well known perovskite and widely investigated dielectric material, was prepared using a simple and instantaneous combustion technique from T. V. Anuradha *et al.* [92]. The synthesis of nanosize $BaTiO_3$ by the combustion of redox mixture containing different Ba-precursors (nitrate, acetate or peroxide), $TiO(NO_3)_2$ and fuel (carbohydrazide, glycine or citric acid) was described. XRD patterns of the $BaTiO_3$ obtained showed cubic phase with significant peak broadening, which indicated formation of nanostructured $BaTiO_3$. The crystallite sizes calculated using Debye Scherrer's equation were found to be in the range of 50-60 nm, while particle sizes indicated by TEM studies were found to be in the range of 10-50 nm. SEM micrographs indicated the variation of pore size, depending upon the precursors and fuel. A high order of porosity was observed, especially when citric acid and glycine were used as fuels with barium nitrate and barium acetate, respectively.

A.S. Mukasyan *et al.* [93] identified optimum synthesis, and compacting and sintering conditions in order to achieve a fully densified pure phase $La_{0.8}Sr_{0.2}CrO_3$ (LSC) perovskite membrane using the aqueous solution of metal nitrates (oxidizer) and glycine (fuel). Depending on the fuel/oxidizer ratio, ϕ, the reaction can proceed in three different modes: smoldering combustion synthesis (SCS) with a maximum temperature of T_m < 600°C; volume combustion synthesis (VCS) at 1,150°C < T_m < 1,350°C; and self-propagating high-temperature synthesis (SHS) at 800°C < T_m < 1,100°C. The characteristics of synthesized powders depended on the combustion mode. The crystalline structure of as-synthesized powders became more defined as the amount of fuel increased. It can be seen from the SEM micrograph that SHS powders have a larger specific surface when compared to SCS and VCS products. After calcinations, microstructures of all powders changed dramatically. It can be seen that the calcined powders did not exhibit flake or a waffle type microstructure, but were extremely uniform with well defined morphology of each particle. This led to large decreases in the specific surface area of powders. Powder synthesized in SHS mode was found to be the most homogeneous, with the highest surface area among all calcined samples. The highest relative density of sintered specimens was found to be 85%, which belonged to the membrane produced from SHS powders.

R.D. Purohit *et al.* [94] synthesized ultrafine ceria (CeO_2) powders by the combustion technique through auto-ignition of viscous liquids containing cerium nitrate (oxidizer) and glycine (fuel). From X-ray line broadening, as presented in Figure 2.29, the increase in crystallite size with that in the glycine-to-nitrate molar ratio was attributed to an increase in flame temperature, which assisted the crystal growth. The very high flame temperature in the case of stoichiometric and fuel-rich precursors can affect the powder characteristics adversely, for example, increase in the crystallite size, and premature partial local sintering among the active primary particles, produced during combustion, thereby reduce the surface area. Figure 2.30 (a) and (b) show the HRTEM micrographs of nanocrystalline ceria powder agglomerates, which also confirmed lower particle size distribution when comparing the fuel-deficient ratio with the stoichiometric ratio. Additionally, the color of the ceria powder also was found to change with the fuel-to-oxidant ratio used in the process. The powder color may be related to variation of the crystallite (particle) size.

C.C. Hwang *et al.* [14] developed a novel combustion synthesis method to prepare the electronic oxide powders, $Ni_{0.5}Zn_{0.5}Fe_2O_4$, ZnO, $LiCoO_2$, $BaFe_{12}O_{19}$ and $YBa_2Cu_3O_{7-x}$ ($x \leq 0.25$),

using organic compounds (e.g., glycine, urea, citric acid, alanine, or carbohydrazide) mixed directly with metal nitrates without adding water. Combustion reaction was started by igniting the mixture using a mini gas burner. In this work, the initial temperature (T_{in}), which was when the sample weight started to change rapidly during chemical reaction, was defined by using thermogravimetric analysis (TGA). The synthesis using glycine, alanine and carbohydrazide as organic fuels was found to produce a single-phased Ni-Zn ferrite, because only the characteristic peaks of a Ni-Zn ferrite were seen in XRD patterns. However, by using glycine as fuel, the Ni-Zn ferrite possessed better quality with good chemical homogeneity. Also, as glycine is inexpensive, it was selected to acquire other ferrites. Figure 2.31 demonstrates a TEM photograph taken after the as-synthesized product had been fully ground and treated with oscillation procedures. It was found that the size of the spherical particles was dispersed with negligible agglomeration and homogeneously distributed in a range of 30-40 nm. Additionally, 97% theoretical density of sintered samples was obtained after 2 hr at a relatively low temperature of 950°C.

S.V. Chavan *et al.* [95] reported the synthesis of yttria (Y_2O_3) by the combustion technique using glycine as fuel. The effect of oxidant-to-fuel molar ratio on powder characteristics was investigated. The XRD data of all the powders calcined at 600°C for 1 hr are shown in Figure 2.32. All the patterns conformed to that of pure phase Y_2O_3, with considerable peak broadening attributed to very small crystallite sizes. It was reported that using the stoichiometric ratio (oxidant-to-molar ratio of 1:1.66) produced the highest flame temperature, which was as high as 1,440°C and led to large 30 nm crystallites and a low surface area. The flame temperature for the fuel rich ratio (oxidant-to-molar ratio of 1:2.5) was lower than the stoichiometric ratio (1050°C), which led to finer 9 nm crystallites. The decrease process in surface area was described as neither uniform nor spontaneous, despite a higher number of gas moles. The best powders, with a crystallite size of 8 nm, were obtained for an oxidant-to-molar ratio of 1:1 (fuel-deficient), due to the gaseous evolution that was very intense, and the combustion process occurred very rapidly for a very short duration when compared to all the other ratios. It can be noted that two competing effects govern the final powder properties, viz., the high exothermicity and flame temperature cause the powders to coarsen, whereas the evolved gases tend to improve the powder properties.

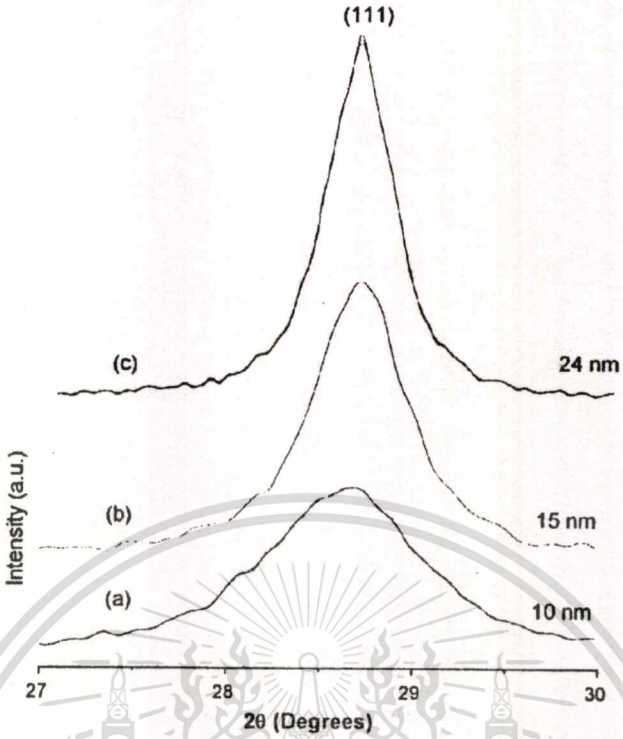

Figure 2.29 X-ray line broadening for ceria powder obtained through (a) the fuel-deficient, (b) the stochiometric, and (c) the fuel-rich precursor [94].

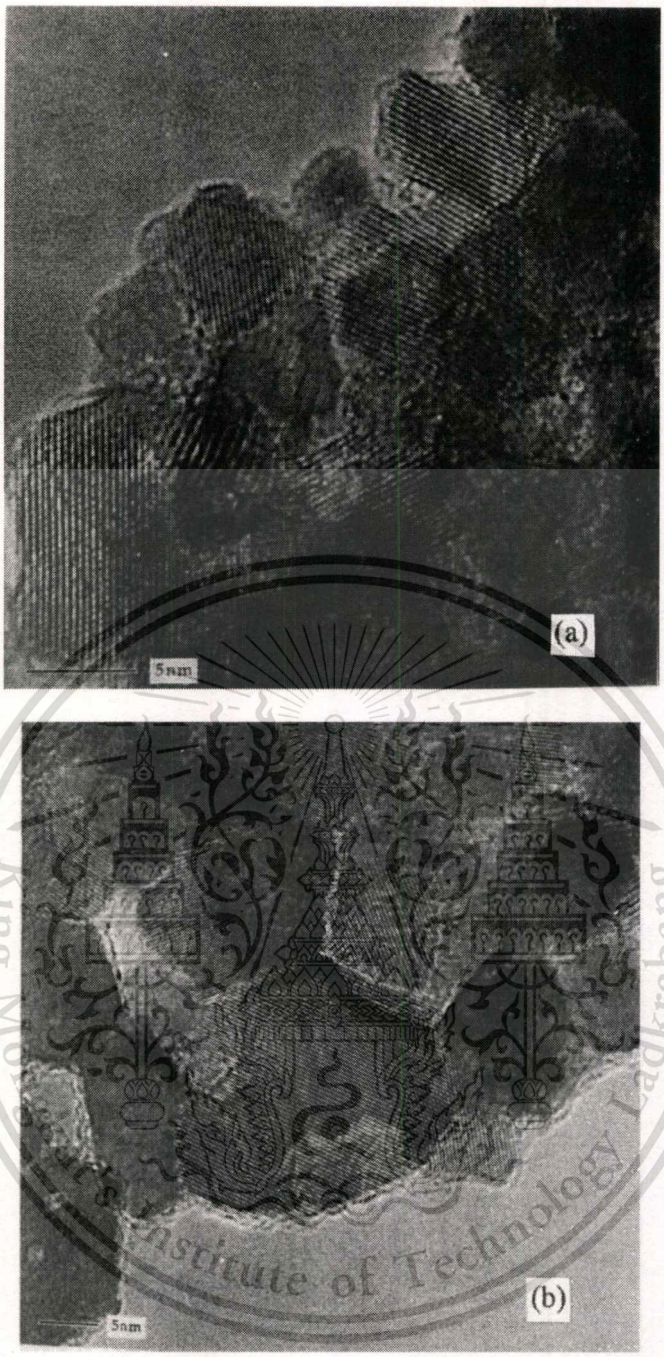

Figure 2.30 HRTEM micrographs of ceria powder obtained through (a) the fuel-deficient, and (b) the stoichiometric precursor [94].

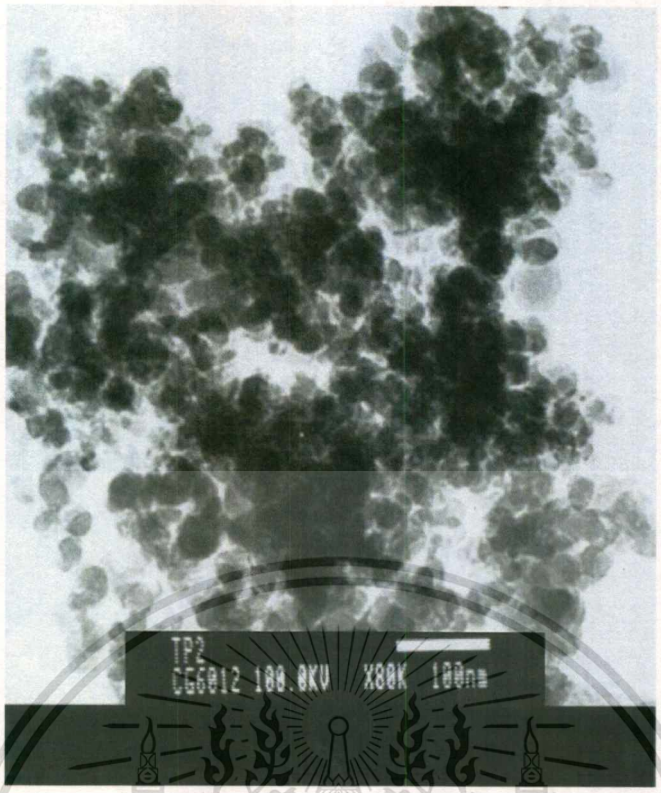

Figure 2.31 TEM photograph of the synthesized Ni–Zn ferrite powders [14].

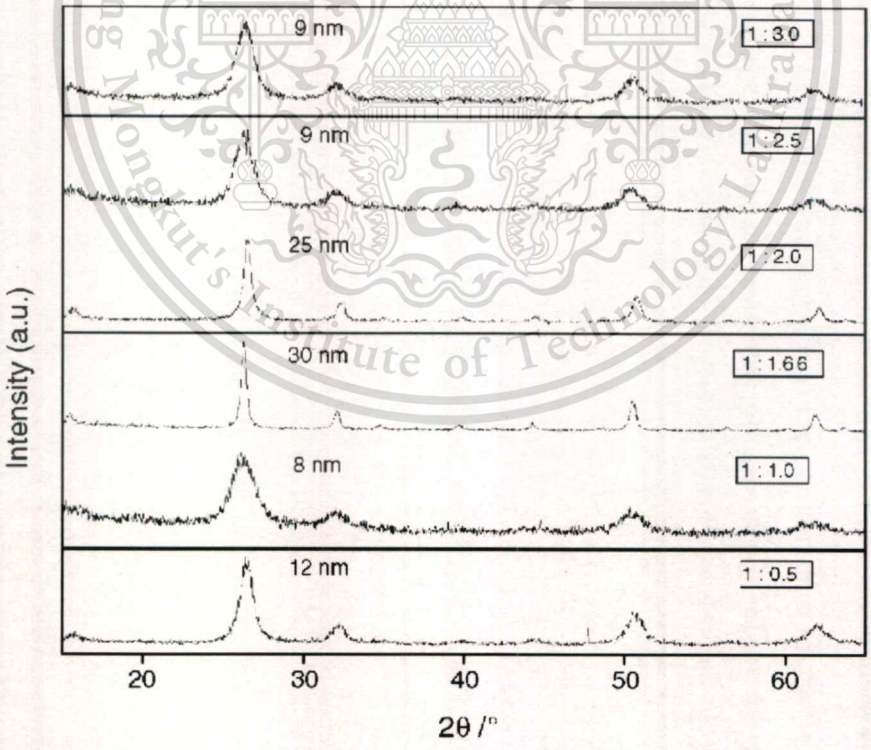

Figure 2.32 XRD patterns for products from different oxidant-to-fuel ratios [95].

CHAPTER 3

EXPERIMENTAL PROCEDURES

The experimental procedures used for the preparation and characterization of lead-free piezoelectric alkali niobate perovskite ABO_3 (A = K, Na; B = Nb) powders are described in this chapter. Firstly, the synthesis method used was divided into two parts. For a modified solid state reaction, potassium niobate ($KNbO_3$; KN) and sodium niobate ($NaNbO_3$; NN) powders were produced. The influence of calcination temperatures and dwell times on the preparation of $KNbO_3$ and $NaNbO_3$ powders was investigated. For a combustion synthesis, sodium niobate ($NaNbO_3$; NN) powders were produced. The influence of the fuel-to-oxidizer molar ratio and calcination temperatures for the preparation of $NaNbO_3$ powders was examined.

The chemical purity and supplier of starting materials are listed in Table 3.1. Potassium oxalate monohydrate ($K_2C_2O_4 \cdot H_2O$), sodium oxalate ($Na_2C_2O_4$) and niobium pentaoxide (Nb_2O_5) were employed as the starting material for a modified solid state reaction. For combustion synthesis, sodium nitrate ($NaNO_3$) and niobium pentoxide (Nb_2O_5) were used as the oxidizer, and glycine (NH_2CH_2COOH) was applied as fuel.

Table 3.1 Specifications of the starting material powders used in this study.

Materials	Purity (%)	Formula weight	Manufacturer
Potassium oxalate monohydrate $K_2C_2O_4 \cdot H_2O$	≥99.00	184.24	Fluka GmBH, Germany
Sodium oxalate $Na_2C_2O_4$	≥99.90	134.00	Fluka GmBH, Germany
Niobium pentaoxide Nb_2O_5	99.95	265.81	CERAC Company Inc., USA
Sodium nitrate $NaNO_3$	≥99.5	84.99	Riedel-deHaën
Glycine NH_2CH_2COOH	99.7-101	75.07	Sigma-Aldrich Company Inc., USA

3.1 Modified solid state reaction

Potassium niobate ($KNbO_3$; KN) and sodium niobate ($NaNbO_3$; NN) powders were produced using a modified solid state reaction method. This modified technique was similar to the conventional solid state mixed oxide method, except when using oxalate compound as starting material instead of oxide and/or carbonate compound. Reagent-grade potassium oxalate monohydrate ($K_2C_2O_4 \cdot H_2O$, ≥99.9%) and niobium pentaoxide (Nb_2O_5, 99.95%) were employed as starting materials for $KNbO_3$ preparation. The raw materials were weighed in stoichiometric quantities following the equation below, with a 3 mol% excess of $K_2C_2O_4 \cdot H_2O$ added in order to compensate weight loss during the calcination step.

$$K_2C_2O_4 \cdot H_2O_{(s)} + Nb_2O_{5(s)} \rightarrow 2KNbO_{3(s)} + CO_{2(g)} + CO_{(g)} + H_2O_{(g)} \quad (3.1)$$

Reagent-grade sodium oxalate ($Na_2C_2O_4$, 99.9%) and niobium pentaoxide (Nb_2O_5, 99.95%) were employed as raw material for $NaNbO_3$ preparation. All starting materials were weighed according to the required stoichiometric ratio, which related to the reaction below, with a 3 mol% excess of $Na_2C_2O_4$ added in order to compensate weight loss during the calcination step.

$$Na_2C_2O_{4(s)} + Nb_2O_{5(s)} \rightarrow 2NaNbO_{3(s)} + CO_{(g)} + CO_{2(g)} \quad (3.2)$$

All raw materials were mixed by the mixing process, as used in the routine processing procedure of the conventional solid state mixed oxide method. Schematic of the mixing process is illustrated in Figure 3.1. These starting materials were mixed by the ball-milling method using ethyl alcohol as medium and partially stabilized zirconia balls for 18 h. Then, the mixture was dried on a hotplate, with regular stirring for a suitable period. After drying, the precursor mixture was determined by thermogravimetric analysis (TGA, Perkin Elmer) and differential thermal analysis (DTA, Perkin Elmer) for investigating thermal behavior during heat treatment and finding the appropriate calcination temperature. Based on the TG-DTA results, the mixture was placed subsequently in a closed alumina crucible and calcined for different periods at various temperatures, ranging from 300°C to 700°C, in order to investigate formation of the alkali niobate perovskite phase.

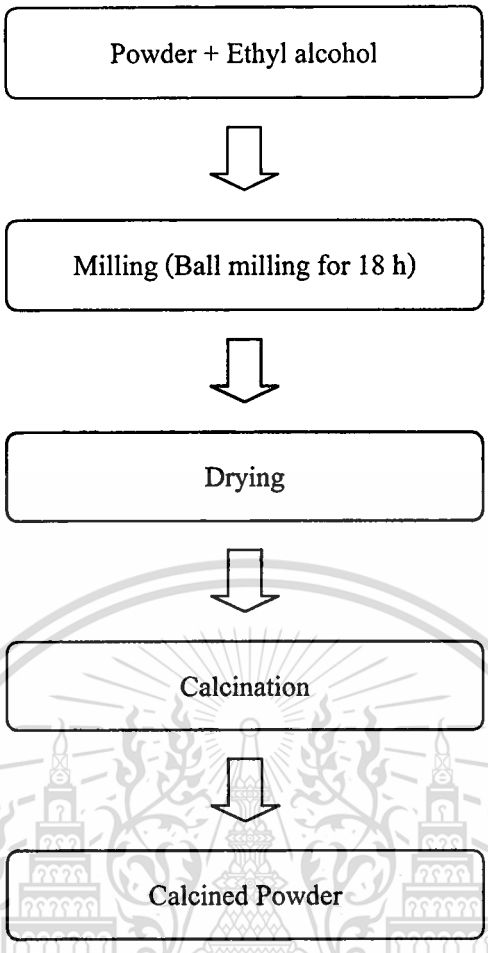

Figure 3.1 Mixed and calcination Processes (MCP) for powder preparation.

3.2 Combustion synthesis

Combustion synthesis (CS) was found to be a potential method for synthesizing powder rapidly with the desired composition, and high porosity and sinterability. AR grade sodium nitrate ($NaNO_3$, ≥99.50%) and niobium pentoxide (Nb_2O_5, 99.95%) were used as the oxidizer, and glycine (NH_2CH_2COOH, 99.7%) was applied as fuel for the combustion synthesis of perovskite alkaline niobate $NaNbO_3$ powders in this study.

Based on the fundamental thermochemical concepts used in propellant chemistry, an exothermic redox reaction of the combustion synthesis process could be initiated only when the oxidizer and fuel are mixed thoroughly in a fixed proportion. This method consists of establishing a simple valency balance, irrespective of whether the elements are present in the oxidizer or fuel components of the mixture, and then calculating the stoichiometric composition of the starting mixture, which is equivalent to the release of maximum energy. The elemental stoichiometric coefficient, ϕ, which is the ratio between the total valencies of fuel (glycine; NH_2CH_2COOH) and that of the oxidizer (nitrate compound), can be calculated following the method proposed by Jain *et al.* [86]. To calculate the total valencies, carbon and hydrogen are considered as reducing elements with the corresponding valencies of +4 and +1; oxygen is seen as an oxidizer with the valence of –2; and nitrogen is considered to have the valence of 0. In extrapolating these concepts for the combustion synthesis of oxide powder in this study, metals were considered as reducing elements with their corresponding valences (e.g. +3 for lanthanum, +2 for magnesium, +1 for potassium and sodium). Additionally, in the case of multiple valence elements, the valence of the element in the product was used in the calculation. The elemental stoichiometric coefficient, ϕ, could be calculated by:

$$\phi = \mathrm{n}\frac{\text{total valaencies of fuel}}{\text{total valaencies of oxidizer}} \tag{3.3}$$

where n is the mole of glycine. According to the propellant chemistry for stoichiometric redox reaction between fuel and an oxidizer, the ϕ ratio should be unified (stoichiometric). A $\phi < 1$ means oxidant-rich condition and $\phi > 1$ means fuel-rich condition. This ϕ ratio was referred to as the fuel-to-oxidizers ratio. To satisfy the principle in the present system of $NaNbO_3$ preparation, the following calculation could be performed:

$$\phi = n \frac{(0_{(N)}+2\times1_{(H)}+4_{(C)}+2\times1_{(H)}+4_{(C)}-2_{(O)}-2_{(O)}+1_{(H)})}{1_{(Na)}+0_{(N)}-2\times3_{(O)}} \quad (3.4)$$

Sodium nitrate possessed the oxidizing valency of 5– and glycine had the reducing valency of 9+, and, as the mole of glycine (n) was found to be 0.56, the molar ratio of fuel (glycine; NH_2CH_2COOH) to oxidizer was 0.56:1. This ratio was referred to as the fuel-to-oxidizers molar ratio. Therefore, the comprehensive reaction that formed $NaNbO_3$ could be written as:

$$18NaNO_{3(aq)} + 9Nb_2O_{5(s)} + 10NH_2CH_2COOH_{(aq)} \longrightarrow$$

$$18NaNbO_{3(s)} + 25H_2O_{(g)} + 14N_{2(g)} + 20CO_{2(g)} \quad (3.5)$$

It must be noted that various fuel-to-oxidizers molar ratios should be used for investigating and comparing the effect of fuel-rich/fuel-lean mixtures on the synthesis of niobate powder. Different fuel-to-oxidizers molar ratios such as fuel-deficient (<0.56), equivalent stoichiometric (0.56) and fuel-rich (>0.56) conditions were applied.

The appropriate amounts of metal nitrate starting materials were weighed according to the chemical reactions mentioned above. Schematic of the combustion synthesis procedure is illustrated in Figure 3.2. The metal nitrates were mixed with de-ionized water in a glass beaker, followed by adding Nb_2O_5 and stirring regularly for 30 min. Glycine (NH_2CH_2COOH) was then added into the solution and the mixture was stirred again for 30 min. After that, the solution precursor was boiled on a hotplate inside a fume-cupboard under ventilation. Then the solution was evaporated after it had thickened. Once the solution had begun to dry, ignition took place when the temperature increased rapidly, which resulted in self-sustaining combustion, with rapid evolution of a large volume of gas products, and formation of voluminous powders.

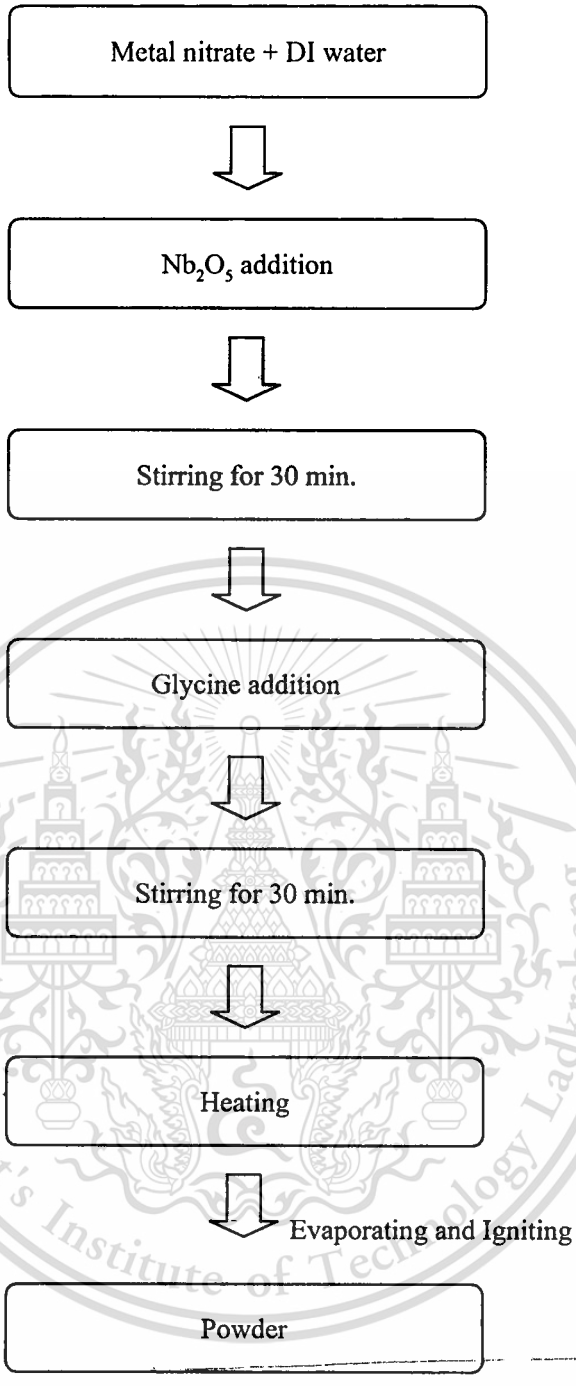

Figure 3.2 Schematic flow chart of the combustion synthesis process (CSP).

3.3 Characterization

The mixture of starting material was determined using thermogravimetric analysis (TGA) and differential thermal analysis (DTA) for investigating thermal behavior of the precursor. The crystal structure, phase nucleation and influence of the fuel-to-oxidizers molar ratio, calcination temperatures and dwell times of calcination to phase formation of as-synthesized and calcined powders, were studied and characterized by the X-ray diffraction technique (XRD) and Fourier transform infrared (FTIR) spectroscopy. The morphology and particle size of the powders obtained were investigated through a scanning electron microscope (SEM).

3.3.1 Thermogravimetric analysis (TGA) and differential thermal analysis (DTA)

Thermogravimetric analysis (TGA) was defined as a technique in which the mass change of a substance is measured as a function of temperature, whilst the substance is subjected to a controlled temperature program. This mass loss is seen only if a process occurs where a volatile component is lost, thus, the reaction may take place with no mass loss being detected. Therefore, simultaneous thermogravimetry-differential thermal analysis (TG-DTA) could be applied to provide all information required to understand the thermal behavior of the mass change. In preparation of the powder, thermal behavior of all precursors was investigated using TG-DTA (Perkin Elmer), with a heating rate of 10 K min^{-1} in a temperature range from room temperature to 1,573 K in N_2 atmosphere at a rate of 100 cm^3 min^{-1}.

3.3.2 X-ray diffraction technique (XRD)

The automated X-ray diffractometer (XRD, Advance D8) was used on the precursor, and as-synthesized and calcined powder, using Ni-filtered CuK_α radiation for phase identification, lattice parameters and mean crystalline size estimation. The volume fraction of the perovskite phase formation was considered for phase purity at various calcination temperatures and dwell times. These relative amounts of perovskite and others phases were approximated by calculating the ratio of the main X-ray peak intensities of perovskite, residual starting component (R = $K_2C_2O_4{\cdot}H_2O$, $Na_2C_2O_4$, KNO_3 and/or $NaNO_3$), Nb_2O_5 and other secondary phases (pyrochlore), using the following equation [96]:

$$\text{Wt\% perovskite} = \frac{I_{\text{perov}}}{I_{\text{perov}}+I_R+I_{Nb_2O_5}+I_{\text{pyro}}} \times 100 \qquad (3.8)$$

where I_{perov}, I_R, $I_{Nb_2O_5}$ and I_{pyro} stand for intensities belonging to the strongest reflection peak of perovskite, residual starting component (R = $K_2C_2O_4 \cdot H_2O$, $Na_2C_2O_4$, KNO_3 and/or $NaNO_3$), (180) Nb_2O_5 and pyrochlore phases, respectively.

The average crystallite size of the powders obtained could be determined from the XRD pattern, according to Scherrer's equation [97]:

$$D = \frac{k\lambda}{\beta \cos\theta_B} \tag{3.9}$$

where D is the average crystallite size, k a constant equal to 0.94, λ the wavelength of X-ray radiation, β the full width at half maximum (FWHM) and θ_B the diffraction angle. The constant of proportionality, k (the Scherrer constant) depends on the how the width is determined, the shape of the crystal, and the size distribution. The most common values for k are 0.94 for FWHM of spherical crystals with cubic symmetry.

3.3.3 Fourier transform infrared (FTIR) spectroscopy

To confirm phase identification, the precursor and final powder product were characterized by using the Fourier transform infrared (FTIR) technique, which determines the adsorption of infrared radiation, due to characteristic vibrations and rotations of atoms in molecules and solid compound. The room temperature FTIR spectra were recorded in the range of 4,000–400 cm^{-1}, with 8 scans on a Perkin Elmer, FT-IR SPECTRUM GX and a resolution of 4 cm^{-1} using KBr pellets (KBr, spectroscopy grade, Merck).

3.3.4 Scanning electron microscope (SEM)

The morphology and particle size of the powders obtained were investigated through the scanning electron microscope (SEM). The powders were dispersed firstly in ethyl alcohol using an ultrasonic bath for 20 min. Then, dispersion was dropped on alumina tape and dried. The morphology of the resulting selected samples was examined with the scanning electron microscope (SEM, Hitachi S4700, JEOL JSM-6335F and Leo 1455VP) after gold coating for 1 min. The average particle size of powders obtained was examined using the linear intercept method.

CHAPTER 4

RESULTS AND DISCUSSIONS

4.1 Solid state reaction synthesis of sodium niobate ($NaNbO_3$) powder at low temperature

Overview - A modified solid state reaction was applied to produce lead-free piezoelectric sodium niobate ($NaNbO_3$) powders. The mixture of $Na_2C_2O_4$ and Nb_2O_5 was identified by thermo gravimetric analysis (TGA) and differential thermal analysis (DTA). The powders were characterized using a scanning electron microscope (SEM) and the X-ray diffraction technique (XRD). The SEM image suggested that the particle size of the powders obtained ranged from 180 to 360 nm. The XRD pattern showed that the pure perovskite phase of $NaNbO_3$ could be synthesized at the low temperature of 475°C for 1 h, with an average crystallite size of 25.89 ± 5.64 nm. This temperature was about 300°C lower than that when using the conventional solid-state method with Na_2CO_3 as reactant, which resulted in a cost-, energy-, and time-saving method.

4.1.1 Introduction

Alkaline niobate materials are considered a lead-free candidate for the substitution of widely used commercial lead-based piezoelectric material, based on the aim to avoid highly harmful lead compounds [57, 64, 98-99]. Among several compounds, sodium niobate ($NaNbO_3$) has attracted considerable attention because of its unique properties [98] and high dielectric constant (2000–3000) at Curie temperature [100]. Unlike most oxidic perovskite, $NaNbO_3$ possesses six phase transitions from the ferroelectric phase at low temperature (rhombohedral) to the antiferroelectric room temperature phase (orthorhombic) and non-polar cubic structure at 640°C [101]. It can form solid solution with other niobate compounds, such as $LiNbO_3$ and $KNbO_3$, to acquire good ferroelectric and piezoelectric properties [50, 62, 102-103]. Traditionally, alkali metal niobate powders have been synthesized via the solid state reaction of alkali metal carbonates and Nb_2O_5 [98, 104]. This method requires a high calcination temperature (about 750°C or more) for a long period of time, possibly causing volatilization of the alkali metal

and leading to poor compositional homogeneity [98-99, 104]. The powders can be agglomerated during heating, which affects their properties [98, 105]. Thereafter, powders with high sinterability and stoichiometric control are necessary for developing $NaNbO_3$-based piezoelectric ceramics. Numerous alternative methods are used to prepare $NaNbO_3$ such as hydrothermal [106], chemical [105], and polymeric precursor processes [16], and the mechanochemical process [15, 98, 107]. Although $NaNbO_3$ was performed by mechanochemical activation after thermal treatment of a stoichiometric Na_2CO_3/Nb_2O_5 mixture at 600°C, this procedure required a long operational period of up to 30 days [98]. Moreover, $NaNbO_3$ was also obtained at a low temperature (450°C) by the wet-chemical method using a water-soluble malic acid complex [108]. However, most chemical techniques require specialized experimental apparatus and high purity reactant, which are more expensive. Interestingly, sodium tantalate ($NaTaO_3$) powder, with high crystallinity has been successfully synthesized at 600°C through a simple method called modified solid state reaction or combustion synthesis, in which urea plays an important role. Unusual starting material ($Na_2C_2O_4$ instead of Na_2CO_3/Na_2O) has been described. This method was found to produce $NaTaO_3$ as a general route at the lower temperature of 500-600°C, when compared with conventional solid state reaction [18]. On the other hand, urea, which was added as fuel in order to achieve the final product, could cause problems in this method, due to risks if performing on a large scale. Nonetheless, the aim of the present study was to produce $NaNbO_3$ using a simple, rapid, low cost, and environment friendly route, such as a solid state reaction of $Na_2C_2O_4$ and Nb_2O_5 without the addition of any fuel.

4.1.2 Experimental procedure

$NaNbO_3$ was synthesized by a solid state reaction method. Reagent-grade sodium oxalate ($Na_2C_2O_4$, 99.9%) and niobium oxide (Nb_2O_5, 99.9%) were employed as raw material. Firstly, starting materials were weighed according to the required stoichiometric ratio that related to the reaction below.

$$Na_2C_2O_{4(s)} + Nb_2O_{5(s)} \rightarrow 2NaNbO_{3(s)} + CO_{(g)} + CO_{2(g)} \quad (4.1)$$

Then, raw materials were mixed together by ball-milling in ethyl alcohol using partially stabilized zirconia balls for 18 h. After drying on a hot plate by regularly stirring at about 80°C for an approximate period, the thermal behavior during heat treatment was determined by thermo gravimetric analysis (TGA, Perkin Elmer) and differential thermal analysis (DTA, Perkin Elmer). According to TG-DTA results, the mixture was subsequently placed in a closed alumina crucible and calcined for different periods of time in air at various temperatures, ranging from 300 to 600°C, in order to investigate the formation of $NaNbO_3$. Afterward, calcined powders were subsequently inspected by room temperature X-ray diffraction (XRD, Advance D8), using Ni-filtered Cu K_α radiation, to examine the effect of thermal treatment on phase development and the optimal calcination condition for the formation of crystalline $NaNbO_3$ powders. Powder morphologies and particle size were figured directly using a scanning electron microscope (SEM, LEO1455 VP).

4.1.3 Results and discussion

The TGA and DTA of a powder mixed in the stoichiometric proportions of $NaNbO_3$ are illustrated in Figure 4.1. The TG curve accordingly revealed a weight loss of 16.8%, occurring during the temperature rise from 400 to 500°C. This observation corresponded to the endothermic peak of the DTA curve, which centered at 484.8°C. This endotherm may be related to the decomposition of $Na_2C_2O_4$ to Na_2CO_3, which lies on the temperature of 450-550°C, and abruptly to the decomposition of Na_2CO_3 to Na_2O (decomposition temperature in the range of 400°C) before releasing CO and CO_2 molecules, as revealed below [19].

$$Na_2C_2O_{4(s)} \longrightarrow Na_2CO_{3(s)} + CO_{(g)} \quad (4.2)$$

$$Na_2CO_{3(s)} \longrightarrow Na_2O_{(s)} + CO_{2(g)} \quad (4.3)$$

It is interesting to note that there was no weight loss or thermal effect at a temperature of about 100°C, at which no decomposition occurrence was indicated. The endothermic peak correlates at the range of 100°C with the release of water molecules.

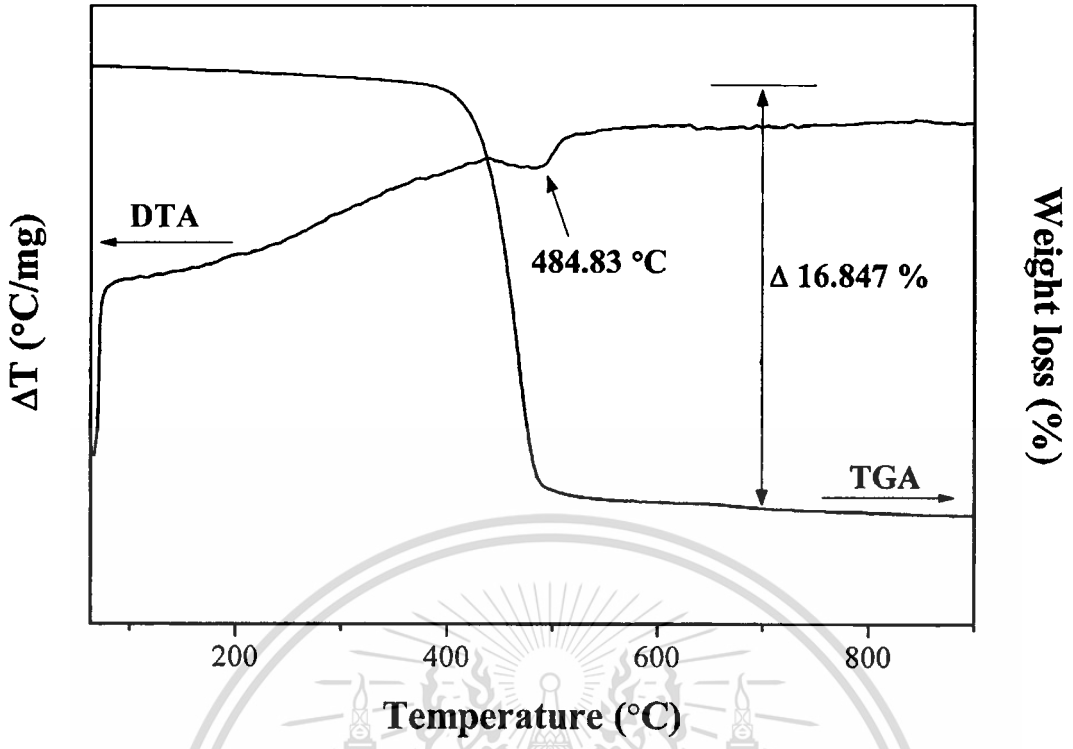

Figure 4.1 TG-DTA result of an uncalcined powder mixed in the stoichiometric proportion of $NaNbO_3$.

This confirmed that non-absorptive $Na_2C_2O_4$ raw material contrasts with Na_2CO_3, because Na_2CO_3 is the hygroscopic compound which can lead to the erroneous stoichiometric ratio. Therefore, powders with good compositional homogeneity, when comparing with the conventional solid-state method with Na_2CO_3 as reactant, may possibly be produced via this solid-state reaction. Thus, based on TG-DTA data, the powders were calcined at temperatures ranging from 300 to 600°C for 4 h in order to investigate the calcination temperature outcome in the development phase. The mixture of starting material was calcined in air using the steady heating/cooling rate of 20°C at various temperatures, and followed by phase analysis using the XRD technique. Figure 4.2 shows the XRD pattern of the $NaNbO_3$ powders calcined at different temperatures for 4 h. It can be seen that fine $NaNbO_3$ crystallites were developed at a calcination temperature as low as 400°C, accompanied by the phase of unreacted Nb_2O_5 (JCPDS file no. 30-0873) and $Na_2C_2O_4$ (JCPDS file no. 20-1149). This observation suggests that nucleation of the perovskite $NaNbO_3$ phase did occur. In addition, the minor phase of Nb_2O_5 and $Na_2C_2O_4$ was also

decreased with escalating calcination temperature, and disappeared completely after the powders were calcined at the calcinations temperature of 500°C for 4 h. Whereas, the intensity of the perovskite $NaNbO_3$ peak was enhanced further and an essentially monophasic $NaNbO_3$ perovskite phase (yield of 100% within the limitations of the XRD technique) was observed. This $NaNbO_3$ phase could be indexed according to an orthorhombic structure with the space group Pbma (no. 57), which was consistent with JCPDS file No. 33-1270. Although the calcination temperature rose at 550 and 600°C, the monophasic $NaNbO_3$ perovskite phase was also obtained. There was no evidence of the pyrochlore diffraction peak. This result also correlates with the TG-DTA analysis shown above. As the calcinations temperature increased, so too did the amount of the $NaNbO_3$ crystallite phase, and this can be seen as intensity of the amplified peak. Since the diffusion coefficient is a temperature dependence parameter, the higher temperature has the most intense effect on the rate of diffusion [110], and can enhance higher atomic mobility [104]. As the finest calcination temperature was established at 500°C, a dwell time ranging from 15 min to 4 h was applied at 475°C (instead of 500°C). This temperature was preferred because of the rapid diffraction peak change of the powder calcined at 450 and 500°C.

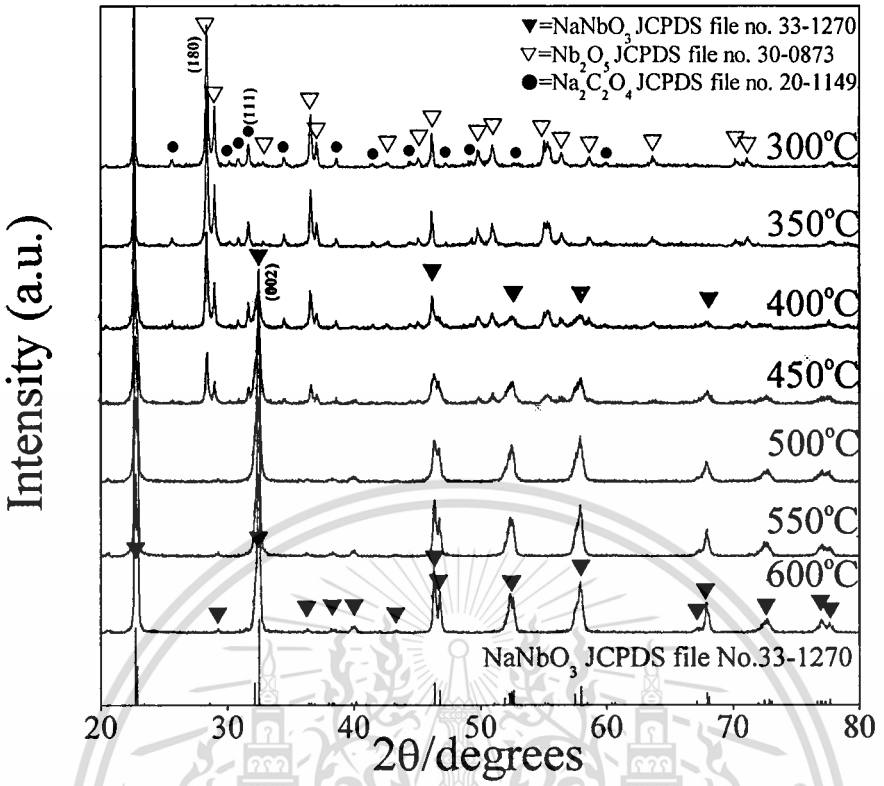

Figure 4.2 XRD patterns of $NaNbO_3$ powder calcined at various temperatures for 4 h with a heating/cooling rate of 20°C/min.

The XRD pattern of the $NaNbO_3$ powders, which were calcined at 475°C with different dwell times, is shown in Figure 4.3. It was found that the single-phase of $NaNbO_3$ powder was also successfully synthesized at the calcination temperature of 475°C, with a dwell time of 60 min or more applied. The increase in crystallinity of the $NaNbO_3$ phase was seen to relate with the escalation of dwell time. Although the calcination temperature of 475°C was higher than the nucleation temperature of the powder obtained by a polymeric precursor [16], this was a single-step and low-cost starting material method that could save time, energy, and cost. Likewise, this temperature was much lower than the conventional solid state reaction process with Na_2CO_3 as reactant, which was in the range of 750°C [98]. This observation indicated that calcination temperature and dwell time might play an important role in evolution of the pure phase product and also be consistent with other systems [111].

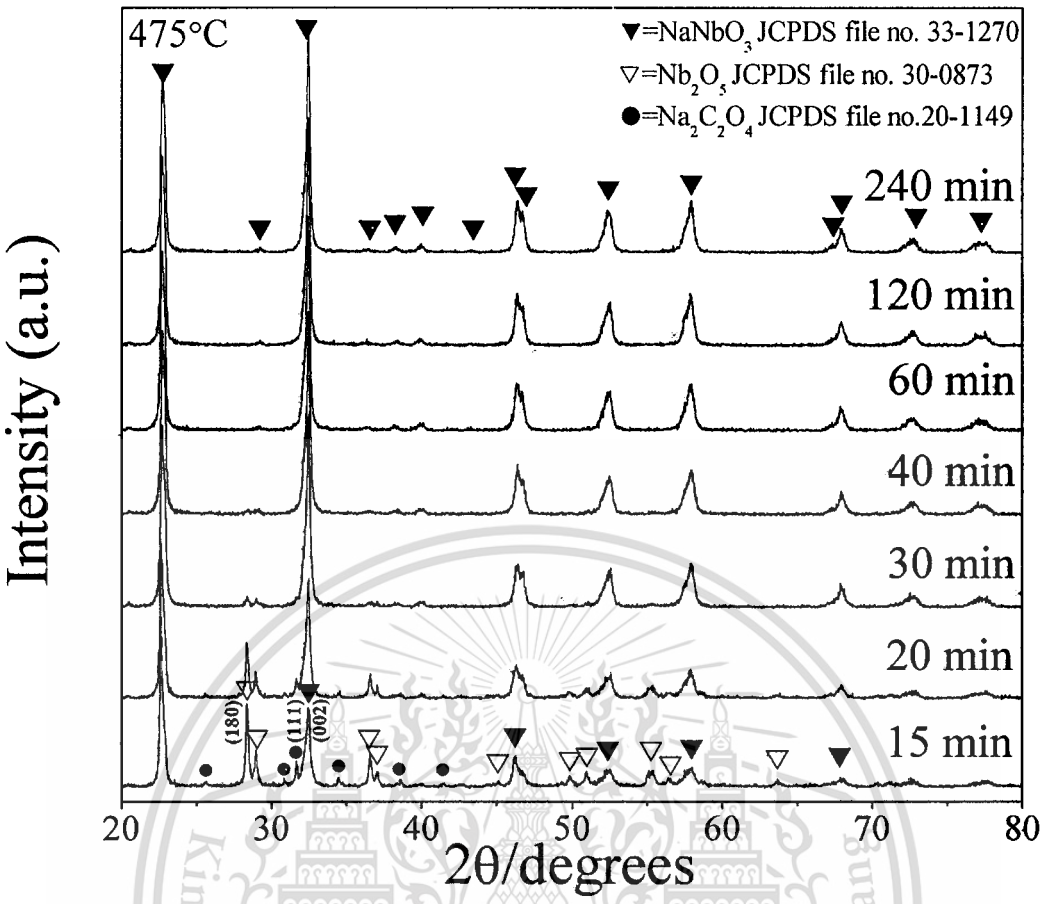

Figure 4.3 XRD patterns of $NaNbO_3$ powder calcined at the calcinations temperature of 475°C for various dwell times with a heating/cooling rate of 20°C/min.

The volume fraction of the perovskite phase formation was considered at various calcination temperatures and dwell times. These relative amounts of perovskite, $Na_2C_2O_4$ and Nb_2O_5 phases, were approximated by calculating the ratio of the main X-ray peak intensities of perovskite $NaNbO_3$, $Na_2C_2O_4$, and Nb_2O_5 phase using the following equation [96]:

$$\text{Wt\% perovskite} = \frac{I_{perov}}{I_{perov}+I_{Na_2C_2O_4}+I_{Nb_2O_5}} \times 100 \qquad (4.4)$$

where I_{perov}, $I_{Na_2C_2O_4}$ and $I_{Nb_2O_5}$ stand for the intensities belonging to the strongest reflection peak of (002) perovskite, (111) $Na_2C_2O_4$, and (180) Nb_2O_5, respectively. A volume fraction increase of the perovskite $NaNbO_3$ phase formation of the calcined powders, resulting from the calcinations process at various temperatures and dwell times, is shown in Table 4.1. As the

calcination temperature rose, the yield of the perovskite phase increased significantly until the temperature reached 500°C, and a pure phase of $NaNbO_3$ was established. Likewise, in observing powders calcined at 475°C for different dwell times, the $NaNbO_3$ phase was enlarged as the dwell time increased up to 60 min, and the monophasic phase of $NaNbO_3$ was seen to form.

Accordingly, the Johnson–Mehl–Avrami, or JMA equation was used in the present study. This equation was found appropriate for describing a wide variety of isothermal solid-state transformations [112-113]. It was used to study the kinetic of the reaction and mechanism involving nucleation and growth, and has the general form of:

$$x(t)=1-\exp[-(kt)^n] \tag{4.5}$$

where x is the volume fraction of the perovskite phase formed, k the reaction rate constant, t the calcination time, and n the Avrami exponent. For analyzing the results, the relation of ln {ln 1/(1 - x)] versus ln t was plotted. Figure 4.4 shows a good linear fit of the Avrami plot for $NaNbO_3$ powders calcined at 475°C. This shows that the isothermal formation of the perovskite phase can be described accurately by the theory of phase transformations. The constant n, which can be calculated from the slope of this Avrami plot, was found to be 1.79. This indicated that the reaction of solid solution formation is diffusion controlled (n is less than 2.5) [114]. The beginning stage of transformation is a fixed number of perovskite nuclei [115]. The average crystallite size of the powders obtained can be determined from the XRD pattern according to Scherrer's equation [97]:

$$D = \frac{k\lambda}{\beta \cos\theta_B} \tag{4.6}$$

where D is the average crystallite size, k a constant equal to 0.94, λ the wavelength of X-ray radiation, β the full width at half maximum (FWHM), and θ_B the diffraction angle. The average crystallite size of powders calcined at 475°C for 15 min to 4 h was found to be from 20.92 ± 2.41 to 28.64 ± 4.99 nm, and that of powders calcined at the optimum condition (475°C for 60 min) was about 25.89 ± 5.64 nm. The increase in crystallinity of the $NaNbO_3$ phase was affected by

increasing dwell time. This may confirm that the dwell time also plays an important role in development of the pure phase creation. SEM micrographs of the powder calcined at 475°C for 60 min are given in Figure 4.5. The particle size, which can be estimated from these micrographs, was found to be in the range of 180 to 360 nm. This value is greater than the average crystallite size calculated from XRD patterns. The inconsistency value could point out the agglomeration of the calcined powders. No evidence of difference phase or pyrochlore phase was found. This outcome relates to the XRD result, in which the monophasic perovskite phase of $NaNbO_3$ can be established after calcination at 475°C for 60 min.

Table 4.1 Fraction of perovskite phase formed as a function of calcinations temperature and dwell time.

$NaNbO_3$	Calcination temperature °C						
	300	350	400	450	500	550	600
wt% perovskite	0	0	35.42	62.86	100.00	100.00	100.00
$NaNbO_3$	Dwell time (min) at 475°C						
	15	20	30	40	60	120	240
wt% perovskite	41.89	60.56	89.13	97.00	100.00	100.00	100.00

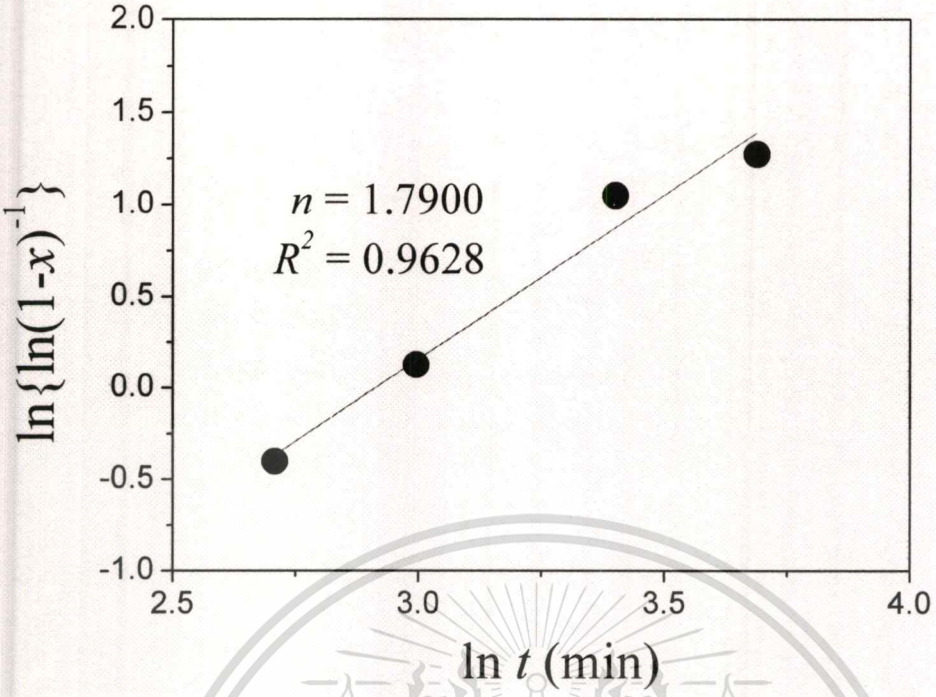

Figure 4.4 Johnson–Mehl–Avrami for the formation of perovskite phase in $NaNbO_3$ powders isothermally heat treated at 475°C.

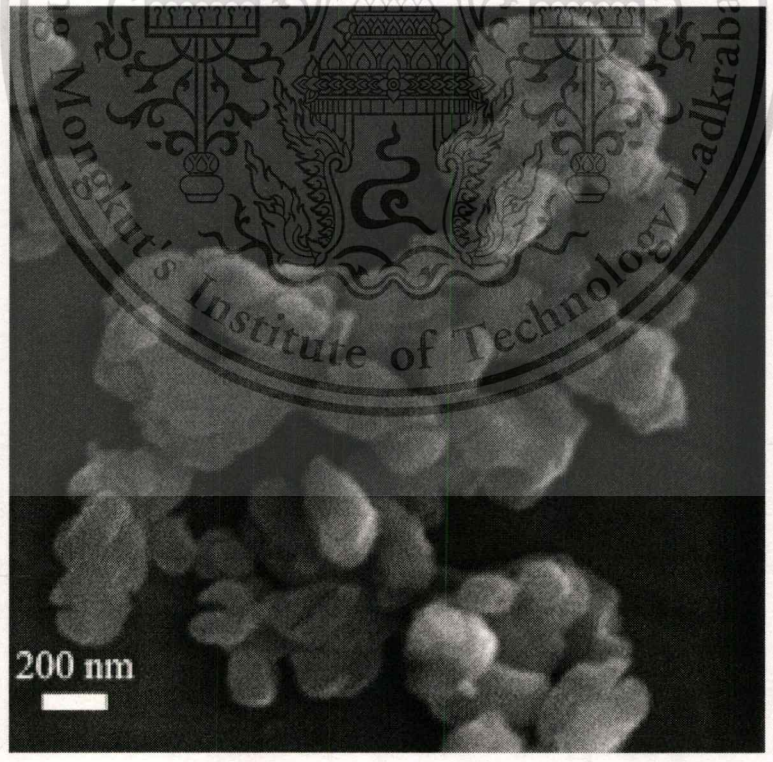

Figure 4.5 SEM micrographs showing $NaNbO_3$ powders synthesized at 475°C for 60 min, with a heating/cooling rate of 20°C/min.

4.1.4 Conclusions

Crystalline powders of sodium niobate $NaNbO_3$ were synthesized from a modified solid state reaction of $Na_2C_2O_4$ and Nb_2O_5. This method is an excellent, simple and cost effective way to prepare stoichiometric, homogeneous, and fine powders. The perovskite phase of $NaNbO_3$ was successfully synthesized at the low temperature of 475°C for 1 h, with an average crystallite size of 25.89 ± 5.64 nm. This temperature is about 275°C lower than that used in the conventional method, which lies in the 750°C range. As dwell time increased, XRD peaks became narrower, and a pattern similar to that expected for orthorhombic $NaNbO_3$ was achieved, as indicated by the separate peaks. The resulting $NaNbO_3$ powders comprised agglomerated particles of 180 to 360 nm in size.

4.2 Synthesis of potassium niobate ($KNbO_3$) nano-powder by a modified solid state reaction

Overview - Crystalline lead-free piezoelectric potassium niobate ($KNbO_3$) powders have been synthesized through a modified solid state reaction method. The thermal behavior of the $K_2C_2O_4 \cdot H_2O$ and Nb_2O_5 raw material mixture was investigated by thermogravimetric analysis (TGA) and differential thermal analysis (DTA). The X-ray diffraction technique (XRD) was used to investigate the phase formation and purity. The morphology of the powder obtained was characterized using a scanning electron microscope (SEM). The XRD pattern showed that the monophasic perovskite phase of $KNbO_3$ could be synthesized successfully at a temperature as low as 550°C for 240 min, with an average crystallite size of 37.27 ± 10.84 nm. The SEM images suggested that the average particle size of the powder obtained was 278 ± 75 nm.

4.2.1 Introduction

Lead zirconate titanate (PZT) ceramics are used widely in piezoelectric applications, due to their superior piezoelectric properties near the morphotropic phase boundary (MPB) [1, 116]. However, more than 50% of the lead-based piezoelectric material contains poisonous lead, which is a major drawback [2]. It has been reported that the use of lead-based ceramics causes serious environmental problems and numerous physical symptoms [2]. Furthermore, EU legislation will enforce draft directives for waste from electrical and electronic equipment (WEEE); and restrictions on the use of certain hazardous substances in electrical and electronic equipment (RoHS) and end-of life vehicles (ELV) [3-4, 117]. According to these issues, lead and other heavy metals should be phased out, and alternative lead-free piezoelectric materials are receiving considerable attention. Among various alternative families, perovskite type (ABO_3) ceramics have attracted much consideration. Among alkali metal niobates, potassium niobate ($KNbO_3$) is a well-known perovskite oxide that possesses attractive physical and piezoelectric properties [117-119]. Furthermore, the electromechanical coupling factor of the thickness extensional mode, k_t, was reported to reach as high as 0.69 for the 49.5°-rotated X-cut on the Y-axis. This value of k_t is the highest among current lead-free piezoelectrics [5]. However, the main hindrance regarding this alkali niobate-based material lies in the difficulty of preparing dense and stoichiometric controlled ceramics using the conventional solid state reaction and ordinary air sintering methods

[120-121]. These difficulties are caused by potassium volatility at high temperatures and excessive reactivity with moisture [122-123]. Thus, different additive methods, hot pressing and spark plasma sintering have been used to improve ceramic densification [41, 66, 121, 124-126]. Several alternative ways for preparing alkali niobates have been investigated and developed: the hydrothermal [127], nitrate–tartarate precursor technique [128], hydrothermal-assisted sol–gel method [129], and glycothermal [130], etc. However, most chemical synthesis routes require high purity reactants, which are more expensive and demand complicated procedures and specific apparatus. A modified solid state reaction method has been used to synthesize the $NaTaO_3$ perovskite type material successfully, with reduced reaction temperature [18]. In this method, the carbonate compound was replaced by oxalate, and the addition of urea played an important role. Recently, this method also has been applied to synthesize lead-free sodium niobate ($NaNbO_3$) powders (without fuel) [131]. By replacing sodium carbonate using oxalate as the raw material, a lower calcination temperature and fine powders with an average crystallite size of 31.45 ± 5.28 nm were achieved.

In this study, a modified solid state reaction method, with an expected lower reaction temperature, was used to synthesize $KNbO_3$ particles, using potassium oxalate as raw material without the addition of any fuel. Effects of the calcination conditions on the $KNbO_3$ phase development were investigated by the X-ray diffraction technique (XRD), the Fourier transform infrared (FTIR) spectroscopy and a scanning electron microscope (SEM).

4.2.2 Experimental procedure

$KNbO_3$ was synthesized by a modified solid state reaction method. Reagent-grade potassium oxalate monohydrate ($K_2C_2O_4 \cdot H_2O$, 99.9%) and niobium oxide (Nb_2O_5, 99.9%) were employed as the starting material. The raw materials were weighed in stoichiometric quantities following the equation below.

$$K_2C_2O_4 \cdot H_2O_{(s)} + Nb_2O_{5(s)} \rightarrow 2KNbO_{3(s)} + CO_{2(g)} + CO_{(g)} + H_2O_{(g)} \qquad (4.7)$$

These starting materials were mixed by the ball-milling method using ethyl alcohol and partially stabilized zirconia balls for 18 h. Then, the mixture was dried on a hot plate with regular stirring for a suitable period. After drying, the precursor mixture was determined by thermo gravimetric analysis (TGA, Perkin Elmer) and differential thermal analysis (DTA, Perkin Elmer) for investigating the thermal behavior during heat treatment and finding the appropriate calcination temperature. Based on TG-DTA results, the mixture was placed subsequently in a closed alumina crucible, and calcined for different periods of time at various temperatures ranging from 300 to 700°C, to investigate formation of the $KNbO_3$ phase. Subsequently, calcined powders were inspected by room temperature X-ray diffraction (XRD, Advance D8), using Ni-filtered CuK_α radiation to examine the effect of thermal treatment on the phase development and optimal calcinations condition of crystalline $KNbO_3$ powder formation. The room temperature FTIR spectra were recorded in the range of 4,000-400 cm^{-1} (Perkin-Elmer, Spectrum GX spectrometer), with eight scans and a resolution of 4 cm^{-1} using KBr pellets. Powder morphologies and particle size were figured directly using a scanning electron microscope (SEM, Hitachi S4700).

4.2.3 Results and discussion

Figure 4.6 shows the TG-DTA curves of the stoichiometric precursor of $KNbO_3$. The thermogravimetric (TG) curve of the $KNbO_3$ precursor shows three stages of weight loss from room temperature to 1,300°C. Four endothermic peaks at 123, 398, 524 and 1,066°C were observed in the differential thermal analysis (DTA) curve. Three weight loss steps were observed in the ranges of 50-121, 121-172, and 416-532°C. The corresponding weight losses seen were 3.92, 1.07, and 16.00%. The overall weight loss was found to be about 21%, which is close to the theoretical value of 20.01%, and corresponds to the release of 1 mol H_2O, 1 mol CO, and 1 mol CO_2 related to Eq. 4.7. In the temperature range from 50 to 121°C (first stage), the initial weight loss of 3.92% showed decomposition of the oxalate molecule releasing water molecules (0.98 mol H_2O), which concurred with the theoretical value for releasing 1.00 mol H_2O (4.00%). This weight-loss corresponded to the endothermic peak, centered at 123°C. The second and third weight-loss steps illustrated the highest weight loss (~17%), which indicated a large elimination

of organic compound that could be related to the release of CO and CO_2 by combustion reactions according to Eqs. 4.8 and 4.9 (16% theoretically). In the temperature range from 121 to 532°C, the DTA curve shows corresponding endothermic peaks (398 and 524°C) that agree with the TG result.

$$K_2C_2O_{4(s)} \rightarrow K_2CO_{3(s)} + CO_{(g)} \quad (4.8)$$

$$K_2CO_{3(s)} \rightarrow K_2O_{(s)} + CO_{2(g)} \quad (4.9)$$

However, an exothermic DTA peak was found centered at 565°C. This implied that the third decomposition stage could lead to the formation of potassium niobate compound, which could be expected from the exothermic peak at 565°C (as confirmed by XRD analysis in Fig. 4.7). As the temperature increased to 695°C, weight loss was found to start again in the TGA curve, which could be correlated to the decomposition of the activated-K_2CO_3 residue. It is well known that $K_2C_2O_4$ decomposes to K_2CO_3 at a higher temperature; however, this carbonate residue could decompose at a lower temperature when its degree of arrangement is lower than its initial state [104]. When heating further, an endothermic peak (without the observed weight-loss stage) could correspond to the phase transformation at 1,066°C. Therefore, temperatures from the above TG-DTA analysis, which ranged from 300 to 700°C, were selected for calcinations and investigation of the phase formation. The mixture of raw materials in the required stoichiometric ratio was calcined in air using a heating/cooling rate of 20°C/min at various temperatures and followed by the phase analysis using an X-ray diffractometer.

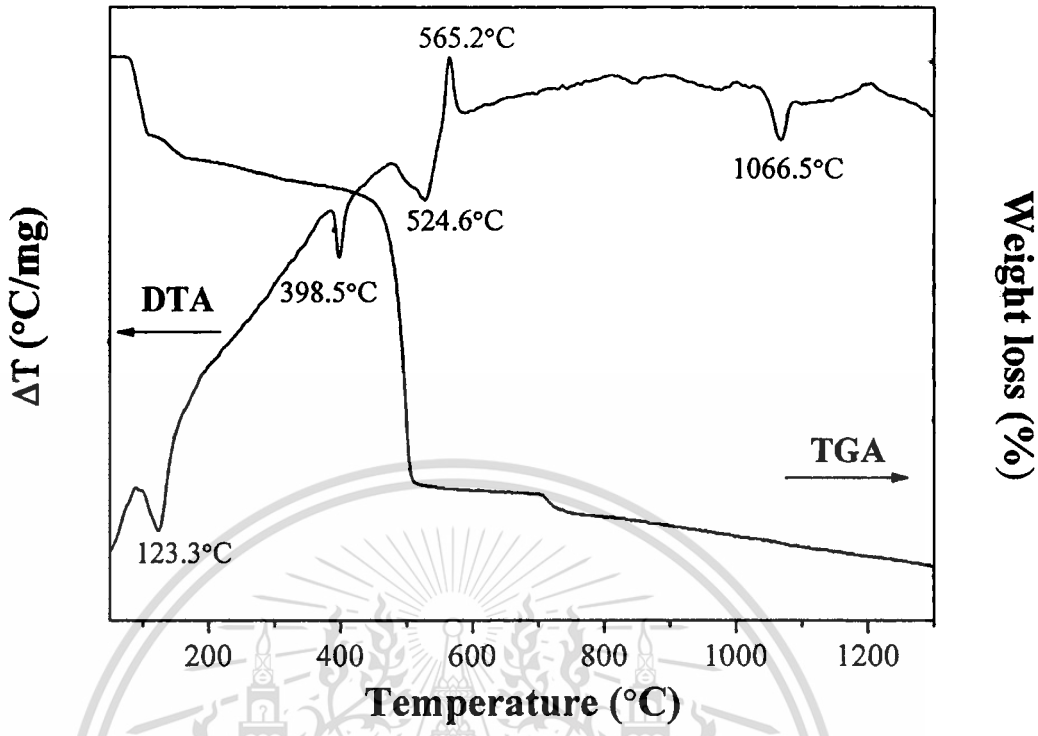

Figure 4.6 TG–DTA curves of an uncalcined powder mixed in the stoichiometric proportion of $KNbO_3$.

The X-ray diffraction (XRD) patterns of potassium niobate ($KNbO_3$) powders, calcined for 4 h at different temperatures, are illustrated in Figure 4.7. The diffraction pattern of the powder calcined at 300°C suggests a composition of potassium oxalate (◇) (JCPDS no.22-1232) and niobium oxide (●) (JCPDS no.30-0873) raw materials. No evidence of the $KNbO_3$ perovskite phase was found. As calcination temperatures increased to 500°C, diffraction peaks of un-reacted raw materials were also found, but with lower intensity. This could demonstrate that the completed reaction cannot occur at such a low temperature range. As the diffusion coefficient is a temperature dependent parameter, the rate of diffusion is affected greatly by higher temperatures [104], which also could improve higher atomic mobility [110]. Nonetheless, the powders calcined from 550 to 700°C showed diffraction peaks that could correspond to the orthorhombic potassium niobate perovskite phase ($KNbO_3$) JCPDS no.32-0822 (▼). Amplified peak intensities can be seen after calcinations at increased temperatures. However, this result

indicates the formation of $KNbO_3$ perovskite phase powder, which passes through the calcination temperatures from 550 to 700°C in 4 h. These temperatures were lower than those in the chemical synthesis of $KNbO_3$,, which used the polymerized complex method (PC method). This technique achieved the $KNbO_3$ compound after the calcination step at 900°C [132], or once the citrate precursor route had obtained $KNbO_3$ nanopowder after heat treatment at 800°C [133]. In addition, other chemical methods always require high purity reagent, which is more expensive, and involves complex procedures. For a verdict on fine $KNbO_3$ nucleation condition, a temperature of 550°C was chosen to find the effect of calcination dwell time. The mixture of raw material powder was calcined at 550°C for 15-360 min. The XRD analysis of calcined powder, with a different dwell time (Figure 4.8), revealed an amorphous phase for a calcinations period of 15 min, and no distinct crystalline phase could be detected. The absence of reflection peaks that correspond to $K_2C_2O_4{\cdot}H_2O$ and Nb_2O_5 indicated the amorphous nature of the powder obtained. The presence of reflection peaks for the XRD pattern of powder calcined at 550°C for 20 min or longer could be ascribed to the crystalline phase of the sample. The different diffraction pattern of the powder, calcined for 20 min, suggests the nucleation condition of the $KNbO_3$ phase, which was confirmed by further soaking time. After the calcination step at 550°C for 20 min or longer, the powder showed an XRD pattern that could be matched with the perovskite potassium niobate (KN) phase JCPDS no.32-0822. These XRD analyses agreed with the TG-DTA analysis, in which crystallization of the $KNbO_3$ phase was found around the previously mentioned temperature range. During the course of calcinations, the rise in calcination temperature and dwell time resulted in increased diffraction peak intensities, which related to higher crystallinity of the powder. This was supported by the increase in lattice parameters and average crystallite size, as revealed below. Nevertheless, it has been confirmed that this modified solid state reaction method can synthesize pure $KNbO_3$ phase powder by using potassium oxalate monohydrate as starting material at the calcinations temperature of 550°C for 20 min. This calcination temperature is much lower than that used in a mixed oxide powder process, which lies in the range of 800°C [50, 119-120, 122, 134], or solution process (sol-gel and precipitation methods) that requires calcination temperatures of over 600°C [135-136].

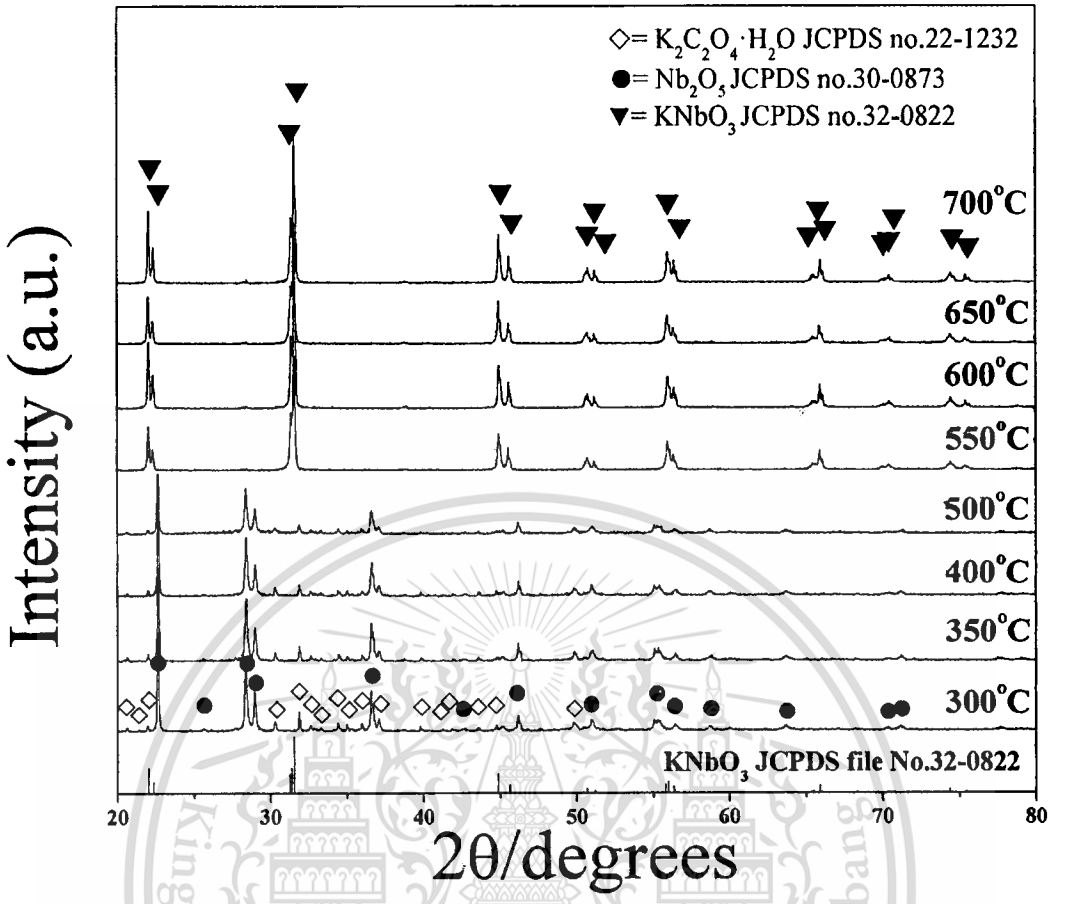

Figure 4.7 X-ray diffraction patterns of $KNbO_3$ powder calcined at various temperatures for 4 h with a heating/cooling rate of 20°C/min.

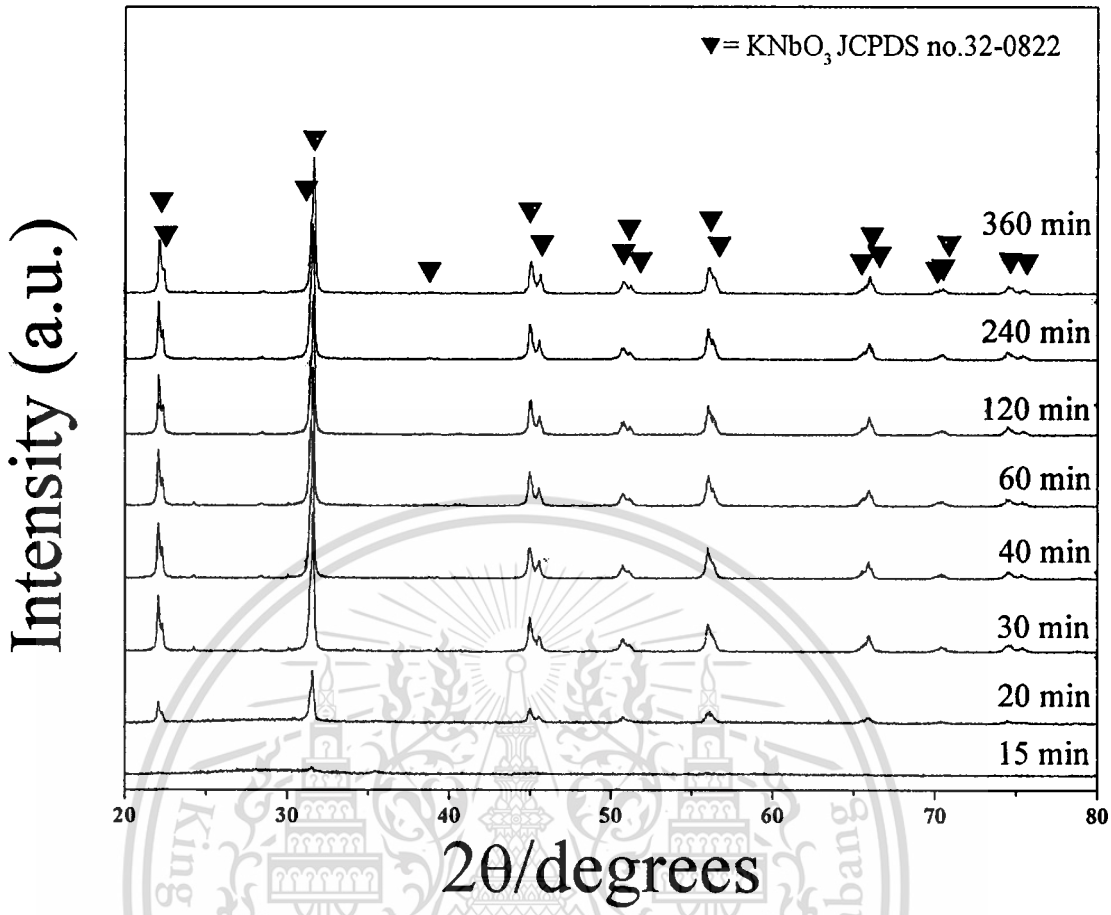

Figure 4.8 X-ray diffraction patterns of $KNbO_3$ powder calcined at the calcination temperature of 550°C for various dwell times with a heating/cooling rate of 20°C/min.

Since XRD analysis suggested an orthorhombic crystal structure for preparing $KNbO_3$ powder, lattice parameters of the sample could be deliberate by means of the UnitCell program package (ftp://rock.esc.cam.ac.uk/pub/minp/UnitCell/). The corresponding cell parameters, which are close to those reported from JCPDS file No.32-0822 (a = 5.695 nm, b = 5.721 nm, and c = 3.973 nm) are given in Table 4.2. The suggested orthorhombic crystal structure, obtained from matching with the JCPDS file, could be supported by this correlation of lattice parameters. The average crystallite size of $KNbO_3$ powders was considered as a function of calcination temperature, and time for broadening the X-ray line of the reflection peak using Scherrer's equation [97]:

$$D = \frac{k\lambda}{\beta \cos \theta_B} \tag{4.10}$$

where D is the average crystallite size, k a constant taken as 0.94, λ the wavelength of X-ray radiation, β the full width at half maximum (FWHM), and θ_B the diffraction angle. The corresponding values are reported in Table 4.3. The average crystallite size of powders, calcined from 550 to 700°C for 4 h, was found to be about 48.38 ± 11.48 to 53.47 ± 12.04 nm. As the dwell time increased, it was found that the average crystallite size of calcined powders was increasing from 34.68 ± 12.12 to 36.48 ± 10.67 nm. The low D values suggest that the surface area of calcined powder was high enough to support high sinterability sufficiently [105]. The increase in crystallinity of the $KNbO_3$ phase was affected by increasing dwell time and calcination temperature. This consequence may confirm that the dwell time and calcination temperatures also play an important role in developing the pure phase creation.

Table 4.2 Lattice parameters of the $KNbO_3$ powder calcined at various calcination temperatures for 4 h.

$KNbO_3$	Calcinations temperature °C			
Lattice parameter (Å)	550	600	650	700
a	5.6929±0.0005	5.6876±0.0070	5.7019±0.0022	5.6952±0.0028
b	5.6989±0.0080	5.6994±0.0048	5.7153±0.0108	5.6980±0.0060
c	3.9802±0.0005	3.9768±0.0006	3.9912±0.0155	3.9777±0.0030

Table 4.3 Mean crystalline size, D, of the $KNbO_3$ powder calcined at different temperatures for 4 h and for a different dwell time at 550°C.

$KNbO_3$	Calcination temperature °C					
	550	600	650	700		
D (nm)	36.40±8.25	41.46±8.84	53.59±6.56	57.81±6.31		
550°C	dwell time (min.)					
	20	30	40	60	120	240
D (nm)	33.15±9.22	34.36±7.92	34.54±8.128	35.30±8.30	35.97±6.47	36.40±8.25

Figure 4.9 shows the FTIR spectroscopic studies of the crystalline potassium niobate ($KNbO_3$) before and after the calcination step. The IR band for the uncalcined precursor was observed at 3,253 cm^{-1}, due to O–H asymmetric stretching (ν_3), which related to the moisture content of the KBr pellet and scissor bending mode (ν_2) of HO–H at 1,600 cm^{-1} and 1,310 cm^{-1}. When $KNbO_3$ powders were calcined at 550°C for 4 h, the absorption of bands at a low wave number range of 620 cm^{-1} suggested occurrence of Nb–O bond formation, which was believed to be the vibration (ν_3) mode in the corner-shared NbO_6 octahedron, according to the reported IR spectra of niobate glass ceramics [137]. This result shows that the perovskite $KNbO_3$ phase was synthesized, which correlated with other results. The TG result indicated that the mass loss in the TG curve at around 700°C could be the result of the K_2CO_3 residue decomposition, however, the FTIR band corresponding to the C–O stretching mode of carbonate at 1,450 cm^{-1} [138] was not found in $KNbO_3$ powders calcined at 550°C for 4 h. This observation could be described as the effect of dwell time. Figure 4.10 shows SEM micrographs of $KNbO_3$ powder prepared using a modified solid state reaction method at 550 and 700°C for 240 min. The $KNbO_3$ powder was found to be polyhedral in shape, with uniform features. The secondary phase could not be observed, which suggested the homogeneous character of the powder prepared. The mean particle sizes, which can be estimated from the micrographs, were found to be 278 ± 75 nm and 341 ± 80 nm for powder obtained at 550 and 700°C, respectively. Particle growth was detected in powder calcined at a higher temperature. This value is greater than the average crystallite size, calculated from X-ray line broadening. It was believed that this contradictory value could indicate the agglomerate of the calcined powders. As reported by other studies [138-140], the firing process tends to produce agglomerated particles and grain growth. No evidence of a different or pyrochlore phase was found. This outcome relates to the XRD result, in which the monophasic perovskite phase of $KNbO_3$ can be established after calcinations at 550°C for 240 min.

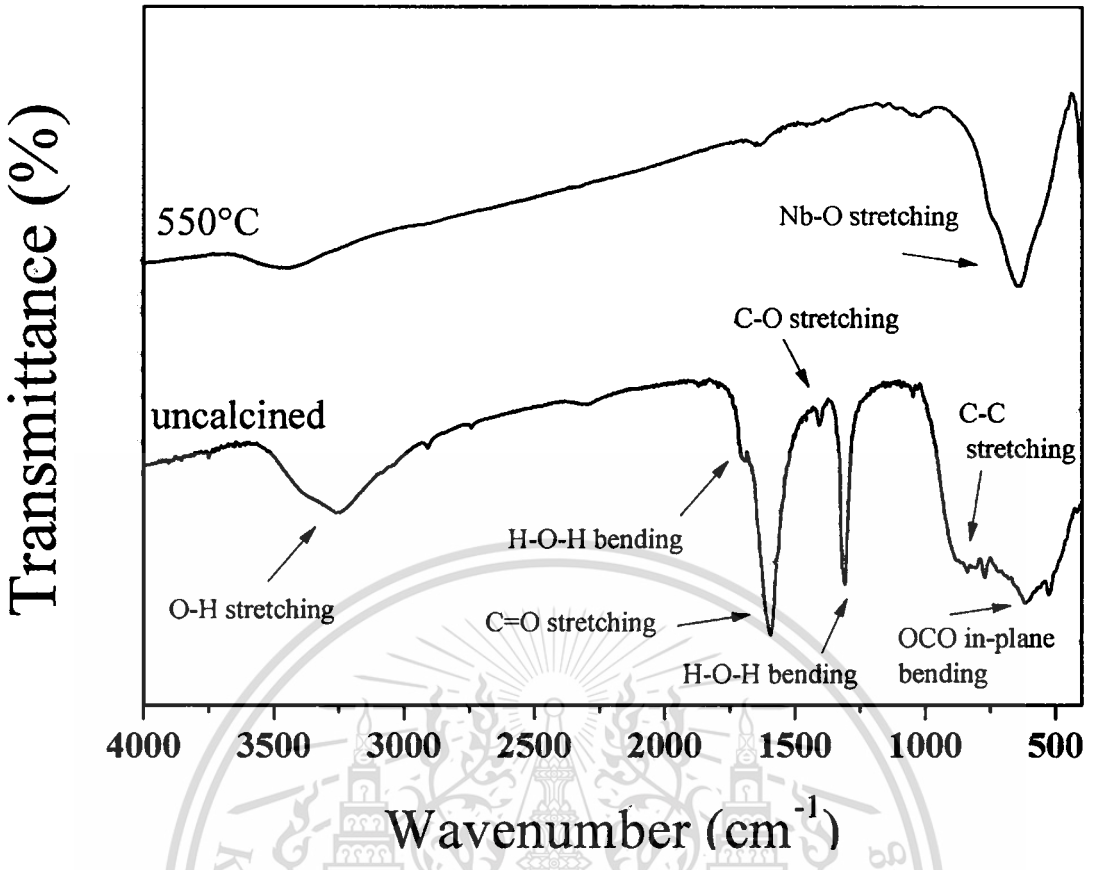

Figure 4.9 FT-IR spectra of an uncalcined powder mixed in the stoichiometric proportion of $KNbO_3$ and $KNbO_3$ particles calcined at 550°C.

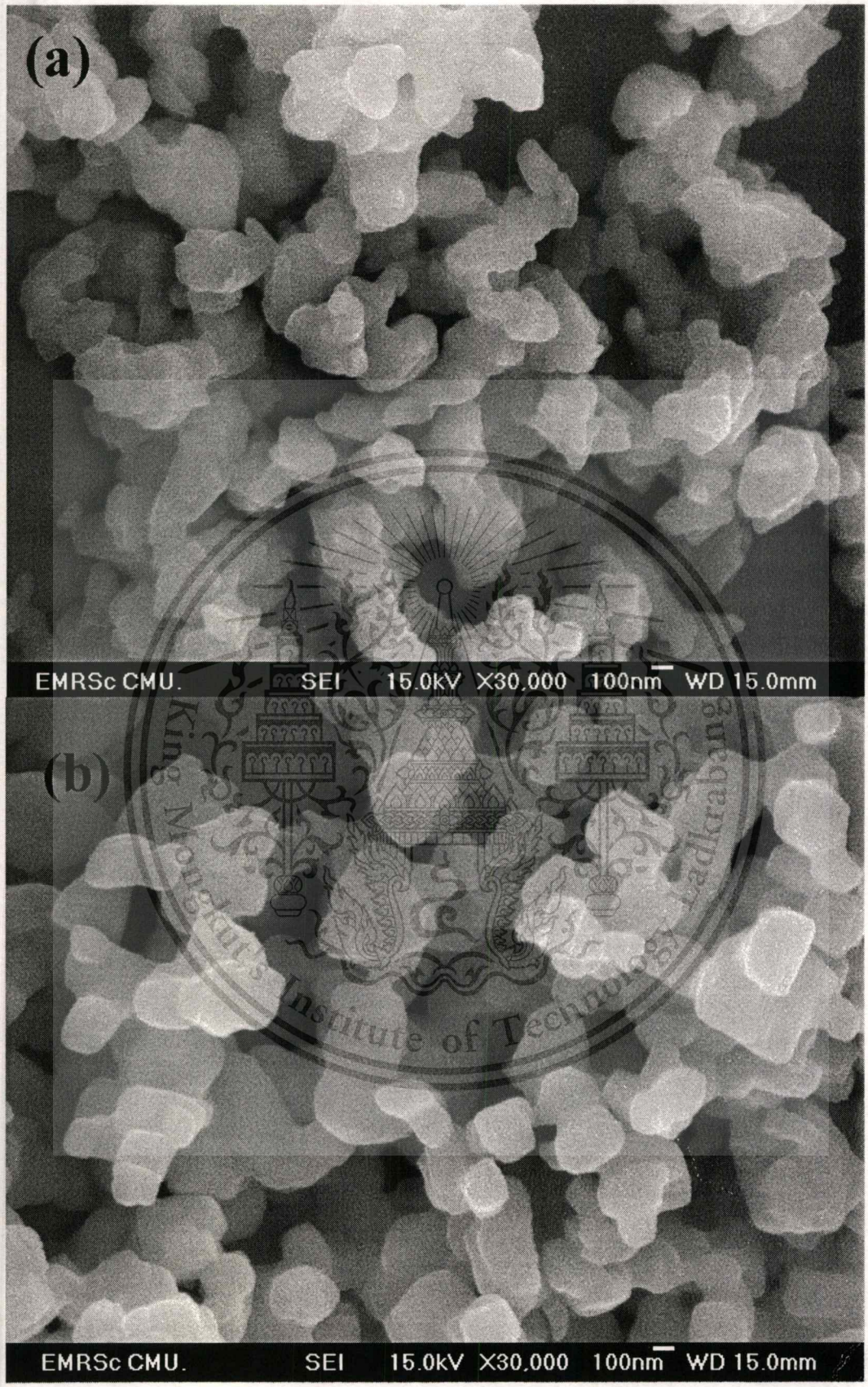

Figure 4.10 SEM micrographs showing $KNbO_3$ powder synthesized at 550°C (a) and 700°C (b), for 4 h with a heating/cooling rate of 20°C/min.

4.2.4 Conclusions

Crystalline $KNbO_3$ powder was prepared from a modified solid state reaction of $K_2C_2O_4 \cdot H_2O$ and Nb_2O_5. The final product was confirmed by XRD and SEM techniques. This is a simple cost- and time-saving method for synthesizing stoichiometric, homogeneous, and fine $KNbO_3$ powder, with a low calcination temperature of 550°C for 240 min. This temperature is about 250°C lower than others used, even in conventional methods. The powder obtained was found to be a uniform agglomerated particle that possesses an average crystallite size (defined by XRD) of between 48.38 ± 11.48 nm and 53.47 ± 12.04 nm, and a mean particle size (defined by SEM micrograph) of 278 ± 75 nm.

4.3 Solution combustion synthesis and characterization of lead-free piezoelectric sodium niobate ($NaNbO_3$) powders

Overview - Nano-crystalline sodium niobate ($NaNbO_3$) powder was synthesized by the solution combustion synthesis of sodium nitrate ($NaNO_3$) and Nb_2O_5 using glycine as the fuel. The chemical reaction, nucleation mechanisms and influence of the fuel-to-oxidizer ratio to phase formation were studied. The precursor and product powders were characterized, using thermo gravimetric analysis (TGA), differential thermal analysis (DTA), the X-ray diffraction technique (XRD), scanning electron microscope (SEM) and Fourier transform infrared (FTIR) spectroscopy. As-prepared powder possesses an orthorhombic crystal structure with an X-ray diffraction pattern that could be matched with the perovskite, $NaNbO_3$ JCPDS no. 82-0606. Perovskite $NaNbO_3$ phase, with a mean crystalline size (calculated by X-ray line broadening) ranging from 47.01 ± 12.66 nm (ratio of 0.7) to 27.58 ± 14.45 nm (ratio of 2.0) was obtained. The SEM image shows polyhedral-shaped powder with a mean particle size of 137 ± 52 nm and 226 ± 46 nm for as-prepared and calcined powder, respectively.

4.3.1 Introduction

Sodium niobate ($NaNbO_3$) is a perovskite with an inorganic complex oxide and the empirical formula, ABO_3. It is among the candidates for lead-free substances that avoid toxicity of leadbased piezoelectric materials (e.g. PZT [29, 141]), and is concerned about the environment. $NaNbO_3$ has been studied widely for its unusual structural transition series [6-9, 131]. It has a ferroelectric rhombohedral phase below -100°C, and is antiferroelectric with orthorhombic symmetry between -100°C and 640°C [6]. Finally, it possesses cubic paraelectric above 640°C [7], and in addition, its antiferroelectric, perovskite-type nature can transform into a ferroelectric one by chemical doping, i.e. K^+ [8-9] and Li^+ [12]. Generally, alkali niobate powders are synthesized by conventional solid state reaction, where alkali metal carbonate or oxide compound of starting materials are heated at high temperature (800°C or above) for a long duration [12-13]. High calcination temperature can cause volatilization of alkali metal, thus causing this classical

method difficulty in achieving a homogeneous mixture of the component [12-14]. Powder agglomeration can occur during heating, which could affect properties such as low surface area and low sinterability [14]. Thus, this method does not always allow for the production of dense, homogeneous single phase ceramics. Therefore, development of alternative methods that can produce powder with high sinterability and controlled stoichiometric composition is necessary. In recent years, ultra fine ceramic powder, which is synthesized using mechanochemical synthesis [15], polymeric precursors [16], and hydrothermal and polymerized complex methods [17], has been described in the literature to enable production of desired compositions. While synthesizing powder rapidly, with the desired composition, high porosity and high sinterability remains a challenge, combustion synthesis (CS) has been found as a potential solution for this problem. Combustion synthesis (CS) or self-propagating high temperature synthesis (SHS) is an effective, low-cost method for producing various industrially useful materials. It has been introduced as a quick, straightforward preparation process for producing homogeneous, very fine, crystalline and unagglomerated multicomponent oxide ceramic powders, without intermediate decomposition and/or calcination steps [19-20]. The combustion synthesis technique begins with a mixture of easily oxidized reactants (such as nitrates) and a suitable organic fuel (such as urea [21], tartalic acid [22], alanine [23], glycine [24], etc.), which acts as a reducing agent. The mixture is then heated until it ignites, which is when the temperature of rapid exothermal chemical reaction commences, and a self-sustaining combustion reaction starts. This highly exothermic reaction produces a high temperature and duration long enough for the synthesis to occur, even in the absence of an external heating source [25]. Ultrafine nano-sized powder also can be prepared by releasing a large amount of gas from the system. This process results in a dry, fluffy, crystalline, unagglomerated and fine oxide powder. Metal nitrate was found to be the salt preferred, due to its water solubility, and homogeneous solution could be achieved easily by melting at a low temperature [21]. However, it was reported that an exothermic redox reaction (oxidation and reduction reaction taking place simultaneously) could be initiated only when the oxidizer and fuel are mixed intimately in a fixed proportion. The basis of the combustion synthesis process derives from the thermochemical concepts used in propellant chemistry [86, 142]. The method consists of

establishing a simple valency balance, irrespective of whether the elements are present in the oxidizer or fuel components of the mixture, and then calculating the stoichiometric composition of the starting mixture, which is equivalent to the release of maximum energy. The assumed valencies, which are presented as usual products of the combustion reaction, consist of CO_2, H_2O and N_2. Therefore, carbon and hydrogen are considered as reducing elements with the corresponding valencies of +4 and +1, whereas oxygen is thought to be an oxidizing agent with a valency of –2, and nitrogen a valency of 0. To extrapolate the concept of combustion synthesis of ceramic oxide meansconsidering metals as reducing agents with their valencies in the corresponding oxide or nitrate, i.e. +2 for magnesium (oxide), +3 for cerium (nitrate) and +4 for cerium (oxide). In the case of multiple valence elements, the final product is used for calculation. The elemental stoichiometric coefficient, □, which is the ratio between the total valencies of fuel (glycine; NH_2CH_2COOH) and that of the oxidizer (sodium nitrate), can be calculated following the method proposed by Jain et al. [86]:

$$\phi = n\frac{(0_{(N)}+2\times1_{(H)}+4_{(C)}+2\times1_{(H)}+4_{(C)}-2_{(O)}-2_{(O)}+1_{(H)})}{1_{(Na)}+0_{(N)}-2\times3_{(O)}} \quad (4.11)$$

where n is the mole of glycine. According to the propellant chemistry for stoichiometric redox reaction between fuel and an oxidizer, the □ ratio should be united (stoichiometric). A □ < 1 means oxidant-rich condition and □ > 1 means fuel-rich condition. To satisfy the principle in the present system, the sodium nitrate (oxidizing valency = 5–) to glycine (reducing valency = 9+) molar ratio was found to be 1:0.56. The comprehensive reaction that formed $NaNbO_3$ can be written as:

$$18NaNO_{3(aq)} + 9Nb_2O_{5(s)} + 10NH_2CH_2COOH_{(aq)} \longrightarrow$$

$$18NaNbO_{3(s)} + 25H_2O_{(g)} + 14N_{2(g)} + 20CO_{2(g)} \quad (4.12)$$

It should be noted that various fuel-to-oxidizer ratios should be carried out for investigating and comparing the effect of fuel-rich/ fuel-lean mixtures on the synthesis of sodium niobate powder. In this study, sodium niobate powder was synthesized via the combustion synthesis technique for

the first time. This process used sodium nitrate and niobium pentoxide as starting materials, and glycine was used as fuel. The different fuel-to-oxidizer molar ratios such as fuel-deficient (< 0.56), equivalent stoichiometric (0.56) and fuel-rich (> 0.56) condition were applied.

4.3.2 Experimental procedure

For the combustion synthesis of perovskite sodium niobate powder, AR grade sodium nitrate ($NaNO_3$ 99.5%) and niobium pentoxide (Nb_2O_5 99.95%) were used as the oxidizer, and glycine (NH_2CH_2COOH 99.7%) as fuel. The appropriate amount of starting materials was weighed, mixed with de-ionized water in a glass beaker and stirred regularly for 30 min. The fuel (glycine) was then added and the mixture stirred for 30 min. After that, the solution precursor was boiled on a hotplate and then evaporated. Once the solution had thickened and begun to dry, the ignition took place when the temperature rapidly increased, which resulted in self-sustaining combustion with rapid evolution of a large volume of gas products, and formation of voluminous powder. For investigating thermal behavior of the precursor, the mixture of starting material was determined using thermo gravimetric analysis (TGA) and differential thermal analysis (DTA). The X-ray diffraction (XRD, Advance D8) technique was carried out on the combustion synthesized powder, using Ni-filtered CuK_α radiation for phase identification and mean crystalline size estimation. The final powder product was characterized by using the Fourier transform infrared (FTIR) technique and scanning electron microscope (SEM, Hitachi S4700).

4.3.3 Results and discussion

Figure 4.11 shows the TG/DTA plots of the stoichiometric precursor for $NaNbO_3$ powder synthesis. From observations of the TGA curve, there appeared to be three-stages of weight loss from room temperature to 800°C. The definition of initial temperature (T_{in}) is when the sample weight starts changing rapidly during the chemical reaction [143]. As the precursor was heated, a significant weight loss was observed as the temperature reached 170°C, indicating that the T_{in} was around this heat. The weight loss did not stop until the temperature reached 480°C. It was indicated clearly that this reaction belongs to a multi-stage reaction. The overall weight loss was

found to be about 40%, which is close to the theoretical value of 36.87% that corresponds to the release of 50 mol H_2O, 28 mol N_2 and 40 mol CO_2 related to Eq. (4.12). This outcome supported our conception that a hotplate can be used as a heating source because it is capable of initiating the combustion reaction at a temperature as low as that of the T_{in}. The evolution XRD pattern of the combustion synthesized ceramic powder, with the fuel-to-oxidizer molar ratio, is illustrated in Figure 4.12. The fuel-deficient (0.5) and equivalent stoichiometric ratio (0.56), were found (according to experimental observation) to have no ignition and combustion reaction in those compositions. Their XRD patterns correlated to detection results of the diffraction peaks of Nb_2O_5 (●) (JCPDS file no. 30-0873) and $NaNO_3$ (■) (JCPDS file no. 85-0859) starting materials, with no evidence of perovskite $NaNbO_3$ phase found. Although the equivalent stoichiometric ratio (0.56) was calculated for maximum energy release, auto-ignition did not occur in this study. This could indicate that oxygen deficiency in the system and its environment might lead to combustion reaction and fail to follow the theory. The fuel-to-oxidizer molar ratio was increased by using the fuel-rich condition (> 0.56), which was found to produce the perovskite $NaNbO_3$ ceramic powder, due to its diffraction peaks being detected for all different fuel contents (fuel-to-oxidizer molar ratio ranging from 0.7 to 2.0). This $NaNbO_3$ phase (▼) was consistent with JCPDS file no. 82-0606, which corresponded to an orthorhombic structure with the space group, $P2_1ma$ (26). For a fuel-rich condition (fuel-to-oxidizer molar ratio of 0.7, 0.8 and 0.9), the $NaNbO_3$ phase (▼) was detected with the accompanying pyrochlore phase of $Na_2Nb_4O_{11}$ (◆), which matched JCPDS file no. 20-1145. No evidence of unreacted Nb_2O_5 and/or $NaNO_3$ diffraction peak was found. As fuel content increased from the fuel-to-oxidizer molar ratio of 1.0-2.0, unreacted Nb_2O_5 (●) (JCPDS file no. 30-0873) was found together with a majority of $NaNbO_3$ diffraction peaks.

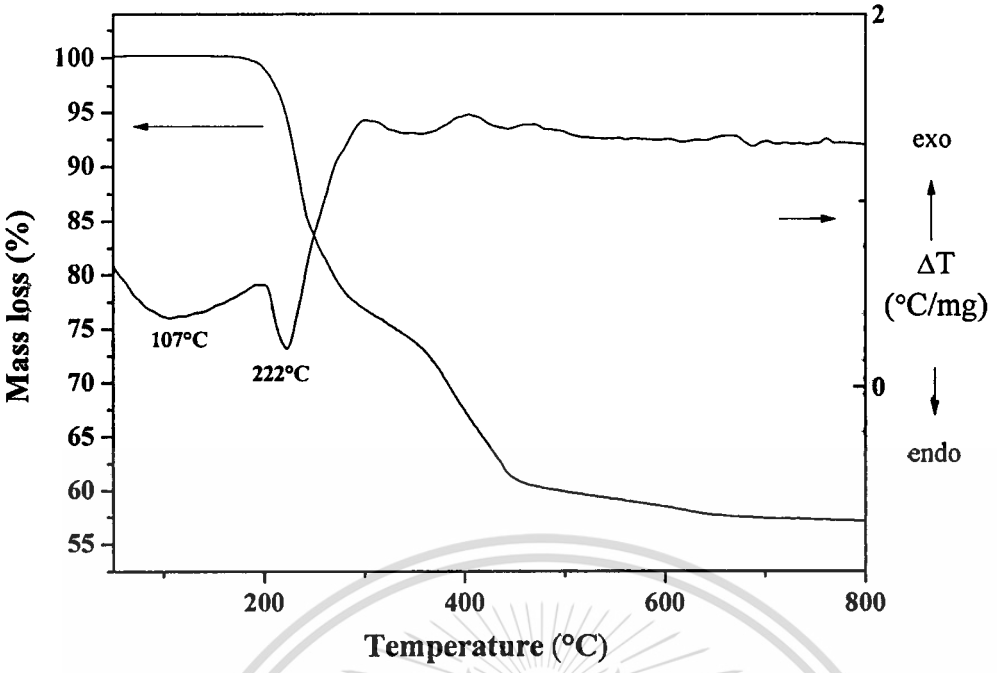

Figure 4.11 TG-DTA curves of the precursor mixed in the stoichiometric proportion of $NaNbO_3$.

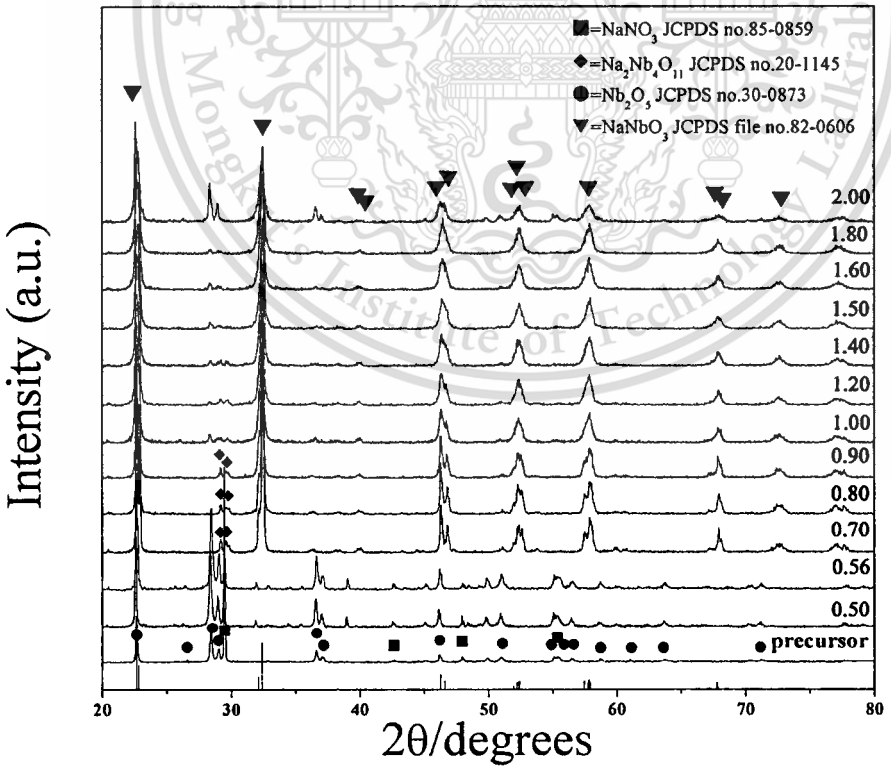

Figure 4.12 X-ray diffraction patterns of $NaNbO_3$ powder obtained from various fuel-to-oxidant molar ratios.

From the reflection peak, the average crystalline size (D) of $NaNbO_3$ powders was considered as a function of fuel content by using X-ray line broadening through Scherrer's equation [97]:

$$D = \frac{k\lambda}{\beta \cos\theta_B} \tag{4.13}$$

where D is the average crystalline size, k a constant taken as 0.94, λ the wavelength of X-ray radiation, β the full width at half maximum (FWHM) and θ_B the diffraction angle. The consequent values are reported in Table 4.4. As the fuel content increased, the average crystalline size (D) was found to decreased from 47.01 ± 12.66 nm (ratio of 0.7) to 27.58 ± 14.45 nm (ratio of 2.0). This suggested that elevated fuel content could lead to the production of a smaller crystalline size (related to a small particle size) of powder. Nevertheless, as a consequence of additional cost and more carbon residual, an extremely high fuel-to-oxidizer molar ratio (fuel-rich ratio) did not always result in the desired production of powder [144]. Therefore, from findings on the fine nucleation condition of monophasic $NaNbO_3$ phase, the fuel-to-oxidizer molar ratio of 1.0 was selected to investigate the effect of calcination temperature. From this ratio, the volume fraction of the perovskite phase formation (wt% perovskite) of as-prepared powder was found to be as high as 93%. This relative value was considered by approximately calculating the ratio of the main X-ray peak intensities of $NaNbO_3$ and Nb_2O_5 phases [96], according to the following equation;

$$\text{wt\% perovskite} = I_{\text{perovskite}}/(I_{\text{perovskite}}+I_{Nb_2O_5})\times 100\% \tag{4.14}$$

Thus, the as-prepared powder was calcined at different temperatures for 4 h with a heating/cooling rate of 20°C/min. The X-ray diffraction (XRD) patterns of sodium niobate ($NaNbO_3$) powder, calcined for 4 h at different temperatures, are illustrated in Figure 4.13. As the XRD pattern of as-prepared powder was composed of a slight Nb_2O_5 (●) (JCPDS file no. 30-0873) phase, the intensity of that phase was found to decrease with increasing calcination temperature. The diffraction peak corresponded to the Nb_2O_5, which disappeared after calcination

at 400°C for 4 h, whereas monophasic perovskite $NaNbO_3$ phase was obtained. This result suggested that the perovskite $NaNbO_3$ powder could be synthesized by using the combustion synthesis process and calcinations at 400°C for 4 h. This process was found to be a simple, rapid and cost-effective method when compared with the traditional solid state reaction, which takes longer time and requires higher temperature [12-13]. In addition, the mean crystalline size (D), which is reported in Table 4.4, was not significantly varied between as-prepared powder (30.71 ± 5.59 nm) and increasing calcination temperatures of up to 400°C (29.40 ± 7.52 nm). It can be suggested that calcinations at this low temperature also produced a lower crystalline size when compared with the traditional solid state reaction method.

Figure 4.14 shows the FTIR spectroscopic studies of the crystalline $NaNbO_3$ obtained after combustion synthesis, its precursor without heat treatment and powder calcined at 400°C for 4 h. For all powder, an IR band of around 3400 cm^{-1} was assigned to O–H asymmetric stretching (ν_3) [145], and on observation, it related to the moisture content of KBr. Regarding the precursor of $NaNbO_3$ powders without heat treatment, and as-prepared powder with a stoichiometric ratio (0.56), the IR spectrum indicated peaking of the characteristic band at ~1612, ~1385 and ~890 cm^{-1}, which corresponded to the anti-symmetric carboxyl group stretching vibration, anti-symmetry NO_3^{-1} stretching and bending vibration, respectively [145]. This result proved existence of the carboxyl and NO_3^{-1} group (belonging to the starting material) in those samples. With regard to fuel-rich ratios (0.7 and 1.2), the new broad absorption bands appeared after combustion at a low wave number of ~673 cm^{-1}, suggesting that the Nb–O bond formation did occur. This Nb–O bond was believed to be the vibration (ν_3) mode in the corner-shared NbO_6 octahedron, according to reported IR spectra of niobate glass ceramics [146]. This result led to the assumption that the perovskite $NaNbO_3$ phase was synthesized (which correlated to XRD analysis). However, the IR band of anti-symmetric COO^- and that of anti-symmetry NO_3^{-1} stretching vibration also were observed. This clearly indicated traces of existent carboxyl group and nitrate in as-prepared $NaNbO_3$ powder, which cannot be detected when using the XRD technique. For powder calcined at 400°C for 4 h, the spectra band of vibration (ν_3) mode belonging to the Nb–O bond was found

without observation of any starting material band. This can indicate that monophasic perovskite $NaNbO_3$ has been synthesized successfully after calcinations at a temperature as low as 400°C for 4 h. Figure 4.15 shows an SEM micrograph of the as-prepared $NaNbO_3$ powder using the fuel-tooxidizer molar ratio of 1.0 (a) and powder calcined at 400°C for 4 h (b). The powder was found to be polyhedral in shape, with uniform features. No evidence of a different or pyrochlore phase was found, which suggested the homogeneous character of the prepared powder. The average particle size, which can be estimated from micrographs, was found to be 137 ± 52 nm and 226 ± 46 nm for as-prepared and calcined powder, respectively. These particle size values are greater than the average crystalline size calculated from X-ray line broadening because a particle can be formed generally of many crystallites [147-149]. The particle growth for calcined powder seemed to be detected. It can be said that the firing process tends to produce agglomerated particles and grain growth, as reported by other works [139-140].

4.3.4 Conclusions

Crystalline $NaNbO_3$ powder, with a volume fraction of the perovskite phase formation (wt% perovskite) as high as 93%, was synthesized directly via the solution combustion process using $NaNO_3$, Nb_2O_5 and glycine. Monophasic perovskite $NaNbO_3$ powder was obtained after calcination at 400°C for 4 h. The fuel-to-oxidizer molar ratio was found to affect the combustion reaction and character of the powder obtained. The average crystalline size (D) was found to decrease from 47.01 ± 12.66 nm (ratio of 0.7) to 27.58 ± 14.45 nm (ratio of 2.0). This method is a simple, rapid, cost and time-saving way of synthesizing stoichiometric, homogeneous and fine $NaNbO_3$ powder with a low calcination temperature. The powder obtained was found to be a uniform soft agglomerated particle.

Table 4.4 Mean crystalline size, D, of $NaNbO_3$ powder obtained from various fuel-to-oxidant molar ratios.

As-prepared	Fuel-to-oxidant molar ratios								
	0.7	0.8	0.9	1.0	1.2	1.4	1.6	1.8	2.0
D (nm)	47.01±12.66	44.99±12.19	39.41±9.02	30.72±5.58	28.99±6.19	27.76±6.30	25.77±5.20	25.12±5.83	27.58±14.45
Calcined Powder	Calcination temperature °C								
	200	300	400	500	600	700	800	900	
D (nm)	31.63±4.77	33.28±4.24	29.40±7.52	32.55±5.73	41.02±8.55	64.13±8.54	74.85±9.74	90.06±16.52	

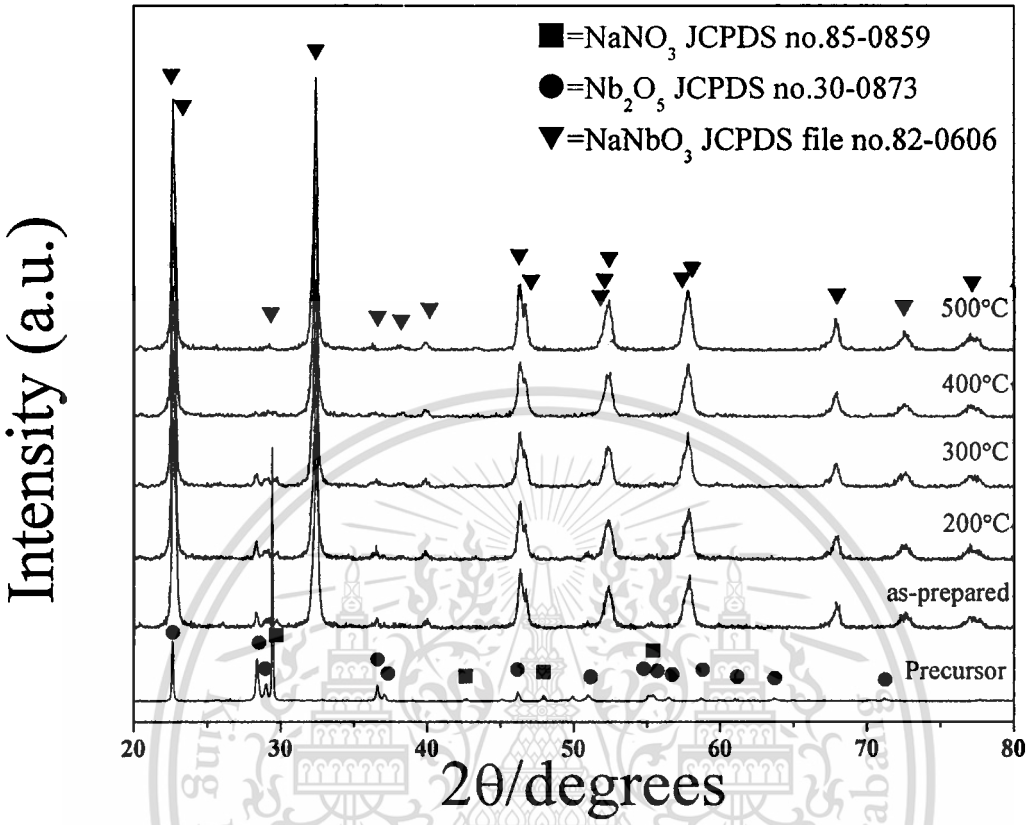

Figure 4.13 X-ray diffraction patterns of $NaNbO_3$ powder (obtained from the fuel-to-oxidant molar ratio of 1.0) calcined at various temperatures for 4 h with a heating/cooling rate of 20°C/min.

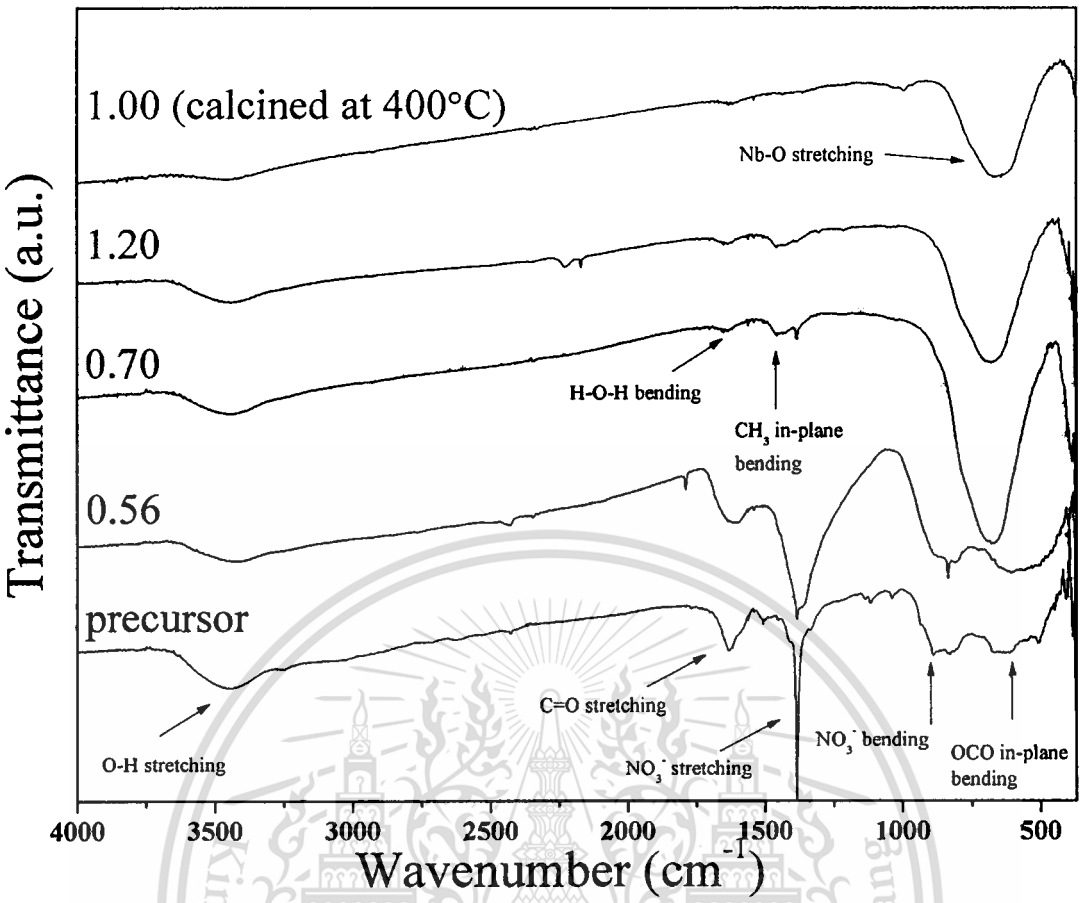

Figure 4.14 FTIR spectra of the precursor mixed in the stoichiometric proportion of $NaNbO_3$ powder obtained from various fuel-to-oxidant molar ratios and after the calcination step.

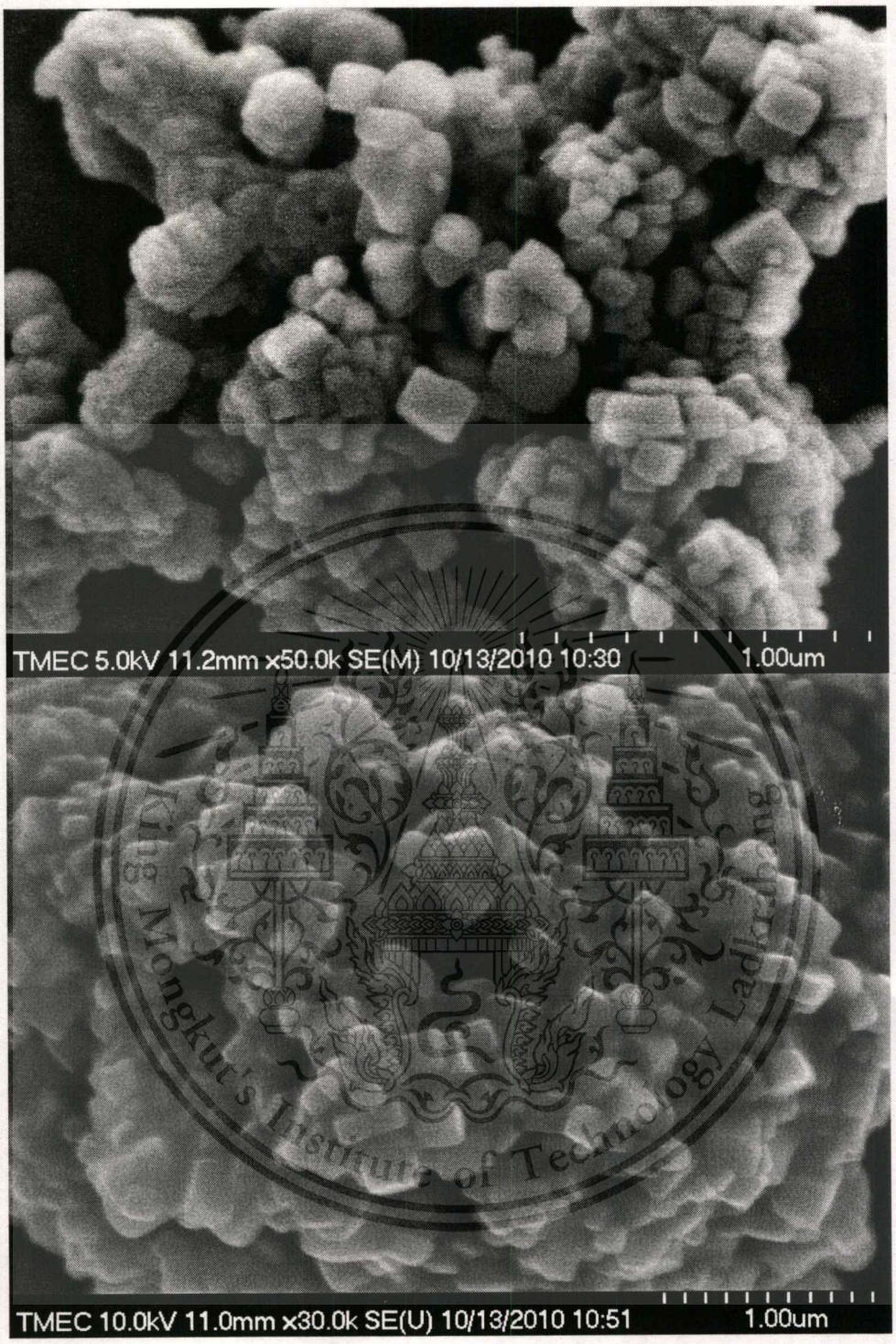

Figure 4.15 SEM micrograph showing as-prepared $NaNbO_3$ powder synthesized using the fuel-to-oxidant molar ratio of 1.0 (a) and powder calcined at 400°C for 4 h (b).

CHAPTER 5

CONCLUSIONS

5.1 Modified solid state reaction

Crystalline powders of sodium niobate $NaNbO_3$ were synthesized from a modified solid state reaction of $Na_2C_2O_4$ and Nb_2O_5. This method is an excellent, a simple and cost effective way of preparing stoichiometric, homogeneous, and fine powders. The perovskite phase of $NaNbO_3$ was synthesized successfully at the low temperature of 475°C for 1 h, with an average crystallite size of 25.89 ± 5.64 nm (defined by XRD). This calcination temperature was about 275°C lower than that used in the conventional method, which lies in the 750°C range. As dwell time increased, XRD peaks became narrower, and a pattern similar to that expected for orthorhombic $NaNbO_3$ was achieved, as indicated by separate peaks. The resulting $NaNbO_3$ powders comprised agglomerated particles of 180 to 360 nm in size (defined by SEM micrograph).

Crystalline potassium niobate $KNbO_3$ powder was prepared from a modified solid state reaction of $K_2C_2O_4 \cdot H_2O$ and Nb_2O_5, which is a simple cost- and time-saving method for synthesizing stoichiometric, homogeneous, and fine $KNbO_3$ powder, with a low calcination temperature of 550°C for 240 min. This temperature is about 250°C lower than others used, even in conventional methods. The powder obtained was found to be a uniform agglomerated particle that possessed an average crystallite size (defined by XRD) of between 33.67 ± 8.60 and 53.47 ± 12.03 nm, and a mean particle size (defined by SEM micrograph) of 278 ± 75 nm. The optimal calcination conditions for the single perovskite phase and their characteristics are shown in Table 5.1.

Table 5.1 The optimal calcination conditions for the single perovskite phase and their characteristics.

Characteristics	$NaNbO_3$	$KNbO_3$
Optimal calcination condition	475°C for 1 h	500°C for 6 h
Average crystallite size (nm)	25.89 ± 5.64	36.48 ± 10.67
Average particle size (nm)	249 ± 84	278 ± 75
Morphology	polyhedral	Polyhedral

5.2 Combustion synthesis

Crystalline $NaNbO_3$ powder, with a volume fraction of the perovskite phase formation (% perovskite) as high as 93%, was synthesized directly via the solution combustion process using $NaNO_3$, Nb_2O_5 and glycine. Monophasic perovskite $NaNbO_3$ powder was obtained after calcination at 400°C for 4 h. This calcination temperature is lower than that when using the modified solid state reaction method. The fuel-to-oxidizer molar ratio was found to affect the combustion reaction and character of the powder obtained. The average crystalline size (D) was found to decrease from 47.01 ± 12.66 nm (ratio of 0.7) to 27.58 ± 14.45 nm (ratio of 2.0). This method is a simple, rapid, cost and time-saving way of synthesizing stoichiometric, homogeneous and fine $NaNbO_3$ powder with a low calcination temperature. The powder obtained was found to be uniform soft agglomerated particles. The average particle size, which can be estimated from micrographs, was found to be 137 ± 52 nm and 226 ± 46 nm for as-prepared and calcined powder, respectively.

REFERENCES

[1] C. Miclea, C. Tanasoiu, C.F. Miclea, L. Amarande, A. Gheorghiu, I. Spanulescu, C. Plavitu, C.T. Miclea, M.C. Cioangher, L. Trupina and A. Iuga, "Effect of lead content on the structure and piezoelectric properties of hard type lead titanate–zirconate ceramics", *J. Eur. Ceram. Soc.*, **27**, 4055–4059 (2007).

[2] Lead and you: a guide to working safely with lead (2003) HSE (UK Health and Safety Executive). http://www.hse.gov.uk/pubns/indg305.pdf. Accessed 25 Apr 2004

[3] DIRECTIVE 2002/96/EC OF THE EUROPEAN PARLIAMENT AND OF THE COUNCIL of 27 January 2003 on waste electrical and electronic equipment (WEEE), Official Journal of the European Union

[4] DIRECTIVE 2002/96/EC OF THE EUROPEAN PARLIAMENT AND OF THE COUNCIL of 27 January 2003 on waste electrical and electronic equipment (WEEE), Official Journal of the European Union

[5] K. Nakamura and Y. Kawamura, "Electromechanical coupling factor of $KNbO_3$", *Proc. IEEE Ultrason. Symp.*, **2**, 1013–1018 (1999).

[6] H.D. Megaw, "The seven phases of sodium niobate", *Ferroelectrics*, **7**, 87–89 (1974).

[7] L.E. Cross and B. Nicholson, "The optical and electrical properties of single crystals of sodium niobate", *J. Phil. Magn. Ser.*, **46**, 453–466 (1955).

[8] G. Shirane, R. Newnham and R. Pepinsky, "Dielectric Properties and Phase Transitions of $NaNbO_3$ and (Na, K)NbO_3", *Phys. Rev.*, **96**, 581–588 (1954).

[9] Y. Shiratori, A. Magrez and C. Pithan, "Particle size effect on the crystal structure symmetry of $K_{0.5}Na_{0.5}NbO_3$", *J. Eur. Ceram. Soc.*, **25**, 2075–2079 (2005).

[10] M.D. Maeder, D. Damjanovic and N. Setter, "Lead Free Piezoelectric Materials", *J. Electroceram.*, **13**, 385–392 (2004).

[11] L. Egerton and D.M. Dillon, "Piezoelectric and Dielectric Properties of Ceramics in the System Potassium–Sodium Niobate", *J. Am. Ceram. Soc.*, **42**, 438–442 (1959).

[12] T. Nitta, "Properties of sodium-lithium niobate solid solution ceramics with small lithium concentrations", *J. Am. Ceram. Soc.*, **51**, 626–629 (1968).

[13] T. Rojac, O. Masson, R. Guinebretière, M. Kosec, B. Malič and J. Holc, "A study of the mechanochemical synthesis of $NaNbO_3$", *J. Eur. Ceram. Soc.*, **17**, 2265–2271 (2007).

[14] C.C. Hwang, T.Y. Wu, J. Wan and J.S. Tsai, "Development of a novel combustion synthesis method for synthesizing of ceramic oxide powders", *Mater. Sci. Eng., B,* **111**, 49–56 (2004).

[15] T. Rojac, M. Kosec, B. Malič and J. Holc, "Mechanochemical synthesis of $NaNbO_3$", *Mater. Res. Bull.*, **40**, 341–345 (2005).

[16] M.A.L. Nobre, E. Longo, E.R. Leite and J.A. Varela, "Synthesis and sintering of ultra fine $NaNbO_3$ powder by use of polymeric precursors", *Mater. Lett.*, **28**, 215–220 (1996).

[17] G. Li, T. Kako, D. Wang, Z. Zou and J. Ye, "Synthesis and enhanced photocatalytic activity of $NaNbO_3$ prepared by hydrothermal and polymerized complex methods", *J. Phys. Chem.*, **69**, 2487–2491 (2008).

[18] J. Xu, D. Xue and C. Yan, "Chemical synthesis of $NaTaO_3$ powder at low-temperature", *Mater. Lett.*, **59**, 2920–2922 (2005).

[19] K.C. Patil, S.T. Aruna and S. Ekambaram, "Combustion synthesis", *Curr. Opin. Solid State Mater. Sci.*, **2**, 158–165 (1997).

[20] K.C. Patil, S.T. Aruna and T. Mimani, "Combustion synthesis; an update", *Curr. Opin. Solid State Mater. Sci.*, **6**, 507–512 (2002).

[21] D.A. Fumor, M.R. Morelli and A.M. Segadães, "Combustion Synthesis of Calcium Aluminates", *Mater. Res. Bull.*, **31**, 1243–1255 (1996).

[22] M.A. Raza, I.Z. Rahman and S. Beloshapkin, "Synthesis of nanoparticles of $La_{0.75}Sr_{0.25}Cr_{0.5}Mn_{0.5}O_{3-\delta}$ (LSCM) perovskite by solution combustion method for solid oxide fuel cell application", *J. Alloys Compd.*, **485**, 593–597 (2009).

[23] M.W. Raja, S. Mahanty, P. Ghosh, R.N. Basu and H.S. Maiti, "Alanine-assisted low-temperature combustion synthesis of nanocrystalline $LiMn_2O_4$ for lithium-ion batteries", *Mater. Res. Bull.*, **42**, 1499–1506 (2007).

[24] S.V. Chavan, P.U.M. Sastry and A.K. Tyagi, "Combustion synthesis of nano-crystalline Nd-doped ceria and Nd_2O_3 and their fractal behavior as studied by small angle X-ray scattering", *J. Alloys Compd.*, **456**, 51–56 (2008).

[25] N.P. Bansal and Z. Zhong, "Combustion synthesis of $Sm_{0.5}Sr_{0.5}CoO_{3-x}$ and $La_{0.6}Sr_{0.4}CoO_{3-x}$ nanopowders for solid oxide fuel cell cathodes", *J. Power Sources*, **158**, 148–153 (2006).

[26] T. Ikeda, *Fundamentals of piezoelectricity*, NY, Oxford University Press, 1984.

[27] G.H. Haertling, "Ferroelectric Ceramics: History and technology", *J. Am. Ceram. Soc.*, **82** [4], 797-818 (1999).

[28] J. Nowotny, *Electronic ceramic materials*, America, Tran Tech Publications, 1992.

[29] B. Jaffe, W.R. Cook and H. Jaffe, *Piezoelectric ceramic*, London, Academic Press, 1971.

[30] A.S. Bhalla, R. Gou and R. Roy, "The perovskite structure-a review of its role in ceramic science and technology", *Mat. Res. Innovat.*, **4**, 3–26 (2000).

[31] http://www.3dchem.com

[32] E. Cross, "Materials science: Lead-free at last", *nature*, **432**, 24–25 (4 November 2004), doi:10.1038/nature03142

[33] B. Noheda, J. A. Gonzalo, R. Guo, S.E. Park, L.E. Cross and D.E. Cox, *The monoclinic phase in PZT: new light on morphotropic phase boundaries*, New York, AIP, 2000.

[34] M.D. Maeder, D. Damjanovic and N. Setter, "Lead Free Piezoelectric Materials", *J. Electroceram.*, **13**, 385–392 (2004).

[35] T. Takenaka and H. Nagata, "Current status and prospects of lead-free piezoelectric ceramics", *J. Eur. Ceram. Soc.*, **25**, 2693–2700 (2005).

[36] S. Jofre and T. Morioka, "Waste management of electric and electronic equipment: comparative analysis of end-of-life strategies", *J. Mater. Cycles Waste Manag.,* **7** [1], 24–32 (2005).

[37] W. He, G. Li, , X. Ma, H. Wang, J. Huang, M. Xu and C. Huang, "WEEE recovery strategies and the WEEE treatment status in China", *J. Hazard. Mater.,* B, **36**, 502–512 (2006).

[38] X. Wang, H.L.-W. Chan and C.-L. Choy, "$(Bi_{1/2}Na_{1/2})TiO_3$-$Ba(Cu_{1/2}W_{1/2})O_3$ Lead-Free Piezoelectric Ceramics", *J. Am. Ceram. Soc.*, **86** [10], 1809–1811 (2003).

[39] L. Egerton and D.M. Dillon, "Piezoelectric and Dielectric Properties of Ceramics in the System Potassium–Sodium Niobate", *J. Am. Ceram. Soc.*, **42,** 438–442 (1959).

[40] H. Birol, D. Damjanovic and N. Setter, "Preparation and characterization of $(K_{0.5}Na_{0.5})NbO_3$ ceramics", *J. Eur. Ceram. Soc.*, **26**, 861–866 (2006).

[41] R.E. Jaeger and L. Egerton, "Hot pressing of potassium-sodium niobate", *J. Am. Ceram. Soc.*, **45**, 209–213 (1962).

[42] L. Egerton and C.A. Bieling, "Isostatically hot-pressed sodium-potassium niobate transducer material for ultrasonic devices", *Ceram. Bull.*, **47** [12], 1151–1156 (1968).

[43] R. Wang, R. Xie, T. Sekiya and Y. Shimojo, "Fabrication and characterization of potassium-sodium niobate piezoelectric ceramics by spark-plasma-sintering method", *Mater. Res. Bull.,* **39**, 1709–1715 (2004).

[44] B.P. Zhang, J.F. Li, K. Wang and H. Zhang, "Compositional Dependence of Piezoelectric Properties in $Na_xK_{1-x}NbO_3$ Lead-Free Ceramics Prepared by Spark Plasma Sintering", *J. Am. Ceram. Soc.*, **89** [5], 1605–1609 (2006).

[45] J.F. Li and K. Wang, "Ferroelectric and Piezoelectric Properties of Fine-Grained $Na_{0.5}K_{0.5}NbO_3$ Lead-Free Piezoelectric Ceramics Prepared by Spark Plasma Sintering", *J. Am. Ceram. Soc.*, **89** [2], 706–709 (2006).

[46] Y. Saito, H. Takao, T. Tani, T. Nonoyama, K. Takatori, T. Homma, T. Nagaya and M. Nakamura, "Lead-free piezoceramics", *Nature*, **432**, 84–87 (2004).

[47] Y. Guo, K. Kakimoto and H. Ohsato, "$(Na_{0.5}K_{0.5})NbO_3$–$LiTaO_3$ lead-free piezoelectric ceramics", *Mater. Lett.*, **59**, 241–244 (2005).

[48] E. Hollenstein, M. Davis, D. Damjanovic and N. Setter, "Piezoelectric properties of Li- and Ta- modified "$(K_{0.5}Na_{0.5})NbO_3$ ceramics", *Appl. Phys. Lett.*, **87**, 182905 (2005).

[49] P. Zhao, B.P. Zhang and J.F. Li, "Enhancing piezoelectric d_{33} coefficient in Li/Ta-codoped lead-free (Na, K)NbO_3 ceramics by compensating Na and K at a fixed ratio", *Appl. Phys. Lett.*, **91**, 172901 (2007).

[50] Y. Chang, Z. Yang, D. Ma, Z. Liu and Z.Wang, "Phase transitional behavior, microstructure, and electrical properties in Ta-modified $[(K_{0.458}Na_{0.542})_{0.96}Li_{0.04}]NbO_3$ lead-free piezoelectric ceramics", *J. Appl. Phys.*, **104**, 024109 (2008).

[51] P. Zhao, B.P. Zhang and J.F. Li, "Enhanced dielectric and piezoelectric properties in $LiTaO_3$-doped lead-free (K,Na)NbO_3 ceramics by optimizing sintering temperature", *Scr. Mater.*, **58**, 429–432 (2008).

[52] N.M. Hagh, B. Jadidian and A. Safari, "Property-processing relationship in lead-free (K, Na, Li)NbO_3-solid solution system", *J. Electroceram.*, **18**, 339–346 (2007).

[53] L.Wu, D. Xiao, J. Wu, Y. Sun, D. Lin , J. Zhu, P. Yu, Y. Zhuang and Q. Wei, "Good temperature stability of $K_{0.5}Na_{0.5}NbO_3$ based lead-free ceramics and their applications in buzzers", *J. Eur. Ceram. Soc.*, **28**, 2963–2968 (2008).

[54] F.S. Tang, H.L. Du, Z.M. Li, W.C. Zhou, S.B. Qu and Z.B. Pei, "Preparation and properties of $(K_{0.5}Na_{0.5})NbO_3$-$LiNbO_3$ ceramics", *Trans. Nonferrous Met. Soc. China*, **16**, s466–s469 (2006).

[55] Y. Guo, K. Kakimoto and H. Ohsato, "Dielectric and piezoelectric properties of lead-free $(Na_{0.5}K_{0.5})NbO_3$–$SrTiO_3$ ceramics", *Solid State Commun.*, **129**, 279–284 (2004).

[56] R.C. Chang, S.Y. Chua, Y.P. Wong, Y.F. Lin and C.S. Hong, "Properties of $(Na_{0.5}K_{0.5})NbO_3$–$SrTiO_3$ based lead-free ceramics and surface acoustic wave devices", *Sens. Actuators, A*, **136**, 267–272 (2007).

[57] H. Dua, F. Luo, S. Qu, Z. Pei, D. Zhu and W. Zhou, "Phase structure, microstructure, and electrical properties of bismuth modified potassium-sodium niobium lead-free ceramics", *J. Appl. Phys.*, **102**, 054102 (2007).

[58] H. Du, W. Zhou, F. Luo, D. Zhu, S. Qu, Y. Li and Z.Pei, "Design and electrical properties' investigation of $(K_{0.5}Na_{0.5})NbO_3$–$BiMeO_3$ lead-free piezoelectric ceramics", *J. Appl. Phys.*, **104**, 034104 (2008).

[59] C.W. Ahn, H.Y. Park, S. Nahma, K. Uchino, H.G. Lee and H.J. Lee, "Structural variation and piezoelectric properties of $0.95(Na_{0.5}K_{0.5})NbO_3$–$0.05BaTiO_3$ ceramics", *Sens. Actuators, A*, **136**, 255–260 (2007).

[60] H. Du, W. Zhou, D. Zhu and L. Fa, "Sintering Characteristic, Microstructure, and Dielectric Relaxor Behavior of $(K_{0.5}Na_{0.5})NbO_3$–$(Bi_{0.5}Na_{0.5})TiO_3$ Lead-Free Ceramics", *J. Am. Ceram. Soc.*, **91** [9], 2903–2909 (2008).

[61] C. Xu, D.Lin and K.W. Kwok, "Electrical properties of $(K_{0.5}Na_{0.5})_{1-x}Ag_xNbO_3$ lead-free piezoelectric ceramics", *J Mater Sci: Mater Electron*, **19**, 1054–1057 (2008).

[62] C. Lei and Z G.Ye, "Lead-free piezoelectric ceramics derived from the $K_{0.5}Na_{0.5}NbO_3$–$AgNbO_3$ solid solution system", *Appl. Phys. Lett.*, **93**, 042901 (2008).

[63] M. Matsubara, T.Yamaguchi, K. Kikuta and S. Hirano, "Sinterability and Piezoelectric Properties of $(K,Na)NbO_3$ Ceramics with Novel Sintering Aid", *Jpn. J. Appl. Phys.*, **43**, 7159–7163 (2004).

[64] M. Matsubara, T.Yamaguchi, W. Sakamoto, K. Kikuta, T. Yogo and S. Hirano, "Processing and piezoelectric properties of lead-free $(K,Na)(Nb,Ta)O_3$ ceramics", *J. Am. Ceram. Soc.*, **88** [5], 1190–1196 (2005).

[65] R. Zuo and J. Rödel, "Sintering and Electrical Properties of Lead-Free $Na_{0.5}K_{0.5}NbO_3$ Piezoelectric Ceramics", *J. Am. Ceram. Soc.*, **89** [6], 2010–2015 (2006).

[66] M.S. Kim, D.S. Lee, E.C. Park, S.J. Jeong and J.S. Song, "Effect of Na_2O additions on the sinterability and piezoelectric properties of lead-free $95(Na_{0.5}K_{0.5})NbO_3$–$5LiTaO_3$ ceramics", *J.Eur. Ceram. Soc.*, **27**, 4121–4124 (2007).

[67] J. Hao, Z. Xu, R. Chu, Y. Zhang, G. Li and Q. Yin, "Effects of MnO_2 on phase structure, microstructure and electrical properties of $(K_{0.5}Na_{0.5})_{0.94}Li_{0.06}NbO_3$ lead-free ceramics", *Mater. Chem. Phys.*, **118**, 229–233 (2009).

[68] K. Nonaka, M. Akiyama, T. Hagio and A. Takase, "Effect of Pb/(Zr+Ti) Molar Ratio on the Photovoltaic Properties of Lead Zirconate-titanate Ceramics", *J. Eur. Ceram. Soc.*, **19**, 1143–1148 (1999).

[69] V. Lingwal, B.S. Semwal and N.S. Panwar, "Dielectric properties of $Na_{1-x}K_xNbO_3$ in orthorhombic phase", *Bull. Mater. Sci.*, **26** [6], 619–625 (2003).

[70] J.J. Moore and H.J. Feng, "Combustion synthesis of Advanced Materials: Part I Reaction Parameters", *Progress in Mater. Sci.*, **39**, 243–273 (1995).

[71] J.J. Berzelius, "One-step Synthesis of GDC-NiO-C Anode for IT SOFC with GNP Method", *Prog. Ann.*, **4**, 126 (1825).

[72] V. Hlavacek, "Combustion Synthesis: a Historical Perspective", *Ceram. Bull.*, **70**, 240–243 (1991).

[73] A.G. Merzhanov, V.M. Shkiro and I.P. Borovinskaya, "Synthesis of Refractory Inorganic Compounds", *USSR Inventor's Certificate* No. 255221 (1967).

[74] K.C. Patil and R. Soundararajan, "Pyrotechniques for entertainment", *Ind. J. Chem. Edn.*, **6**, 29–30 (1979).

[75] K.C. Patil and M.M.A. Sekar, "Synthesis, structure and reactivity of metel hydrazine carboxylates: combustible precursors to fine particle oxide materials", *Int. J. Self-Propag. High-Temp. Synth.*, **3**, 181–196 (1994).

[76] A. Varma, "Form from fire" *Sci. Am.*, **283**, 44–47 (2001).

[77] A.G. Merzhanov, *SHS research and development handbook*, Chernogolovka, Russia, Russian Academy of Sciences, 1999.

[78] G. Xanthoupoulou, "Oxide catalysts for pyrolysis of diesel fuel made by self propagating high temperature synthesis (SHS) Part II: Fe–Cr oxide catalysts based on chromite concentrates", *Appl. Catal.*, **187**, 79–88 (1999).

[79] Q. Ming, M.D. Nersesyan, A. Wagner, J. Ritchie, J.T. Richardson, D. Luss, A.J. Jacobson and Y.L. Yang, "Combustion synthesis and characterization of Sr and Ga doped LaFeO", *Solid State Ionics*, **122**, 113–121 (1999).

[80] A.L. Wagner, A.J. Jacobson, J.T. Richardson and D. Luss, "Reaction characteristics of $La_{0.84}Sr_{0.16}CrO_3$", *J. Mater. Sci.*, **34**, 3035–3041 (1999).

[81] Q. Ming, J. Hung, Y.L. Yang, M.D. Nersesyan, A.J. Jacobson, J.T. Richardson and D. Luss, "Combustion synthesis of $La_{0.2}Sr_{0.8}Cr_{0.2}Fe_{0.8}O_{3-x}$", *Combust. Sci. Technol.*, **138**, 279–285 (1998).

[82] Q. Ming, M.D. Nersesyan, S. Lin, J.T. Richardson, D. Luss and A.A. Shiryaev, "A new route to synthesize $La_{1-x}Sr_xMnO_3$", *J. Mater. Sci.*, **35**, 3599–3606 (2000).

[83] L. Li, T. Akiyama and J. Yagi, "Activity and capacity of hydrogen storage alloy Mg NiH produced by hydriding combustion synthesis", *J. Alloys. Comp.*, **308**, 98–103 (2000).

[84] L. Yong-hua, L. Rong and L.Yi-yi, "Pore characteristics of porous NiTi alloy fabricated by combustion synthesis", *J. Alloys Comp.*, **319**, 108–118 (2001).

[85] J.J. Kingsley and K.C. Patil, "A novel combustion process for the synthesis of fine particle a-alumina and related oxide materials", *Mater. Lett.*, **6**, 427–432 (1988).

[86] S.R. Jain, K.C. Adiga and V.R.P. Verneker, "A New Approach to Thermochemical Calculations of Condensed Fuel-Oxidizer Mixtures", *Combus. Flame*, **40**, 71–79 (1981).

[87] A.M. Segadães, M.R. Morelli and R.G.A. Kiminam, "Combustion Synthesis of Aluminium Titanate", *J. Eur. Ceram. Soc.*, **18**, 771–778 (1998).

[88] V.C. Sousa, A.M. Segadães, M.R. Morelli and R.G.A. Kiminami, "Combustion synthesized ZnO powders for varistor ceramics", *Int. J. Inor. Mater.*, **1**, 235–241 (1999).

[89] A. Civera, M. Pavese, G. Saracco and V. Specchia, "Combustion synthesis of perovskite-type catalysts for natural gas combustion", *Catal. Today*, **83**, 199–211 (2003).

[90] Z.S. Macedoa, C.R. Ferrari, A.C. Hernandes, "Self-propagation high-temperature synthesis of bismuth titanate", *Powder Tech.*, **139**, 175– 179 (2004).

[91] T. Mimani and K.C. Patil, "Solution Combusiton Synthesis of Nanoscale Oxides and Their Composites", *Mater. Phys. Mech.*, **4**, 134–137 (2001).

[92] T.V. Anuradha, S. Ranganathan, T. Mimani and K.C. Patil, "Combustion synthesis of nanostructured barium titanate", *Scripta Mater.*, **44**, 2237–2241 (2001).

[93] A.S. Mukasyan, C. Costello, K.P. Sherlock, D. Lafarga and A. Verma, "Perovskite menbranes by aqueous combustion synthesis: synthesis and properties", *Sep. Purif. Technol.*, **25**, 117–126 (2001).

[94] R.D. Purohit, B.P. Sharma, K.T. Pillai and A.K. Tyagi, "Ultrafine ceria powders via glycine-nitrate combustion", *Mater. Res. Bull.*, **36**, 2711–2721 (2001).

[95] S.V. Chavan, K.T. Pillai and A.K. Tyagi, "Combustion synthesis of nanocrystalline yttria: Tailoring of powder properties", *Mater. Sci. Eng., B,* **132**, 266–271 (2006).

[96] S.L. Swartz and T.R. Shrout, "Fabrication of perovskite lead mahnesium niobate", *Mater. Res. Bull.*, **17** [10], 1245–1250 (1982).

[97] H.P. Klug and L.E. Alexander, *X-ray Diffraction Procedure of Polycrystalline and Amorphous Materials*, New York, JonhWiley & Sons, 1974.

[98] T. Hungría, L. Pardo, A. Moure and A. Castro, "Effect of mechanochemical activation on the synthesis of $NaNbO_3$ and processing of environmentally friendly piezoceramics", *J. Alloys Compd.*, **395**, 166–173 (2005).

[99] T.-Y. Ke, H.-A. Chen, H.-S. Sheu, J.-W. Yeh, H.-N. Lin, C.-Y. Lee and H.-T. Chiu, "Sodium Niobate Nanowire and Its Piezoelectricity", *J. Phys. Chem., C.*, **112**, 8827–8831 (2008).

[100] F. Jona and G. Shirane, *Ferroelectric crystals*, Dover Publications, New York, 1993.

[101] X.-B. Wang, Z. Shen, Z.-P. Hu, L. Qin, S.H. Tang and M.H. Kuok, "High temperature Raman study of phase transitions in antiferroelectric $NaNbO_3$", *J. Mol. Struct.*, **385**, 1–6 (1996).

[102] H. Du, W. Zhou, F. Luo, D. Zhu, S. Qu, Y. Li and Z. Pei, "Design and electrical properties' investigation of $(K_{0.5}Na_{0.5})NbO_3$-$BiMeO_3$ lead-free piezoelectric ceramics", *J. Appl. Phys.*, **104**, 034104–7 (2008).

[103] J. Wu, D. Xiao, Y. Wang, W. Wu, B. Zhang and J. Zhu, "Improved temperature stability of $CaTiO_3$-modified $[(K_{0.5}Na_{0.5})_{0.96}Li_{0.04}](Nb_{0.91}Sb_{0.05}Ta_{0.04})O_3$ lead-free piezoelectric ceramics", *J. Appl. Phys.*, **104**, 024102–4 (2008).

[104] Y.-J. Hsiao, Y.-H. Chang, Y.-S. Chang, T.-H. Fang, Y.-L. Chai, G.-J. Chen, T.-W. Huang, "Growth and characterization of $NaNbO_3$ synthesized using reaction-sintering method", *Mater. Sci. Eng., B*, **136**, 129–133 (2007).

[105] S. Lanfredi, L. Dessemond and A.C.M. Rodrigue, "Dense ceramics of $NaNbO_3$ produced from powders prepared by a new chemical route", *J. Eur. Ceram. Soc.*, **20**, 983–990 (2000).

[106] G.K.L. Goh, F.F. Lange, S.M. Haile and C.G. Levi, "Hydrothermal synthesis of $KNbO_3$ and $NaNbO_3$ powders", *J. Mater. Res.*, **18**, 338–345 (2003).

[107] A. Moure, T. Hungría, A. Castro adn L Pardo, "Quantitative microstructural analysis and piezoelectricity of highly dense, submicron-structured $NaNbO_3$ ceramics from mechanically activated precursors", *J. Eur. Ceram. Soc.*, **29**, 2297–2308 (2009).

[108] E.R. Camargo, M. Popa and M. Kakihana, "Sodium Niobate ($NaNbO_3$) Powders Synthesized by a Wet-Chemical Method Using a Water-Soluble Malic Acid Complex", *Chem. Mater.*, **14**, 2365–2368 (2002).

[109] L.H. McAlexander, C.M. Beck, J.J. Burdeniuc and R.H. Crabtree, "Fluoroalkane aromatization over hot sodium oxalate", *J. Fluorine Chem.*, **99**, 67–71 (1999).

[110] W.D. Callister, *Materials science and engineering: an introduction*, Wiley, New York, 2007.

[111] N. Chaiyo and N. Vittayakorn, "Effect of calcination conditions on phase formation of microwave dielectric cobalt niobate ($CoNb_2O_6$) powders via a mixed oxide synthesis route", *J. Ceram. Process Res.*, **9**, 381–384 (2008).

[112] S. Sheibani, A. Atai and S. Heshmati-Manesh, "Kinetics analysis of mechano-chemically and thermally synthesized Cu by Johnson–Mehl–Avrami model", *J. Alloys Compd.*, **455**, 447–453 (2008).

[113] Z.-J. Yan, S.-E. Dang, X.-H. Wang and P.-X. Lian, "Applicability of Johnson-Mehl-Avrami model to crystallization kinetics of $Zr_{60}Al_{15}Ni_{25}$ bulk amorphous alloy", *Trans. Nonferrous Met. Soc. China,* **18**, 138–144 (2008).

[114] H.M. Jang, S.R. Cho and K.-M. Lee, "Mechanism of Formation of Perovskite Phase and Dielectric Properties of $Pb(Zn,Mg)_{1/3}Nb_{2/3}O_3$ Ceramics Prepared by Columbite Precursor Routes", *J. Am. Ceram. Soc.*, **78**, 297–304 (1995).

[115] Y. Shen, H.H. Hng and J.T. Oh, "Formation kinetics of Ni–15% Fe–5% Mo during ball milling", *Mater. Lett.*, **58**, 2824–2828 (2004).

[116] N. Setter, *Piezoelectric materials in devices*, Ceramic lab, EPFL, Switzerland, 2002.

[117] M. Ichiki, L. Zhang, M. Tanaka and R. Maeda, "Electrical properties of piezoelectric sodium-potassium niobate", *J. Eur. Ceram. Soc.*, **24**, 1693–1697 (2004).

[118] J.-F. Liu, X.-L. Li, Y.-D. Li, "Synthesis and characterization of nanocrystalline niobates", *J. Cryst. Growth*, **247**, 419–424 (2003).

[119] K. Yamanouchi, H. Odagawa, T. Kojima and T. Matsumura, "Theoretical and experimental study of super-high electromechanical coupling surface acoustic wave propagation in $KNbO_3$ single crystal", *Electron Lett.*, **33**, 193–194 (1997).

[120] K. Matsumoto, Y. Hiruma, H. Nagata and T. Takenaka, "Electric-field-induced strain in Mn-doped $KNbO_3$ ferroelectric ceramics", *Ceram. Int.*, **34**, 787–791 (2008).

[121] D. Makovec, I. Pribošič and M. Drofenik, "TiO_2 as a sintering additive for $KNbO_3$ ceramics", *Ceram. Int.*, **34**, 89–94 (2008).

[122] C.H. Lu, S.Y. Lo and H.C. Lin, "Hydrothermal synthesis of nonlinear optical potassium niobate ceramic powder", *Mater. Lett.*, **34**, 172–176 (1998).

[123] H. Muthurajan, H.H. Kumar, V. Samuel, U.N. Gupta and V. Ravi, "Novel hydroxide precursors to prepare $NaNbO_3$ and $KNbO_3$", *Ceram. Int.*, **34**, 671–673 (2008).

[124] H.E. Mgbemere, R.-P. Herber and G.A. Schneider, "Effect of MnO_2 on the dielectric and piezoelectric properties of alkaline niobate based lead free piezoelectric ceramics", *J. Eur. Ceram. Soc.*, **29**, 1729–1733 (2009).

[125] R. Wang, R. Xie, T. Sekiya, Y. Shimojo, Y. Akimune, N. Hirosaki, M. Itoh, "Piezoelectric properties of spark-plasma-sintered $(Na_{0.5}K_{0.5})NbO_3$–$PbTiO_3$ ceramics", *Jpn. J. Appl. Phys.*, **41**, 7119–7122 (2002).

[126] Z.S. Ahn and W.A. Schulze, "Conventionally sintered $(Na_{0.5}K_{0.5})NbO_3$ with barium additions", *J. Am. Ceram. Soc.*, **70**, 18–21 (1987).

[127] Y. Chang, Z. Yang, L. Wei, Liu B, "Effects of $AETiO_3$ additions on phase structure, microstructure and electrical properties of $(K_{0.5}Na_{0.5})NbO_3$ ceramics", *Mater. Sci. Eng., A*, **437**, 301–305 (2006).

[128] K. Bhattacharyya and A.K. Tyagi, "A novel soft-chemical method for the synthesis of nanocrystallin $MNbO_3$ (M = Na, K)", *J. Alloys Compd.*, **470**, 580–583 (2009).

[129] M.M. Amini and M. Mirzaee, "Effect of solvent and temperature on the preparation of potassium niobate by hydrothermal-assisted sol–gel processing", *Ceram. Int.*, **35**, 2367–2372 (2009).

[130] C.-H. Lu, S.-Y. Lo and Y.-L. Wang, "Glycothermal preparation of potassium niobate ceramic particles under supercritical condition", *Mater. Lett.*, **55**, 121–125 (2002).

[131] N. Chaiyo, B. Boonchom and N. Vittayakorn, "Solid-state reaction synthesis of sodium niobate ($NaNbO_3$) powder at low temperature", *J. Mater. Sci.*, **45**, 1443–1447 doi:10.1007/s10853-009-4098-z (2010).

[132] I. Pribošič, D. Makovec and M. Drofenik, "Chemical synthesis of $KNbO_3$ and $KNbO_3$-$BaTiO_3$ ceramics", *J. Eur. Ceram. Soc.*, **25**, 2713–2717 (2005).

[133] K. Kakimoto, T. Ito and H. Ohsato, "Synthesis of $KNbO_3$ piezoelectric ceramics using citrate precursors", *Jpn. J. Appl. Phys.*, **47**, 7669–7672 (2008).

[134] B. Malic, J. Bernard, A. Bencan and M. Kosec, "Influence of zirconia addition on the microstructure of $K_{0.5}Na_{0.5}NbO_3$ ceramics", *J. Eur. Ceram. Soc.*, **28**, 1191–1196 (2008).

[135] M.M. Amini and M.D. Sacks, "Synthesis of potassium niobate from metal alkoxides", *J. Am. Ceram. Soc.*, **74**, 53–59 (1991).

[136] K.J. Kim and E. Matijevic, "Preparation and characterization of uniform submicrometer metal niobate particles: Part II. Magnesium niobate and potassium niobate", *J. Mater. Res.*, **7**, 912–918 (1992).

[137] J.S. de Andrade, A.G. Pinheiro, I.F. Vasconcelos, J.M. Sasaki, J.A.C. Paiva de, M.A. Valente and A.S.B. Sombra, "Raman and infrared spectra of $KNbO_3$ in niobate glass-ceramics", *J. Phys. Condens Matter.*, **11**, 4451–4460 (1999).

[138] H.A Böke, Akkurt S, Özdemir S, Göktürk EH, Saltik ENC, "Quantification of $CaCO_3$–$CaSO_3 \cdot 0.5H_2O$–$CaSO_4 \cdot 2H_2O$ mixtures by FTIR analysis and its ANN model", *Mater. Lett.*, **58**, 723–726 (2004).

[139] Y. Terashi, A. Purwanto, W.N. Wang, F. Iskandar and K. Okuyama, "Role of urea addition in the preparation of tetragonal $BaTiO_3$ nanoparticles using flame-assisted spray pyrolysis", *J. Eur. Ceram. Soc.*, **28**, 2573–2580 (2008).

[140] R. Wongmaneerung, W. Chaisan, O. Khamman, R. Yimnirun and S. Ananta, "Potential of vibro-milling technique for preparation of electroceramic nanopowders", *Ceram. Int.*, **34**, 813–817 (2008).

[141] B. Jaffe, R.S. Roth and S. Marzullo, "Piezoelectric Properties of Lead Zirconate–Lead Titanate Solid-Solution Ceramics", *J. Appl. Phys.*, **25**, 809–810 (1954).

[142] S.S. Manoharan and K.C. Patil, "Combustion Synthesis of Metal Chromite Powders", *J. Am. Ceram. Soc.*, **75**, 1012–1015 (1992).

[143] L.A. Chick, L.R. Pederson, G.D. Maupin, J.L. Bates, L.E. Thomas and G.J. Exarthos, "Glycine-nitrate combustion synthesis of oxide ceramic powders", *Mater. Lett.*, **10**, 6–12 (1990).

[144] A. Civera, M. Pavese, G. Saracco and V. Specchia, "Combustion synthesis of perovskite-type catalysts for natural gas combustion", *Catal. Today*, **83**, 199–211 (2003).

[145] C. Weifan, L. Fengsheng, L. Leili and L. Yang, "One-step synthesis of nanocrystalline perovskite $LaMnO_3$ powders via microwave-induced solution combustion route", *J. Rare Earths*, **24**, 782–787 (2006).

[146] S.H Xiao, W.F. Jiang, L.Y. Li and X.J. Li, "Low-temperature auto-combustion synthesis and magnetic properties of cobalt ferrite nanopowder", *Mater. Chem. Phys.*, **106**, 82–87 (2007).

[147] M.L. Lavčević and A. Turković, "The measurements of particle/crystallite size in nanostructured TiO_2 films by SAXS/WAXD method", *Scripta Mater.*, **46**, 501–505 (2002).

[148] W.-N. Wang, W. Widiyastuti, T. Ogi and I.W. Lenggoro, "Correlations between Crystallite/Particle Size and Photoluminescence Properties of Submicrometer Phosphors", *Chem. Mater.*, **19**, 1723–1730 (2007).

[149] N. Izu, W. Shin, I. Matsubara and N. Murayama, "The effects of the particle size and crystallite size on the response time for resistive oxygen gas sensor using cerium oxide thick film", *Sens. Actuators, B*, **94**, 222–227 (2003).

APPENDIXS

1. The fuel-to-oxidizer molar ratio calculation

Based on the fundamental thermochemical concepts used in propellant chemistry, an exothermic redox reaction of the combustion synthesis process could be initiated only when the oxidizer and fuel are mixed thoroughly in a fixed proportion. The elemental stoichiometric coefficient, ϕ, could be calculated by:

$$\phi = \text{n}\frac{\text{total valaencies of fuel}}{\text{total valaencies of oxidizer}}$$

where n is the mole of glycine. The assumed valencies, which are presented as usual products of the combustion reaction, consist of CO_2, H_2O and N_2. Therefore, carbon and hydrogen are considered as reducing elements with the corresponding valencies of +4 and +1, whereas oxygen is thought to be an oxidizing agent with a valency of –2, and nitrogen a valency of 0. To extrapolate the concept of combustion synthesis of ceramic oxide meansconsidering metals as reducing agents with their valencies in the corresponding oxide or nitrate, i.e. +2 for magnesium (oxide), +3 for cerium (nitrate) and +4 for cerium (oxide). In the case of multiple valence elements, the final product is used for calculation. According to the propellant chemistry for stoichiometric redox reaction between fuel and an oxidizer, the ϕ ratio should be unified (stoichiometric). A $\phi < 1$ means oxidant-rich condition and $\phi > 1$ means fuel-rich condition. This ϕ ratio was referred to as the fuel-to-oxidizers ratio. To satisfy the principle in the present system of $NaNbO_3$ preparation, the following calculation could be performed:

$$\phi = \text{n}\frac{(0_{(N)}+2\times1_{(H)}+4_{(C)}+2\times1_{(H)}+4_{(C)}-2_{(O)}-2_{(O)}+1_{(H)})}{1_{(Na)}+0_{(N)}-2\times3_{(O)}}$$

Sodium nitrate possessed the oxidizing valency of 5– and glycine had the reducing valency of 9+, and, as the mole of glycine (n) was found to be 0.56, the molar ratio of fuel (glycine; NH_2CH_2COOH) to oxidizer was 0.56:1. This ratio was referred to as the fuel-to-oxidizers molar ratio. Therefore, the comprehensive reaction that formed $NaNbO_3$ could be written as:

$$18NaNO_{3(aq)} + 9Nb_2O_{5(s)} + 10NH_2CH_2COOH_{(aq)} \longrightarrow 18NaNbO_{3(s)} + 25H_2O_{(g)} + 14N_{2(g)} + 20CO_{2(g)}$$

From reaction above, if 5 g (0.0305 mol) of $NaNbO_3$ was expected, 0.0305 mol of $NaNO_3$ and NH_2CH_2COOH and 0.0152 of Nb_2O_5 were used. The results were shown in Table 1. For other fuel-to-oxidizers molar ratios can be calculated in the same method.

Table 1 Data of the preparation and the calculation of the amount of starting materials for combustion synthesis using the stoichiometric fuel-to-oxidizers molar ratio (0.56).

Data	$NaNO_3$	Nb_2O_5	NH_2CH_2COOH	$NaNbO_3$
molecular weight (g/mol)	84.9947	265.8098	75.0666	163.8944
amount (mol)	0.0305	0.0152	0.0305	0.0305
amount (g)	2.5930	4.0546	2.2901	5

2. Wt% perovskite calculation

These relative amounts of perovskite and others phases were approximated by calculating the ratio of the main X-ray peak intensities of perovskite, residual starting component (R = $K_2C_2O_4{\cdot}H_2O$, $Na_2C_2O_4$, KNO_3 and/or $NaNO_3$), Nb_2O_5 and other secondary phases (pyrochlore), using the following equation [96]:

$$\text{Wt\% perovskite} = \frac{I_{\text{perov}}}{I_{\text{perov}}+I_R+I_{Nb_2O_5}+I_{\text{pyro}}} \times 100 \qquad (3.8)$$

where I_{perov}, I_R, $I_{Nb_2O_5}$ and I_{pyro} stand for intensities belonging to the strongest reflection peak of perovskite, residual starting component (R = $K_2C_2O_4{\cdot}H_2O$, $Na_2C_2O_4$, KNO_3 and/or $NaNO_3$), (180) Nb_2O_5 and pyrochlore phases, respectively.

3. The average crystallite size calculation

The average crystallite size of the powders obtained could be determined from the XRD pattern, according to Scherrer's equation [97]:

$$D = \frac{k\lambda}{\beta \cos\theta_B}$$

where D is the average crystallite size, k a constant equal to 0.94, λ the wavelength of X-ray radiation, β the full width at half maximum (FWHM) and θ_B the diffraction angle. The constant of proportionality, k (the Scherrer constant) depends on the how the width is determined, the shape of the crystal, and the size distribution. The most common values for k are 0.94 for FWHM of spherical crystals with cubic symmetry

VITA

Name-Surename	:	Nopsiri Chaiyo
Date of birth	:	8 September 1986
Province	:	Chiang Rai
Education	:	B.Sc. (First Class Honors in Industrial Chemistry-Analytical Instrumentation), King Mongkut's Institute of Technology Ladkrabang, Bangkok (2008)
Scholarship	:	M.Sc. Scholarship from Thailand Graduate Institute of Science and Technology (TGIST)

Conference and Publications

International Conferences:

1. Synthesis and Morphology Evolution of Lead-Free Piezoelectric $K_{1/2}Na_{1/2}NbO_3$ Powder at Low Temperature "*6th Asian Meeting on Ferroelectrics*" Taipei, TAIWAN (2008) **N. Chaiyo**, A. Ruangphanit, R. Muanghlua, S. Niemcharoen, A. Sangseud, S. Taopen, S. Leelapattana, W. C. Vittayakorn, N. Vittayakorn

2. Preparation and Properties of Lead Free Bismuth Sodium Titanate-Bismuth Zinc Titanate Ceramics "*6th Asian Meeting on Ferroelectrics*" Taipei, TAIWAN (2008) R. Muanghlua, S. Niemcharoen, W. C. Vittayakorn, N. Tungsitvisetkul, P. Chinwaro, A. Ruangphanit , **N. Chaiyo**, N. Vittayakorn.

3. Synthesis, phase formation and characterization of $Co_4Nb_2O_9$ powders synthesized by solid-state reaction "*International Conference on Smart Materials-Smart/Intelligent Materials and Nano Technology & 2nd International Workshop on Functional Materials and Nanomaterials*" Chiang Mai, THAILAND (2008) **N. Chaiyo,** N. Vittayakorn.

4. Effect of Annealing on the Structure and Dielectric Properties in PZT-PCoN Ceramics "*International Conference on Smart Materials-Smart/Intelligent Materials and Nano Technology & 2nd International Workshop on Functional Materials and Nanomaterials*" Chiang Mai, THAILAND (2008) N. Vittayakorn, **N. Chaiyo**, R. Muanghlua, A. Ruangphanit, W. C. Vittayakorn.

5. Synthesis and Morphology evolution of lead-free piezoelectric $KNbO_3$ powder using a modified solid state reaction "*The Twenty-sixth annual Conference of the Microscopy Society of Thailand* " Chiang Mai, THAILAND (2009) **N. Chaiyo**, A. Ruangphanit, N. Vittayakorn.

6. Hydrothermal synthesis and Characterization of Lead-free piezoelectric $KNbO_3$ powders. "*The Twenty-sixth annual Conference of the Microscopy Society of Thailand*" Chiang Mai, THAILAND (2009) C. Chansi, N. Adam, S. Vuttivong, **N. Chaiyo**, N. Vittayakorn.

7. Effect of calcination condition on lead-free piezoelectric $NaNbO_3$ powder through a modified solid state reaction synthesis. "*The Twenty-sixth annual Conference of the Microscopy Society of Thailand*" Chiang Mai, THAILAND (2009) **N. Chaiyo**, A. Ruangphanit, N. Vittayakorn.

8. A modified solid-state reaction synthesis and characterization of sodium niobate ($NaNbO_3$) powders "*The 3rd International Symposium on Functional Materials (ISFM2009)"* Jinju, KOREA (2009) **N. Chaiyo**, N. Vittayakorn.

9. Solution Combustion Synthesis of Lead-free Piezoelectric Sodium Niobate ($NaNbO_3$) Powders "*The Twenty-seventh annual Conference of the Microscopy Society of Thailand*" Samui, THAILAND (2010) **N. Chaiyo**, A. Ruangphanit, N. Vittayakorn.

10. Facile Synthesis of Lead-free Piezoelectric Sodium Niobate ($NaNbO_3$) Powders via the Solution Combustion Method "*The 10th Russia/CIS/Baltic/Japan Symposium on Ferroelectricity (RCBJSF-10)*" Yokohama, JAPAN (2010) **N. Chaiyo**, A. Ruangphanit, B. Boonchom, N. Vittayakorn.

International Publications

1. **N. Chaiyo**, N. Vittayakorn. "Effect of calcination conditions on phase formation of microwave dielectric cobalt niobate ($CoNb_2O_6$) powders via a mixed oxide synthesis route" *Journal of Ceramic Processing Research* **9**:381–384 (2008)

2. N. Vittayakorn, **N. Chaiyo**, R. Muanghlua, A. Ruangphanit, W. C. Vittayakorn. "Effect of Annealing on the Structure and Dielectric Properties in PZT-PCoN Ceramics" *Advanced Materials Research* **55-57**:49–52(2008)

3. **N. Chaiyo**, R. Muanghlua, A. Ruangphanit, W. C. Vittayakorn and N. Vittayakorn. "Synthesis, Phase Formation and Characterization of $Co_4Nb_2O_9$ Powders Synthesized by Solid-State Reaction" *Advanced Materials Research* **55-57**:873–876 (2008)

4. R. Muanghlua, S. Niemcharoen, W. C. Vittayakorn, N. Tungsitvisetkul, P. Chinwaro, A. Ruangphanit , **N. Chaiyo**, N. Vittayakorn. "Preparation and Properties of Lead Free Bismuth Sodium Titanate-Bismuth Zinc Titanate Ceramics" *Ferroelectrics* **383**:1–7 (2009)

5. **N. Chaiyo**, A. Ruangphanit, R. Muanghlua, S. Niemcharoen, A. Sangseud, S. Taopen, S. Leelapattana, W. C. Vittayakorn, N. Vittayakorn. "Synthesis and Morphology Evolution of Lead-Free Piezoelectric $K_{1/2}Na_{1/2}NbO_3$ Powder at Low Temperature" *Ferroelectrics* 383:8–14 (2009)

6. **N. Chaiyo**, B. Boonchom, N. Vittayakorn. "Solid-state reaction synthesis of sodium niobate ($NaNbO_3$) powder at low temperature" *Journal of Material Science* **45**:1443–1447 DOI 10.1007/s10853-009-4098-z (2010)

7. **N. Chaiyo**, R. Muanghlua, S. Niemcharoen, B. Boonchom, N. Vittayakorn. "Solution combustion synthesis and characterization of lead-free piezoelectric sodium niobate ($NaNbO_3$) powders" *Journal of Alloys and Compounds* **509**:2445–2449 (2011)

8. **N. Chaiyo**, A. Ruangphanit, R. Muanghlua, S. Niemcharoen, B. Boonchom, N. Vittayakorn. "Synthesis of potassium niobate ($KNbO_3$) nano-powder by a modified solid-state reaction" *Journal of Material Science* **46**:1585–1590 DOI 10.1007/s10853-010-4967-5 (2011)

9. **N. Chaiyo**, A. Ruangphanit, B. Boonchom, N. Vittayakorn. "Facile Synthesis of Lead-Free Piezoelectric Sodium Niobate ($NaNbO_3$) Powders via the Solution Combustion Method" *Ferroelectrics* **415**:75–82 (2011)

10. **N. Chaiyo**, R. Muanghlua, S. Niemcharoen, B. Boonchom, P. Seeharaj, N. Vittayakorn. "Non-isothermal kinetics of the thermal decomposition of sodium oxalate $Na_2C_2O_4$" *Journal of Thermal Analysis and Calorimetry* DOI 10.1007/s10973-011-1675-6 (2011)

Journal of Ceramic Processing Research. Vol. 9, No. 4, pp. 381~384 (2008)

J O U R N A L O F
Ceramic Processing Research

Effect of calcination conditions on phase formation of microwave dielectric cobalt niobate ($CoNb_2O_6$) powders via a mixed oxide synthesis route

Nopsiri Chaiyo and Naratip Vittayakorn*

King Mongkut's Institute of Technology Ladkrabang Nanotechnology Research Center (NRC), King Mongkut's Institute of Technology Ladkrabang, Bangkok, Thailand 10520

Cobalt niobate ($CoNb_2O_6$) powders have been prepared using a mixed oxide synthesis route. The formation of the $CoNb_2O_6$ phase in the calcined powders has been investigated as a function of calcination conditions by differential thermal analysis (DTA) and X-ray diffraction (XRD) techniques. The morphological evolution was determined by scanning electron microscopy (SEM). It has been found that the minor phases of unreacted Co_3O_4 and the orthorhombic-Nb_2O_5 and monoclinic-β-Nb_2O_5 phase tend to form together with the columbite $CoNb_2O_6$ phase, depending on calcination conditions. It is seen that optimization of calcination conditions can lead to a single-phase orthorhombic $CoNb_2O_6$. The calcination temperature and dwell time have been found to have a pronounced effect on the phase formation of the calcined cobalt niobate ($CoNb_2O_6$) powders. Optimization of calcination conditions can lead to a single-phase $CoNb_2O_6$ in a columbite phase.

Key words: $CoNb_2O_6$, Calcination, Powder synthesis.

Introduction

Advances in wireless communication systems are very dependent upon improvements in microwave dielectric materials. In particular, centimetre and millimetre wave wireless applications require high-Q materials that would be less expensive than the known high-Q perovskite-structure, barium-tantalate-based microwave dielectrics and would not need high sintering temperatures [1]. Cobalt niobate $CoNb_2O_6$ is a potential candidate for mechanical filter coatings and electrical applications such as for resonators and capacitors which has a columbite structure having the general formula AB_2O_6, with a *Pcan (no.60)* space group and can be used for capacitors or dielectric resonators for microwave applications due to its low tangent loss (tan δ) and high dielectric constant (ε_r) [1, 2]. Figure 1 shows the columbite structure of $CoNb_2O_6$. Regarding the structure, [M-O_6] (M = Co or Nb) octahedra share edges forming chains along the *c*-axis. Parallel Co-O_6 and Nb-O_6 chains alternate along the *b*-axis. $CoNb_2O_6$ is well known as the key precursor for the successful preparation of single-phase perovskite $Pb(Co_{1/3}Nb_{2/3})O_3$ (PCoN), which is becoming increasingly important for multilayer ceramic capacitor, transducer, electrostrictor and actuator applications [3, 4]. The objective of this investigation was to study the reaction between the starting cobalt oxide and niobium oxide precursors, phase formation, microstructure and microwave dielectric properties of columbite-structure cobalt niobate ceramics.

*Corresponding author:
Tel : +66-9-700-2136
Fax: +66-2-3264415
E-mail: naratipcmu@yahoo.com

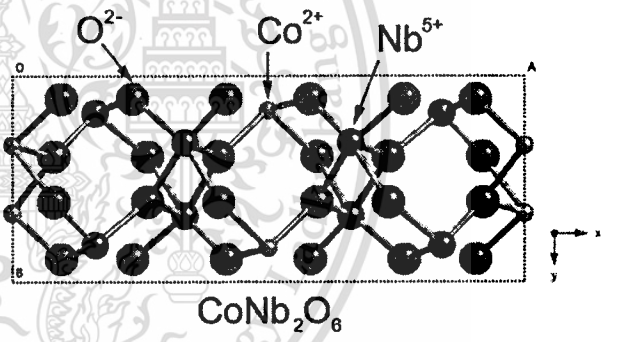

Fig. 1. Crystal structure of $CoNb_2O_6$ compound.

Experimental

Ceramics with the composition $CoNb_2O_6$ were produced by the conventional mixed-oxide route. All samples in this study were prepared from reagent-grade oxides: Co_3O_4 (99.99%, Aldrich, U.S.A.) and Nb_2O_5 (99.9%, Aldrich, U.S.A.). Co_3O_4 and Nb_2O_5 powders were weighed and mixed by ball-milling in a polyethylene bottle together with methyl alcohol and partially stabilized zirconia media. Methyl alcohol was removed by heating at 80 °C for appropriate durations. After drying, the reaction of the uncalcined powders taking place during heat treatment was investigated by differential thermal analysis (DTA; Perkin-Elmer 7 series) using a heating rate of 10 Kminute^{-1} in air from room temperature up to 1350 °C. Based on the DTA results, various calcinations conditions, i.e. temperature ranging from 700-1100 °C and dwell time ranging from 15 to 240 minutes, were applied with a heating/cooling rate of 5 Kminute^{-1}, in order to investigate the formation of $CoNb_2O_6$.

All powders were subsequently examined by room temperature X-ray diffraction (XRD; Bruker D8 Advance) using Ni-filtered CuK_α radiation to identify the phases formed and optimum calcination conditions for the formation of $CoNb_2O_6$ powders. The relative proportions of $CoNb_2O_6$, Co_3O_4, orthorhombic-Nb_2O_5 and monoclinic-β-Nb_2O_5 have been calculated according to the following approximate relationship, by analogy with our treatment of the yield of $CoNb_2O_6$ in a related synthesis [5, 6]:

$$Wt\%\ \text{columbite phase} = \left(\frac{I_{col}}{I_{col} + I_{Co_3O_4} + I_{Otho-Nb_2O_5} + I_{\beta-Nb_2O_5}}\right) \times 100 \quad (1)$$

here I_{col}, $I_{Co_3O_4}$, $I_{Otho-Nb_2O_5}$ and $I_{\beta-Nb_2O_5}$ refer to the intensities of the (311) columbite peak, (311) cubic-Co_3O_4 peak, (180) orthorhombic-Nb_2O_5 and (400) monoclinic-β-Nb_2O_5 peak respectively, these being the strongest reflections in all cases. Microstructural analysis of the ceramic samples was performed by means of scanning electron microscopy (LEO 1455VP, Cambridge, England).

Results and Discussions

Figure 2 shows the DTA curves for the mixture of Co_3O_4 and Nb_2O_5 with a molar ratio of 1 : 3. From Fig. 2, three endothermic peaks centered at 100.6, 357 and 810 °C are observed. The first endothermic peak at 100.6 °C is attributed to the evaporation of water molecules [7]. The second endothermic peak occurring at 357 °C should correspond to the decomposition of the organic species from the milling process [8]. The different temperature, intensities, and shapes of the thermal peaks are probably related to the different nature of the organic species and consequently, caused by the removal of species bounded differently in the network [7, 8]. The third endothermic peak at 810 °C is assigned to the formation of $CoNb_2O_6$ by combination reactions of Co_3O_4 and Nb_2O_5. According

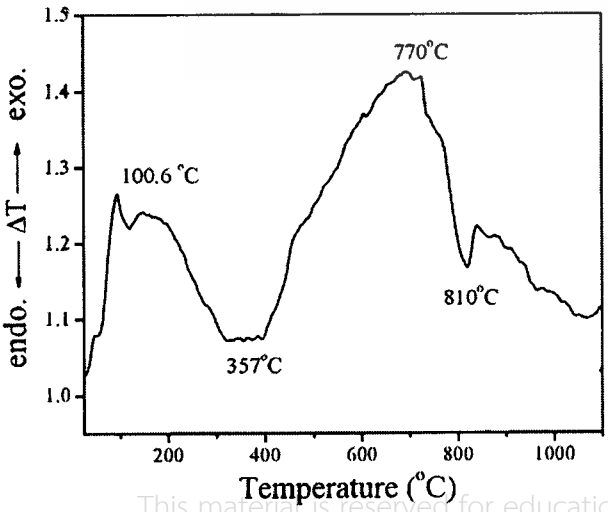

Fig. 2. DTA curve for the mixture of Co_3O_4-Nb_2O_5 powders.

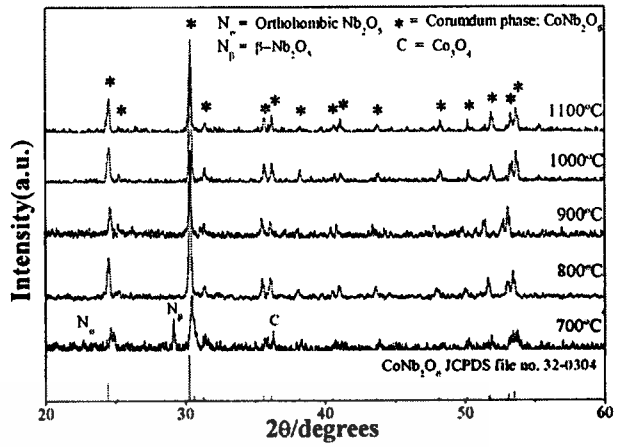

Fig. 3. XRD patterns of $CoNb_2O_6$ powder calcined at various temperatures for 4 h with heating/cooling rates of 20 $Kminute^{-1}$.

to the DTA measurements, these data were used to define the range of calcination temperature for XRD investigation between 700 °C and 1100 °C.

XRD paterns of all calcined powders are given in Fig. 3. It is seen that $CoNb_2O_6$ crystallites were already developed in the powder at a calcination temperature as low as 700 °C, accompanied with cubic-Co_3O_4 (JCPDS files No 78-1969), orthorhombic-Nb_2O_5 (JCPDS files No 27-1003), monoclinic-β-Nb_2O_5 (JCPDS files No 26-0885). No evidence of a cubic phase of CoO was found. The strongest reflection from Co_3O_4, (200), was located at $2\theta = 36.8$ whereas the observed temperature variation of Nb_2O_5 in terms of the intensity and position of the peaks attested to a number of phase changes. In niobium oxide synthesis through precipitation from solution, the calcination temperature has a significant effect on the crystal structure of the resulting oxide. The XRD patterns show that the transformation from the orthorhombic-Nb_2O_5 to monoclinic-β-Nb_2O_5 takes place as the calcination temperature increases, which was reported earlier by Belous et al. [9]. As the temperature increased to 800 °C, the intensity of the columbite $CoNb_2O_6$ peaks was further enhanced and it became the only phase. Upon calcination at 900, 1000 and 1100 °C, an essentially single of $CoNb_2O_6$ phase was obtained. This $CoNb_2O_6$ phase was able to be indexed according to an orthorhombic columbite-type structure with lattice parameters a = 571 pm, b = 1414 pm and c = 504 pm, space group *Pcan (no. 60)*, consistent with JCPDS file number 32-0304. Having established the optimum calcination temperature, dewll times ranging from 15 minute to 120 minute with constant heating/cooling rate of 5 $Kminute^{-1}$ were applied at 800 °C, as shown in Fig. 4. It can be seen that a single-phase of $CoNb_2O_6$ powders was also successfully obtained with a calcinations temperature of 800 °C and a dwell time of 120 minutes or more applied. This was apparently a consequence of the enhancement in crystallinity of the $CoNb_2O_6$ phase with increasing dwell time. The disappearance of monoclinic-β-Nb_2O_5 and orthorhombic-Nb_2O_5 phase indicated that full crystallization has occurred at relative shorter calcinations

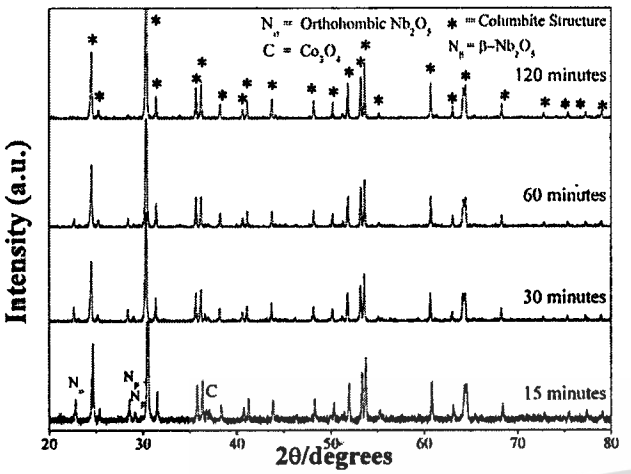

Fig. 4. XRD patterns of $CoNb_2O_6$ powder calcined with heating/cooling rates of 20 Kminute^{-1} at 800 °C for 15-240 minutes.

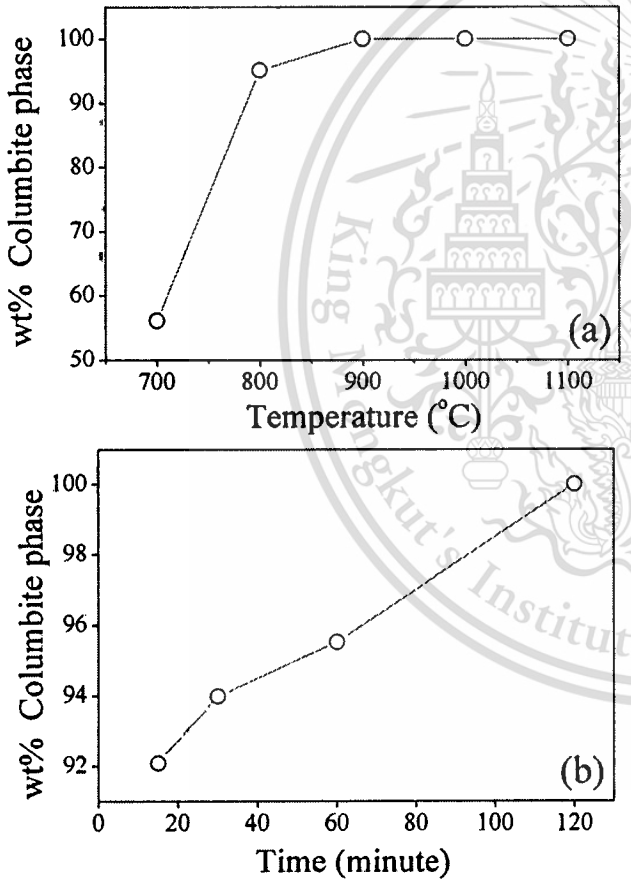

Fig. 5. Fraction of the columbite phase formed in $CoNb_2O_6$ specimens (a) as a function of calcination temperature (calcined for 4 hours) (b) as a function of calcination time (calcined at 800 °C).

times. The observation that the dwell time may also play an important role in obtaining a single phase product is also consistent with other systems [10, 11]. The columbite phase formation at various calcination temperatures and time is shown in Fig. 5(a) and (b). By increasing the calcination temperature from 700 to 1100 °C, the yield of the columbite phase increased significantly until at 800 °C, a single phase of $CoNb_2O_6$ was formed. However, form the present study, there are no significant differences between the powders calcined at temperatures ranging from 800 to 1100 °C. This observation agrees well with those derived from the DTA results. Apart from the calcination temperature, the effect of dwell time was also found to be quite significant (Fig. 4). It is seen that the single phase of $CoNb_2O_6$ (yield 100% within the limitations of the XRD technique) was found to be in powders, calcined at 800 °C with a dwell time of 120 minutes or more. The average grain sizes were determined from XRD patterns according to the Scherrer's equation:

$$D=\frac{k\lambda}{\beta\cos\theta_B} \tag{2}$$

where D is the average grain size, k is a constant equal to 0.89, θ_B is the (311) peak angle, λ is the X-ray wavelength equal to 1.5406 Å and β is the half peak width. The average grain size of $CoNb_2O_6$ powders at 800 °C with a dwell time of 120 minutes was about 280 nm.

Because the raw materials used were multiphase, the formation reaction of the columbite phase belongs to a heterogeneous system. A model used to treat multiphase reaction kinetics was derived by Johnson and Mehl and the equation for this reaction is:

$$\ln[1/(1-y)]=(kt)^n \tag{3}$$

where y is the constant of the columbite phase formed, k the reaction rate constant, t the calcination time and n is the reaction order [12, 13]. The relation of ln [ln $1/(1-y)$] versus ln t is plotted in Fig. 6. From this graph, it was found that the phase transformation of the columbite phase obeys this theory of phase transformations [14]. This phenomenological model is based on the theory of nucleation and growth and is accurate for a large number of systems. The fact that the data in Fig. 6 closely follow Eq. (3) indicates that the columbite phase grows at a constant rate from a random distribution of point nuclei [14]. SEM micrographs of the calcined $CoNb_2O_6$ powders are given in Fig. 7(a) and 7(b). In general, the particles are agglomerated

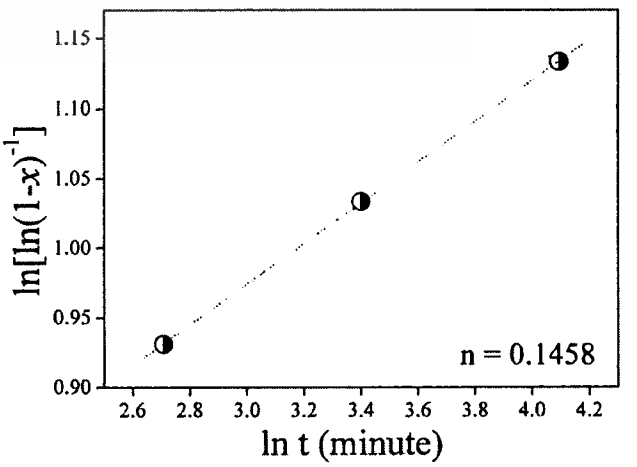

Fig. 6. Johnson-Mehl-Avrami-type for the formation of columbite phase in $CoNb_2O_6$ specimens isothermally heat treated at 800 °C.

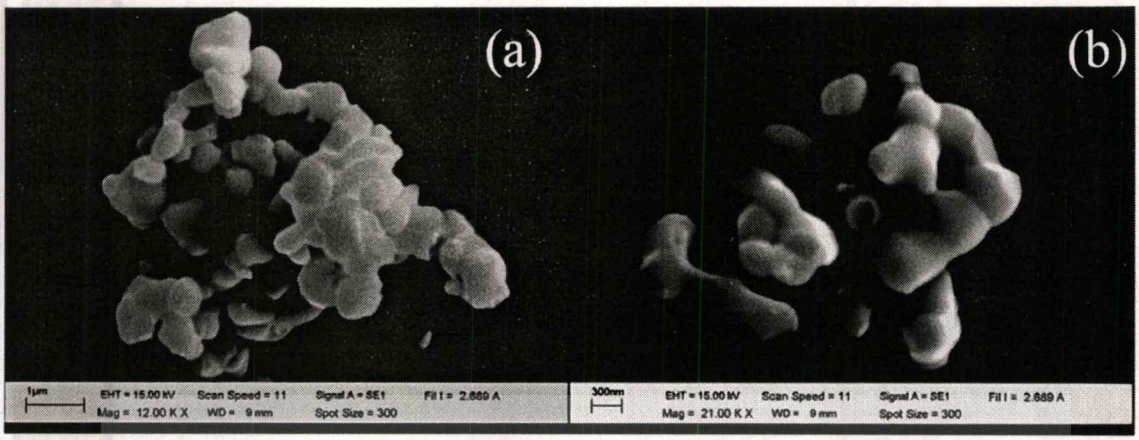

Fig. 7. Scanning electron micrographs of the $CoNb_2O_6$ powders calcined at 800 °C for 2 h, with heating/cooling rate 5 °C/min.

and basically irregular in shape, with a substantial variation in particle size and morphology. The particle size can be estimated from SEM micrographs to be in the range of 70-300 nm. A detailed study at higher magnification (Fig. 7(b)) showed that the particles had spherical secondary particles, composed of nano-sized primary particulates.

Conclusions

Polycrystalline powder of $CoNb_2O_6$ was synthesized using solid state synthesis using oxides as starting materials. Evidence has been obtained for a 100% yield of $CoNb_2O_6$ at a calcination temperature of 800 °C for 120 minutes with heating/cooling rates of 5 $Kminute^{-1}$. XRD showed the compound to have the columbite structure, having orthorhombic lattice parameters of a = 5.06880(± 0.0014)Å, b = 14.1348 (± 0.0046)Å and c = 5.2230 (± 0.0072)Å.

Acknowlegements

This work was supported by the Thailand Research Fund (TRF), the Commission on Higher Education (CHE), Thailand Graduate Institute of Science and Technology (TGIST), National Research Council of Thailand (NRCT) and King Mongkut's Institute of Technology Ladkrabang.

References

1. A.J. Moulson and J.M. Herbert, Electroceramics: Materials, Properties, Appications, Chapman and Hall, New York (1990).
2. A.S. Bhalla, R. Guo and R. Roy, Mat. Res. Innovat. 1 (2000) 3-26.
3. N. Vittayakorn and T. Tunkasiri, Phys. Scr. T129 (2007) 199-204.
4. T.R. Shrout and A. Halliyal, Am. Ceram. Soc. Bull. 66[4] (1987) 704-711.
5. S.L. Swartz and T.R. Shrout, Mater. Res. Bull. 17 (1982) 1245-1250.
6. N. Vittayakorn, J. Ceram. Process. Res. 7 (2006) 288-291.
7. N. Vittayakorn and S. Wirunchit, Smart Mater. Struct. 16 (2007) 851-857.
8. A. Ngamjarurojana, O. Khamman, R. Yimnirun and S. Ananta, Materials Letters 60 (2006) 2867-2872.
9. A.G. Belous, O.V. Ovchar, D.O. Mishchuk, A.V. Kramarenko, B. Jancar, J. Bezjak and D. Suvorov, Inorg. Mater. 43 (2007) 412-417.
10. R. Wongmaneerung, R. Yimnirun and S. Ananta, Materials Letters 60 (2006) 2666-2671.
11. R. Wongmaneerung, T. Sarakonsri, R. Yimnirun and S. Ananta, Mat. Sci. Eng. B-Solid. 132 (2006) 292-299.
12. M.J. Avrami, J. Chem. Phys. 8 (1940) 212-224.
13. M.J. Avrami, J. Chem. Phys. 9 (1941) 177-184.
14. J.W. Christian, The Theory of Transformations in Metals and Alloys: Part I., Pergamon Press, Oxford (2002).

Advanced Materials Research Vols. 55-57 (2008) pp 49-52
online at http://www.scientific.net

Effect of Annealing on the Structure and Dielectric Properties in PZT-PCoN Ceramics

N. Vittayakorn[1,5,a], N. Chaiyo[1], R. Muanghlua[2], A. Ruangphanit[3] and W. C. Vittayakorn[4]

[1] King Mongkut's Institute of Technology Ladkrabang Nanotechnology Research Center(NRC), King Mongkut's Institute of Technology Ladkrabang, Bangkok, Thailand 10520

[2]Electronics Research Center, Faculty of Engineering, King Mongkut's Institute of Technology Ladkrabang, Bangkok Thailand 10520

[3] Department of Physics, Faculty of Science, Chiang Mai University, Chiang Mai, Thailand 50200

[4] Thai Microelectronics Center (TMEC), National Electronics and Computer Technology Center, Nation Science and Technology Development Agency, Ministry of Science and Technology, Chachoengsao 24000, Thailand

[5] Materials Science Research Unit, Department of Chemistry, Faculty of Science, King Mongkut's Institute of Technology Ladkrabang, Bangkok, Thailand 10520

[a] e-mail: naratipcmu@yahoo.com

Keyword: Ferroelectric Materials, Lead Zirconate Titanate, Lead Cobolt Niobate

Abstract The solid solution between the normal ferroelectric $Pb(Zr_{1/2}Ti_{1/2})O_3$ (PZT) and relaxor ferroelectric $Pb(Co_{1/3}Nb_{2/3})O_3$ (PCoN) was synthesized by the solid state reaction method. Sintered PZT-PCoN ceramics were annealed at temperatures ranging from 850 to 1,100°C for 4 h. X-ray diffraction patterns revealed changes of crystalline structure after annealing, which could be correlated to the accompanied changes in dielectric properties. Furthermore, significant improvements in the dielectric responses were observed in this system. After annealing, a huge increase of up to 200% occurred in the dielectric constants, especially near the temperature of maximum dielectric constant.

Introduction

Piezoelectric lead zirconate titanate (PZT) ceramic material has been widely used for transducer applications, due to its excellent piezoelectric properties, and was a candidate in a number of recent investigations [1, 2]. It is well known that PZT material is almost always used with a dopent, modifier or other chemical constituents to improve and optimize its basic properties for a particular application [1, 3]. Lead zirconate titanate ceramics and their solid solution, along with several complex perovskite oxides represented by $Pb(B'B'')O_3$, have been investigated [4-6]. Among the various complex ferroelectric oxide materials, several niobates with transition temperatures below room temperature are $Pb(Mg_{1/3}Nb_{2/3})O_3$, $Pb(Ni_{1/3}Nb_{2/3})O_3$, and $Pb(Co_{1/3}Nb_{2/3})O_3$. Among them, lead cobalt niobate [$Pb(Co_{1/3}Nb_{2/3})O_3$ (PCoN)] is also a typical ferroelectric relaxor material with a transition temperature of -70°C, as reported by Smolenskii *et al.* [7] in 1958 . In this compound, the octahedral sites of the crystal are occupied randomly by Co^{2+} and Nb^{5+} ions. Recently, our previous work has shown promise in producing phase pure perovskite PZT–PCoN ceramics with the solid state reaction method [5, 8]. A morphotropic phase boundary (MPB) between the PCoN-rich pseudo-cubic phase and the PZT-rich tetragonal phase was reported at $0.7Pb(Zr_{1/2}Ti_{1/2})O_3$:$0.3Pb(Co_{1/3}Nb_{2/3})O_3$ [5].

In this study, we emphasized the effect of annealing on the crystal structure, and dielectric properties in PZT–PCoN ceramics. Based on our previous results for the PZT–PCoN system, PZT containing 30 mol% of PCoN was selected as the starting composition, which is close to the rhombohedral MPB in this system. For annealing, the samples were heat treated at 850-1,100°C for

4 hours in a sealed Al_2O_3 crucible, with PbO-rich atmosphere. This paper reports evolution of the perovskite phase, and crystal structure of the PZT–PCoN ceramics. Next, the temperature and frequency dependence of the dielectric constant are given for as-sintered and annealed samples. The results of influence on the post-sintering annealing of these properties are shown in brief.

Experiment

The $0.7Pb(Zr_{1/2}Ti_{1/2})O_3$-$0.3Pb(Co_{1/3}Nb_{2/3})O_3$ ceramics were prepared by conventionally mixed–oxide processing, in which stoichiometric mixtures of reagent-grade metal oxide powders of 99% + purity (PbO, CoO, TiO_2, ZrO_2 and Nb_2O_5) were used as the starting raw materials. Thermal synthesis of blended and pressed mixture of the starting material was carried out at 900°C for a period of 4 h. Crumbled, milled and sieved material was pressed again in the form of cylinders and then sintered at 1,100°C for 4 h. The sintered pellets were then annealed at various temperatures from 850 to 1,100°C for 4 h. These annealing processes were performed in a double crucible, with interior PbO + ZrO_2 atmosphere, in order to maintain the established composition and, especially, avoid the loss of PbO caused by its sublimation. The Archimedes displacement method with distilled water was employed to evaluate sample density. The ceramic pellets were ground and polished to make parallel surfaces, and densities were determined geometrically. After gold sputtering onto the major faces of the pellets as electrodes, dielectric constants and losses at the frequency decades of 10 kHz were measured, using a computer-interfaced LCR meter.

Results and Discussions

The phase development in the annealed samples was analyzed by XRD and the results are presented in Figure 1. All samples show a single-phase powder diffraction pattern. No secondary reaction phases such as PbO, Pb-based compounds, unreacted oxide and so on, are observed in the pattern.

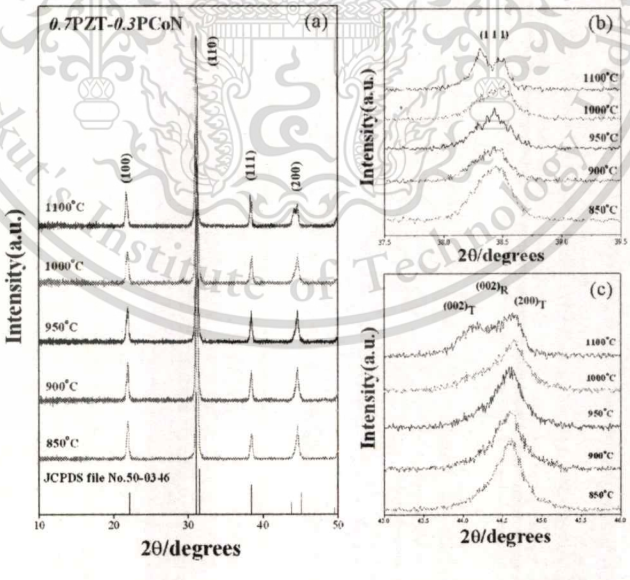

Figure 1 (a) XRD patterns of 0.7PZT-0.3PZN annealed samples at various temperatures for 4 h, (b) XRD pattern of the (1 1 1) peak, (c) XRD pattern of the (2 0 0) peak.

After annealing, a significant change in the crystal structure was observed, especially above an annealing temperature of 1,000°C, where the crystal structure changes from pseudo-cubic to tetragonal and rhombohedral. On the basis of XRD and dielectric experiments, we have identified the MPB in the $(1 - x)$PZT–xPCoN system from our previous work. The MPB resides at around $x \sim 0.2$, separating the tetragonal phase for $x \leq 0.2$ from the rhombohedral phase for $x \geq 0.3$. In this study, the XRD data show that splitting of the (200) and (111) peak is not observed in ceramic

samples annealed at temperatures below 1,000°C. These results indicated that the major phase in this ceramic sample had pseudo-cubic symmetry. Splitting of the (200) peak becomes more pronounced as the annealing temperature approaches 1,100°C, thus indicating stabilization of the tetragonal phase. Furthermore, the unambiguous splitting of the (111) peak indicated the coexistence of the rhombohedral and tetragonal phase. The co-existence of the tetragonal and rhombohedral phase is seen clearly when the XRD profile peak splits with increasing annealing temperature. From these results, it is clear that the composition of the annealed sample has shifted very closely to the MPB.

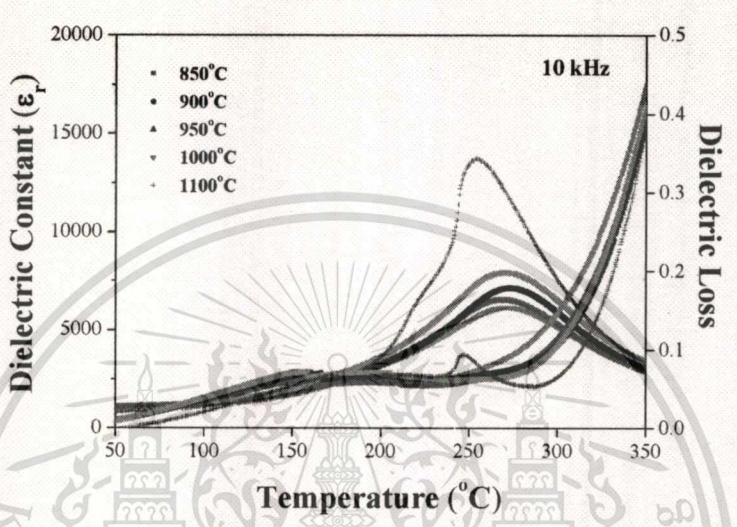

Figure 2 Variation of the dielectric constant (ε_r) and loss tangent (tan δ) with different annealing temperatures at 10 kHz.

Figure 3 SEM photographs of 0.7PZT-0.3PCoN ceramics (a) as-sintered samples (b) annealing at 1,100°C.

Figure 2 shows the dielectric constant (ε_r) at 10 kHz versus the temperature for *0.7*PZT-*0.3*PCoN ceramics annealed at different temperatures for 4 h. After annealing, a significant improvement in the dielectric constant was observed, especially near the temperature of the maximum dielectric constant (ε_m), where the improvement was up to 200%. This change in behavior might be due to a shift in a chemical composition close to the MPB, caused by thermal annealing. This behavior is consistent with the conclusions of Randall *et al.* [9]and Leite *et al.* [10] in the PMN–PT system. Figure 3 shows scanning electron microscopy (SEM) images of the fractured surfaces of 0.7PZT-

0.3PCoN ceramics before and after annealing at 1,100°C. There was no change in the grain size. The density of the samples decreased from 8.120 to 8.015 g/cm^3 after annealing at 1,100°C for 4 h. Obviously, the decrease in density did not lead to an improvement of electrical responses.

Summary

The dielectric properties of 0.7PZT–0.3PCoN ceramics, formed via the solid state reaction, were investigated. Thermal annealing was seen to be effective at improving the dielectric and piezoelectric responses of PZT-based ferroelectric ceramics. The annealing time was found to have an effect on the electrical properties. After annealing at 1,100°C for 4h in a PbO-rich atmosphere, *0.7*PZT–*0.3*PCoN ceramics with ε_m 14,400 were achieved in this study. The large improvements in dielectric properties after annealing were attributed to a shift in the phase composition to the MPB composition.

Acknowledgements

This work was supported by the Thailand Research Fund (TRF), the Commission on Higher Education (CHE), Thailand Graduate Institute of Science and Technology (TGIST), National Research Council of Thailand (NRCT) and King Mongkut's Institute of Technology Ladkrabang (KMITL).

References

[1] G. H. Haertling: J. Am. Ceram. Soc. Vol. 82 (1999), p. 797.
[2] K. Uchino: *Ferroelectric Devices* (Marcel Dekker,Inc., New York, 2000)
[3] K. Uchino: Solid State Ionics Vol. 108 (1998), p. 43.
[4] N. Vittayakorn, G. Rujijanagul, X. Tan, M. A. Marquardt and D. P. Cann: J. Appl. Phys. Vol. 96 (2004), p. 5103.
[5] N. Vittayakorn and T. Tunkasiri: Phys. Scr. Vol. T129 (2007), p. 199.
[6] N. Vittayakorn, G. Rujijanagul, X. Tan, H. He, M. A. Marquardt and D. P. Cann, J. Electroceramic Vol. 16 (2006), p. 141.
[7] G. A. Smolenskii and A. L. Agranovskaya: Sov. Phys.-Tech. Phys. (1958), p. 1380.
[8] N. Vittayakorn, S. Wirunchit, S. Traisak, R. Yimnirun and G. Rujijanagul: Curr. Appl Phys. Vol. 8 (2008), p. 128.
[9] C. A. Randall, A. D. Hilton, D. J. Barber and T. R. Shrout: J. Mater. Res. Vol. 8 (1993), p. 880.
[10] E. R. Leite, A. M. Scotch, A. Khan, T. Li, H. M. Chan, M. P. Harmer, S.-F. Liu and S.-E. Park: J. Am. Ceram. Soc. Vol. 85 (2002), p. 3018.

Advanced Materials Research Vols. 55-57 (2008) pp 873-876
online at http://www.scientific.net

Synthesis, Phase Formation and Characterization of $Co_4Nb_2O_9$ Powders Synthesized by Solid-State Reaction

N. Chaiyo[1], R. Muanghlua[2], A. Ruangphanit[3], W. C. Vittayakorn[4] and N. Vittayakorn[1,5,a]

[1] King Mongkut's Institute of Technology Ladkrabang Nanotechnology Research Center (NRC), King Mongkut's Institute of Technology Ladkrabang, Bangkok, Thailand 10520

[2]Electronics Research Center, Faculty of Engineering, King Mongkut's Institute of Technology Ladkrabang, Bangkok Thailand 10520

[3] Thai Microelectronics Center (TMEC), National Electronics and Computer Technology Center,

Nation Science and Technology Development Agency, Ministry of Science and Technology, Chachoengsao 24000, Thailand

[4] Department of Physics, Faculty of Science, Chiang Mai University, Chiang Mai, Thailand 50200

[5] Materials Science Research Unit, Department of Chemistry, Faculty of Science, King Mongkut's Institute of Technology Ladkrabang, Bangkok, Thailand 10520

[a] e-mail: naratipcmu@yahoo.com

Keywords: $Co_4Nb_2O_9$; Calcinations; Powder synthesis; Microwave dielectric

Abstract. A corundum-type structure of cobalt niobate ($Co_4Nb_2O_9$) has been synthesized by a solid-state reaction. The formation of the $Co_4Nb_2O_9$ phase in the calcined powders was investigated as a function of calcination conditions by differential thermal analysis (DTA) and X-ray diffraction (XRD) techniques. Morphology and particle size have been determined by scanning electron microscopy (SEM). It was found that the minor phases of unreacted Co_3O_4 tend to form together with the columbite $CoNb_2O_6$ phase at a low calcination temperature and short dwell time. It seems that the single-phase of $Co_4Nb_2O_9$ in a corundum phase can be obtained successfully at the calcination conditions of 900°C for 60 min, with heating/cooling rates of 20°C /min.

Introduction

A variety of microwave dielectric ceramics have been utilized for microwave dielectric applications including the filters and resonators in the wireless communication system [1]. There are three important properties required, i.e., a high dielectric constant ε_r, high quality factor $Q \times f$ and low temperature coefficient of resonant frequency τ_f., in order to miniaturize the size of the microwave dielectric resonator and reach suitability for application at high frequency, and the resonant frequency must be stable at various operating temperatures. A high $Q \times f$ value of more than 30,000 GHz is required to withstand high electric loads, especially for microwave dielectric ceramics used in the base stations of mobile phones. However, still higher $Q \times f$ – value materials are required for new digital systems [2]. Over the past few years, the demand for smaller, lighter and temperature stable devices has increased. Cobalt niobate $CoNb_2O_6$ is one of the best known microwave dielectric materials, which recently gained considerable attention. In general, production of single-phase $CoNb_2O_6$ is not straightforward, as a minor concentration of $Co_4Nb_2O_9$ sometimes forms alongside the major phase of $CoNb_2O_6$. The crystal structure of $Co_4Nb_2O_9$ ceramic is known to have a corundum-type structure. The oxygen ions are located at the lattice sites of a hexagonal closed-packed unit cell. In the HCP crystal structure, as in the FCC structure, there are as many octahedral interstitial sites as there are atoms in the unit cell. In recent study, the microwave dielectric properties of a corundum-type structure such as $Mg_4Nb_2O_9$ ceramic was reported to have a high $Q \times f$ value, which was comparable to that of Al_2O_3. Thus far, although $Co_4Nb_2O_9$ is identical

in stoichiometry to $Mg_4Nb_2O_9$, it has not been synthesized to the corundum-type structure. Interestingly, the mixed oxide route for the production of $Co_4Nb_2O_9$ powders has not received detailed attention, and the effects of calcination conditions have not yet been studied extensively. The objective of this work was to study the reaction between the starting cobalt oxide and niobium oxide precursors, phase formation and microstructure of corundum-type structure cobalt niobate powder.

Experimental

Reagent-grade oxides of Co_3O_4 (99.99 %, Aldrich, USA) and Nb_2O_5 (99.9%, Aldrich, USA) were used in this study. $Co_4Nb_2O_9$ powders were synthesized by the solid-state reaction of Co_3O_4 and Nb_2O_5 powders that were homogenized by ball milling with ethyl alcohol in the required stoichiometric ratio. The mixed slurry was dried at 80°C. The reactions of the uncalcined $Co_4Nb_2O_9$ powder, taking place during heat treatment, were investigated by differential thermal analysis (DTA; Perkin-Elmer 7 series) using a heating rate of 10°C /min in air from room temperature to 1,350 °C. According to the DTA results, various calcination conditions (i.e. temperatures ranging from 700 – 1,100°C and dwell times from 15 to 240 min) were applied, with a heating/cooling rate of 20°C/min in order to investigate the formation of $Co_4Nb_2O_9$. Calcined powders were subsequently examined by room temperature X-ray diffraction (XRD; Bruker D8 Advance) using Ni-filtered CuK_α radiation to identify the phase formed and optimum calcination condition for the formation of $Co_4Nb_2O_9$ powders. Powder morphologies and grain size were directly imaged using scanning electron microscopy (LEO, LEO 1455VP, Cambridge, England).

Results and Discussion

The DTA curve for the powder mixed in the stoichiometric proportions of $Co_4Nb_2O_9$ is shown in Figure 1. Three endothermic peaks centered at 121°C, 294°C and 837°C were observed. The first and second endothermic peaks should correspond to the evaporation of water molecules and decomposition of the organic species from the milling process, respectively [3, 4]. The third endothermic peak, at 837 °C, was assigned to the formation of $Co_4Nb_2O_9$ by combination reactions of Co_3O_4 and Nb_2O_5. Based on the DTA measurements, these data were used to define the range of calcination temperature at between 700 to 1,100 °C for XRD investigation.

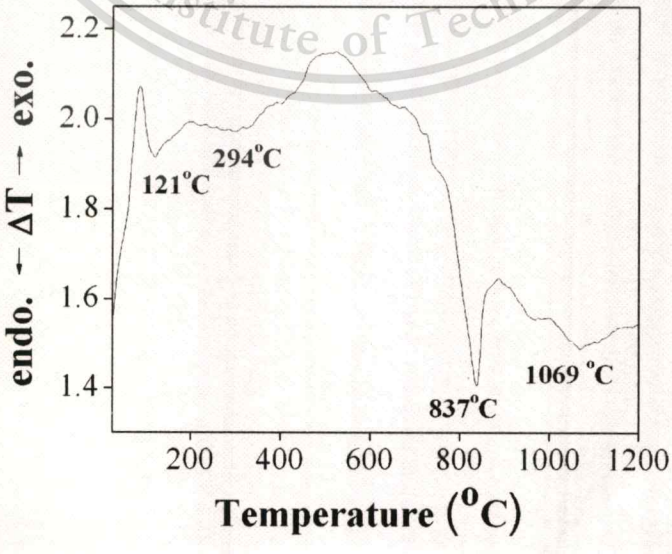

Figure 1. DTA curve for the mixture of Co_3O_4-Nb_2O_5 powder.

XRD patterns of all calcined powders are given in Figure 2. At a clacination temperature as low as 800°C, the strongest reflections were apparent in the majority of the XRD patterns, which indicated the formation of a columbite phase of $CoNb_2O_6$ (A) that could be matched with JCPDS file numbers 32-0304. The minor phase of unreacted cubic-Co_3O_4 (Y), which could be matched with JCPDS files No 78-1969, were found. As the calcination temperature increased to 900°C, intensity of the corundum $Co_4Nb_2O_9$ peaks was enhanced further and became the monophasic phase. This $Co_4Nb_2O_9$ phase was indexable according to a hexagonal corundum-type structure, with a lattice parameter of a = 517 pm and c = 1412 pm, and space group *P3c1* (no. 165), consistent with JCPDS file numbers 38-1457. Upon calcinations at 1,000 and 1,100 °C, an essentially monophasic phase of $Co_4Nb_2O_9$ was obtained. However, in this work, there were no significant differences between the powders calcined at temperatures ranging from 900 to 1,100 °C.

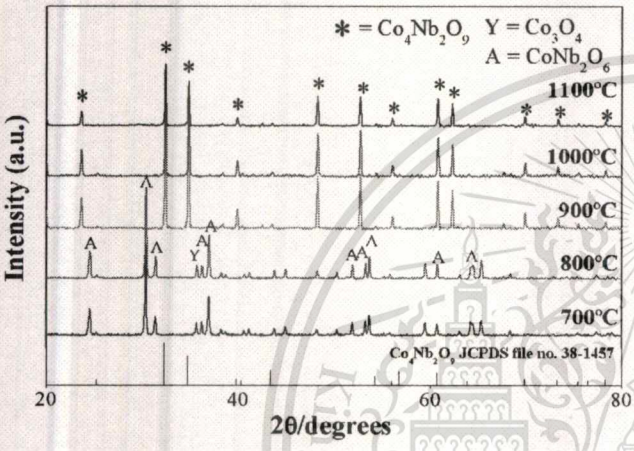

Figure 2. XRD patterns of $Co_4Nb_2O_9$ powder calcined at various temperatures for 4 h with heating/cooling rates of 20 °C /min.

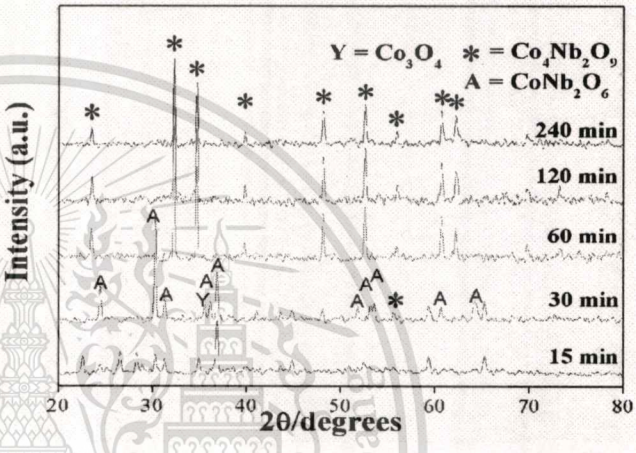

Figure 3. XRD patterns of $Co_4Nb_2O_9$ powder calcined with heating/cooling rates of 20 °C /min at 900 °C for 15-240 min.

After obtaining the optimum calcination temperature, dwell times ranging from 15 min to 120 min, with a constant heating/cooling rate of 20°C/min were applied at 900 °C, as shown in Figure 3. It was observed that the single-phase of $Co_4Nb_2O_9$ (yield of 100% within the limitations of the XRD technique) powder was possible in powders calcined at 900°C, with a dwell time of 60 min or more applied. Observation that the dwell time effect may also play an important role in obtaining a single-phase product is also consistent with other systems [5, 6].

The average grain sizes were determined from the XRD pattern according to the Scherrer's equation

$$D = \frac{k\lambda}{\beta \cos\theta_B}$$

where D is the average grain size, k is a constant equal to 0.89, θ_B is the (3 1 1) peak angle, λ is the X-ray wavelength equal to 1.5406 Å and β is the half peak width. The average grain size of $Co_4Nb_2O_9$ powders was about 280 nm at 900 °C, with a dwell time of 60 min. The morphology of the calcined $Co_4Nb_2O_9$ powders was investigated by scanning electron microscopy (SEM), which is illustrated in Figure 4(a) and 4(b). In general, the particles are agglomerated and basically irregular in shape, with a substantial variation in particle size and morphology. The particle size can be estimated in the range of 300-400 nm from SEM micrographs. A detailed study at higher

magnification [Fig. 5(b)] shows that the particles had spherical secondary particles, composed of nano-sized primary particulates.

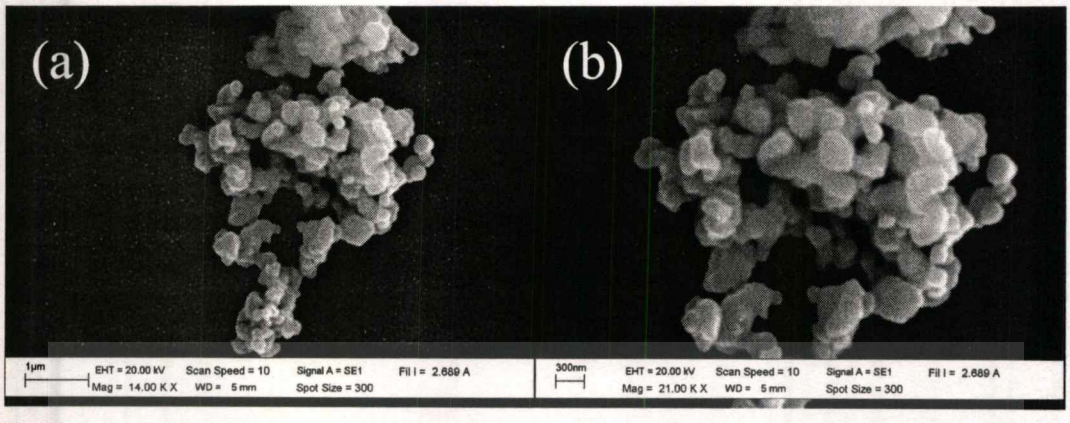

Figure 4. Scanning electron micrographs of the $Co_4Nb_2O_9$ powders calcined at 900 °C for 60 min, with a heating/cooling rate of 20 °C /min.

Summary

The corundum-structure, $Co_4Nb_2O_9$, was synthesized by solid state reaction using oxides as starting materials. The content of the impurity phases decreased with increasing calcination temperature and dwell time. Evidence has been obtained of a 100% yield of $Co_4Nb_2O_9$ at a calcination temperature of 900°C for 60 min, with heating/cooling rates of 20°C/minute. XRD showed the compound to have a corundum structure, with hexagonal lattice parameters of a = 5.1669(± 0.0014) and c = 14.1248 (± 0.0072). The particle size can be estimated in the range of 300-400 nm from SEM micrographs.

Acknowledgements

This work was supported by the Thailand Research Fund (TRF), the Commission on Higher Education (CHE), Thailand Graduate Institute of Science and Technology (TGIST), National Research Council of Thailand (NRCT) and King Mongkut's Institute of Technology Ladkrabang (KMITL).

References

[1] A. Kan, H. Ogawa, A. Yokoi and Y. Nakamura: J. Euro. Ceram. Soc. Vol. 27 (2007), p. 2977.
[2] A. J. Moulson and J. M. Herbert: *Electroceramics: Materials, Properties, Appications* (Chapman and Hall, New York, 1990)
[3] S. Ananta, Mater. Lett. Vol. 58 (2004), p. 2530.
[4] R. Wongmaneerung, T. Sarakonsri, R. Yimnirun and S. Ananta: Materials Science and Engineering: B. Vol. 130 (2006), p. 246.
[5] R. Wongmaneerung, R. Yimnirun and S. Ananta: Mater. Lett. Vol. 60 (2006), p. 2666.
[6] S. Wongsaenmai, R. Yimnirun and S. Ananta: Mater. Lett. Vol. 61 (2007), p. 2426.

Ferroelectrics, 383:1–7, 2009

ISSN: 0015-0193 print / 1563-5112 online
DOI: 10.1080/00150190902873303

Taylor & Francis
Taylor & Francis Group

Preparation and Properties of Lead Free Bismuth Sodium Titanate–Bismuth Zinc Titanate Ceramics

RANGSON MUANGHLUA,[1] SURASAK NIEMCHAROEN,[1] WANWILAI C. VITTAYAKORN,[2] NATTAPONG TUNGSITVISETKUL,[3] PIMJAN CHINWARO,[3] ANUCHA RUANGPHANIT,[4] NOPSIRI CHAIYO,[5] AND NARATIP VITTAYAKORN[3,5,*]

[1]Department of Electronics, Faculty of Engineering, King Mongkut's Institute of Technology, Ladkrabang, Bangkok, Thailand 10520
[2]Department of Physics and Materials Science, Faculty of Science, Chiang Mai University, Chiang Mai 50200, Thailand
[3]Materials Science Research Units, Department of Chemistry, Faculty of Science, King Mongkut's Institute of Technology, Ladkrabang, Bangkok 10520, Thailand
[4]Thai Microelectronics Center (TMEC), National Electronics and Computer Technology Center, Nation Science and Technology Development Agency, Ministry of Science and Technology, Chachoengsao 24000, Thailand
[5]Collage of KMITL Nanotechnology King Mongkut's Institute of Technology, Ladkrabang, King Mongkut's Institute of Technology, Ladkrabang, Bangkok 10520, Thailand

Lead-free piezoelectric ceramics based on $(1-x)Bi_{1/2}Na_{1/2}TiO_3 - x\ Bi(Zn_{1/2}Ti_{1/2})O_3$ *(*$x = 0.0, 0.02, 0.04, 0.06, 0.08, 0.10, 0.20, 0.30, 0.40$, *and* 0.5*) were obtained via solid-state processing techniques. The influence of BZT addition on BNT characteristics, sintering, microstructure and properties was investigated. A single perovskite phase with rhombohedral symmetry was obtained for* $Bi(Zn_{1/2}Ti_{1/2})O_3$ *substitutions of up to 10 mole%. A small amount of BZT was effective for improving both sintering behavior and dielectric properties of BNT ceramics. Optimized dielectric properties were obtained for samples with a maximum density of* $\rho = 98.3\%$ *for the composition,* $x = 0.1$.

Keywords Lead-free piezoelectric ceramics; dielectric properties; perovskite structure; $(Bi_{0.5}Na_{0.5})TiO_3$; $Bi(Zn_{0.5}Ti_{0.5})O_3$

PACS: 64.70.K-, 77.22.Ch, 81.05.Je, 85.80.-n and 77.84.Dy

Introduction

The effects of toxic lead oxide, a major constituent of the most widely used piezoelectric materials $PbZrO_3$-$PbTiO_3$ (PZT), are considered a danger to nature. For protection of the

Received August 3, 2008; in final form December 31, 2008.
*Corresponding author. E-mail: naratipcmu@yahoo.com

environment, Restriction of Hazardous Substances (RoHS) regulations, European Union's Waste Electrical and Electronics Equipment (WEEE) and other requirements have been established [1, 2]. As of July 1st, 2006, all new electrical and electronic products put on the European Market and falling under the scope of the European Union directive, RoHS, have to comply with stated requirements. Every homogeneous material within covered products is restricted to a maximum concentration of 0.1% by weight of lead, mercury, hexavalent chromium, PBB and PBDE, and a maximum of 0.01% by weight of cadmium. According to supporting requirements, there was an increase in the attentiveness of lead-free materials. As many researches have reported, $Bi_{0.5}Na_{0.5}TiO_3$; BNT (which was discovered by Smolensky et al. in 1960 [3]) is one of the most important lead-free piezoelectric materials with a perovskite structure. BNT possesses strong ferroelectric properties at a relatively high Curie temperature ($T_c = 320°C$) and phase transition point from ferroelectric to antiferroelectric ($T_p = 200°C$), with a relatively large remanent polarization ($P_r = 38\ \mu C/cm^2$) and coercive field ($E_c = 73$ kV/cm) at room temperature [3–8]. Apart from its strong ferroelectric, when compared with PZT, BNT-based materials possess high anisotropic electromechanical coupling properties ($k_t \geq 0.48$, $k_p \approx 0.165$–0.255), high frequency constant ($N_t \geq 2550$ Hz · m) and lower dielectric constant ($\varepsilon_{33}^T \approx 290$–$524$) [6]. Nevertheless, it is hard to pole pure BNT for its large coercive field and relatively large conductivity. To improve some poor properties of BNT, numerous modifications of BNT-based ceramics have been developed. Many researches have suggested that the improvement of piezoelectric properties can be achieved by forming solid solution with other perovskite oxides. Several solid solutions of BNT, with $SrTiO_3$, $La_2(TiO_3)_3$, $NaNbO_3$, and $BaTiO_3$, have been investigated [4].

$Bi(Zn_{1/2}Ti_{1/2})O_3$ (BZT) is a ferroelectric material, which has a Zn^{2+} and Ti^{4+} complex on the B-site of the ABO_3 perovskite structure, with a tetragonal symmetry [9]. The solid solution of $(x)PbTiO_3$–$(1–x)Bi(Zn_{1/2}Ti_{1/2})O_3$ has been studied by Suchomel et al.[10]. The $(x)PbTiO_3 - (1–x)Bi(Zn_{1/2}Ti_{1/2})O_3$ system exhibits a high c/a ratio of 1.11 for $x = 0.60$. However, there have been no systematic investigations on the solid solution of BNT-BZT ceramics. In this paper, the preparation of bismuth zinc titanate (BZT) —modified bismuth sodium titanate (BNT) ceramics, with compositions $(1 - x)Bi_{1/2}Na_{1/2}TiO_3 - x\ Bi(Zn_{1/2}Ti_{1/2})O_3$ ($x = 0.0$, 0.2, 0.4, 0.6, 0.8, 0.10, 0.20, 0.30, 0.40, and 0.5) ceramics through the solid-state processing techniques, was investigated. The influence of BZT addition on the powder, crystal structure, microstructure and dielectric properties was examined.

Experimental Procedure

Bismuth zinc titanate (BZT) — modified bismuth sodium titanate (BNT) ceramics with compositions $(1\text{-}x)Bi_{1/2}Na_{1/2}TiO_3 - x\ Bi(Zn_{1/2}Ti_{1/2})O_3$ ($x = 0.0$, 0.2, 0.4, 0.6, 0.8, 0.10, 0.20, 0.30, 0.40, and 0.5) were prepared by the solid-state processing techniques. High-purity oxides and carbonates; Na_2CO_3 (99.5%), Bi_2O_3 (99.97%), ZnO (99.9%) and TiO_2 (99.9%) were used as starting materials, which had been treated carefully by a special drying process before use, particularly for sodium carbonates. In the first stage, Bi_2O_3, Na_2CO_3 and TiO_2 were thoroughly mixed in the stoichiometric ratio, and then calcined at 900°C for 24 h to form $(Bi_{0.5}Na_{0.5})TiO_3$; BNT. In the second stage, the precursor (BNT) was mixed in the stoichiometric ratio with other starting materials. After drying at 80°C for 16 h, powders were calcined in a closed alumina crucible at 900°C for 4 h, with a heating/cooling rate of 20°C/min. The calcined powders were then mixed with 5 wt% polyvinyl alcohol (PVA) and pressed into discs, 1.5 cm in diameter. The green discs were sintered at 1,150°C for 6

h, with a heating/cooling rate of 5°C/min and covered with calcined powders in order to protect from the loss of bismuth. Formation of the perovskite phase and crystal structure of BNT-BZT was examined by room temperature X-ray diffraction (XRD, Advance D8) using Ni-filtered CuK_α radiation. Morphologies and grain size were imaged directly using a scanning electron microscope (SEM, LEO1455 VP). Dielectric measurements were carried out at room temperature by an LCR meter (Hewlett-Packard, 4284A).

Results and Discussion

Figure 1 illustrates the X-ray diffraction patterns of $(1-x)$BNT-xBZT; $x = 0.0$–0.5 powders calcined at 900°C for 4 h, with a heating/cooling rate of 20°C/min. At a BZT ratio of up to 0.10, X-ray diffraction patterns showed that a pure perovskite structure was obtained with no impurity phases, and/or no individual phases from the precursors were presented. As the fraction of BZT in the solid solution was increased to above 0.10, the pyrochlore phase began to develop and increase in intensity with increasing BZT concentration. These results indicate that the presence of BZT in the solid solution decreases the structural stability of the BNT perovskite phase. In other words, this result indicates that BZT has limited solubility in BNT ceramics, which tends to be solved at a concentration of 0.1mol. In addition, the X-ray diffraction patterns revealed that the crystal structure was influenced by BZT addition. Without BZT doping, the pure BNT possesses a rhombohedral phase, with a (110) peak detectable at 32.48° (2θ), which could be matched with $Bi_{1/2}Na_{1/2}TiO_3$ JCPDS file no. 36-0340. As the BZT content in the compounds is increased, the diffraction angle of (1 1 1) peaks in the BNT-BZT powders and shifts downwards to lower 2θ angles, as illustrated in Fig. 2(a). This phenomenon indicated that a consecutive increase in lattice constant is a function of BZT fraction. As we know, the ionic radius of Zn^{2+} ($r_{Zn^{2+}} =$ 88 pm) is larger than that of Ti^{4+} ($r_{Ti^{4+}} = 74.5$ pm), which results in lattice distortion and an increased lattice constant of the ceramic. The X-ray diffraction patterns of these

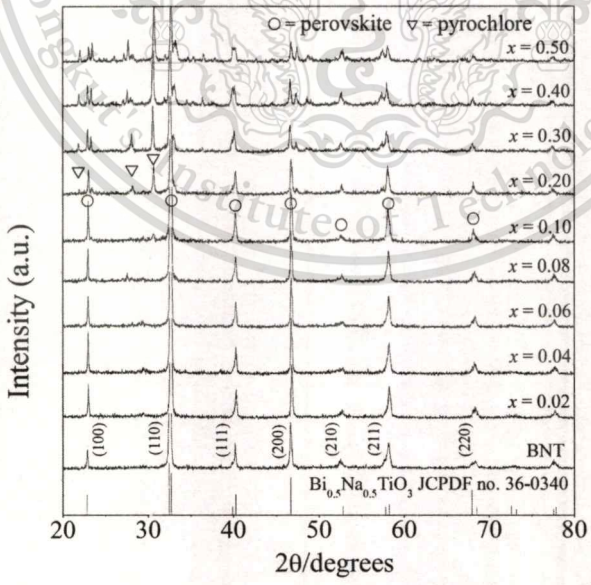

Figure 1. X-ray diffraction patterns of (1-x)BNT-xBZT; $x = 0.0$–0.5 powders calcined at 900°C for 4 h, with a heating/cooling rate of 20°C/min.

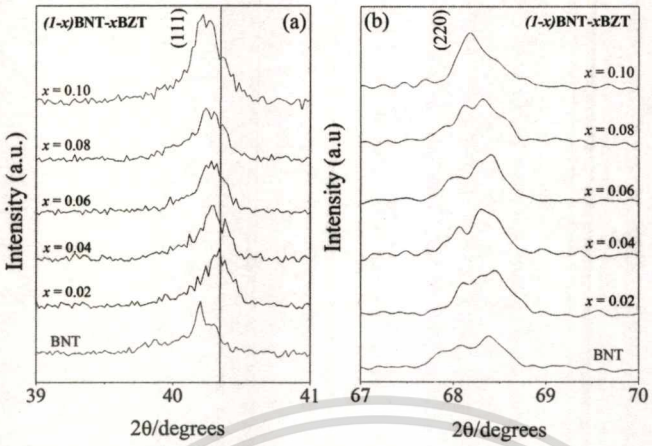

Figure 2. X-ray diffraction patterns of (1-x)BNT-xBZT; $x = 0.0$-0.1 powders calcined at 900°C for 4 h, with a heating/cooling rate of 20°C/min.

powders also indicate a phase transition from rhombohedral to cubic, with increasing BZT concentration. The rhombohedral symmetry of BNT ceramics can be characterized at room temperature by a (2 2 0)/(1 4 0) peak split between 66° and 69°, and a single peak of (2 0 0) between 45° and 48° [5]. The rhombohedral (2 2 0)/(1 4 0) peak split remains until $x = 0.08$ and then combines into a slightly asymmetric peak at $x = 0.1$[Fig. 2(b)]. The microstructure of the $(1-x)$BNT$-x$BZT ceramics sintered at 1,150°C for 6 h, with a heating/cooling rate of 5°C/min, is presented in Fig. 3. The SEM observation confirms that the BNT-BZT ceramics are densely sintered. Furthermore, all BNT-BZT samples have a high density of around 92.5–98.3% of the theoretical density, as reported in Table 1. The theoretical densities of each composition were calculated based on the rule of BNT mixture and the theoretical densities of BZT. The microstructure of the ceramics clearly showed the apparent increase in density, as shown in Fig. 3. The density increased to the maximum value of 98.3% compared to the theoretical density of 10 mol% BZT. Beyond 10 mol% BZT, a decrease in density resulted. The fracture mode of pure BNT ceramics was preferentially intergranular, but it became a more transgranular oriented fracture with

Table 1

Physical and dielectric properties of (1-x)BNT-xBZT; $x = 0.0 - 0.2$ ceramics sintered at 1,150°C for 6 h (P = perovskite, P_y = pyroclore, R = rhombohedrol, C = cubic)

x	Phase	Crystal structure	Grain size (μm)	Density (%)	Dielectric constant	tan δ
0.00	P	R	2.02 ± 0.37	92.5	420	0.73
0.02	P	R	1.78 ± 0.26	95.6	750	0.35
0.04	P	R	2.35 ± 0.40	96.1	760	0.42
0.06	P	R	1.97 ± 0.32	96.5	710	0.22
0.08	P	R	1.83 ± 0.24	96.6	770	0.17
0.10	P	C	2.24 ± 0.57	98.3	840	0.04
0.20	$P+P_y$	C	2.08 ± 0.35	97.6	950	0.28

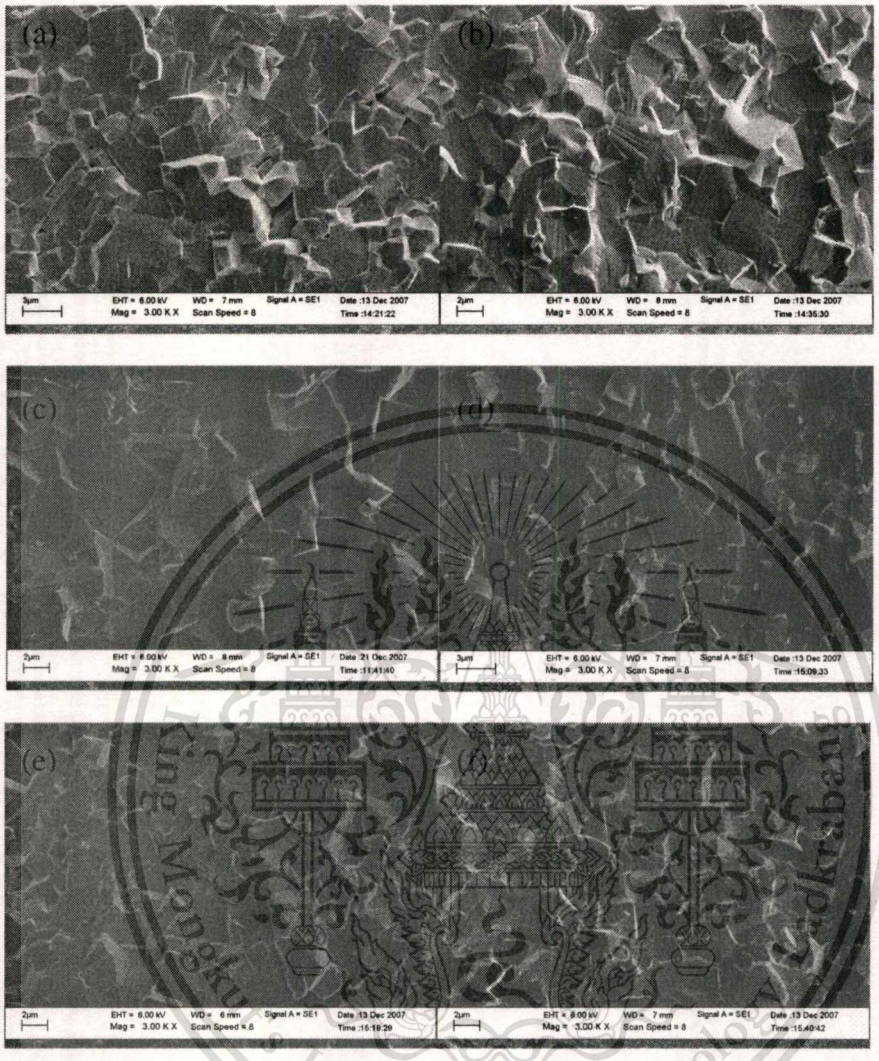

Figure 3. SEM micrograph of (1-x)BNT-xBZT; (a) $x = 0.0$, (b) $x = 0.02$, (c) $x = 0.04$, (d) $x = 0.06$, (e) $x = 0.08$, and (f) $x = 0.1$ ceramics sintered at 1,150°C for 6 h, with a heating/cooling rate of 5°C/min.

increasing amounts of added BZT. Figure 4 shows the relative permittivity (ε_r) and loss tangent (tan δ) at room temperature of $(1-x)$BNT-xBZT; $x = 0.0$-0.2 ceramics as a function of the BZT fraction. The ε_r of pure BNT was only about 420, but it increased significantly with increasing BZT content to about 750, 760 and 840 for 0.02, 0.04 and 0.10 mol BZT-doped BNT ceramics, respectively. Moreover, dielectric loss was decreased. The decrement in dielectric loss is believed to be proportional to the sintered density. However, higher dielectric loss observed at composition $x = 0.2$ is due to the formation of the pyrochlore phase. This was related to the result from the X-ray diffraction technique, which indicated that pyroclore phases were found in ceramics of BZT mole fractions above 0.10. In addition, the lower transition temperature of BNT-BZT ceramics may have increased the relative permittivity.

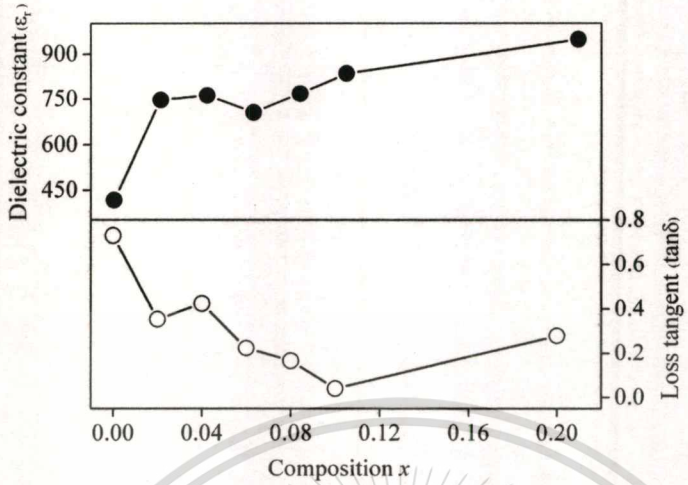

Figure 4. Dielectric constant (ε_r) and loss tangent (tan δ) at room temperature of (1-x)BNT-xBZT; $x = 0.0$-0.2 ceramics sintered at 1,150°C for 6 h, with a heating/cooling rate of 5°C/min in a bismuth atmosphere.

Conclusion

The microstructure, crystal structure and dielectric properties of $(1-x)Bi_{1/2}Na_{1/2}TiO_3 - x\,Bi(Zn_{1/2}Ti_{1/2})O_3$ piezoelectric ceramics were investigated with different contents of $Bi(Zn_{1/2}Ti_{1/2})O_3$. A single perovskite phase with rhombohedral symmetry was obtained for $Bi(Zn_{1/2}Ti_{1/2})O_3$ substitutions of up to 10 mole%. A small amount of BZT was effective for improving both sintering behavior and dielectric properties of BNT ceramics. The density of BNT ceramics was increased with BZT addition to a relative density of approximately 98.3% for 10 mol% of BZT added.

Acknowledgments

This work was supported by the Thailand Research Fund (TRF), the Commission on Higher Education (CHE), Thailand Graduate Institute of Science and Technology (TGIST), National Research Council of Thailand (NRCT), and the National Nanotechnology Center (NANOTEC) NSTDA, Ministry of Science and Technology, Thailand through its program of Center of Excellence Network.

References

1. RoHS and WEEE compliant flame retardants developed for electrical connectors. *Reinforced Plastics* **51**(8), 12–12 (2007).
2. Endwave transceivers comply with upcoming ROHS deadline. *III-Vs Review* **19**(2), 11–11 (2006).
3. C. Peng, J. F. Li, and W. Gong, Preparation and properties of $(Bi_{1/2}Na_{1/2})TiO_3$-$Ba(Ti,Zr)O_3$ lead-free piezoelectric ceramics. *Mater. Lett.* **59**(12), 1576–1580 (2005).
4. L. Gao, Y. Huang, Y. Hu, and H. Du, Dielectric and ferroelectric properties of (1 - x)$BaTiO_3$-x$Bi_{0.5}Na_{0.5}TiO_3$ ceramics. *Ceramics International* **33**(6), 1041–1046 (2007).
5. H. Y. Tian, D. Y. Wang, D. M. Lin, J. T. Zeng, K. W. Kwok, H. L. W. Chan, Diffusion phase transition and dielectric characteristics of $Bi_{0.5}Na_{0.5}TiO_3$-$Ba(Hf,Ti)O_3$ lead-free ceramics. *Solid State Commu.* **142**(1–2), 10–14 (2007).

6. X. Jing, Y. Li, and Q. Yin, Hydrothermal synthesis of $Na_{0.5}Bi_{0.5}TiO_3$ fine powders. *Mater. Sci. Eng. B* **99**(1–3), 506–510 (2003).
7. T. Motohashi and T. Kimura, Development of texture in $Bi_{0.5}Na_{0.5}TiO_3$ prepared by reactive-templated grain growth process. *J. Eur. Ceram. Soc.* **27**(13–15), 3633–3636 (2007).
8. H. Nagata and T. Takenaka, Additive effects on electrical properties of $(Bi_{1/2}Na_{1/2})TiO_3$ ferroelectric ceramics. *J. Eur. Ceram. Soc.* **21**(10–11), 1299–1302 (2001).

Ferroelectrics, 383:8–14, 2009

ISSN: 0015-0193 print / 1563-5112 online
DOI: 10.1080/00150190902873311

Taylor & Francis
Taylor & Francis Group

Synthesis and Morphology Evolution of Lead-Free Piezoelectric $K_{1/2}Na_{1/2}NbO_3$ Powder at Low Temperature

NOPSIRI CHAIYO,[1] ANUCHA RUANGPHANIT,[2] RANGSON MUANGHLUA,[3] SURASAK NIEMCHAROEN,[3] ATCHARA SANGSEUB,[4] SAOWANEE TAOPEN,[4] SUNANTA LEELAPATTANA,[4] WANWILAI C. VITTAYAKORN,[5] AND NARATIP VITTAYAKORN[1,4,*]

[1]College of KMITL Nanotechnology King Mongkut's Institute of Technology, Ladkrabang, King Mongkut's Institute of Technology, Ladkrabang, Bangkok 10520, Thailand
[2]Thai Microelectronics Center (TMEC), National Electronics and Computer Technology Center, Nation Science and Technology Development Agency, Ministry of Science and Technology, Chachoengsao 24000, Thailand
[3]Department of Electronics, Faculty of Engineering, King Mongkut's Institute of Technology, Ladkrabang, Bangkok, Thailand 10520
[4] Materials Science Research Units, Department of Chemistry, Faculty of Science, King Mongkut's Institute of Technology, Ladkrabang, Bangkok 10520, Thailand
[5]Department of Physics and Materials Science, Faculty of Science, Chiang Mai University, Chiang Mai 50200, Thailand

A synthetic route for modified solid state reaction has been developed for the synthesis of the perovskite phase of potassium sodium niobate, $K_{1/2}Na_{1/2}NbO_3$ (KNN). Potassium oxalate monohydrate ($K_2C_2O_4.H_2O$) and sodium oxalate ($Na_2C_2O_4$) were employed as a source of potassium and sodium, respectively. The formation of the $K_{1/2}Na_{1/2}NbO_3$ phase was investigated as a function of calcination conditions by TG-DTA and XRD techniques. Morphology and particle size were determined via an SEM technique. It was found that the minor phases of Na_2CO_3 and K_2CO_3 tend to form together with $K_{1/2}Na_{1/2}NbO_3$, depending on calcination conditions. The perovskite phase was successfully synthesized at a low temperature of 400°C. As calcination temperatures increased from 600° to 850°C, the KNN solid solution became more homogeneous, XRD peaks became narrower, and a pattern similar to that expected for orthorhombic $K_{1/2}Na_{1/2}NbO_3$ was achieved after 600°C, as indicated by the separate peaks of 0 2 2 and 2 0 0.

Keywords Materials preparation; piezoceramics; potassium compounds and sodium compounds

PACS: 64.70.K-; 77.22.Ch, 81.05.Je; 85.80.-n; 77.84.Dy

Received August 3, 2008; in final form December 31, 2008.
*Corresponding author. E-mail: naratipcmu@yahoo.com

Introduction

For almost half a century, lead zirconate titanate (PZT) and PZT-based ceramics have been widely investigated and used as actuators, sensors, transducers, resonators, surface acoustic wave (SAW) filters and other piezoelectric devices, due to their excellent dielectric, piezoelectric and electromechanical properties [1–5]. Lead-based PZT materials contain more than 60 wt% of lead oxide, which cause various environmental problems and numerous medical symptoms, i.e. headaches, constipation, nausea, anemia and reduced fertility [6]. In terms of legislation at the EU level, two recent directives have put severe restrictions on the use of hazardous substances in electronic equipment. According to these, lead and other heavy metals should have been phased out by 1st July, 2006 [7]. Therefore, lead-free and/or low-lead-content piezoelectric compositions have been studied and developed for replacing the lead-based compositions in commercial application [1, 5]. Alkali niobates of the general form, $ANbO_3$ (*A*: alkali metal), were proposed as alternative piezoelectric materials [7]. Among various candidates, potassium sodium niobate [(K,Na)NbO_3; KNN] is the most promising one, because of its outstanding piezoelectric and ferroelectric properties. Although KNN has been studied since the 1950s, research on it has not been intensive. A recent article in *Nature* by Saito et al. attracted more attention on this lead-free piezoelectric ceramic [8]. KNN powders have been prepared by a conventional solid-state reaction method using oxide or carbonate compound as raw materials [9]. This reaction creates several problems, which are caused by moisture-sensitive compound [7]. Moreover, high calcination temperature can lead to the evaporation of volatile compound. It was found that potassium niobate ($KNbO_3$) powder has been successfully synthesized at a temperature as low as 500°C through a modified solid state reaction [10] and other compositions such as $NaTaO_3$ powder, which also was synthesized by using this method [11].

Thus, the purpose of this study was to explore a modified solid state reaction method for the production of $K_{1/2}Na_{1/2}NbO_3$ powder at a low calcination temperature. The phase evolution, morphology and particle size of the powder calcined at various temperatures were investigated and discussed.

Experimental Procedure

Potassium sodium niobate ($K_{1/2}Na_{1/2}NbO_3$) powders were prepared by the modified solid state reaction method. Reagent grade potassium oxalate monohydrate ($K_2C_2O_4.H_2O$, 99.9%), sodium oxalate ($Na_2C_2O_4$, 99.9%) and niobium oxide (Nb_2O_5, 99.9%), in required stoichiometric ratio related to reaction bellow, were mixed by the ball-milling method in isopropanol for 18 h.

$$0.5K_2C_2O_4.H_2O_{(s)} + 0.5Na_2C_2O_{4(s)} + Nb_2O_{5(s)} + O_{2(g)} \rightarrow 2K_{0.5}Na_{0.5}NbO_{3(s)} + 2CO_{2(g)} + 0.5O_{2(g)} + 0.5H_2O_{(g)} \quad (1)$$

The mixture was dried at 80°C for an approximate length of time. After drying, the reaction of the uncalcined powders taking place during heat treatment was determined by thermo gravimetric and differential thermal analysis (TG-DTA, Perkin Elmer). Based on the TG-DTA results, the mixture was calcined in air at various temperatures ranging from 300°C to 850°C in a closed alumina crucible in order to investigate the formation of KNN.

All powders were subsequently inspected by room temperature X-ray diffraction (XRD, Advance D8) using Ni-filtered CuK_α radiation to examine the phases formed and the optimum calcination condition for the formation of KNN powder. Powder morphologies and

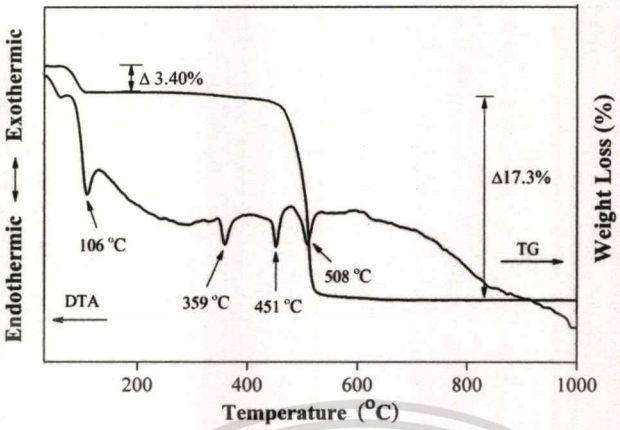

Figure 1. TG-DTA result of an uncalcined powder mixed in the stoichiometric proportion of $K_{1/2}Na_{1/2}NbO_3$.

particle size were directly imaged using a scanning electron microscope (SEM, LEO1455 VP).

Results and Discussion

The TG-DTA simultaneous analysis of a powder mixed in the stoichiometric proportions of $K_{1/2}Na_{1/2}NbO_3$ is illustrated in Fig.1. From Fig. 1, four endothermic peaks centered at 106, 359, 451 and 508°C are observed. The first endothermic peak is attributed to the dehydration of potassium oxalate monohydrate with mass loss of 3.4% on the TG curve [12]. The second endothermic peak can be ascribed to the formation of potassium carbonate through potassium oxalate decomposition [12]. The third endothermic peak also results from the formation of sodium carbonate through sodium oxalate decomposition [13]. The fourth endothermic peak is assigned to the formation of $K_{1/2}Na_{1/2}NbO_3$ by combination reactions of Na_2O, K_2O and Nb_2O_5. In addition, there is an obvious mass loss of 17.3% during the temperature rise from 460 to 530°C on the TG curve, which indicates the decarbonation of K_2CO_3 and Na_2CO_3. These data were used to define the range of calcination temperatures for XRD investigation between 300°C to 850°C.

Therefore, to investigate the effect of calcination temperature on the phase development, the mixed powders were calcined for 2 h in air at various temperatures up to 850°C, followed by phase analysis using XRD. Figure 2 shows the XRD pattern of the KNN powders calcined at different temperatures for 2 h. It can be seen that fine KNN crystallites were developed in the powder at a calcination temperature as low as 350°C, accompanied by Nb_2O_5, K_2CO_3 and Na_2CO_3. Upon calcinations at 400°C, an essentially monophasic of perovskite phase (yield of 100% within the limitations of the XRD technique) was observed. This phase was indexed based on a simple orthorhombic perovskite cell, as proposed by Stannek [14]. However, for the composition, $K_{1/2}Na_{1/2}NbO_3$, a JCPDS-ICDD powder diffraction card did not exist. The material was orthorhombic and isostructural with orthorhombic $KNbO_3$, with a unit cell derived from the simple perovskite cell by rotating two axes by 45°[15, 16]. We successfully synthesized the single perovskite phase by firing at a low temperature of 400°C. The results of the X-ray diffraction measurement

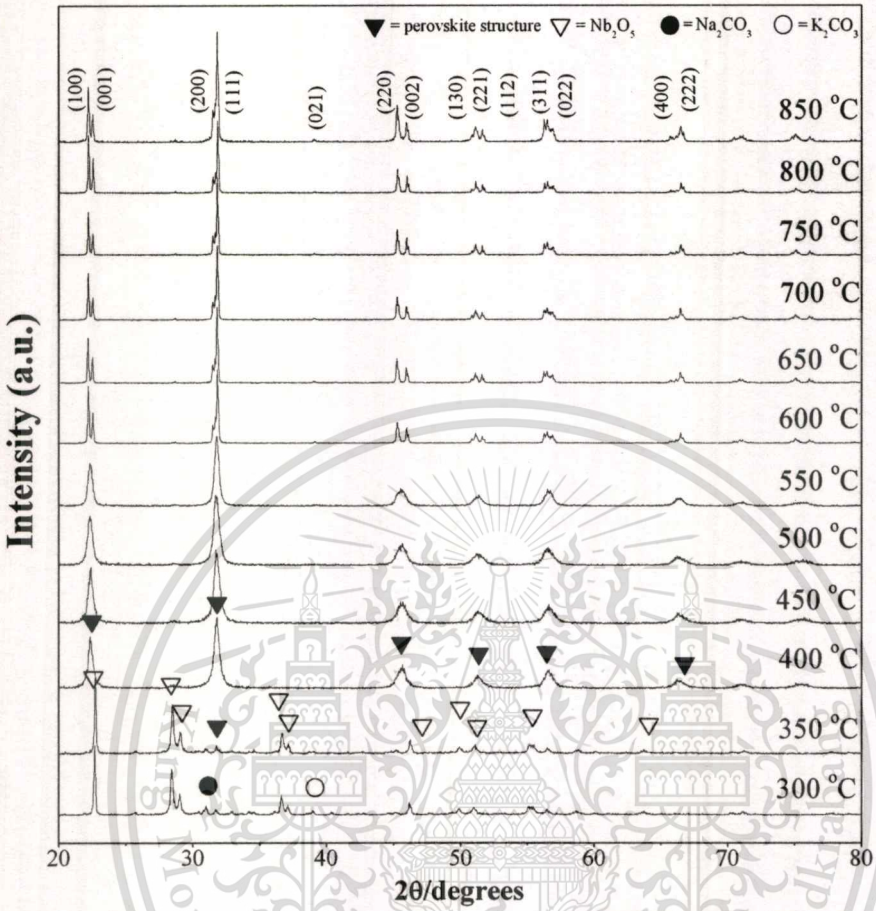

Figure 2. XRD patterns of $K_{1/2}Na_{1/2}NbO_3$ powder calcined at various temperatures for 2 h with heating/cooling rates of 20°C /min.

support the DTA observation (Fig. 1) that the perovskite phase is formed at a temperature of ~400−500°C. This temperature was more than 350°C lower than the ordinary synthesis temperature of solid state reaction.

Although the pure perovskite phase was obtained at a low temperature of 400°C, broadening of the XRD peaks was observed at temperatures between 400–550°C. This indicated that the KNN powder at 400–550°C was not a good homogeneous solid solution phase. Any spatial variations in the Na and K ratios, due to imperfect mixing and incomplete reaction, would produce a series of $K_{(1-x)}Na_xNbO_3$ solid solution compositions with differing values of x, in different regions of the sample. Because of the small shifts in d-spacings with changing composition reported for intermediate values of x, an overlap of XRD peaks from compositionally inhomogeneous regions would occur, and result in single broad peaks for temperatures $\leq$ 550°C, as shown in Fig. 2. As calcination temperatures increased from 600° to 850°C, the KNN solid solution became more homogeneous, XRD peaks became narrower, and a pattern similar to that expected for orthorhombic $K_{1/2}Na_{1/2}NbO_3$ was achieved after 600°C, as indicated by the separate peaks of 0 2 2 and 2 0 0 in Fig. 3. Estimated lattice parameters were a = 5.56 Å, b =15.70 Å, and c = 5.62 Å for powder

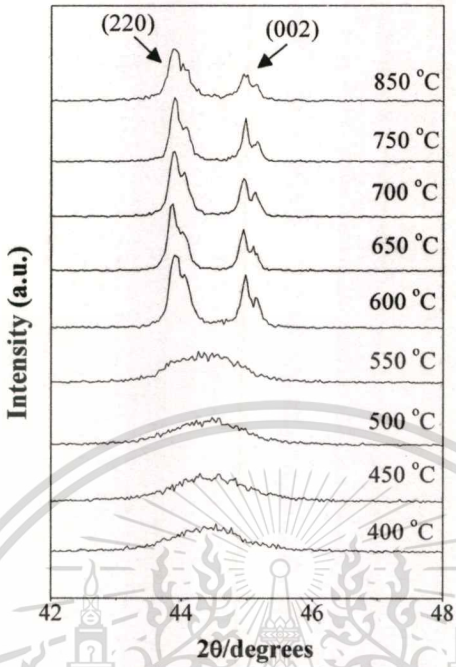

Figure 3. XRD pattern of the $K_{1/2}Na_{1/2}NbO_3$ powder, showing doublets (2 2 0) and (0 0 2).

that was calcined at 600°C; which is close to the values reported in the literature [17]. This study also shows that crystalline orthorhombic KNN is the only detectable phase in the powder, after calcinations in the range of 600–850°C. The experimental work carried out here suggests that the optimal calcination conditions for the single orthorhombic phase, $K_{1/2}Na_{1/2}NbO_3$ (with impurities undetected by the XRD technique), is 600°C for 2, with heating/cooling rates of 20°C/min. Moreover, the formation temperature and dwell time for the production of $K_{1/2}Na_{1/2}NbO_3$ powders observed in this work are also lower than those reported by Ichiki et al. [18] (950°C for 5 h) and Singh et al. [19] (900°C for 1 h). The morphology evolution and particle sizes can be directly investigated using scanning electron microscopy (SEM). Micrograph of KNN powders calcined at 400°C for 2 h, with a heating/cooling rate of 20°C/min. is displayed in Fig.4(a) and 4(b). In general, the particles are conglomerated and irregular in shape and the morphology of the calcined powders are

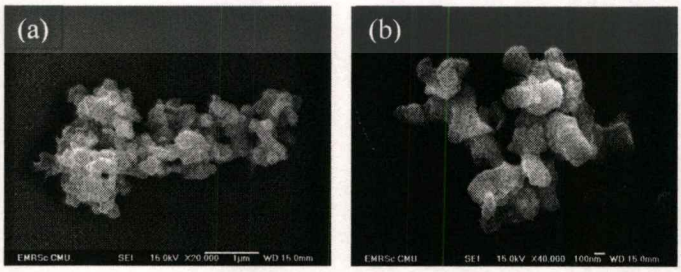

Figure 4. Scanning electron micrograph of the $K_{1/2}Na_{1/2}NbO_3$ powders calcined at 400°C for 2 h, with a heating/cooling rate of 20°C/min. (a) low magnification and (b) higher magnification.

about the same. The range of particle size was found to be about 70 to 300 nm. No evidence of secondary phase was found. This observation was in good agreement with the evidence suggested from the XRD technique. A detailed study at higher magnification [Fig. 4(b)] showed that the smallest particle size estimated from SEM micrographs was ~40 nm.

Conclusions

In summary, we have exploited a simple method to synthesize perovskite-type $K_{1/2}Na_{1/2}NbO_3$ powder, with high crystallinity at a lower temperature. A pyrochlore-free perovskite $K_{1/2}Na_{1/2}NbO_3$ phase was obtained in this study by using potassium oxalate monohydrate and sodium oxalate as a source of potassium and sodium, respectively, together with a careful calcination treatment. The perovskite phase was successfully synthesized at the low temperature of 400°C. As calcination temperatures increased from 600° to 850°C, the KNN solid solution became more homogeneous, XRD peaks became narrower, and a pattern similar to that expected for orthorhombic $K_{1/2}Na_{1/2}NbO_3$ was achieved after 600 °C, as indicated by the separate peaks of 0 2 2 and 2 0 0. The resulting KNN powders consisted of agglomerated particles of 70 to 300 nm in size. As a final remark, the present method could also be applicable to the preparation of other materials such as $KNbO_3$, $NaNbO_3$ etc.

Acknowledgments

This work was supported by the Thailand Research Fund (TRF), the Commission on Higher Education (CHE), Thailand Graduate Institute of Science and Technology (TGIST), National Research Council of Thailand (NRCT), and the National Nanotechnology Center (NANOTEC) NSTDA, Ministry of Science and Technology, Thailand through its program of Center of Excellence Network.

References

1. Z. X. Ruzhong Zuoa and L. Li, Dielectric and piezoelectric properties of Fe_2O_3-doped $(Na_{0.5}K_{0.5})_{0.96}Li_{0.04}Nb_{0.86}Ta_{0.1}Sb_{0.04}O_3$ lead-free ceramics. *J. Phys. Chem. Sol.* **69**, 1728–1732 (2008).
2. Y. G. Lv, C. L. Wang, J. L. Zhang, M. L. Zhao, M. K. Li, and H. C. Wang, Modified $(K_{0.5}Na_{0.5})(Nb_{0.9}Ta_{0.1})O_3$ ceramics with high Qm. *Mater. Lett.* **62**, 3425–3427 (2008).
3. Y. Wang, J. Wu, D. Xiao, J. Zhu, P. Yu, L. Wu, and X. Li, Piezoelectric properties of (Li, Ag) modified $(Na_{0.50}K_{0.50})NbO_3$ lead-free ceramics with high Curie temperature. *J. Alloys Compd.* **459**, 414–417 (2008).
4. S. J. Park, H. Y. Park, K. H. Cho, S. Nahm, H. G. Lee, D. H. Kim, and B. H. Choi, Effect of CuO on the sintering temperature and piezoelectric properties of lead-free $0.95(Na_{0.5}K_{0.5})NbO_3$-$0.05CaTiO_3$ ceramics. *Mater. Res. Bull.*, vol. In Press, Corrected Proof.
5. R. C. Chang, S. Y. Chu, Y. P. Wong, C. S. Hong, and H. H. Huang, The effects of sintering temperature on the properties of lead-free $(Na_{0.5}K_{0.5})NbO_3$-$SrTiO_3$ ceramics. *J. Alloys Compd.* **456**, 308–312 (2008).
6. T. Takenaka and H. Nagata, Current status and prospects of lead-free piezoelectric ceramics. *J. Eur. Ceram. Soc.* 25, 2693–2700 (2005).
7. [7] E. Ringgaard and T. Wurlitzer, Lead-free piezoceramics based on alkali niobates. *J. Eur. Ceram. Soc.* 25, 2701–2706 (2005).
8. Y. Saito, H. Takao, T. Tani, T. Nonoyama, K. Takatori, T. Homma, T. Nagaya, and M. Nakamura, Lead-free piezoceramics. *Nature* **432**, 84–87 (2004).

9. K. Singh, V. Lingwal, S. C. Bhatt, N. S. Panwar, and B. S. Semwal, Dielectric properties of potassium sodium niobate mixed system. *Mater. Res. Bull.* **36**, 2365–2374 (2001).
10. A. S. T. Wada and T. Saito, Fabrication of lead-free piezoelectric $KNbO_3$ ceramics by modified solid state reaction method. *Jpn. Soc. Appl. Phys.* **45**, 7431–7434 (2006).
11. J. Xu, D. D. Xue, and C. Yan, Chemical synthesis of $NaTaO_3$ powder at low-temperature. *Mater. Lett.* **59**, 2920–2922 (2005).
12. M. A. Mohamed, A. K. Galwey, and S. A. Halawy, The activities of some metal oxides in promoting the thermal decomposition of potassium oxalate. *Thermochim. Acta.* **387**, 63–74 (2002).
13. L. H. McAlexander, C. M. Beck, J. J. Burdeniuc, and R. H. Crabtree, Fluoroalkane aromatization over hot sodium oxalate. *J. Fluor. Chem.* **99**, 67–72 (1999).
14. W. Stanek, Characterization of sintering phenomena of $K_{0.5}Na_{0.5}NbO_3$. vol. M. Sc. Berkeley: University of Californa, 1970.
15. B. Jaffe and W. R. Cook, Piezoelectric ceramic: R.A.N. Publishers, 1971.
16. L. Katz and H. D. Megaw, The structure of potassium niobate at room temperature: the solution of pseudosymmetric structure by fourier mathods. *Acta Crystallogr.* **22**, 639–684 (1967).
17. V. Lingwal, B. S. Semwal, and N. S. Panwar, Dielectric properties of $Na_{1-x}K_xNbO_3$ in orthorhombic *Phase. Bull. Mater. Sci.* **26**, 619–625 (2003).
18. M. Ichiki, L. Zhang, M. Tanaka, and R. Maeda, Electrical properties of piezoelectric sodium-potassium niobate. *J. Eur. Ceram. Soc.* **24**, 1693–1697 (2004).
19. K. Singh, V. Lingwal, S. C. Bhatt, N. S. Panwar, and B. S. Semwal, Dielectric properties of potassium sodium niobate mixed system. *Mater. Res. Bull.* **36**, 2365–2374 (2001).
20. J. H. Lv, M. Zhang, M. Guo, and W. C. Li, Hydrothermal synthesis and characterization of $K_xNa_{(1-x)}NbO_3$ powders. *Int. J. Appl. Ceram. Technol.* **4**, 571–577 (2007).

J Mater Sci (2010) 45:1443–1447
DOI 10.1007/s10853-009-4098-z

Solid-state reaction synthesis of sodium niobate ($NaNbO_3$) powder at low temperature

Nopsiri Chaiyo · Banjong Boonchom · Naratip Vittayakorn

Received: 16 September 2009 / Accepted: 30 November 2009 / Published online: 15 December 2009

Abstract A modified solid-state reaction was applied to produce lead-free piezoelectric sodium niobate ($NaNbO_3$) powders. The mixture of $Na_2C_2O_4$ and Nb_2O_5 was identified by thermo gravimetric analysis (TGA) and differential thermal analysis (DTA). The powders were characterized using a scanning electron microscope (SEM) and the X-ray diffraction technique (XRD). The SEM image suggested that the particle size of the powders obtained ranged from 180 to 360 nm. The XRD pattern showed that the pure perovskite phase of $NaNbO_3$ could be synthesized at the low temperature of 475 °C for 1 h, with an average crystallite size of 31.45 ± 5.28 nm. This temperature was about 300 °C lower than that when using the conventional solid-state method with Na_2CO_3 as reactant, which resulted in a cost-, energy-, and time-saving method.

N. Chaiyo · N. Vittayakorn
Electroceramic Research Laboratory, College of KMITL Nanotechnology, King Mongkut's Institute of Technology Ladkrabang, Bangkok 10520, Thailand

B. Boonchom
King Mongkut's Institute of Technology Ladkrabang, Chumphon Campus, 17/1 M. 6 Pha Thiew District, Chumphon 86160, Thailand

N. Vittayakorn (✉)
Advanced Materials Science Research Unit, Department of Chemistry, Faculty of Science, King Mongkut's Institute of Technology Ladkrabang, Bangkok 10520, Thailand
e-mail: naratipcmu@yahoo.com

N. Chaiyo · N. Vittayakorn
ThEP Center, CHE, 328 Si Ayutthaya Rd., Bangkok 10400, Thailand

Introduction

Alkaline niobate materials are considered a lead-free candidate for the substitution of widely used commercial lead-based piezoelectric material, based on the aim to avoid highly harmful lead compounds [1–4]. Among several compounds, sodium niobate ($NaNbO_3$) has attracted considerable attention because of its unique properties [3] and high dielectric constant (2000–3000) at Curie temperature [5]. Unlike most oxidic perovskite, $NaNbO_3$ possesses six phase transitions from the ferroelectric phase at low temperature (rhombohedral) to the antiferroelectric room temperature phase (orthorhombic) and non-polar cubic structure at 640 °C [6]. It can form solid solution with other niobate compounds, such as $LiNbO_3$ and $KNbO_3$, to acquire good ferroelectric and piezoelectric properties [7–10]. Traditionally, alkali metal niobate powders have been synthesized via the solid-state reaction of alkali metal carbonates and Nb_2O_5 [3, 11]. This method requires a high calcination temperature (about 750 °C or more) for a long period of time, possibly causing volatilization of the alkali metal and leading to poor compositional homogeneity [3, 4, 11]. The powders can be agglomerated during heating, which affects their properties [3, 12]. Thereafter, powders with high sinterability and stoichiometric control are necessary for developing $NaNbO_3$-based piezoelectric ceramics. Numerous alternative methods are used to prepare $NaNbO_3$ such as hydrothermal [13], chemical [12], and polymeric precursor processes [14], and the mechanochemical process [3, 15, 16]. Although $NaNbO_3$ was performed by mechanochemical activation after thermal treatment of a stoichiometric Na_2CO_3/Nb_2O_5 mixture at 600 °C, this procedure required a long operational period of up to 30 days [3]. Moreover, $NaNbO_3$ was also obtained at a low temperature (450 °C) by the wet-chemical method

using a water-soluble malic acid complex [17]. However, most chemical techniques require specialized experimental apparatus and high purity reactant, which are more expensive. Interestingly, sodium tantalate ($NaTaO_3$) powder, with high crystallinity has been successfully synthesized at 600 °C through a simple method called modified solid-state reaction or combustion synthesis, in which urea plays an important role. Unusual starting material ($Na_2C_2O_4$ instead of Na_2CO_3/Na_2O) has been described. This method was found to produce $NaTaO_3$ as a general route at the lower temperature of ~500–600 °C, when compared with conventional solid-state reaction [18]. On the other hand, urea, which was added as fuel in order to achieve the final product, could cause problems in this method, due to risks if performing on a large scale. Nonetheless, the aim of the present study was to produce $NaNbO_3$ using a simple, rapid, low cost, and environment friendly route, such as a solid-state reaction of $Na_2C_2O_4$ and Nb_2O_5 without the addition of any fuel.

Experiment

$NaNbO_3$ was synthesized by a solid-state reaction method. Reagent grade sodium oxalate ($Na_2C_2O_4$, 99.9%) and niobium oxide (Nb_2O_5, 99.9%) were employed as raw material. Firstly, starting materials were weighed according to the required stoichiometric ratio that related to the reaction below.

$$Na_2C_2O_{4(s)} + Nb_2O_{5(s)} \rightarrow 2NaNbO_{3(s)} + 2CO_{2(g)} \quad (1)$$

Then, raw materials were mixed together by ball-milling in ethyl alcohol using partially stabilized zirconia balls for 18 h. After drying on a hot plate by regularly stirring at about 80 °C for an approximate period, the thermal behavior during heat treatment was determined by thermo gravimetric analysis (TGA, Perkin Elmer) and differential thermal analysis (DTA, Perkin Elmer). According to TG-DTA results, the mixture was subsequently placed in a closed alumina crucible and calcined for different periods of time in air at various temperatures, ranging from 300 to 600 °C, in order to investigate the formation of $NaNbO_3$.

Afterward, calcined powders were subsequently inspected by room temperature X-ray diffraction (XRD, Advance D8), using Ni-filtered Cu K_α radiation, to examine the effect of thermal treatment on phase development and the optimal calcination condition for the formation of crystalline $NaNbO_3$ powders. Powder morphologies and particle size were figured directly using a scanning electron microscope (SEM, LEO1455 VP).

Results and discussion

The TGA and DTA of a powder mixed in the stoichiometric proportions of $NaNbO_3$ are illustrated in Fig. 1. The TG curve accordingly revealed a weight loss of 16.8%, occurring during the temperature rise from 400 to 500 °C. This observation corresponded to the endothermic peak of the DTA curve, which cantered at 484.8 °C. This endotherm may be related to the decomposition of $Na_2C_2O_4$ to Na_2CO_3, which lies on the temperature of 450–550 °C, and abruptly to the decomposition of Na_2CO_3 to Na_2O (decomposition temperature in the range of 400 °C) before releasing CO and CO_2 molecules, as revealed below [19].

$$Na_2C_2O_4 \rightarrow Na_2CO_3 + CO \quad (2)$$

$$Na_2CO_3 \rightarrow Na_2O + CO_2 \quad (3)$$

It is interesting to note that there was no weight loss or thermal effect at a temperature of about 100 °C, at which no decomposition occurrence was indicated. The endothermic peak correlates at the range of 100 °C with the release of water molecules. This confirmed that non-absorptive $Na_2C_2O_4$ raw material contrasts with Na_2CO_3, because Na_2CO_3 is the hygroscopic compound which can lead to the erroneous stoichiometric ratio. Therefore, powders with good compositional homogeneity, when comparing with the conventional solid-state method with Na_2CO_3 as reactant, may possibly be produced via this solid-state reaction.

Thus, based on TG-DTA data, the powders were calcined at temperatures ranging from 300 to 600 °C for 4 h in order to investigate the calcination temperature outcome in the development phase. The mixture of starting material was calcined in air using the steady heating/cooling rate of 20 °C at various temperatures, and followed by phase analysis using the XRD technique. Figure 2 shows the XRD pattern of the $NaNbO_3$ powders calcined at different

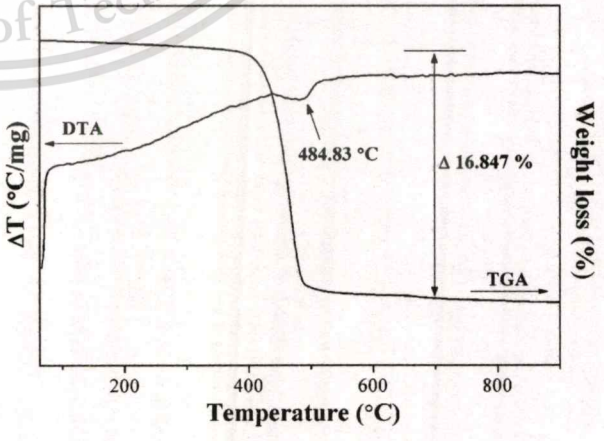

Fig. 1 TG-DTA result of an uncalcined powder mixed in the stoichiometric proportion of $NaNbO_3$

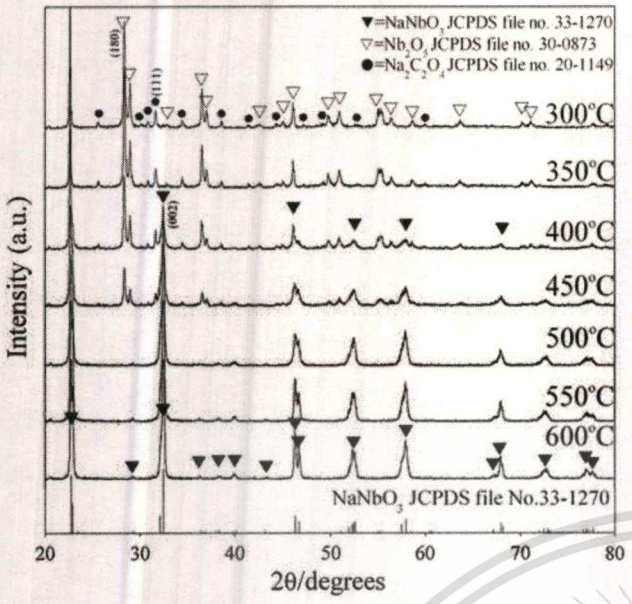

Fig. 2 XRD patterns of $NaNbO_3$ powder calcined at various temperatures for 4 h with a heating/cooling rate of 20 °C/min

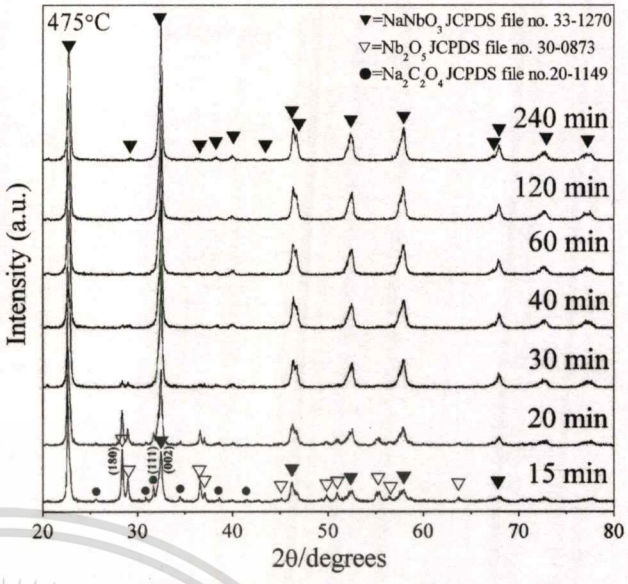

Fig. 3 XRD patterns of $NaNbO_3$ powder calcined at the calcination temperature of 475 °C for various dwell times with a heating/cooling rate of 20 °C/min

temperatures for 4 h. It can be seen that fine $NaNbO_3$ crystallites were developed at a calcination temperature as low as 400 °C, accompanied by the phase of unreacted Nb_2O_5 (JCPDS file no. 30-0873) and $Na_2C_2O_4$ (JCPDS file no. 20-1149). This observation suggests that nucleation of the perovskite $NaNbO_3$ phase did occur. In addition, the minor phase of Nb_2O_5 and $Na_2C_2O_4$ was also decreased with escalating calcination temperature, and disappeared completely after the powders were calcined at the calcination temperature of 500 °C for 4 h. Whereas, the intensity of the perovskite $NaNbO_3$ peak was enhanced further and an essentially monophasic $NaNbO_3$ perovskite phase (yield of 100% within the limitations of the XRD technique) was observed. This $NaNbO_3$ phase could be indexed according to an orthorhombic structure with the space group *Pbma* (no. 57), which was consistent with JCPDS file No. 33-1270. Although the calcination temperature rose at 550 and 600 °C, the monophasic $NaNbO_3$ perovskite phase was also obtained. There was no evidence of the pyrochlore diffraction peak. This result also correlates with the TG-DTA analysis shown above. As the calcination temperature increased, so too did the amount of the $NaNbO_3$ crystallite phase, and this can be seen as intensity of the amplified peak. Since the diffusion coefficient is a temperature dependence parameter, the higher temperature has the most intense effect on the rate of diffusion [20], and can enhance higher atomic mobility [11].

As the finest calcination temperature was established at 500 °C, a dwell time ranging from 15 min to 4 h was applied at 475 °C (instead of 500 °C). This temperature was preferred because of the rapid diffraction peak change of the powder calcined at 450 and 500 °C. The XRD pattern of the $NaNbO_3$ powders, which were calcined at 475 °C with different dwell times, is shown in Fig. 3. It was found that the single-phase of $NaNbO_3$ powder was also successfully synthesized at the calcination temperature of 475 °C, with a dwell time of 60 min or more applied. The increase in crystallinity of the $NaNbO_3$ phase was seen to relate with the escalation of dwell time. Although the calcination temperature of 475 °C was higher than the nucleation temperature of the powder obtained by a polymeric precursor [14], this was a single-step and low-cost starting material method that could save time, energy, and cost. Likewise, this temperature was much lower than the conventional solid-state reaction process with Na_2CO_3 as reactant, which was in the range of 750 °C [3]. This observation indicated that calcination temperature and dwell time might play an important role in evolution of the pure phase product and also be consistent with other systems [21].

The volume fraction of the perovskite phase formation was considered at various calcination temperatures and dwell times. These relative amounts of perovskite, $Na_2C_2O_4$ and Nb_2O_5 phases, were approximated by calculating the ratio of the main X-ray peak intensities of perovskite $NaNbO_3$, $Na_2C_2O_4$, and Nb_2O_5 phase using the following equation [22]:

$$\text{Wt\% perovskite} = \frac{I_{\text{perov}}}{I_{\text{perov}} + I_{Na_2C_2O_4} + I_{Nb_2O_5}} \times 100 \qquad (4)$$

where I_{perov}, $I_{Na_2C_2O_4}$, and $I_{Nb_2O_5}$ stand for the intensities belonging to the strongest reflection peak of (002)

Table 1 Fraction of perovskite phase formed as a function of calcination temperature and dwell time

$NaNbO_3$	Calcination temperature (°C)						
	300	350	400	450	500	550	600
%Perovskite	0	0	35.42	62.86	100.00	100.00	100.00
$NaNbO_3$	Dwell time (min) at 475 °C						
	15	20	30	40	60	120	240
%Perovskite	41.89	60.56	89.13	97.00	100.00	100.00	100.00

perovskite, (111) $Na_2C_2O_4$, and (180) Nb_2O_5, respectively. A volume fraction increase of the perovskite $NaNbO_3$ phase formation of the calcined powders, resulting from the calcinations process at various temperatures and dwell times, is shown in Table 1. As the calcination temperature rose, the yield of the perovskite phase increased significantly until the temperature reached 500 °C, and a pure phase of $NaNbO_3$ was established. Likewise, in observing powders calcined at 475 °C for different dwell times, the $NaNbO_3$ phase was enlarged as the dwell time increased up to 60 min, and the monophasic phase of $NaNbO_3$ was seen to form.

Accordingly, the Johnson–Mehl–Avrami, or JMA equation was used in the present study. This equation was found appropriate for describing a wide variety of isothermal solid-state transformations [23, 24]. It was used to study the kinetic of the reaction and mechanism involving nucleation and growth, and has the general form of:

$$x(t) = 1 - \exp[-(kt)^n]. \quad (5)$$

where x is the volume fraction of the perovskite phase formed, k the reaction rate constant, t the calcination time, and n the Avrami exponent. For analyzing the results, the relation of ln [ln $1/(1 - x)$] versus ln t was plotted. Figure 4 shows a good linear fit of the Avrami plot for $NaNbO_3$ powders calcined at 475 °C. This shows that the isothermal formation of the perovskite phase can be described accurately by the theory of phase transformations. The constant n, which can be calculated from the slope of this Avrami plot, was found to be 1.79. This indicated that the reaction of solid solution formation is diffusion controlled (n is less than 2.5) [25]. The beginning stage of transformation is a fixed number of perovskite nuclei [26].

The average crystallite size of the powders obtained can be determined from the XRD pattern according to Scherrer's equation [27]:

$$D = \frac{k\lambda}{\beta \cos\theta_B} \quad (6)$$

where D is the average crystallite size, k a constant equal to 0.89, λ the wavelength of X-ray radiation, β the full width at half maximum (FWHM), and θ_B the diffraction angle. The average crystallite size of powders calcined at 475 °C for 15 min to 4 h was found to be from 21.52 to 35.56 nm, and that of powders calcined at the optimum condition (475 °C for 60 min) was about 31.45 nm. The increase in crystallinity of the $NaNbO_3$ phase was affected by increasing dwell time. This may confirm that the dwell time also plays an important role in development of the pure phase creation.

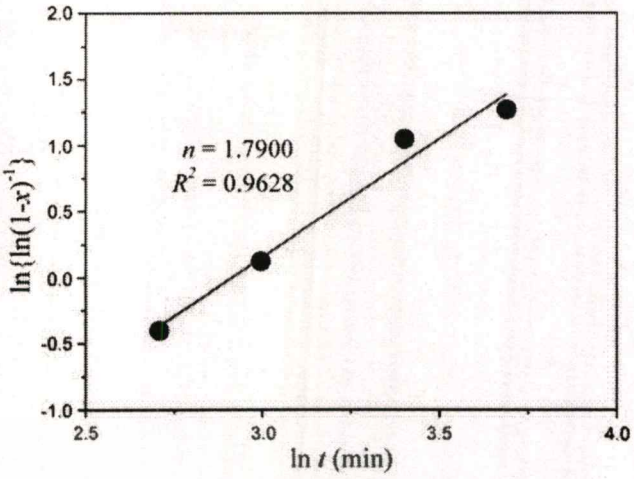

Fig. 4 Johnson–Mehl–Avrami for the formation of perovskite phase in $NaNbO_3$ powders isothermally heat treated at 475 °C

SEM micrographs of the powder calcined at 475 °C for 60 min are given in Fig. 5. The particle size, which can be estimated from these micrographs, was found to be in the range of 180 to 360 nm. This value is greater than the average crystallite size calculated from XRD patterns. The inconsistency value could point out the agglomeration

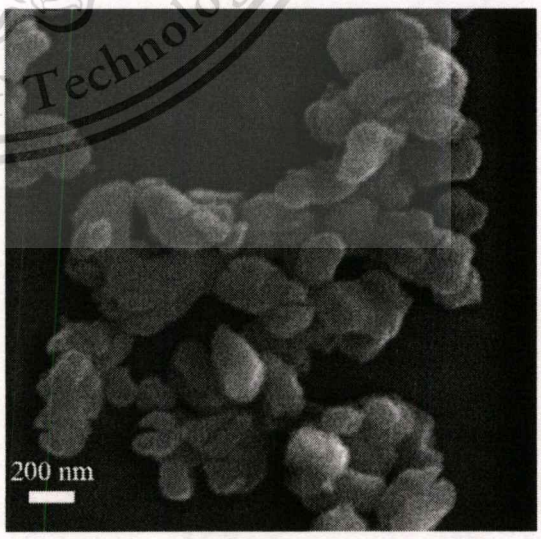

Fig. 5 SEM micrographs showing $NaNbO_3$ powders synthesized at 475 °C for 60 min, with a heating/cooling rate of 20 °C/min

of the calcined powders. No evidence of difference phase or pyrochlore phase was found. This outcome relates to the XRD result, in which the monophasic perovskite phase of $NaNbO_3$ can be established after calcination at 475 °C for 60 min.

Conclusion

Crystalline powders of sodium niobate $NaNbO_3$ were synthesized from a modified solid-state reaction of $Na_2C_2O_4$ and Nb_2O_5. This method is an excellent, simple and cost effective way to prepare stoichiometric, homogeneous, and fine powders. The perovskite phase of $NaNbO_3$ was successfully synthesized at the low temperature of 475 °C for 1 h, with an average crystallite size of 31.45 ± 5.28 nm. This temperature is about 275 °C lower than that used in the conventional method, which lies in the 750 °C range. As dwell time increased, XRD peaks became narrower, and a pattern similar to that expected for orthorhombic $NaNbO_3$ was achieved, as indicated by the separate peaks. The resulting $NaNbO_3$ powders comprised agglomerated particles of 180 to 360 nm in size.

Acknowledgements This work was supported by the Thailand Research Fund (TRF), Thailand Graduate Institute of Science and Technology (TGIST), National Research Council of Thailand (NRCT), and the National Nanotechnology Center (NANOTEC) NSTDA, Ministry of Science and Technology, Thailand through its "Center of Excellence Network" Program.

References

1. Matsubara M, Yamaguchi T, Sakamoto W, Kikuta K, Yogo T, Hirano S-I (2005) J Am Chem Soc 88:1190
2. Zhaoa P, Zhanga B-P, Lib J-F (2008) Scripta Mater 58:429
3. Hungría T, Pardo L, Moure A, Castro A (2005) J Alloys Compd 395:166
4. Ke T-Y, Chen H-A, Sheu H-S, Yeh J-W, Lin H-N, Lee C-Y, Chiu H-T (2008) J Phys Chem C 112:8827
5. Jona F, Shirane G (1993) Ferroelectric crystals. Dover Publications, New York
6. Wang X-B, Shen Z, Hu Z-P, Qin L, Tang SH, Kuok MH (1996) J Mol Struct 385:1
7. Du H, Zhou W, Luo F, Zhu D, Qu S, Li Y, Pei Z (2008) J Appl Phys 104:034104-7
8. Chang Y, Yang Z-P, Ma D, Liu Z, Wang Z (2008) J Appl Phys 104:024109-8
9. Wu J, Xiao D, Wang Y, Wu W, Zhang B, Zhu J (2008) J Appl Phys 104:024102-4
10. Lei C, Ye Z-G (2008) Appl Phys Lett 93:042901-3
11. Hsiao Y-J, Chang Y-H, Chang Y-S, Fang T-H, Chai Y-L, Chen G-J, Huang T-W (2007) Mater Sci Eng B 136:129
12. Lanfredi S, Dessemond L, Rodrigue ACM (2000) J Eur Ceram Soc 20:983
13. Goh GKL, Lange FF, Haile SM, Levi CG (2003) J Mater Res 18:338
14. de Lima Nobre MA, Longo E, Leite ER, Varela JA (1996) Mater Lett 28:215
15. Moure A, Hungría T, Castro A, Pardo L (2009) J Eur Ceram Soc 29:2297
16. Rojac T, Kosec M, Malic B, Holc J (2005) Mater Res Bull 40:341
17. Camargo ER, Popa M, Kakihana M (2002) Chem Mater 14:2365
18. Xu J, Xue D, Yan C (2005) Mater Lett 59:2920
19. McAlexander LH, Beck CM, Burdeniuc JJ, Crabtree RH (1999) J Fluorine Chem 99:67
20. Callister WD (2007) Materials science and engineering: an introduction. Wiley, New York
21. Chaiyo N, Vittayakorn N (2008) J Ceram Process Res 9:381
22. Feng G, Rongzi H, Jiaji L, Zhen L, Lihong C, Changsheng T (2009) J Eur Ceram Soc 29:1687
23. Sheibani S, Ataie A, Heshmati-Manesh S (2008) J Alloys Compd 455:447
24. Yan Z-J, Dang S-E, Wang X-H, Lian P-X (2008) Trans Nonferrous Met Soc China 18:138
25. Jang HM, Cho SR, Lee K-M (1995) J Am Ceram Soc 78:297
26. Shen Y, Hng HH, Oh JT (2004) Mater Lett 58:2824
27. Klug HP, Alexander LE (1974) X-ray diffraction procedure of polycrystalline and amorphous materials. Wiley, New York

Journal of Alloys and Compounds 509 (2011) 2445–2449

Contents lists available at ScienceDirect

Journal of Alloys and Compounds

journal homepage: www.elsevier.com/locate/jallcom

Solution combustion synthesis and characterization of lead-free piezoelectric sodium niobate ($NaNbO_3$) powders

Nopsiri Chaiyo[a,b], Rangson Muanghlua[c], Surasak Niemcharoen[c], Banjong Boonchom[d], Naratip Vittayakorn[a,b,e,*]

[a] Electroceramic Research Laboratory, College of KMITL Nanotechnology, King Mongkut's Institute of Technology Ladkrabang, Bangkok 10520, Thailand
[b] ThEP Center, CHE, 328 Si Ayutthaya Rd., Bangkok 10400, Thailand
[c] Department of Electronics, Faculty of Engineering, King Mongkut's Institute of Technology Ladkrabang, Bangkok 10520, Thailand
[d] King Mongkut's Institute of Technology Ladkrabang, Chumphon Campus, 17/1 M. 6 Pha Thiew District, Chumphon 86160, Thailand
[e] Department of Chemistry, Faculty of Science, King Mongkut's Institute of Technology Ladkrabang, Bangkok 10520, Thailand

ARTICLE INFO

Article history:
Received 20 July 2010
Received in revised form 27 October 2010
Accepted 8 November 2010
Available online 13 November 2010

Keywords:
Sodium niobate
Modified solid state reaction

ABSTRACT

Nano-crystalline sodium niobate ($NaNbO_3$) powder was synthesized by the solution combustion synthesis of sodium nitrate ($NaNO_3$) and Nb_2O_5 using glycine as the fuel. The chemical reaction, nucleation mechanisms and influence of the fuel-to-oxidizer ratio to phase formation were studied. The precursor and product powders were characterized, using thermo gravimetric analysis (TGA), differential thermal analysis (DTA), the X-ray diffraction technique (XRD), scanning electron microscope (SEM) and Fourier transform infrared (FTIR) spectroscopy. As-prepared powder possesses an orthorhombic crystal structure with an X-ray diffraction pattern that could be matched with the perovskite, $NaNbO_3$ JCPDS no. 82-0606. Perovskite $NaNbO_3$ phase, with a mean crystalline size (calculated by X-ray line broadening) ranging from 44.51 ± 11.99 nm (ratio of 0.7) to 26.11 ± 13.69 nm (ratio of 2.0) was obtained. The SEM image shows polyhedral-shaped powder with a mean particle size of 137 ± 52 nm and 226 ± 46 nm for as-prepared and calcined powder, respectively.

1. Introduction

Sodium niobate ($NaNbO_3$) is a perovskite with an inorganic complex oxide and the empirical formula, ABO_3. It is among the candidates for lead-free substances that avoid toxicity of lead-based piezoelectric materials (e.g. PZT [1,2]), and is concerned about the environment. $NaNbO_3$ has been studied widely for its unusual structural transition series [3–7]. It has a ferroelectric rhombohedral phase below −100 °C, and is antiferroelectric with orthorhombic symmetry between −100 °C and 640 °C [4]. Finally, it possesses cubic paraelectric above 640 °C [5], and in addition, its antiferroelectric, perovskite-type nature can transform into a ferroelectric one by chemical doping, i.e. K^+ [6,7] and Li^+ [8].

Generally, alkali niobate powders are synthesized by conventional solid state reaction, where alkali metal carbonate or oxide compound of starting materials are heated at high temperature (800 °C or above) for a long duration [8,9]. High calcination temperature can cause volatilization of alkali metal, thus causing this classical method difficulty in achieving a homogeneous mixture of the component [8–10]. Powder agglomeration can occur during heating, which could affect properties such as low surface area and low sinterability [10]. Thus, this method does not always allow for the production of dense, homogeneous single phase ceramics. Therefore, development of alternative methods that can produce powder with high sinterability and controlled stoichiometric composition is necessary. In recent years, ultra fine ceramic powder, which is synthesized using mechanochemical synthesis [11], polymeric precursors [12], and hydrothermal and polymerized complex methods [13], has been described in the literature to enable production of desired compositions. While synthesizing powder rapidly, with the desired composition, high porosity and high sinterability remains a challenge, combustion synthesis (CS) has been found as a potential solution for this problem.

Combustion synthesis (CS) or self-propagating high temperature synthesis (SHS) is an effective, low-cost method for producing various industrially useful materials. It has been introduced as a quick, straightforward preparation process for producing homogeneous, very fine, crystalline and unagglomerated multicomponent oxide ceramic powders, without intermediate decomposition and/or calcination steps [14,15]. The combustion synthesis technique begins with a mixture of easily oxidized reactants (such as nitrates) and a suitable organic fuel (such as urea [16], tartalic acid

* Corresponding author at: Department of Chemistry, Faculty of Science, King Mongkut's Institute of Technology Ladkrabang, Bangkok 10520, Thailand. Fax: +66 2 326 4415.
E-mail address: naratipcmu@yahoo.com (N. Vittayakorn).

0925-8388/$ – see front matter © 2010 Elsevier B.V. All rights reserved.
doi:10.1016/j.jallcom.2010.11.043

[17], alanine [18], glycine [19], etc.), which acts as a reducing agent. The mixture is then heated until it ignites, which is when the temperature of rapid exothermal chemical reaction commences, and a self-sustaining combustion reaction starts. This highly exothermic reaction produces a high temperature and duration long enough for the synthesis to occur, even in the absence of an external heating source [20]. Ultrafine nano-sized powder also can be prepared by releasing a large amount of gas from the system. This process results in a dry, fluffy, crystalline, unagglomerated and fine oxide powder. Metal nitrate was found to be the salt preferred, due to its water solubility, and homogeneous solution could be achieved easily by melting at a low temperature [16].

However, it was reported that an exothermic redox reaction (oxidation and reduction reaction taking place simultaneously) could be initiated only when the oxidizer and fuel are mixed intimately in a fixed proportion. The basis of the combustion synthesis process derives from the thermochemical concepts used in propellant chemistry [21,22]. The method consists of establishing a simple valency balance, irrespective of whether the elements are present in the oxidizer or fuel components of the mixture, and then calculating the stoichiometric composition of the starting mixture, which is equivalent to the release of maximum energy. The assumed valencies, which are presented as usual products of the combustion reaction, consist of CO_2, H_2O and N_2. Therefore, carbon and hydrogen are considered as reducing elements with the corresponding valencies of +4 and +1, whereas oxygen is thought to be an oxidizing agent with a valency of −2, and nitrogen a valency of 0. To extrapolate the concept of combustion synthesis of ceramic oxide means considering metals as reducing agents with their valencies in the corresponding oxide or nitrate, i.e. +2 for magnesium (oxide), +3 for cerium (nitrate) and +4 for cerium (oxide). In the case of multiple valence elements, the final product is used for calculation.

The elemental stoichiometric coefficient, φ, which is the ratio between the total valencies of fuel (glycine; NH_2CH_2COOH) and that of the oxidizer (sodium nitrate), can be calculated following the method proposed by Jain et al. [21]:

$$\varphi = \frac{n(0_{(N)} + 2 \times 1_{(H)} + 4_{(C)} + 2 \times 1_{(H)} + 4_{(C)} - 2_{(O)} - 2_{(O)} + 1_{(H)})}{1_{(Na)} + 0_{(N)} + 3 \times -2_{(O)}} \quad (1)$$

where n is the mole of glycine. According to the propellant chemistry for stoichiometric redox reaction between fuel and an oxidizer, the φ ratio should be united (stoichiometric). A $\varphi < 1$ means oxidant-rich condition and $\varphi > 1$ means fuel-rich condition. To satisfy the principle in the present system, the sodium nitrate (oxidizing valency = 5−) to glycine (reducing valency = 9+) molar ratio was found to be 1:0.56. The comprehensive reaction that formed $NaNbO_3$ can be written as:

$$36NaNO_3 + 18Nb_2O_5 + 20NH_2CH_2COOH \rightarrow 36NaNbO_3 + 50H_2O + 28N_2 + 40CO_2 \quad (2)$$

It should be noted that various fuel-to-oxidizer ratios should be carried out for investigating and comparing the effect of fuel-rich/fuel-lean mixtures on the synthesis of sodium niobate powder. In this study, sodium niobate powder was synthesized via the combustion synthesis technique for the first time. This process used sodium nitrate and niobium pentoxide as starting materials, and glycine was used as fuel. The different fuel-to-oxidizer molar ratios such as fuel-deficient (<0.56), equivalent stoichiometric (0.56) and fuel-rich (>0.56) condition were applied.

2. Experimental procedure

For the combustion synthesis of perovskite sodium niobate powder, AR grade sodium nitrate ($NaNO_3$ 99.5%) and niobium pentoxide (Nb_2O_5 99.95%) were used as the oxidizer, and glycine (NH_2CH_2COOH 99.7%) as fuel. The appropriate amount of starting materials was weighed, mixed with de-ionized water in a glass beaker and stirred regularly for 30 min. The fuel (glycine) was then added and the mixture stirred for 30 min. After that, the solution precursor was boiled on a hotplate and then evaporated. Once the solution had thickened and begun to dry, the ignition took place when the temperature rapidly increased, which resulted in self-sustaining combustion with rapid evolution of a large volume of gas products, and formation of voluminous powder. For investigating thermal behavior of the precursor, the mixture of starting material was determined using thermo gravimetric analysis (TGA) and differential thermal analysis (DTA). The X-ray diffraction (XRD, Advance D8) technique was carried out on the combustion synthesized powder, using Ni-filtered CuK_α radiation for phase identification and mean crystalline size estimation. The final powder product was characterized by using the Fourier transform infrared (FTIR) technique and scanning electron microscope (SEM, Hitachi S4700).

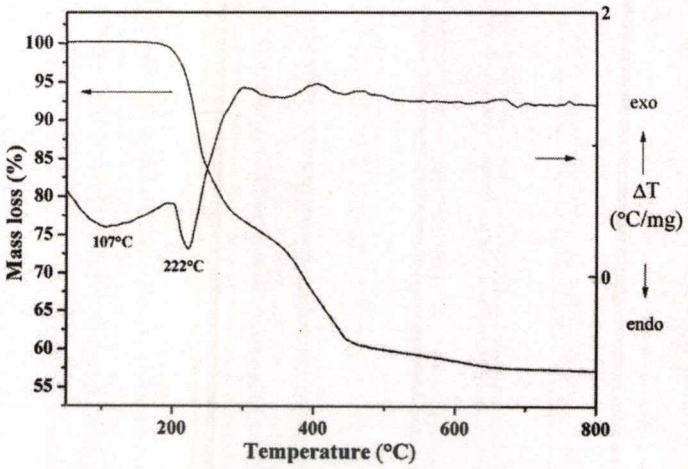

Fig. 1. TG-DTA curves of the precursor mixed in the stoichiometric proportion of $NaNbO_3$.

3. Results and discussion

Fig. 1 shows the TG/DTA plots of the stoichiometric precursor for $NaNbO_3$ powder synthesis. From observations of the TGA curve, there appeared to be three-stages of weight loss from room temperature to 800 °C. The definition of initial temperature (T_{in}) is when the sample weight starts changing rapidly during the chemical reaction [23]. As the precursor was heated, a significant weight loss was observed as the temperature reached 170 °C, indicating that the T_{in} was around this heat. The weight loss did not stop until the temperature reached 480 °C. It was indicated clearly that this reaction belongs to a multi-stage reaction. The overall weight loss was found to be about 40%, which is close to the theoretical value of 36.87% that corresponds to the release of 50 mol H_2O, 28 mol N_2 and 40 mol CO_2 related to Eq. (2). This outcome supported our conception that a hotplate can be used as a heating source because it is capable of initiating the combustion reaction at a temperature as low as that of the T_{in}.

The evolution XRD pattern of the combustion synthesized ceramic powder, with the fuel-to-oxidizer molar ratio, is illustrated in Fig. 2. The fuel-deficient (0.5) and equivalent stoichiometric ratio (0.56), were found (according to experimental observation) to have no ignition and combustion reaction in those compositions. Their XRD patterns correlated to detection results of the diffraction peaks of Nb_2O_5 (●) (JCPDS file no. 30-0873) and $NaNO_3$ (■) (JCPDS file no. 85-0859) starting materials, with no evidence of perovskite $NaNbO_3$ phase found. Although the equivalent stoichiometric ratio (0.56) was calculated for maximum energy release, auto-ignition did not occur in this study. This could indicate that oxygen deficiency in the system and its environment might lead to combustion reaction and fail to follow the theory. The fuel-to-oxidizer molar ratio was increased by using the fuel-rich condition (>0.56), which was found to produce the perovskite $NaNbO_3$ ceramic powder, due to its diffraction peaks being detected for all different fuel contents

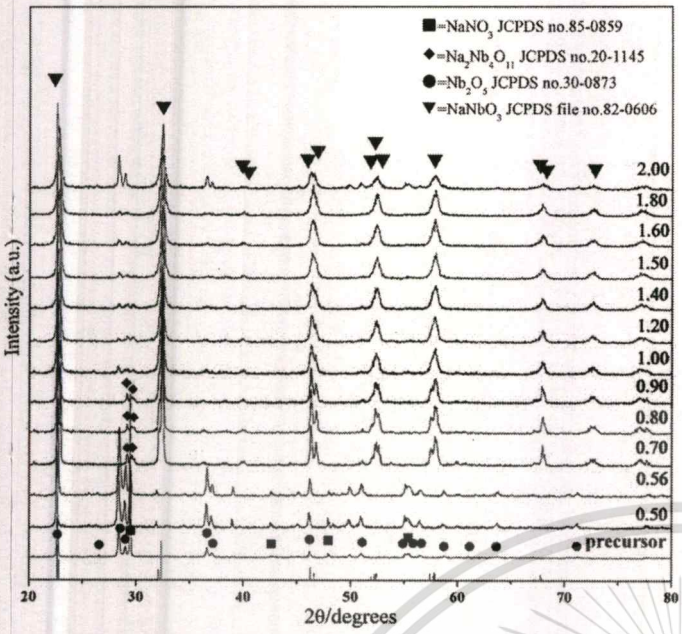

Fig. 2. X-ray diffraction patterns of $NaNbO_3$ powder obtained from various fuel-to-oxidant molar ratios.

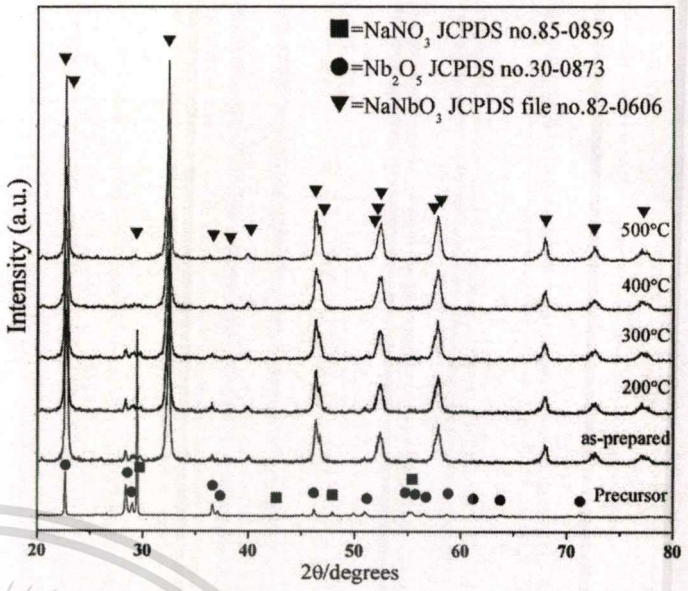

Fig. 3. X-ray diffraction patterns of $NaNbO_3$ powder (obtained from the fuel-to-oxidant molar ratio of 1.0) calcined at various temperatures for 4 h with a heating/cooling rate of 20 °C/min.

(fuel-to-oxidizer molar ratio ranging from 0.7 to 2.0). This $NaNbO_3$ phase (▼) was consistent with JCPDS file no. 82-0606, which corresponded to an orthorhombic structure with the space group, $P2_1ma$ (26). For a fuel-rich condition (fuel-to-oxidizer molar ratio of 0.7, 0.8 and 0.9), the $NaNbO_3$ phase (▼) was detected with the accompanying pyrochlore phase of $Na_2Nb_4O_{11}$ (♦), which matched JCPDS file no. 20-1145. No evidence of unreacted Nb_2O_5 and/or $NaNO_3$ diffraction peak was found. As fuel content increased from the fuel-to-oxidizer molar ratio of 1.0–2.0, unreacted Nb_2O_5 (●) (JCPDS file no. 30-0873) was found together with a majority of $NaNbO_3$ diffraction peaks. From the reflection peak, the average crystalline size (D) of $NaNbO_3$ powders was considered as a function of fuel content by using X-ray line broadening through Scherrer's equation [24]:

$$D = \frac{k\lambda}{\beta \cos\theta_B} \quad (3)$$

where D is the average crystalline size, k a constant taken as 0.89, λ the wavelength of X-ray radiation, β the full width at half maximum (FWHM) and θ_B the diffraction angle. The consequent values are reported in Table 1. As the fuel content increased, the average crystalline size (D) was found to decreased from 44.51 ± 11.99 nm (ratio of 0.7) to 26.11 ± 13.69 nm (ratio of 2.0). This suggested that elevated fuel content could lead to the production of a smaller crystalline size (related to a small particle size) of powder. Nevertheless, as a consequence of additional cost and more carbon residual, an extremely high fuel-to-oxidizer molar ratio (fuel-rich ratio) did not always result in the desired production of powder [25].

Therefore, from findings on the fine nucleation condition of monophasic $NaNbO_3$ phase, the fuel-to-oxidizer molar ratio of 1.0 was selected to investigate the effect of calcination temperature. From this ratio, the volume fraction of the perovskite phase formation (%perovskite) of as-prepared powder was found to be as high as 93%. This relative value was considered by approximately calculating the ratio of the main X-ray peak intensities of $NaNbO_3$ and Nb_2O_5 phases [26], according to the following equation; % perovskite $= (I_{perovskite}/(I_{perovskite} + I_{Nb_2O_5})) \times 100$. Thus, the as-prepared powder was calcined at different temperatures for 4 h with a heating/cooling rate of 20 °C/min. The X-ray diffraction (XRD) patterns of sodium niobate ($NaNbO_3$) powder, calcined for 4 h at different temperatures, are illustrated in Fig. 3. As the XRD pattern of as-prepared powder was composed of a slight Nb_2O_5 (●) (JCPDS file no. 30-0873) phase, the intensity of that phase was found to decrease with increasing calcination temperature. The diffraction peak corresponded to the Nb_2O_5, which disappeared after calcination at 400 °C for 4 h, whereas monophasic perovskite $NaNbO_3$ phase was obtained. This result suggested that the perovskite $NaNbO_3$ powder could be synthesized by using the combustion synthesis process and calcinations at 400 °C for 4 h. This process was found to be a simple, rapid and cost-effective method when compared with the traditional solid-state reaction, which takes longer time and requires higher temperature [8,9]. In addition, the mean crystalline size (D), which is reported in Table 1, was not significantly varied between as-prepared powder (29.28 ± 5.29 nm) and increasing calcination temperatures of up to 400 °C (27.84 ± 7.12 nm). It can be suggested that calcina-

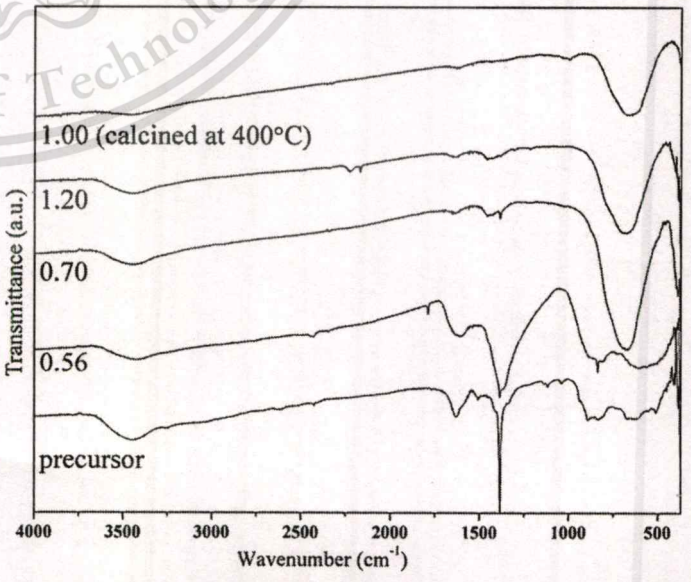

Fig. 4. FT-IR spectra of the precursor mixed in the stoichiometric proportion of $NaNbO_3$ powder obtained from various fuel-to-oxidant molar ratios and after the calcination step.

Table 1
Mean crystalline size, D, of $NaNbO_3$ powder obtained from various fuel-to-oxidant molar ratios.

	Fuel-to-oxidant molar ratios								
	0.7	0.8	0.9	1.0	1.2	1.4	1.6	1.8	2.0
As-prepared	44.51 ± 11.99	42.59 ± 11.54	37.31 ± 8.54	29.09 ± 5.29	27.45 ± 5.86	26.29 ± 5.97	24.40 ± 4.92	23.79 ± 5.52	26.12 ± 13.69
	Calcination temperature (°C)								
	200 °C	300 °C	400 °C	500 °C	600 °C	700 °C	800 °C	900 °C	
Calcined powder	29.95 ± 4.51	31.51 ± 4.02	27.84 ± 7.12	30 ± 82 ± 5.43	38.84 ± 8.09	60.72 ± 8.09	70.87 ± 9.22	85.27 ± 15.65	

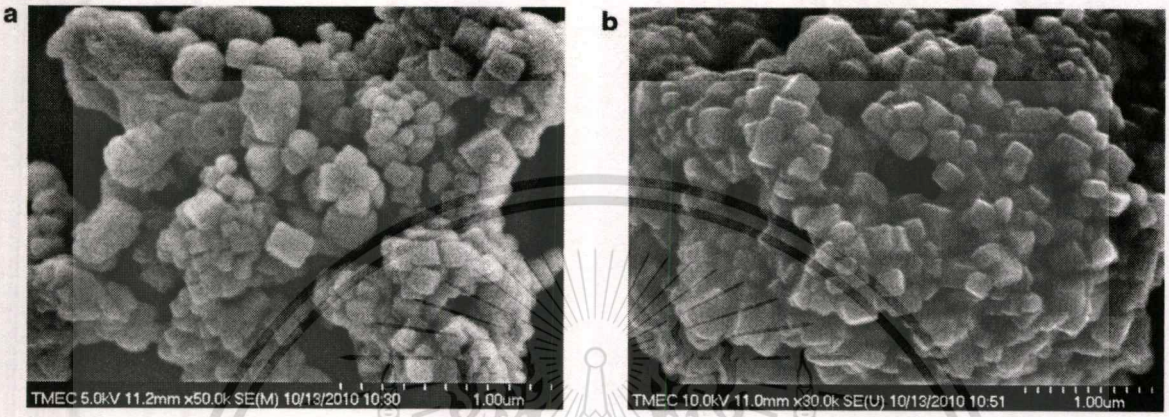

Fig. 5. SEM micrograph showing as-prepared $NaNbO_3$ powder synthesized using the fuel-to-oxidant molar ratio of 1.0 (a) and powder calcined at 400 °C for 4 h (b).

tions at this low temperature also produced a lower crystalline size when compared with the traditional solid state reaction method.

Fig. 4 shows the FT-IR spectroscopic studies of the crystalline $NaNbO_3$ obtained after combustion synthesis, its precursor without heat treatment and powder calcined at 400 °C for 4 h. For all powder, an IR band of around 3400 cm^{-1} was assigned to O–H asymmetric stretching (ν_3) [27], and on observation, it related to the moisture content of KBr. Regarding the precursor of $NaNbO_3$ powders without heat treatment, and as-prepared powder with a stoichiometric ratio (0.56), the IR spectrum indicated peaking of the characteristic band at ~1612, ~1385 and ~890 cm^{-1}, which corresponded to the anti-symmetric carboxyl group stretching vibration, anti-symmetry $NO_3{}^{-1}$ stretching and bending vibration, respectively [28]. This result proved existence of the carboxyl and $NO_3{}^{-1}$ group (belonging to the starting material) in those samples. With regard to fuel-rich ratios (0.7 and 1.2), the new broad absorption bands appeared after combustion at a low wave number of ~673 cm^{-1}, suggesting that the Nb–O bond formation did occur. This Nb–O bond was believed to be the vibration (ν_3) mode in the corner-shared NbO_6 octahedron, according to reported IR spectra of niobate glass ceramics [28]. This result led to the assumption that the perovskite $NaNbO_3$ phase was synthesized (which correlated to XRD analysis). However, the IR band of anti-symmetric COO^- and that of anti-symmetry $NO_3{}^{-1}$ stretching vibration also were observed. This clearly indicated traces of existent carboxyl group and nitrate in as-prepared $NaNbO_3$ powder, which cannot be detected when using the XRD technique. For powder calcined at 400 °C for 4 h, the spectra band of vibration (ν_3) mode belonging to the Nb–O bond was found without observation of any starting material band. This can indicate that monophasic perovskite $NaNbO_3$ has been synthesized successfully after calcination at a temperature as low as 400 °C for 4 h. Fig. 5 shows an SEM micrograph of the as-prepared $NaNbO_3$ powder using the fuel-to-oxidizer molar ratio of 1.0 (a) and powder calcined at 400 °C for 4 h (b). The powder was found to be polyhedral in shape, with uniform features. No evidence of a different or pyrochlore phase was found, which suggested the homogeneous character of the prepared powder. The average particle size, which can be estimated from micrographs, was found to be 137 ± 52 nm and 226 ± 46 nm for as-prepared and calcined powder, respectively. These particle size values are greater than the average crystalline size calculated from X-ray line broadening because a particle can be formed generally of many crystallites [29–31]. The particle growth for calcined powder seemed to be detected. It can be said that the firing process tends to produce agglomerated particles and grain growth, as reported by other works [32,33].

4. Conclusions

Crystalline $NaNbO_3$ powder, with a volume fraction of the perovskite phase formation (% perovskite) as high as 93%, was synthesized directly via the solution combustion process using $NaNO_3$, Nb_2O_5 and glycine. Monophasic perovskite $NaNbO_3$ powder was obtained after calcination at 400 °C for 4 h. The fuel-to-oxidizer molar ratio was found to affect the combustion reaction and character of the powder obtained. The average crystalline size (D) was found to decrease from 44.51 ± 11.99 nm (ratio of 0.7) to 26.11 ± 13.69 nm (ratio of 2.0). This method is a simple, rapid, cost- and time-saving way of synthesizing stoichiometric, homogeneous and fine $NaNbO_3$ powder with a low calcination temperature. The powder obtained was found to be a uniform soft agglomerated particle.

Acknowledgements

This work was supported by the Thailand Research Fund (TRF), Thailand Graduate Institute of Science and Technology (TGIST), King Mongkut's Institute of Technology Ladkrabang Research (KMITL Research), and the National Nanotechnology Center (NANOTEC) NSTDA, Ministry of Science and Technology, Thailand through its "Center of Excellence Network" Program.

References

[1] B. Jaffe, W.R. Cook Jr., H. Jaffe, Piezoelectric Ceramics, Academic Press, New York, 1971.
[2] B. Jaffe, R.S. Roth, S. Marzullo, J. Appl. Phys. 25 (1954) 809–810.
[3] N. Chaiyo, B. Boonchom, N. Vittayakorn, J. Mater. Sci. 45 (2010) 1443.
[4] H.D. Megaw, Ferroelectrics 7 (1974) 87–89.
[5] L.E. Cross, B. Nicholson, J. Phil. Magn. Ser. 46 (1955) 453–466.
[6] G. Shirane, B. Newnham, R. Pepinsky, Phys. Rev. 96 (1954) 581–588.
[7] Y. Shiratori, A. Magrez, C. Pithan, J. Eur. Ceram. Soc. 25 (2005) 2075–2079.
[8] T. Nitta, J. Am. Ceram. Soc. 51 (1968) 626–629.
[9] T. Rojac, O. Masson, R. Guinebretière, M. Kosec, B. Malič, J. Holc, J. Eur. Ceram. Soc. 17 (2007) 2265–2271.
[10] C.C. Hwang, T.Y. Wu, J.S. Tsai, Mater. Sci. Eng. B 111 (2004) 49–56.
[11] T. Rojac, M. Kosec, B. Malič, J. Holc, Mater. Res. Bull. 40 (2005) 341–345.
[12] M.A.L. Nobre, E. Longo, E.R. Leite, J.A. Varela, Mater. Lett. 28 (1996) 215–220.
[13] G. Li, T. Kako, D. Wang, Z. Zou, J. Ye, J. Phys. Chem. 69 (2008) 2487–2491.
[14] K.C. Patil, S.T. Aruna, S. Ekambaram, Curr. Opin. Solid State Mater. Sci. 2 (1997) 158–165.
[15] K.C. Patil, S.T. Aruna, T. Mimani, Curr. Opin. Solid State Mater. Sci. 6 (2002) 507–512.
[16] D.A. Fumo, M.R. Morelli, A.M. Segadães, Mater. Res. Bull. 31 (1996) 1243–1255.
[17] M.A. Raza, I.Z. Rahman, S. Beloshapkin, J. Alloys Compd. 485 (2009) 593–597.
[18] M.W. Raja, S. Mahanty, P. Ghosh, R.N. Basu, H.S. Maiti, Mater. Res. Bull. 42 (2007) 1499–1506.
[19] S.V. Chavan, P.U.M. Sastry, A.K. Tyagi, J. Alloys Compd. 456 (2008) 51–56.
[20] N.P. Bansal, Z. Zhong, J. Power Sources 158 (2006) 148–153.
[21] S.R. Jain, K.C. Adiga, V.R.P. Verneker, Combus. Flame 40 (1981) 71–79.
[22] S.S. Manoharan, K.C. Patil, J. Am. Ceram. Soc. 75 (1992) 1012–1015.
[23] L.A. Chick, L.R. Pederson, G.D. Maupin, J.L. Bates, L.E. Thomas, G.J. Exarthos, Mater. Lett 10 (1990) 6–12.
[24] H.P. Klug, L.E. Alexander, X-ray Diffraction Procedure of Polycrystalline and Amorphous Materials, Jonh Wciley & Sons, New York, 1974.
[25] A. Civera, M. Pavese, G. Saracco, V. Specchia, Catal. Today 83 (2003) 199–211.
[26] G. Feng, H. Rongzi, L. Jiaji, L. Zhen, C. Lihong, T. Changsheng, J. Eur. Ceram. Soc. 29 (2009) 1687–1693.
[27] C. Weifan, L. Fengsheng, L. Leili, L. Yang, J. Rare Earths 24 (2006) 782–787.
[28] S.H Xiao, W.F. Jiang, L.Y. Li, X.J. Li, Mater. Chem. Phys. 106 (2007) 82–87.
[29] M.L. Lavčević, A. Turković, Scripta Mater. 46 (2002) 501–505.
[30] W.-N. Wang, W. Widiyastuti, T. Ogi, I.W. Lenggoro, Chem. Mater. 19 (2007) 1723–1730.
[31] N. Izu, W. Shin, I. Matsubara, N. Murayama, Sens. Actuators B 94 (2003) 222–227.
[32] Y. Terashi, A. Purwanto, W.N. Wang, F. Iskandar, K. Okuyama, J. Eur. Ceram. Soc. 28 (2008) 2573.
[33] R. Wongmaneerung, W. Chaisan, O. Khamman, R. Yimnirun, S. Ananta, Ceram. Int. 34 (2008) 813.

J Mater Sci (2011) 46:1585–1590
DOI 10.1007/s10853-010-4967-5

Synthesis of potassium niobate ($KNbO_3$) nano-powder by a modified solid-state reaction

Nopsiri Chaiyo · Anucha Ruangphanit · Rangson Muanghlua · Surasak Niemcharoen · Banjong Boonchom · Naratip Vittayakorn

Received: 20 July 2010 / Accepted: 29 September 2010 / Published online: 15 October 2010

Abstract Crystalline lead-free piezoelectric potassium niobate ($KNbO_3$) powders have been synthesized through a modified solid-state reaction method. The thermal behavior of the $K_2C_2O_4{\cdot}H_2O$ and Nb_2O_5 raw material mixture was investigated by thermogravimetric analysis (TGA) and differential thermal analysis (DTA). The X-ray diffraction technique (XRD) was used to investigate the phase formation and purity. The morphology of the powder obtained was characterized using a scanning electron microscope (SEM). The XRD pattern showed that the monophasic perovskite phase of $KNbO_3$ could be synthesized successfully at a temperature as low as 550 °C for 240 min, with an average crystallite size of 36 ± 8 nm. The SEM images suggested that the average particle size of the powder obtained was 278 ± 75 nm.

N. Chaiyo · N. Vittayakorn
Electroceramic Research Laboratory, College of KMITL Nanotechnology, King Mongkut's Institute of Technology Ladkrabang, Bangkok 10520, Thailand

N. Chaiyo · N. Vittayakorn
ThEP Center, CHE, 328 Si Ayutthaya Rd, Bangkok 10400, Thailand

A. Ruangphanit
Thai Micro Electronics Center (TMEC), National Electronics and Computer Technology Center, Chachoengsao, Chachoengsao, Thailand

R. Muanghlua · S. Niemcharoen
Faculty of Engineering, Department of Electronics, King Mongkut's Institute of Technology Ladkrabang, Bangkok 10520, Thailand

B. Boonchom
King Mongkut's Institute of Technology Ladkrabang, Chumphon Campus, 17/1 M. 6 Pha Thiew District, Chumphon 86160, Thailand

N. Vittayakorn (✉)
Faculty of Science, Department of Chemistry, King Mongkut's Institute of Technology Ladkrabang, Bangkok 10520, Thailand
e-mail: naratipcmu@yahoo.com

Introduction

Lead zirconate titanate (PZT) ceramics are used widely in piezoelectric applications, due to their superior piezoelectric properties near the morphotropic phase boundary (MPB) [1, 2]. However, more than 50% of the lead-based piezoelectric material contains poisonous lead, which is a major drawback [3]. It has been reported that the use of lead-based ceramics causes serious environmental problems and numerous physical symptoms [3]. Furthermore, EU legislation will enforce draft directives for waste from electrical and electronic equipment (WEEE), and restrictions on the use of certain hazardous substances in electrical and electronic equipment (RoHS) and end-of life vehicles (ELV) [4–6]. According to these issues, lead and other heavy metals should be phased out, and alternative lead-free piezoelectric materials are receiving considerable attention.

Among various alternative families, perovskite type (ABO_3) ceramics have attracted much consideration. Among alkali metal niobates, potassium niobate ($KNbO_3$) is a well-known perovskite oxide that possesses attractive physical and piezoelectric properties [6–9]. Furthermore, the electromechanical coupling factor of the thickness-extensional mode, k_t, was reported to reach as high as 0.69 for the 49.5°-rotated X-cut on the Y-axis. This value of k_t is the highest among current lead-free piezoelectrics [10]. However, the main hindrance regarding this alkali niobate-based material lies in the difficulty of preparing dense and stoichiometric controlled ceramics using the conventional

solid-state reaction and ordinary air sintering methods [11, 12]. These difficulties are caused by potassium volatility at high temperatures and excessive reactivity with moisture [13, 14]. Thus, different additive methods, hot pressing and spark plasma sintering have been used to improve ceramic densification [12, 15–19].

Several alternative ways for preparing alkali niobates have been investigated and developed: the hydrothermal [20] and hydrothermal-assisted sol–gel method [22], and glycothermal [23], nitrate–tartarate precursor technique [21], etc. However, most chemical synthesis routes require high purity reactants, which are more expensive and demand complicated procedures and specific apparatus. A modified solid-state reaction method has been used to synthesize the $NaTaO_3$ perovskite type material successfully, with reduced reaction temperature [24]. In this method, the carbonate compound was replaced by oxalate, and the addition of urea played an important role. Recently, this method also has been applied to synthesize lead-free sodium niobate ($NaNbO_3$) powders (without fuel) [25]. By replacing sodium carbonate using oxalate as the raw material, a lower calcination temperature and fine powders with an average crystallite size of 31.45 ± 5.28 nm were achieved.

In this study, a modified solid-state reaction method, with an expected lower reaction temperature, was used to synthesize $KNbO_3$ particles, using potassium oxalate as raw material without the addition of any fuel. Effects of the calcination conditions on the $KNbO_3$ phase development were investigated by the X-ray diffraction technique (XRD) and a scanning electron microscope (SEM).

Experiment

$KNbO_3$ was synthesized by a modified solid-state reaction method. Reagent-grade potassium oxalate monohydrate ($K_2C_2O_4{\cdot}H_2O$, 99.9%) and niobium oxide (Nb_2O_5, 99.9%) were employed as the starting material. The raw materials were weighed in stoichiometric quantities following the equation below.

$$K_2C_2O_4 \cdot H_2O_{(s)} + Nb_2O_{5(s)} \rightarrow 2KNbO_{3(s)} + CO_{2(g)} + CO_{(g)} + H_2O \quad (1)$$

These starting materials were mixed by the ball-milling method using ethyl alcohol and partially stabilized zirconia balls for 18 h. Then, the mixture was dried on a hot plate with regular stirring for a suitable period. After drying, the precursor mixture was determined by thermo gravimetric analysis (TGA, Perkin Elmer) and differential thermal analysis (DTA, Perkin Elmer) for investigating the thermal behavior during heat treatment and finding the appropriate calcination temperature. Based on TG–DTA results, the mixture was placed subsequently in a closed alumina crucible, and calcined for different periods of time at various temperatures ranging from 300 to 700 °C, to investigate formation of the $KNbO_3$ phase.

Subsequently, calcined powders were inspected by room temperature X-ray diffraction (XRD, Advance D8), using Ni-filtered CuK_α radiation to examine the effect of thermal treatment on the phase development and optimal calcination condition of crystalline $KNbO_3$ powder formation. The room temperature FTIR spectra were recorded in the range of 4,000–400 cm^{-1} (Perkin-Elmer, Spectrum GX spectrometer), with eight scans and a resolution of 4 cm^{-1} using KBr pellets. Powder morphologies and particle size were figured directly using a scanning electron microscope (SEM, Hitachi S4700).

Results and discussion

Figure 1 shows the TG–DTA curves of the stoichiometric precursor of $KNbO_3$. The thermogravimetric (TG) curve of the $KNbO_3$ precursor shows three stages of weight loss from room temperature to 1,300 °C. Four endothermic peaks at 123, 398, 524 and 1,066 °C were observed in the differential thermal analysis (DTA) curve. Three weight-loss steps were observed in the ranges of 50–121, 121–172, and 416–532 °C. The corresponding weight losses seen were 3.92, 1.07, and 16.00%. The overall weight loss was found to be about 21%, which is close to the theoretical value of 20.01%, and corresponds to the release of 1 mol H_2O, 1 mol CO, and 1 mol CO_2 related to Eq. 1. In the temperature range from 50 to 121 °C (first stage), the initial weight loss of 3.92% showed decomposition of the oxalate molecule releasing water molecules (0.98 mol

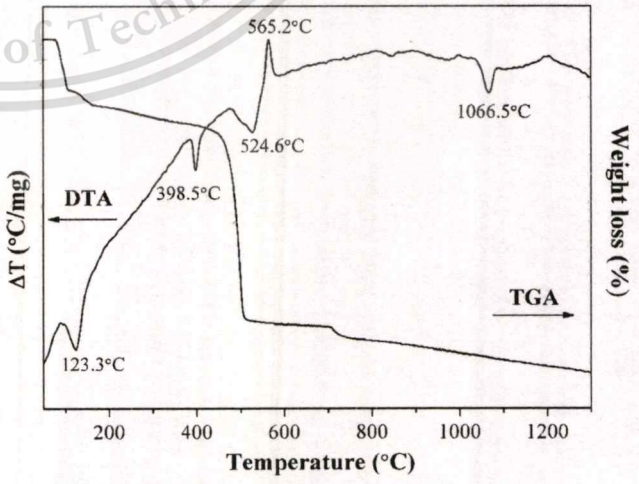

Fig. 1 TG–DTA curves of an uncalcined powder mixed in the stoichiometric proportion of $KNbO_3$

H_2O), which concurred with the theoretical value for releasing 1.00 mol H_2O (4.00%). This weight-loss corresponded to the endothermic peak, centered at 123 °C.

The second and third weight-loss steps illustrated the highest weight loss (~17%), which indicated a large elimination of organic compound that could be related to the release of CO and CO_2 by combustion reactions according to Eqs. 2 and 3 (16% theoretically). In the temperature range from 121 to 532 °C, the DTA curve shows corresponding endothermic peaks (398 and 524 °C) that agree with the TG result.

$$K_2C_2O_4 \rightarrow K_2CO_3 + CO \quad (2)$$

$$K_2CO_3 \rightarrow K_2O + CO_2 \quad (3)$$

However, an exothermic DTA peak was found centered at 565 °C. This implied that the third decomposition stage could lead to the formation of potassium niobate compound, which could be expected from the exothermic peak at 565 °C (as confirmed by XRD analysis in Fig. 2). As the temperature increased to 695 °C, weight loss was found to start again in the TGA curve, which could be correlated to the decomposition of the activated-K_2CO_3 residue. It is well known that $K_2C_2O_4$ decomposes to K_2CO_3 at a higher temperature; however, this carbonate residue could decompose at a lower temperature when its degree of arrangement is lower than its initial state [26]. When heating further, an endothermic peak (without the observed weight-loss stage) could correspond to the phase transformation at 1,066 °C. Therefore, temperatures from the above TG–DTA analysis, which ranged from 300 to 700 °C, were selected for calcinations and investigation of the phase formation. The mixture of raw materials in the required stoichiometric ratio was calcined in air using a heating/cooling rate of 20 °C/min at various temperatures and followed by the phase analysis using an X-ray diffractometer.

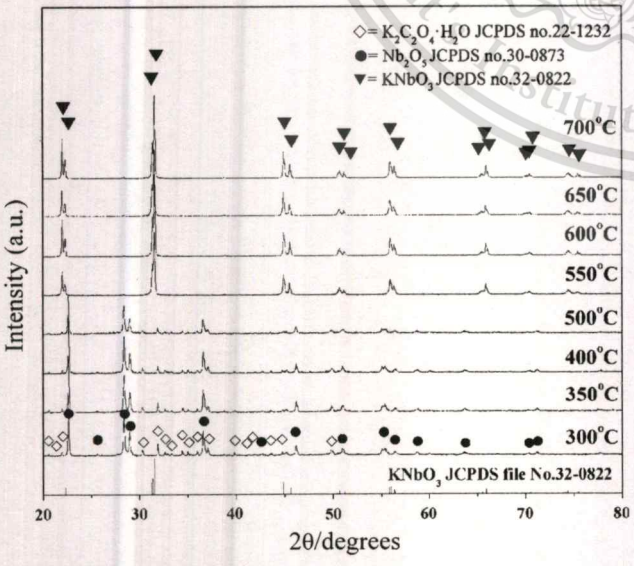

Fig. 2 X-ray diffraction patterns of $KNbO_3$ powder calcined at various temperatures for 4 h with a heating/cooling rate of 20 °C/min

The X-ray diffraction (XRD) patterns of potassium niobate ($KNbO_3$) powders, calcined for 4 h at different temperatures, are illustrated in Fig. 2. The diffraction pattern of the powder calcined at 300 °C suggests a composition of potassium oxalate (◇) (JCPDS no.22-1232) and niobium oxide (●) (JCPDS no.30-0873) raw materials. No evidence of the $KNbO_3$ perovskite phase was found. As calcination temperatures increased to 500 °C, diffraction peaks of un-reacted raw materials were also found, but with lower intensity. This could demonstrate that the completed reaction cannot occur at such a low temperature range. As the diffusion coefficient is a temperature dependent parameter, the rate of diffusion is affected greatly by higher temperatures [27], which also could improve higher atomic mobility [28]. Nonetheless, the powders calcined from 550 to 700 °C showed diffraction peaks that could correspond to the orthorhombic potassium niobate perovskite phase ($KNbO_3$) JCPDS no.32-0822 (▼). Amplified peak intensities can be seen after calcinations at increased temperatures. However, this result indicates the formation of $KNbO_3$ perovskite phase powder, which passes through the calcination temperatures from 550 to 700 °C in 4 h. These temperatures were lower than those in the chemical synthesis of $KNbO_3$, which used the polymerized complex method (PC method). This technique achieved the $KNbO_3$ compound after the calcination step at 900 °C [29], or once the citrate precursor route had obtained $KNbO_3$ nanopowder after heat treatment at 800 °C [30]. In addition, other chemical methods always require high purity reagent, which is more expensive, and involves complex procedures.

For a verdict on fine $KNbO_3$ nucleation condition, a temperature of 550 °C was chosen to find the effect of calcination dwell time. The mixture of raw material powder was calcined at 550 °C for 15–360 min. The XRD analysis of calcined powder, with a different dwell time (Fig. 3), revealed an amorphous phase for a calcination period of 15 min, and no distinct crystalline phase could be detected. The absence of reflection peaks that correspond to $K_2C_2O_4 \cdot H_2O$ and Nb_2O_5 indicated the amorphous nature of the powder obtained. The presence of reflection peaks for the XRD pattern of powder calcined at 550 °C for 20 min or longer could be ascribed to the crystalline phase of the sample. The different diffraction pattern of the powder, calcined for 20 min, suggests the nucleation condition of the $KNbO_3$ phase, which was confirmed by further soaking time. After the calcination step at 550 °C for 20 min or longer, the powder showed an XRD pattern that could be matched with the perovskite potassium niobate (KN) phase

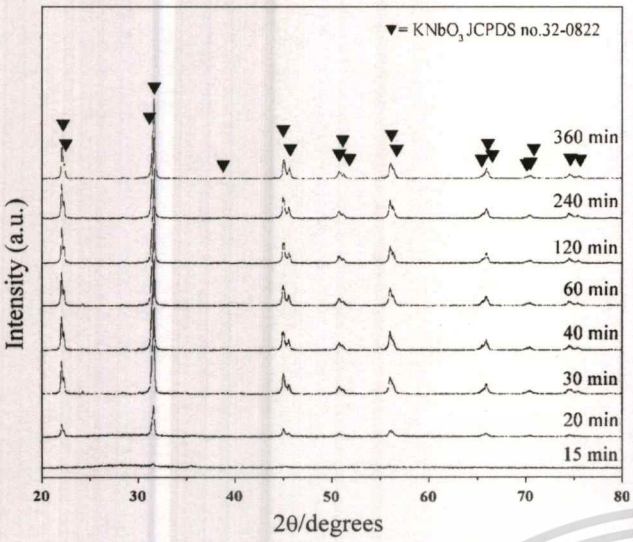

Fig. 3 X-ray diffraction patterns of $KNbO_3$ powder calcined at the calcination temperature of 550 °C for various dwell times with a heating/cooling rate of 20 °C/min

JCPDS no.32-0822. These XRD analyses agreed with the TG–DTA analysis, in which crystallization of the $KNbO_3$ phase was found around the previously mentioned temperature range. During the course of calcinations, the rise in calcination temperature and dwell time resulted in increased diffraction peak intensities, which related to higher crystallinity of the powder. This was supported by the increase in lattice parameters and average crystallite size, as revealed below. Nevertheless, it has been confirmed that this modified solid state reaction method can synthesize pure $KNbO_3$ phase powder by using potassium oxalate monohydrate as starting material at the calcination temperature of 550 °C for 20 min. This calcination temperature is much lower than that used in a mixed oxide powder process, which lies in the range of 800 °C [9, 11, 13, 31, 32], or solution process (sol–gel and precipitation methods) that requires calcination temperatures of over 600 °C [33, 34]. Since XRD analysis suggested an orthorhombic crystal structure for preparing $KNbO_3$ powder, lattice parameters of the sample could be deliberate by means of the UnitCell program package (ftp://rock.esc.cam.ac.uk/pub/minp/UnitCell/). The corresponding cell parameters, which are close to those reported from JCPDS file No.32-0822 ($a = 5.695$ nm, $b = 5.721$ nm, and $c = 3.973$ nm) are given in Table 1. The suggested orthorhombic crystal structure, obtained from matching with the JCPDS file, could be supported by this correlation of lattice parameters.

The average crystallite size of $KNbO_3$ powders was considered as a function of calcination temperature, and time for broadening the X-ray line of the reflection peak using Scherrer's equation [35]: $D = k\lambda/\beta\cos\theta_B$, where D is the average crystallite size, k a constant taken as 0.89, λ the wavelength of X-ray radiation, β the full width at half maximum (FWHM), and θ_B the diffraction angle. The corresponding values are reported in Table 2. The average crystallite size of powders, calcined from 550 to 700 °C for 4 h, was found to be about 36 ± 8 to 58 ± 6 nm. As the dwell time increased, it was found that the average crystallite size of calcined powders was increasing from 33 ± 9 to 36 ± 8 nm. The low D values suggest that the surface area of calcined powder was high enough to support high sinterability sufficiently [36]. The increase in crystallinity of the $KNbO_3$ phase was affected by increasing dwell time and calcination temperature. This consequence may confirm that the dwell time and calcination temperature also play an important role in developing the pure phase creation.

Figure 4 shows the FT-IR spectroscopic studies of the crystalline potassium niobate ($KNbO_3$) before and after the calcination step. The IR band for the uncalcined precursor was observed at 3,253 cm^{-1}, due to O–H asymmetric

Table 1 Lattice parameters of the $KNbO_3$ powder calcined at various calcination temperatures for 4 h

$KNbO_3$	Calcinations temperature (°C)			
Lattice parameter	550	600	650	700
a	5.6929 ± 0.0005	5.6876 ± 0.0070	5.7019 ± 0.0022	5.6952 ± 0.0028
b	5.6989 ± 0.0080	5.6994 ± 0.0048	5.7153 ± 0.0108	5.6980 ± 0.0060
c	3.9802 ± 0.0005	3.9768 ± 0.0006	3.9912 ± 0.0155	3.9777 ± 0.0030

Table 2 Mean crystalline size, D, of the $KNbO_3$ powder calcined at different temperatures for 4 h and for a different dwell time at 550 °C

$KNbO_3$	Calcination temperature (°C)					
	550		600	650		700
D	36.40 ± 8.25		41.46 ± 8.84	53.59 ± 6.56		57.81 ± 6.31
550 °C	Dwell time (min)					
	20	30	40	60	120	240
D	33.15 ± 9.22	34.36 ± 7.92	34.54 ± 8.128	35.30 ± 8.30	35.97 ± 6.47	36.40 ± 8.25

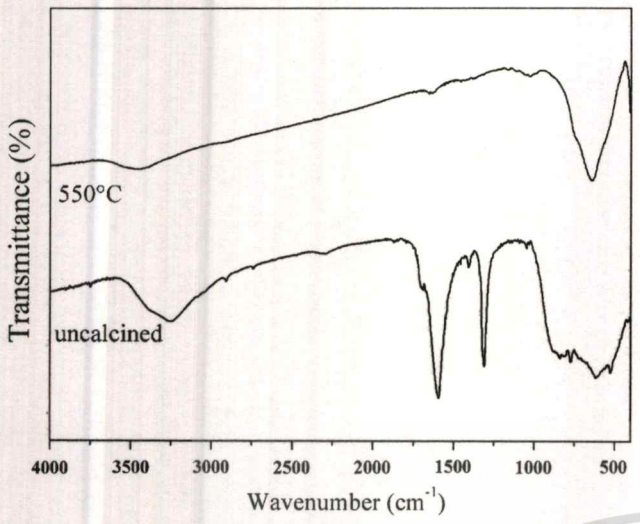

Fig. 4 FT-IR spectra of an uncalcined powder mixed in the stoichiometric proportion of $KNbO_3$ and $KNbO_3$ particles calcined at 550 °C

stretching (ν_3), which related to the moisture content of the KBr pellet and scissor bending mode (ν_2) of HO–H at 1,600 cm^{-1} and 1,310 cm^{-1}. When $KNbO_3$ powders were calcined at 550 °C for 4 h, the absorption of bands at a low wave number range of 620 cm^{-1} suggested occurrence of Nb–O bond formation, which was believed to be the vibration (ν_3) mode in the corner-shared NbO_6 octahedron, according to the reported IR spectra of niobate glass ceramics [37]. This result shows that the perovskite $KNbO_3$ phase was synthesized, which correlated with other results. The TG result indicated that the mass loss in the TG curve at around 700 °C could be the result of the K_2CO_3 residue decomposition, however, the FTIR band corresponding to the C–O stretching mode of carbonate at 1,450 cm^{-1} [38] was not found in $KNbO_3$ powders calcined at 550 °C for 4 h. This observation could be described as the effect of dwell time.

Figure 5 shows SEM micrographs of $KNbO_3$ powder prepared using a modified solid state reaction method at 550 and 700 °C for 240 min. The $KNbO_3$ powder was found to be polyhedral in shape, with uniform features. The secondary phase could not be observed, which suggested the homogeneous character of the powder prepared. The mean particle sizes, which can be estimated from the micrographs, were found to be 278 ± 75 and 341 ± 80 for powder obtained at 550 and 700 °C, respectively. Particle growth was detected in powder calcined at a higher temperature. This value is greater than the average crystallite size, calculated from X-ray line broadening. It was believed that this contradictory value could indicate the agglomerate of the calcined powders. As reported by other studies [39, 40], the firing process tends to produce agglomerated particles and grain growth. No evidence of a different or pyrochlore phase was found. This outcome relates to the XRD result, in which the monophasic perovskite phase of $KNbO_3$ can be established after calcinations at 550 °C for 240 min.

Conclusion

Crystalline $KNbO_3$ powder was prepared from a modified solid state reaction of $K_2C_2O_4{\cdot}H_2O$ and Nb_2O_5. The final product was confirmed by XRD and SEM techniques. This is a simple cost- and time-saving method for synthesizing stoichiometric, homogeneous, and fine $KNbO_3$ powder, with a low calcination temperature of 550 °C for 240 min. This temperature is about 250 °C lower than others used, even in conventional methods. The powder obtained was found to be a uniform agglomerated particle that possesses an average crystallite size (defined by XRD) of between 36 ± 8 and 58 ± 6 nm, and a mean particle size (defined by SEM micrograph) of 278 ± 75 nm.

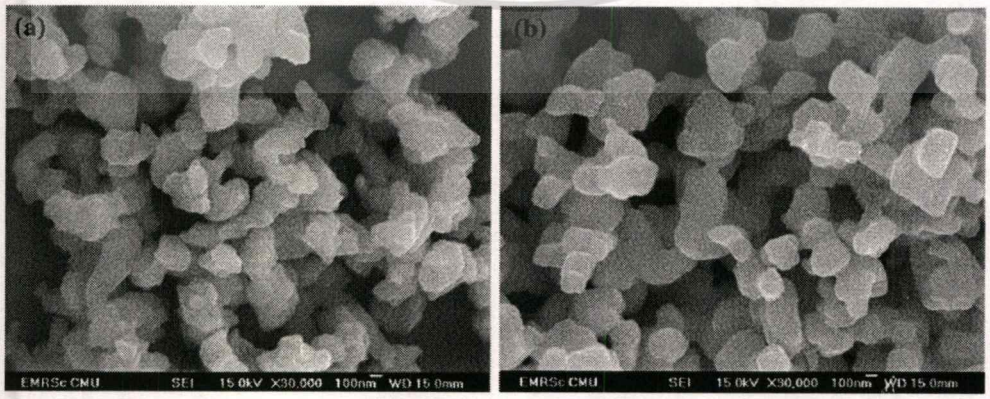

Fig. 5 SEM micrographs showing $KNbO_3$ powder synthesized at 550 °C (**a**) and 700 °C (**b**), for 4 h with a heating/cooling rate of 20 °C/min

Acknowledgements This study was supported by the Thailand Research Fund (TRF), Thailand Graduate Institute of Science and Technology (TGIST), and the National Nanotechnology Center (NANOTEC) NSTDA, Ministry of Science and Technology, Thailand, through its "Center of Excellence Network" Program.

References

1. Miclea C, Tanasoiu C, Miclea CF, Amarande L, Gheorghiu A, Spanulescu I, Plavitu C, Miclea CT, Cioangher MC, Trupina L, Iuga A (2007) J Eur Ceram Soc 27:4055
2. Setter N (2002) Piezoelectric materials in devices. Ceramic lab, EPFL, Switzerland
3. Lead and you: a guide to working safely with lead (2003) HSE (UK Health and Safety Executive). http://www.hse.gov.uk/pubns/indg305.pdf. Accessed 25 Apr 2004
4. Commission of the European Communities (2003) Directive 2002/96/EC of the European Parliament and of the Council of 27 January 2003 on waste electrical and electronic equipment (WEEE). Off J Eur Union, L37, 46:24
5. Commission of the European Communities (2003) Directive 2002/95/EC of the European Parliament and of the Council of 27 January 2003 on the restriction of the use of certain hazardous substances in electrical and electronic equipment. Off J Eur Union, L37, 46:19
6. Ichiki M, Zhang L, Tanaka M, Maeda R (2004) J Eur Ceram Soc 24:1693
7. Liu J-F, Li X-L, Li Y-D (2003) J Cryst Growth 247:419
8. Paula AJ, Parra R, Zaghete MA, Varela JA (2008) Mater Lett 62:2581
9. Yamanouchi K, Odagawa H, Kojima T, Matsumura T (1997) Electron Lett 33:193
10. Nakamura K, Kawamura Y (1999) Proc IEEE Ultrason Symp 2:1013
11. Matsumoto K, Hiruma Y, Nagata H, Takenaka T (2008) Ceram Int 34:787
12. Makovec D, Pribošič I, Drofenik M (2008) Ceram Int 34:89
13. Lu CH, Lo SY, Lin HC (1998) Mater Lett 34:172
14. Muthurajan H, Kumar HH, Samuel V, Gupta UN, Ravi V (2008) Ceram Int 34:671
15. Kim MS, Lee DS, Park EC, Jeong SJ, Song JS (2007) J Eur Ceram Soc 27:4121
16. Mgbemere HE, Herber R-P, Schneider GA (2009) J Eur Ceram Soc 29:1729
17. Wang R, Xie R, Sekiya T, Shimojo Y, Akimune Y, Hirosaki N, Itoh M (2002) Jpn J Appl Phys 41:7119
18. Ahn ZS, Schulze WA (1987) J Am Ceram Soc 70:18
19. Jaeger RE, Egerton L (1962) J Am Ceram Soc 45:209
20. Chang Y, Yang Z, Wei L, Liu B (2006) Mater Sci Eng A 437:301
21. Bhattacharyya K, Tyagi AK (2009) J Alloys Compd 470:580
22. Amini MM, Mirzaee M (2009) Ceram Int 35:2367
23. Lu C-H, Lo S-Y, Wang Y-L (2002) Mater Lett 55:121
24. Xu J, Xue D, Yan C (2005) Mater Lett 59:2920
25. Chaiyo N, Boonchom B, Vittayakorn N (2010) J Mater Sci 45:1443. doi:10.1007/s10853-009-4098-z
26. Vlaev L, Nedelchev N, Gyurova K, Zagorcheva M (2008) J Anal Appl Pyrolysis 81:253
27. Hsiao Y-J, Chang Y-H, Chang Y-S, Fang T-H, Chai Y-L, Chem G-J, Huang T-W (2007) Mater Sci Eng B 136:129
28. Callister WD (2007) Materials science and engineering: an introduction. Wiley, New York
29. Pribošič I, Makovec D, Drofenik M (2005) J Eur Ceram Soc 25:2713
30. Kakimoto K, Ito T, Ohsato H (2008) Jpn J Appl Phys 47:7669
31. Malic B, Bernard J, Bencan A, Kosec M (2008) J Eur Ceram Soc 28:1191
32. Chang Y, Yang Z-P, Ma D, Liu Z, Wang Z (2008) J Appl Phys 104:024109
33. Amini MM, Sacks MD (1991) J Am Ceram Soc 74:53
34. Kim KJ, Matijevic E (1992) J Mater Res 7:912
35. Klug HP, Alexander LE (1974) X-ray diffraction procedure of polycrystalline and amorphous materials. Wiley, New York
36. Lanfredi S, Dessemond L, Rodrigue ACM (2000) J Eur Ceram Soc 20:983
37. de Andrade JS, Pinheiro AG, Vasconcelos IF et al (1999) J Phys Condens Matter 11:4451
38. Böke HA, Akkurt S, Özdemir S, Göktürk EH, Saltik ENC (2004) Mater Lett 58:723
39. Terashi Y, Purwanto A, Wang WN, Iskandar F, Okuyama K (2008) J Eur Ceram Soc 28:2573
40. Wongmaneerung R, Chaisan W, Khamman O, Yimnirun R, Ananta S (2008) Ceram Int 34:813

Ferroelectrics, 415:75–82, 2011

ISSN: 0015-0193 print / 1563-5112 online
DOI: 10.1080/00150193.2011.577374

Taylor & Francis
Taylor & Francis Group

Facile Synthesis of Lead-Free Piezoelectric Sodium Niobate ($NaNbO_3$) Powders via the Solution Combustion Method

NOPSIRI CHAIYO,[1,2] ANUCHA RUANGPHANIT,[3] BANJONG BOONCHOM,[4] AND NARATIP VITTAYAKORN[1,2,5,*]

[1]Electroceramic Research Laboratory, College of Nanotechnology, King Mongkut's Institute of Technology Ladkrabang, Bangkok 10520, Thailand
[2]ThEP Center, CHE, 328 Si Ayutthaya Rd., Bangkok 10400, Thailand
[3]Thai Micro Electronics Center (TMEC), National Electronics and Computer Technology Center Chachoengsao, Chachoengsao, Thailand
[4]King Mongkut's Institute of Technology Ladkrabang, Chumphon Campus, 17/1 M. 6 Pha Thiew District, Chumphon 86160, Thailand
[5]Advanced Materials Science Research Unit, Department of Chemistry, Faculty of Science, King Mongkut's Institute of Technology Ladkrabang, Bangkok 10520, Thailand

Nanocrystalline perovskite sodium niobate, $NaNbO_3$ (NN), was prepared by means of the glycine-nitrate combustion process (GNP). This was achieved by using sodium nitrate and niobium pentoxide as starting materials. The X-ray diffraction technique (XRD) was used to investigate the phase formation and purity of synthesized powder. The morphology of the powder obtained was characterized using a scanning electron microscope (SEM). The amount of glycine in the starting solution was found to have significant influence on the combustion process and the final phase purity. The fuel-rich ratio (fuel-to-oxidant molar ratio of 1.0) was found to produce $NaNbO_3$ powder of an average crystalline size (defined by XRD) of 31.31 ± 4.37 nm. Calcination at 400°C for 4 h produced single phase NN with an average crystalline size of about 26.60 to 37.14 nm.

Keywords Sodium niobate; glycine-nitrate combustion process; combustion method

1. Introduction

Sodium niobate, $NaNbO_3$, is a well known lead-free piezoelectric material, which has attracted considerable attention due to its unique and environmentally friendly properties [1, 2]. Unlike other oxide perovskites, $NaNbO_3$ undergoes six phase transitions from the ferroelectric phase at low temperature (rhombohedral) to the antiferroelectric room temperature phase (orthorhombic) and non-polar cubic structure at 640°C [2, 3]. When $NaNbO_3$ is antiferroelectric at room temperature, it can be induced to ferroelectric via solid solutions combined with Li- or K- based niobates [4]. The production of $NaNbO_3$ by traditional solid

Received June 20, 2010.
*Corresponding author. E-mail: naratipcmu@yahoo.com

state reaction, with high temperature and long duration, provides volatilization of alkali metal, which results in stoichiometric controlled problems [5, 6]. Moreover, agglomerates can occur during heating [6]. These can affect the piezoelectric and physical properties of synthesized powders and ceramics. Thus, alternative processes have been developed to fabricate alkali niobate powder with a controllable condition.

Combustion synthesis (CS); called 'self-propagating high-temperature synthesis (SHS)', is known as a novel process for synthesizing very fine crystalline multi component oxide powders without intermediate decomposition and/or calcination steps [7]. In CS, the energy released by highly exothermic chemical reaction (simultaneous oxidation and reduction reaction between oxidizer and fuel), which is very rapid and self-sustaining, can drive the chemical reaction itself without an external source [8, 9]. The simple nature of CS results in low operational costs and energy efficiency. Solution combustion synthesis is one of many CS categories. Advanced materials with nanoparticles have been prepared through the redox mixture solution of metal nitrate and fuel [8–10]. Numerous fuels, such as urea, glycine, alanine, etc., have been used.

An efficient solution combustion method is the glycine-nitrate combustion process (GNP), which uses metal nitrate and glycine as starting material and fuel, respectively [11, 12]. Glycine is among the cheapest amino acids that can act as a complexing agent, since it has a carboxylic acid group at one end and amino group at the other [13]. This molecular characteristic is known as zwitterionic; an effective complex with metal ions of various ionic sizes.

In this study, $NaNbO_3$ powder was prepared via the solution combustion method or GNP, using sodium nitrate, Nb_2O_5 and glycine. In order to explore the possibility of preparing nano-crystalline $NaNbO_3$ powder by a combustion technique, a composition of sodium and niobium was fixed. Also, different fuel-to-oxidant molar ratios and calcination temperatures were used to investigate the effect of fuel content on the combustion process and powder characteristics.

2. Experiment

Nanoparticles of $NaNbO_3$ were synthesized by a solution combustion technique. The precursor of the composition, $NaNbO_3$, was prepared by mixing AR grade sodium nitrate ($NaNO_3$ 99.5%) and niobium pentoxide (Nb_2O_5 99.95%) in stoichiometric proportions. The starting materials were mixed with de-ionized water in a glass beaker, and then a stoichiometric amount of glycine (NH_2CH_2COOH 99.7%) was added into the mixed solution with regular stirring for 30 min. Different fuel-to-oxidant molar ratios were applied. The mixture in the glass beaker was heated on a hotplate until the ignition and self-sustaining combustion took place, resulting in a fluffy powder. Then, the powder was calcined at different temperatures ranging from 300°C to 900°C for 4 h. As-prepared and calcined powders were subsequently inspected by room temperature X-ray diffraction (XRD, Advance D8), using Ni-filtered CuK_α radiation to examine the effect of fuel content, and thermal treatment was given for the combustion process and phase development of crystalline $NaNbO_3$ powders. Powder morphologies and particle size were figured directly using a scanning electron microscope (SEM, Hitachi S4700).

3. Results and Discussion

In order to alter the properties of synthesized $NaNbO_3$ powder, the fuel-to-oxidant molar ratio was systematically varied. On the principle of propellant chemistry [14], the

stoichiometric redox reaction between fuel and oxidizer could be assumed by estimating the ratio of the net reducing valency of the glycine (9+) to the net oxidizing valency of sodium nitrate (5-), which should be united. In this case, the stoichiometric ratio of the fuel-to-oxidant molar ratio was found to be 0.56, which could represent combustion reaction as follows:

$$36NaNO_3 + 18Nb_2O_5 + 20NH_2CH_2COOH \rightarrow 36NaNbO_3 + 50H_2O + 28N_2 + 40CO_2 \quad (1)$$

In this study, the powder synthesis was studied in detail by varying the fuel-to-oxidant molar ratio on either side of this ratio, i.e. fuel-deficient composition as 0.3 and 0.5, and fuel-rich composition as 1.0 and 2.0.

The X-ray diffraction (XRD) patterns of the powder synthesized from various fuel-to-oxidant molar ratios are illustrated in Fig. 1. In the ratios (0.3 and 0.5) of the fuel-deficient composition, no ignition or combustion reaction was found, according to experimental observations. The XRD patterns belonging to those sample compositions showed that phases of Nb_2O_5 (•) (JCPDS file no. 30-0873) and $NaNO_3$ (■) (JCPDS file no.85–0859) starting materials were detected without evidence of a perovskite $NaNbO_3$ phase. These XRD patterns corresponded with those of the precursor mixture without the combustion process. This observation suggests that the nucleation of the perovskite $NaNbO_3$ phase did not occur without the ignition and exothermic chemical reaction, which was an important source of energy for driving the formation reaction. On the other hand, it can be noted that the ignition did not take place when low fuel content or fuel-deficient composition was applied [9, 15]. As fuel content increased, it could be seen clearly that the perovskite $NaNbO_3$ phase (▼) was obtained by the GNP when using fuel-rich ratios. The volume fraction of the perovskite phase formation was considered at various fuel-rich ratios. These relative amounts of perovskite $NaNbO_3$ phase were approximated by calculating the ratio

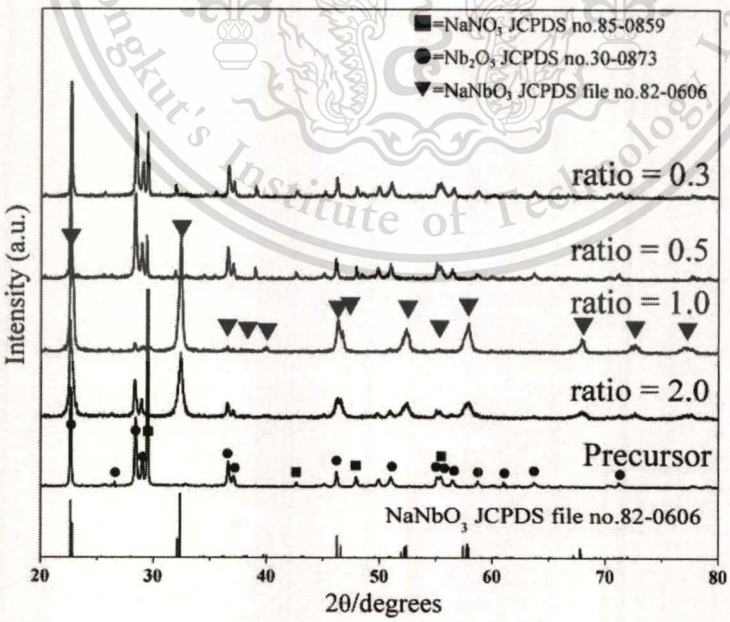

Figure 1. X-ray diffraction patterns of $NaNbO_3$ powder obtained from various fuel-to-oxidant molar ratios.

of the main X-ray peak intensities of $NaNbO_3$ and Nb_2O_5 phases [16], according to the following equation; $\%perovskite = I_{perovskite}/(I_{perovskite} + I_{Nb_2O_5}) \times 100$. The volume fractions of the perovskite phase formation (%perovskite) were found to be 93% and 63% for the fuel-to-oxidant molar ratio of 1.0 and 2.0, respectively. This outcome could support the advantages of the GNP by proposing that this method is a simple, rapid and cost effective way to fabricate perovskite $NaNbO_3$ ceramic powder. This $NaNbO_3$ phase could be indexed according to an orthorhombic structure, with the space group $P2_{1ma}$ (26), which is consistent with JCPDS file no. 82-0606. However, that perovskite $NaNbO_3$ phase was found to accompany the phase of unreacted Nb_2O_5 (•) (JCPDS file no. 30-0873) starting materials in slight content.

In order to observe the morphology and microstructure of the synthesized perovskite powder, a scanning electron microscope (SEM) was used. Figure 2 shows an SEM micrograph of perovskite $NaNbO_3$ powder prepared by using the fuel-to-oxidant molar ratio of 1.0. The synthesized powder was found to be cubic in shape, with uniform features. The other unexpected phase could not be observed, which suggested the homogeneous character of the as-prepared powder. The mean particle size of the primary particle, which can be estimated from SEM micrographs, was found to be 74.56 ± 24.99 nm. This value was found to be about 5 times less than that used in a solid-state reaction method or alternative methods previously reported [17, 18]. This mean particle size was greater than the average crystalline size (31.31 ± 4.37), which was calculated from X-ray line broadening using the Scherrer's equation [19]; $D = k\lambda/\beta\cos\theta$, where D is the average crystallite size, k a constant equal to 0.89, λ the wavelength of X-ray radiation, β the full width at half maximum (FWHM), and θ the diffraction angle. The inconsistency value could indicate the agglomerate of the synthesized powders. However, these observations indicated that the nano-sized powder could be obtained by this proposed method, as previously reported [20].

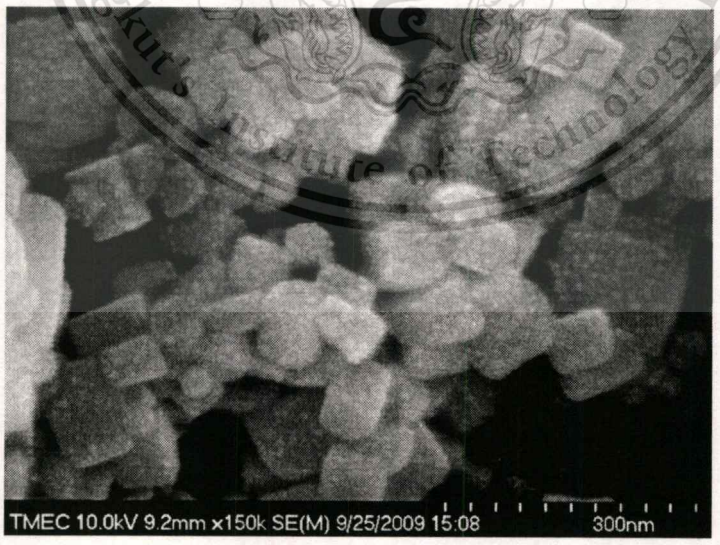

Figure 2. SEM micrograph showing as-prepared $NaNbO_3$ powder synthesized using the fuel-to-oxidant molar ratio of 1.0.

The combustion synthesis has been known and reported as the synthesis process without a calcination step, nevertheless, in this case, those observations suggested that monophasic perovskite $NaNbO_3$ powder could not be synthesized completely through the GNP, which is concordant to the literature [10, 21]. Hence, to investigate the phase formation of monophasic perovskite $NaNbO_3$ powder, the as-prepared powder obtained from the GNP, with a fuel-to-oxidant molar ratio of 1.0, was selected for further calcination steps. As-prepared $NaNbO_3$ powder, with a fuel-to-oxidant molar ratio of 1.0, was calcined at different calcination temperatures that ranged from 300°C to 900°C. Figure 3 shows the XRD pattern of the $NaNbO_3$ powder calcined at different temperatures for 4 h, with a heating/cooling rate of 20°C/min. The X-ray diffraction patterns of the powder calcined at low temperatures of 200°C and 300°C suggests existing composition of perovskite $NaNbO_3$ phase (▼) JCPDS file no. 82-0606, accompanied by the phase of Nb_2O_5 (●) (JCPDS file no.30–0873). As the calcination temperature increased, the refection peaks of unreacted starting material decreased and disappeared when using a calcination temperature of 400°C. In comparison with a solid-state reaction method [22] and other processes [23], this temperature was quite low. In addition, based on the average crystalline size (D) considered by Scherrer's equation, using X-ray line broadening, no significant difference was found between D of the powder calcined at 400°C for 4 h (27.84 ± 7.12) and as-prepared powder (31.31 ± 4.37). This outcome demonstrated that this relatively low calcination temperature was suitable for producing a nano-sized particle and could avoid particle growth. These results have led the combustion synthesis into being a cost- and time-saving process. However, when the calcination temperature was increased further to 900°C, the crystallinity of synthesized powder was amplified, which could be noticed by higher intensity of the refection peak.

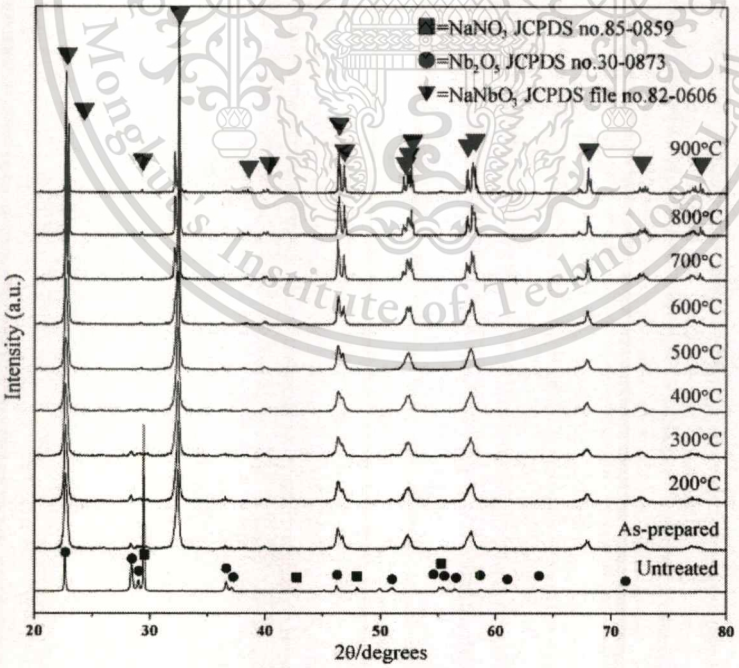

Figure 3. X-ray diffraction patterns of $NaNbO_3$ powder (obtained from the fuel-to-oxidant molar ratio of 1.0) calcined at various temperatures for 4 h with a heating/cooling rate of 20°C /min.

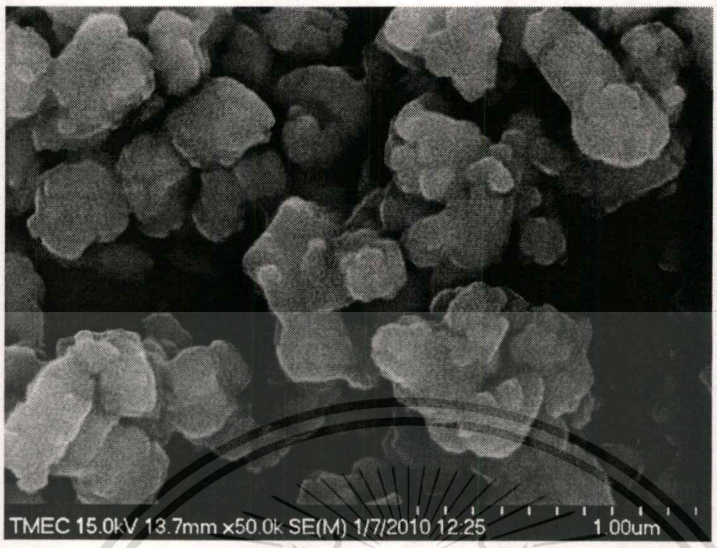

Figure 4. SEM micrographs showing $NaNbO_3$ powder (obtained from the fuel-to-oxidant molar ratio of 1.0) calcined at 400°C for 4 h with a heating/cooling rate of 20°C /min.

Since the increase in calcination temperature affected the increase of crystalline size [24], atomic mobility could be improved, based on the diffusion coefficient being a temperature dependent parameter, with higher temperatures having an extreme effect on the rate of diffusion [25, 26]. A high crystallization temperature leads to a large particle size powder, which can be obviously demonstrated by the increase in average crystalline size (D) from 28 nm (when calcined at 400°C) to 85 nm (when calcined at 900°C).

The SEM micrograph of powders calcined at 400°C for 4 h, with a heating/cooling rate of 20°C/min is illustrated in Figure 4. After the calcination step, the $NaNbO_3$ powder was found to be polyhedral in shape, with uniform features. The other secondary phase could not be observed, which suggested the homogeneous character of the prepared powder. Its particle size, which was estimated from the SEM micrograph, was found to be about 196.48 ± 55.12 nm. This value was found to be higher than the average crystalline size (D) of 27.84 ± 7.12 nm (calculated by Scherrer's equation using X-ray line broadening). The contradictory value could indicate the agglomerate of the calcined powders.

4. Conclusion

Crystalline $NaNbO_3$ powder was successfully synthesized through the glycine-nitrate combustion process (GNP) for the first time. Glycine was used as fuel according to its combustion and complexation nature. The final product was confirmed by XRD and SEM techniques. This method is a relatively simple, rapid and straightforward preparation process for producing homogeneous, very fine, crystalline and unagglomerated $NaNbO_3$ powders, with 93% of phase purity in the as-prepared powder. Monophasic perovskite $NaNbO_3$ can be obtained at a relatively low calcination temperature of 400°C for 4 h. The powder obtained (ratio of 1.0) was found to be a uniform particle that possessed an average crystalline size (defined by XRD) of 27.84 ± 7.12, and a mean particle size (defined by SEM micrograph) of 196.48 ± 55.12 nm. This method is expected to be suitable for mass production of other niobate-based powder.

Acknowledgments

This work was supported by KMITL Research Fund, Thailand Graduate Institute of Science and Technology (TGIST), and the National Nanotechnology Center (NANOTEC) NSTDA, Ministry of Science and Technology, Thailand through its "Center of Excellence Network" Program.

References

1. T. Rojac, O. Masson, R. Guinebretière, M. Kosec, B. Malič, and J. Holc, A study of the mechanochemical synthesis of $NaNbO_3$. *J Eur Ceram Soc.* **27**, 2265–2271 (2007).
2. N. Chaiyo, B. Boonchom, and N. Vittayakorn, Solid-state reaction synthesis of sodium niobate ($NaNbO_3$) powder at low temperature. *J Mater Sci.* **45**, 1443–1447 (2010).
3. X. B. Wang, Z. Shen, Z. P. Hu, L. Qin, S. H. Tang, and M. H. Kuok, High temperature Raman study of phase transitions in antiferroelectric $NaNbO_3$. *J Mol Struct.* **385**, 1–6 (1996).
4. T. Hungría, L. Pardo, A. Moure, and A. Castro, Effect of mechanochemical activation on the synthesis of $NaNbO_3$ and processing of environmentally friendly piezoceramics. *J Alloys Compd.* **395**, 166–173 (2005).
5. S. Lanfredi, L. Dessemond, and A. C. M. Rodrigues, Dense ceramics of $NaNbO_3$ produced from powders prepared by a new chemical route. *J Eur Ceram Soc.* **20**, 983–990 (2000).
6. T. Rojac, M. Kosec, B. Malič, and J. Hol, Mechanochemical synthesis of $NaNbO_3$. *Mater Res Bull.* **40**, 341–345 (2005).
7. D. A. Fumo, M. R. Morelli, and A. M. Segadães, Combustion synthesis of calcium aluminates. *Mater Res Bull.* **31**, 1243–1255 (1996).
8. R. D. Purohit, B. P. Sharma, K. T. Pillai, and A. K. Tyagi, Ultrafine ceria powders via glycine-nitrate combustion. *Mater Res Bull.* **36**, 2711–2721 (2001).
9. M. Liu, D. Xue, and C. Luo, Facile synthesis of lithium niobate squares by a combustion route. *J Am Ceram Soc.* **89**, 1551–1556 (2006).
10. S. H. Xiao, W. F. Jiang, L. Y. Li, and X. J. Li, Low-temperature auto-combustion synthesis and magnetic properties of cobalt ferrite nanopowder. *Mater Chem Phys.* **106**, 82–87 (2007).
11. P. Blennow, K. K. Hansen, L. R. Wallenberg, and M. Mogensen, Synthesis of Nb-doped $SrTiO_3$ by a modified glycine-nitrate process. *J Eur Ceram Soc.* **27**, 3609–3612 (2007).
12. N. P. Bansal and Z. Zhong, Combustion synthesis of $Sm_{0.5}Sr_{0.5}CoO_{3-x}$ and $La_{0.6}Sr_{0.4}CoO_{3-x}$ nanopowders for solid oxide fuel cell cathodes. *J Power Source.* **158**, 148–153 (2006).
13. R. D. Purohit, B. P. Sharma, K. T. Pillai, and A. K. Tyagi, Ultra ceria powders via glycine-nitrate combustion. *Mater Res Bull.* **36**, 2711–2721 (2001).
14. S. R. Jain, K. C. Adiga, and V. R. P. Verneker, New approach to thermochemical calculation of condensed fuel-oxider mixtures. *Combus Flame.* **40**, 71–79 (1981).
15. S. Luo, Z. Tang, W. Yao, and Z. Zhang, Low-temperature combustion synthesis and characterization of nanosized tetragonal barium titanate powders. *Microelectron Eng.* **66**, 147–152 (2003).
16. G. Feng, H. Rongzi, L. Jiaji, L. Zhen, C. Lihong, and T. Changsheng, Phase formation and characterization of high Curie temperature $x\mathrm{BiYbO_3}$–$(1 - x)\mathrm{PbTiO_3}$ piezoelectric ceramics. *J Eur Ceram Soc.* **29**, 1687–1693 (2009).
17. G. Li, T. Kako, D. Wang, Z. Zou, and J. Ye, Synthesis and enhanced photocatalytic activity of $NaNbO_3$ prepared by hydrothermal and polymerized complex methods. *J Phys Chem Solids.* **69**, 2487–2491 (2008).
18. S. Y. Wu, X. Q. Liu, and X. M. Chen, Hydrothermal synthesis of $NaNbO_3$ with low NaOH concentration. *Ceram Inter.* **36**, 871–877 (2010).
19. H. P. Klug and L. E. Alexander, *X-ray diffraction procedure of polycrystalline and amorphous materials*. New York: Wiley; 1974.
20. T. Mimani and K. C. Patil, Solution combustion synthesis of nanoscale oxide and their composites. *Mater Phys Mech.* **4**, 134–137 (2001).

21. Z. Tian, L. Lin, F. Meng, and W. Huang, Combustion synthesis and characterization of nanocrystalline $Ba(Mg_{1/2}Nb_{1/2})O_3$ powders. *Mater Sci Eng B.* **158**, 88–91 (2009).
22. T. Hungrìa, L. Pardo, A. Moure, and A. Castro, Effect of mechanochemical activation on the synthesis of $NaNbO_3$ and processing of environmentally friendly piezoceramics. *J Alloys Compd.* **395**, 166–173 (2005).
23. M. A. L. Nobre, E. Longo, E. R. Leite, and J. A. Varela, Synthesis and sintering of ultra fine $NaNbO_3$ powder by use of polymeric precursors. *Mater Lett.* **28**, 215–220 (1996).
24. S. V. Chavan, P. U. M. Sastry, and A. K. Tyagi, Combustion synthesis of nano-crystalline Ng-doped ceria and Nd_2O_3 and their fractal behavior as studied by small angle X-ray scattering. *J Alloys Compd.* **456**, 51–56 (2008).
25. W. D. Callister, Materials science and engineering: an introduction. New York: Wiley; 2007.
26. Y. J. Hsiao, Y. H. Chang, Y. S. Chang, T. H. Fang, Y. L. Chai, G. J. Chen, and T.-W. Huang, Growth and characterization of $NaNbO_3$ synthesized using reaction-sintering method. *Mater Sci Eng B.* **136**, 129–133 (2007).

J Therm Anal Calorim
DOI 10.1007/s10973-011-1675-6

Non-isothermal kinetics of the thermal decomposition of sodium oxalate $Na_2C_2O_4$

Nopsiri Chaiyo · Rangson Muanghlua · Surasak Niemcharoen · Banjong Boonchom · Panpailin Seeharaj · Naratip Vittayakorn

Received: 22 March 2011 / Accepted: 17 May 2011

Abstract The thermal transformation of $Na_2C_2O_4$ was studied in N_2 atmosphere using thermo gravimetric (TG) analysis and differential thermal analysis (DTA). $Na_2C_2O_4$ and its decomposed product were characterized using a scanning electron microscope (SEM) and the X-ray diffraction technique (XRD). The non-isothermal kinetic of the decomposition was studied by the mean of Ozawa and Kissinger–Akahira–Sunose (KAS) methods. The activation energies (E_α) of $Na_2C_2O_4$ decomposition were found to be consistent. Decreasing E_α at increased decomposition temperature indicated the multi-step nature of the process. The possible conversion function estimated through the Liqing–Donghua method was 'cylindrical symmetry (R_2 or $F_{1/2}$)' of the phase boundary mechanism. Thermodynamic functions (ΔH^*, ΔG^* and ΔS^*), calculated by the Activated complex theory and kinetic parameters, indicated that the decomposition step is a high energy pathway and revealed a very hard mechanism.

Keywords Sodium oxalate · Decomposition · Ozawa method · Kissinger–Akahira–Sunose method

Electronic supplementary material The online version of this article (doi:10.1007/s10973-011-1675-6) contains supplementary material, which is available to authorized users.

N. Chaiyo · N. Vittayakorn
Electroceramic Research Laboratory, Department of Chemistry, Faculty of Science, College of Nanotechnology, King Mongkut's Institute of Technology Ladkrabang, Bangkok 10520, Thailand

N. Chaiyo · N. Vittayakorn
ThEP Center, CHE, 328 Si Ayutthaya Rd, Bangkok 10400, Thailand

R. Muanghlua · S. Niemcharoen
Department of Electronics, Faculty of Engineering, King Mongkut's Institute of Technology Ladkrabang, Bangkok 10520, Thailand

B. Boonchom (✉)
King Mongkut's Institute of Technology Ladkrabang, Chumphon Campus, 17/1 M. 6 Pha Thiew District, Chumphon, 86160, Thailand
e-mail: kbbanjon@gmail.com

P. Seeharaj · N. Vittayakorn (✉)
Department of Chemistry, Faculty of Science, King Mongkut's Institute of Technology Ladkrabang, Bangkok 10520, Thailand
e-mail: naratipcmu@yahoo.com

Introduction

Thermal analysis (TA), e.g., thermogravimetry (TG), differential thermal analysis (DTA), and differential scanning calorimetry (DSC) have been used widely for scientific and practical purposes [1, 2]. These techniques provide important information about physico-chemical parameters, kinetic analysis, polymorphic forms, stability of material, etc., which are reliable and necessary [3]. Thus, the outcomes obtained through this basis can be applied directly in material science for studying thermal behavior, thermal character, and the mechanism and kinetic of solid state reaction. The interpretation of data obtained from these methods, use of various mathematical models and calculation procedures are quite useful. For gaining value of the apparent activation energy, E_a, and pre-exponential factor, A, which is the most probable mechanism function $g(\alpha)$ of the reaction, various equations and methods were described such as the Coats and Redfern equation [4], and iterative procedure, i.e., the Ozawa equation [5], Kissinger–Akahira–Sunose (KAS) equation [6], Senum and Yang approximation formulae [7], etc. The mathematical apparatus and calculation procedures used are related to the mathematical

Published online: 03 June 2011

analysis of thermogravimetric curves. The calculations, based on multiple rates of thermogravimetric curves, are so-called iso-conversional calculation procedures [3].

Thermal decomposition of metal oxalates has been the subject of many researches for more than a century [8]. Decomposition and its non-isothermal kinetics, belonging to some of the oxalates ($Ag_2C_2O_4$, NiC_2O_4, MnC_2O_4, HgC_2O_4, PbC_2O_4, and $SrTiO(C_2O_4)_2{\cdot}4H_2O$), were reported later [3, 8–10]. The dehydration kinetics of $CaC_2O_4{\cdot}H_2O$ were deduced from the multiple rate iso-temperature method, and the apparent activation energy, E_a, was obtained from the Ozawa and KAS method [6]. The kinetic triplet, the activation energy, E_a, the pre-exponential factor, A, and the mechanism functions, $f(\alpha)$, of $MgC_2O_4{\cdot}2H_2O$ were obtained by analyzing the TG-DTG curves of their thermal decomposition using the Popescu and Flynn–Wall–Ozawa method [11]. Furthermore, the decomposed products, e.g., oxide or metal, which possess pores, lattice imperfections and both characteristics, were determined, and the results are necessary data for their function and further study. Although there has been increasing interest in the study of experimental factors and processing parameters, especially in determining the kinetics of thermal decomposition reactions, many features of oxalate decomposition still remain unclear.

In a previous paper, we presented results on the preparation of lead-free piezoelectric sodium niobate ($NaNbO_3$) powders [12]. The use of $Na_2C_2O_4$ as starting material (instead of Na_2CO_3) resulted in a low-temperature solid-state reaction. In general, the sodium oxalate, $Na_2C_2O_4$, serves as a metal cleaning preparation in the textile, leather and tanning industries; potassium oxalate cleans natural fibers in photography, and both of them are used in analytical and solvent extraction chemistry (sodium oxalate as primary volumetric standard for manganometry and acidimetry) [13]. As starting material for versatile industries, it is very important to determine its thermal decomposition mechanism, kinetics and thermodynamic parameter for advantages in cost and time management for industrial production. Many works on the isothermal kinetic of thermal decomposition of oxalate compounds have been published, but there are no reports on the thermal decomposition kinetic of $Na_2C_2O_4$ in the literature.

In this work, the thermal decomposition of $Na_2C_2O_4$ was investigated using non-isothermal thermogravimetry–differential thermal analysis (TG-DTG/DTA), X-ray powder diffraction (XRD), and scanning electron microscopy (SEM). Thus, the non-isothermal kinetics analysis for the decomposition of this compound was carried out, based on the iso-conversional techniques of the Ozawa and Kissinger–Akahira–Sunose (KAS) methods. Possible conversion functions have been estimated by the Liqing–Donghua method [6], combined with 35 algebraic expressions of the conversion functions, $g(\alpha)$. The activation energy, E, and pre-exponential factor, A, were estimated. The transition state thermodynamic functions, ΔH^*, ΔG^* and ΔS^*, were calculated via the activated complex theory.

Experimental procedure

Materials and measurement

Sodium oxalate, $Na_2C_2O_4$ (≥99.0% (RT) 71801, Fluka), was used without further purification. Thermal behavior of $Na_2C_2O_4$ was investigated using TG-DTA (Perkin Elmer). Initial experiments were conducted with a heating rate of 15, 20, 30 and 40 K min^{-1} in a temperature range from room temperature to 1,573 K in N_2 atmosphere at a rate of 100 cm^3 min^{-1}. Then, decomposition of the sample was carried out at 873 K in a furnace for 4 h using a heating/cooling rate of 10 K min^{-1}. $Na_2C_2O_4$ and its thermal transformation products were investigated further. The phase formation was studied by room temperature X-ray diffraction (XRD, Advance D8), using Ni-filtered CuK_α radiation. Sample scanning was done between the angles of 20–80°. Diffraction peaks were analyzed and indexed according to the diffracting planes of different phases. The morphology of samples was examined using a scanning electron microscope (SEM, Hitachi S4700) after gold coating.

Determination of the most probable mechanism function

Since the kinetic parameters depend strongly on the selection of a proper mechanism function for the process, the following equation was used to estimate the most correct reaction mechanism, i.e., $g(\alpha)$ function [6]:

$$\ln g(\alpha) = \left[\ln\frac{AE}{R} + \ln\frac{e^{-x}}{x^2} + \ln h(x)\right] - \ln\beta \qquad (1)$$

where A (the pre-exponential factor/min^{-1}) and E_α (the activation energy/kJ mol^{-1}) are the Arrhenius parameters, and R is the gas constant (8.314 J mol^{-1} K^{-1}). For determination, the degrees of conversion α (extent of conversion, $\alpha = (m_i - m_t)/(m_i - m_f)$, where m_i, m_f, and m_t are the initial, final, and current sample mass, respectively, at moment t), corresponding to four heating rates (β = 15, 20, 30 and 40 K min^{-1}) taken at the same temperature, were substituted into the left side of Eq. 1, which was combined with 35 types of mechanism functions [14–16]. Potting $\ln g(\alpha)$ versus $\ln\beta$ and a linear regression of least square method were conducted. The most probable mechanism function was assumed to be the one for which the

slope of the straight line was closest to −1.0000, and the linear correlation coefficient r^2 should be unity.

Calculation of activation energy by iso-conversional procedure

In the kinetic study, the first Ozawa equation [5] was used to calculate the values of the activation energy, E_α, of the decomposition reaction of $Na_2C_2O_4$, as follows:

$$\ln \beta = \ln \frac{0.0048AE}{g(\alpha)R} - 1.0516\frac{E}{RT} \quad (2)$$

and Kissinger–Akahira–Sunose (KAS) equation [6]:

$$\ln \frac{\beta}{T^2} = \ln \frac{AE}{g(\alpha)R} - \frac{E}{RT} \quad (3)$$

The kinetics of such reactions is described by various equations, taking into account the special features of their mechanisms. Data from four TG curves in the decomposition range were used to determine α from experiments at different heating rates (β = 15, 20, 30 and 40 K min^{-1}). The plots of ln β versus $1/T$ (Eq. 2) and ln (β/T^2) versus $1/T$ (Eq. 3) have provided evidence of apparent activation energy values for decomposition at different values of α. The activation energy, E_α, can be estimated from the slope of these plots. This is a model-free method according to the reaction mechanism, and the shape of $g(\alpha)$ function cannot affect this calculation, which was performed without use of the most probable mechanism function.

Calculation of the transition state thermodynamic function

The pre-exponential factor, A, can be estimated from the intercept of the plots from Ozawa (Eq. 2) and KAS (Eq. 3) through the insertion of the most probable function, $g(\alpha)$, and the calculated activation energy, E_α. According to the theory of the activated complex (transition state) of Eyring [2, 3, 17], the general equation of A may be written as follows:

$$A = \frac{e\chi k_B T_P}{h}\exp\left(\frac{\Delta S^*}{R}\right) \quad (4)$$

where e = 2.7183 is the Neper number; χ is the transition factor, which is unity for monomolecular reactions; k_B is the Boltzmann constant; h is Plank's constant; and T_P is the average temperature of the TG curves at different heating rates. Then, the change of entropy may be calculated according to the formula:

$$\Delta S^* = R \ln \frac{Ah}{e\chi k_B T_P} \quad (5)$$

Therefore, the changes of the enthalpy, ΔH^*, and Gibbs free energy, ΔG^*, for the activated complex formation from the reagent can be calculated using the well-known thermodynamical equation:

$$\Delta H^* = E - RT_P \quad (6)$$

$$\Delta G^* = \Delta H^* - T_P \Delta S^* \quad (7)$$

Results and discussion

Thermogravimetry–differential thermal analysis curves of the thermal decomposition of $Na_2C_2O_4$ at a heating rate of 30 K min^{-1} are illustrated in Fig. 1. The TG curve accordingly revealed a weight loss of ~21%, which occurred during the temperature rise from 800 to 870 K. This observation corresponded to the endothermic peak of the DTA and DTG curve, which centred at 848 and 844 K, respectively. This decomposition step may be related to the decomposition of $Na_2C_2O_4$ to Na_2CO_3 and released CO because the overall weight loss of ~21% is close to the theoretical value of 20.9%, which corresponds to the release of 1 mol of CO. The decomposition reaction is suggested to be as the Eq. 8:

$$Na_2C_2O_4 \rightarrow Na_2CO_3 + CO \quad (8)$$

This decomposition temperature of the decarbonylation stage was higher than those found in the literature, which lie on the temperature of 773 K [18].

The XRD patterns of sodium oxalate ($Na_2C_2O_4$) powder and its calcined product (at 873 K) are illustrated in Fig. 2. The diffraction pattern of $Na_2C_2O_4$ powder could correspond to the monoclinic sodium oxalate (JCPDS file no. 49-1816 (▼), space group $P2_1/_a$ (14)). After calcination at 873 K for 4 h, the diffraction pattern suggests an appearance of the monoclinic, γ-Na_2CO_3 [JCPDS no. 72-0628,

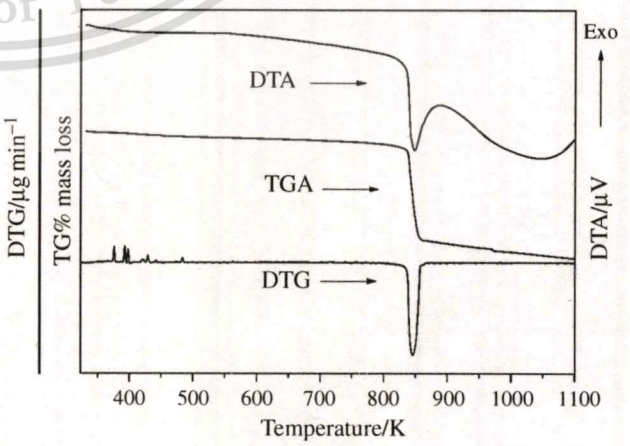

Fig. 1 TGA, DTG, and DTA curves of the thermal decomposition of $Na_2C_2O_4$ at a heating rate β of 30 K min^{-1}

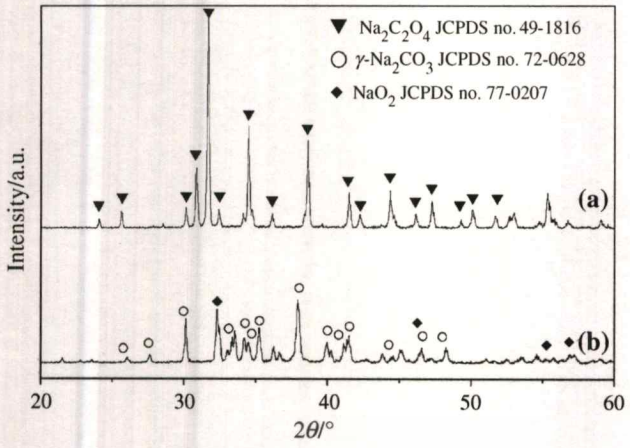

Fig. 2 X-ray diffraction patterns of *a* $Na_2C_2O_4$ and *b* its calcined product heated at 873 K for 4 h with a heating/cooling rate of 10 K min^{-1}

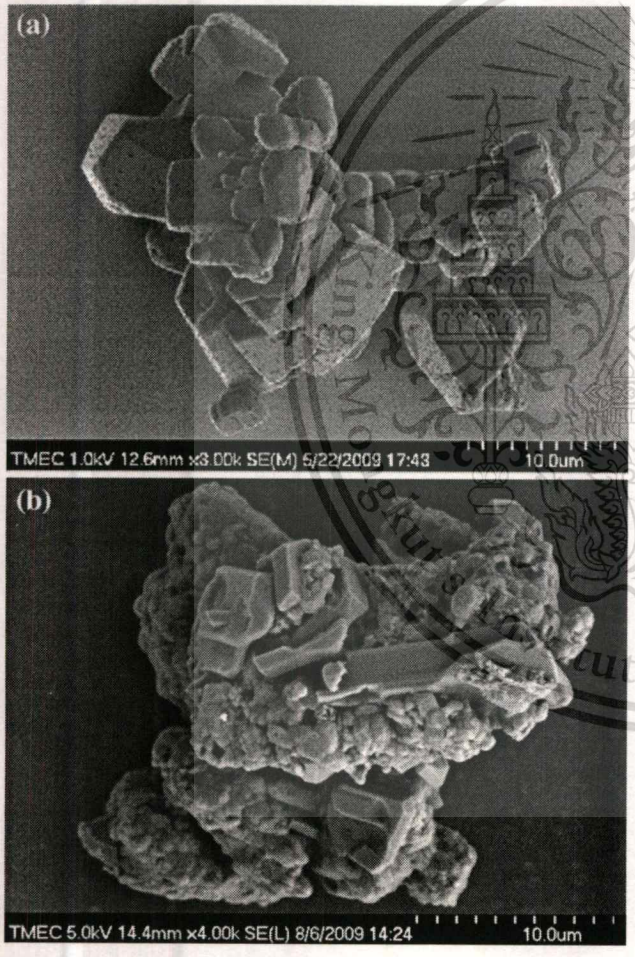

Fig. 3 SEM micrographs of $Na_2C_2O_4$ powder (**a**) and its calcined product heated at 873 K for 4 h with a heating/cooling rate of 10 K min^{-1} (**b**)

space group C2/m (12)], accompanied by the cubic NaO_2 (JCPDS file no. 77-0207, space group Fm3m) as a minority phase. This result could be correlated to TGA-DTG/DTA

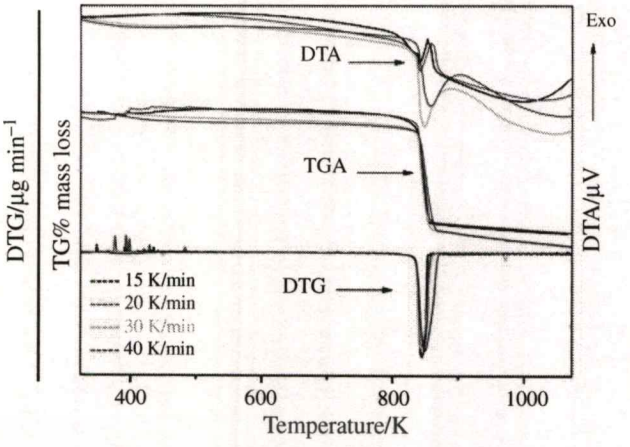

Fig. 4 TGA curves of thermal $Na_2C_2O_4$ decomposition at four heating rates under an N_2 atmosphere

Table 1 The α–T data at different heating rates for the decomposition process of $Na_2C_2O_4$

α	Temperature at four heating rate (β/K min^{-1})				T_p/K
	15	20	30	40	
0.1	837.14	838.99	840.93	842.40	839.86
0.2	839.43	841.15	843.65	845.23	842.36
0.3	840.95	842.23	844.85	846.54	843.64
0.4	843.16	844.70	847.15	849.14	846.04
0.5	844.38	846.00	849.35	851.64	847.84
0.6	846.72	848.48	851.15	852.94	849.82
0.7	848.77	850.68	853.65	855.54	852.16
0.8	849.70	851.67	855.65	858.19	853.80
0.9	851.92	854.35	858.15	860.95	856.34

T_p is the average temperature peak in the DTG curve (K)

analysis, which suggested that the decomposition of $Na_2C_2O_4$ to Na_2CO_3 was in the region of this temperature.

The scanning electron micrographs of $Na_2C_2O_4$ powder and its calcined product (at 873 K) are illustrated in Fig. 3a, b, respectively. $Na_2C_2O_4$ powder was found to have uniform morphological features, with a polyhedral shape and obvious edges. The particle was in the range of micron size. On the contrary, the micrograph of the particle's calcined product (at 873 K) consisted of non-uniform grain. The macropores and agglomeration, which could result from the thermal decomposition process, were found.

Figure 4 shows the TG, DTG, and DTA curves in the decomposition range of $Na_2C_2O_4$, with four heating rates of 15, 20, 30, and 40 K min^{-1}. Data of α and T collected from the TG curves in the decomposition range of $0.1 < \alpha < 0.9$ at various heating rates are illustrated in Table 1, and used to determine the kinetic parameters of the process in all calculation procedures. According to Eq. 3 combined with 35 conversion functions, ln g(α)

calculated different α values at the same temperature, and four heating rates on ln β, must give rise to straight lines, so the slope and linear correlation coefficient, r^2, can be determined. Table 2 lists the results for all of the 35 types of mechanism functions. The slope determined from function no. 18 was found to be the closest to −1.0000 and the correlation coefficient, r^2, was better than others. This function was considered to be the most probable reaction mechanism for the description of $Na_2C_2O_4$ decarbonylation. Therefore, it can be stated that the mechanism function for the decomposition of $Na_2C_2O_4$ (splitting of carbon monoxide) is the mechanism of phase boundary reaction (cylindrical symmetry, R_2 or $F_{1/2}$ model) with integral form $g(\alpha) = 1-(1-\alpha)^{1/2}$ and differential form $f(\alpha) = 2(1-\alpha)^{1/2}$.

Table 2 The most probable mechanism function, $g(\alpha)$, slope and correlation coefficient of the linear regression, r^2

No.	Symbol	Slope	r^2
1	$F_{1/3}$	−0.9571	0.984568
2	$F_{3/4}$	−1.1987	0.980565
3	$F_{3/2}$	−1.5708	0.964395
4	F_2	−1.8641	0.956190
5	F_3	−2.5481	0.946691
6	$P_{3/2}$	−1.2699	0.980378
7	$P_{1/2}$	−0.4233	0.980378
8	$P_{1/3}$	−0.2822	0.980378
9	$P_{1/4}$	−0.2116	0.980378
10	E_1	–	–
11	A_1, F_1	−1.3266	0.974513
12	$A_{3/2}$	−0.8844	0.974513
13	A_2	−0.6633	0.974513
14	A_3	−0.4422	0.974513
15	A_4	−0.3317	0.974513
16	A_u	–	–
17	R_1, F_0, P_1	−0.8466	0.980378
18	R_2, $F_{1/2}$	−1.0327	0.985949
19	R_3, $F_{2/3}$	−1.1326	0.984293
20	D_1	−1.6932	0.980378
21	D_2	−2.1589	0.986125
22	D_3	−2.26526	0.984293
23	D_4	−1.9923	0.984810
24	D_5	−2.9668	0.967651
25	D_6	−1.5714	0.980464
26	D_7	−1.6103	0.980442
27	D_8	−1.4596	0.980466
28	G_1	−0.6622	0.969938
29	G_2	−0.5652	0.961585
30	G_3	−0.5016	0.955476
31	G_4	−2.6533	0.974513
32	G_5	−3.9799	0.974513
33	G_6	−5.3069	0.974513
34	G_7	−0.5163	0.985949
35	G_8	−0.5663	0.984293

Figure 5a, b illustrate the plots of ln β versus $1/T$ (Eq. 1) and ln (β/T^2) versus $1/T$ (Eq. 2) for the decomposition process of $Na_2C_2O_4$, based on the Ozawa and KAS analysis, respectively. The activation energy, E_α, of the decomposition reaction of $Na_2C_2O_4$, which was calculated from the slope of these straight lines and their correlation coefficient, r^2, are tabulated in Table 3a (Ozawa method) and b (KAS method). The calculated activation energies obtained from different equations, in which the values obtained by the KAS method were generally higher, were found to be consistent. It can be seen that the values of E_α tend to decrease with the increase of conversion α. It can be noted also that the E_α values are dependent on α, and the decomposition reaction should be interpreted in terms of a multi-step reaction mechanism [19]. As the dependence can disclose the complexity of a process and identify its kinetic scheme, the shape of the decreasing dependence of E_α on α has been identified from model data [20]. This

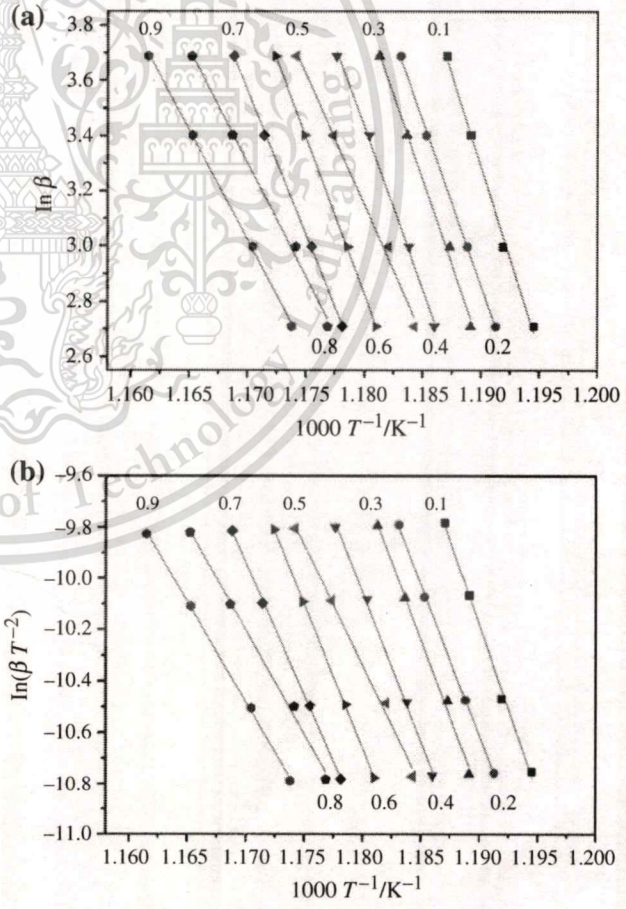

Fig. 5 Ozawa (**a**) and KAS (**b**) plots for the decomposition process of $Na_2C_2O_4$ at four heating rates in various conversions (α = 0.1–0.9, with 0.1 increment)

Table 3 Kinetic (E_α, A), and thermodynamic (ΔS^*, ΔH^* and ΔG^*) parameters for the decarbonylation of $Na_2C_2O_4$ obtained by the Ozawa (a) and KAS (b) methods

α	E_α/kJ mol^{-1}	A/min^{-1}	ΔH^*/kJ mol^{-1}	ΔS^*/J mol^{-1} K^{-1}	ΔG^*/kJ mol^{-1}	r^2
(a) Ozawa method						
0.1	1051.98	1.3231E+66	1044.9943	1003.9768	201.7900	0.9959
0.2	942.49	1.3766E+59	935.4897	870.2758	202.4000	0.9995
0.3	964.60	4.6238E+60	957.5909	899.4801	198.7519	0.9959
0.4	927.96	1.8404E+58	920.9318	853.5098	198.8303	0.9979
0.5	751.04	7.5773E+46	743.9932	635.5338	205.1614	0.9950
0.6	895.87	1.4111E+56	888.8045	812.9774	197.9180	0.9998
0.7	824.27	3.1738E+51	817.1834	723.9749	200.2424	0.9995
0.8	650.67	2.6314E+40	643.5705	511.8200	206.5770	0.9962
0.9	627.76	8.6070E+38	620.6462	483.3606	206.7244	0.9994
AV.	848.52 ± 145.87	1.4701E+65	841.4672	754.9899	202.0440	0.9977
(b) KAS method						
0.1	1092.30	1.17385E+57	1085.3129	830.6884	387.6474	0.9958
0.2	977.12	1.21573E+50	970.1163	696.9493	383.0307	0.9994
0.3	1000.35	4.06853E+51	993.3349	726.1232	380.7471	0.9957
0.4	961.78	1.61107E+49	954.7451	680.1103	379.3461	0.9978
0.5	775.70	6.62753E+37	768.6466	462.1270	376.8362	0.9949
0.6	927.96	1.22539E+47	920.9005	639.5107	377.4298	0.9998
0.7	852.63	2.74479E+42	845.5462	550.4743	376.4552	0.9995
0.8	670.04	2.27637E+31	662.9459	338.3219	374.0857	0.9960
0.9	645.92	7.40872E+29	638.7983	309.8210	373.4858	0.9994
AV.	878.20 ± 153.48	1.30428E+56	871.1496	581.5696	378.7849	0.9976

study reported that the decomposition reaction was complicated by diffusion. This process is met widely in solids decomposed in the following way: solid → solid + gas [21]. In addition, values of the correlation coefficient, r^2, for all cases of calculation were greater than 0.9949. It can be seen that the values of E_α obtained from the Ozawa and KAS methods (Eqs. 2, 3) are reliable.

On the basis of TG curves at four heating rates and using Eqs. 1–3, values of the apparent activation energy, E_α, were calculated, and the most probable reaction mechanism function of the studied reaction was determined. Based on these results, the pre-exponential factor, A, can be estimated from intercept of the plots from the Ozawa (Eq. 2) and KAS (Eq. 3) methods. The related transition state thermodynamic functions (ΔS^*, ΔH^* and ΔG^*) also can be calculated according to Eqs. 5–7. The corresponding values are shown in Table 3a (Ozawa method) and b (KAS method). As seen from Table 3a (Ozawa method) and b (KAS method), the change of the entropy, ΔS^*, for the decomposition of $Na_2C_2O_4$ is positive and can be described as corresponding activated complexes that have a lower degree of arrangement (higher entropy) than the initial state. Regarding the fundamentals of the activated complex theory (transition theory) [2, 3, 13, 14], a positive value of ΔS^* indicates a malleable activated complex that leads to very many degrees of rotation and vibration freedom, which results in a "fast" stage reaction. On the other hand, a negative value of ΔS^* suggests that the degree of structural complexity (arrangement, organization) of the activated complex is higher than that in the non activated complex, and may be indicated as "slow" stage [19, 22–25]. The positive value of the activation enthalpy, ΔH^*, showed that the decomposition stage is connected to the introduction of heat, and agrees well with the endothermic peak in the DTA result. The high ΔH^* value indicated that this decomposition step needs high energy. The positive value of Gibbs energy, ΔG^*, suggested that this is a non-spontaneous process. These results indicated that the decomposition step of $Na_2C_2O_4$ is a high energy pathway and revealed a very hard mechanism.

Conclusions

In conclusion, kinetic parameters of $Na_2C_2O_4$ (decarbonylation reaction) decomposition can be determined on the basis of thermogravimetric data. The kinetics of thermal decomposition of $Na_2C_2O_4$ under non-isothermal

heating was studied using the Ozawa and KAS methods. The results obtained from these two different calculation procedures were found to correlate with each other. Values of the apparent activation energy and pre-exponential factor, and the change of entropy, enthalpy, and Gibbs free energy, the most probable mechanisms and characteristics of the process were reported. These could be the important data for further studies and synthesis of the materials involved.

Acknowledgements This work was supported by the Thailand Research Fund (TRF), Thailand Graduate Institute of Science and Technology (TGIST), and the National Nanotechnology Center (NANOTEC) NSTDA, Ministry of Science and Technology, Thailand through its "Center of Excellence Network" Program.

References

1. Wendlandt WW. Thermal methods of analysis. New York: John Wiley & Sons Inc; 1974.
2. Šesták J. Thermodynamical properties of solids. Prague: Academia; 1984.
3. Vlaev L, Nedelchev N, Gyurova K, Zagorcheva M. A comparative study of non-isothermal kinetics of decomposition of calcium oxalate monohydrate. J Anal Appl Pyrolysis. 2008;81:253–62.
4. Coats AW, Redfern JP. Kinetic parameters from thermogravimetric data. Nature. 1964;201:68–9.
5. Ozawa TA. A new method of analyzing thermogravimetric data. Bull Chem Soc Jpn. 1965;38:1881–6.
6. Liqing L, Donghua C. Application of iso-temperature method of multiple rate to kinetic analysis. J Therm Anal Calorim. 2004; 78:283–93.
7. Senum GI, Yang RT. Rational approximations of the integral of the Arrhenius function. J Therm Anal Calorim. 1977;11:445–9.
8. L'vov BV. Kinetics and mechanism of thermal decomposition of nickel, manganese, silver, mercury and lead oxalates. Thermochim Acta. 2000;364:99–109.
9. Galwey AK, Brown ME. Thermal decomposition of ionic solids. Amsterdam: Elsevier; 1999.
10. Patra BS, Otta S, Bhattamisra SD. A kinetic and mechanistic study of thermal decomposition of strontium titanyl oxalate. Thermochim Acta. 2006;441:84–8.
11. Zhang JJ, Ren N, Bai JH. Non-isothermal decomposition reaction kinetics of the magnesium oxalate dihydrate. Chin J Chem. 2006;24:360–4.
12. Chaiyo N, Boonchom B, Vittayakorn N. Solid-state reaction synthesis of sodium niobate ($NaNbO_3$) powder at low temperature. J Mater Sci. 2010;45:1443–7.
13. Budavari S, O'Neil M, Smith A, editors. The Merck index; An encyclopedia of chemicals, drugs and biologicals. 11th ed. Rahway: Merck Co. Inc.; 1989.
14. Šesták J, Berggren G. Study of the kinetics of the mechanism of solid-state reactions at increasing temperatures. Thermochim Acta. 1971;3:1–12.
15. Heide K, Höland W, Gölker H, Seyfarth K, Müller B, Sauer R. Die bestimmung kinetischer parameter endothermer zersetzungsreaktionen unter nicht-isothermen bedingungen. Thermochim Acta. 1975;13:365–78.
16. Zhang JJ, Ge LG, Zha XL, Dai YJ, Chen HL, Mo LP. Thermal decomposition kinetics of the Zn(II) complex with Norfloxacin in static air atmosphere. J Therm Anal Calorim. 1999;58:269–78.
17. Bamford CH, Tipper CFH. Comprehensive chemical kinetics. Amsterdam: Elsevier; 1980.
18. McAlexander LH, Beck CM, Burdeniuc JJ, Crabtree RH. Fluoroalkane aromatization over hot sodium oxalate. J Fluorine Chem. 1999;99:67–72.
19. Boonchom B, Vittayakorn N. Dehydration behavior of synthetic $Al_{0.5}Fe_{0.5}PO_4{\cdot}2.5H_2O$. J Chem Eng Data. 2010;55:3307–11.
20. Zhang K, Hong J, Cao G, Zhan D, Tao Y, Cong C. The kinetics of thermal dehydration of copper(II) acetate monohydrate in air. Thermochim Acta. 2005;437:145–9.
21. Vyazovkin S. A unified approach to kinetic processing of non-isothermal data. Int J Chem Kinet. 1996;28:95–101.
22. Vlaev LT, Gospodinov GG. Study on the kinetics of the isothermal decomposition of selenites from IIIB group of the periodic system. Thermochim Acta. 2001;370:15–9.
23. Boonchom B, Thongkam M. Kinetics and thermodynamics of the formation of $MnFeP_4O_{12}$. J Chem Eng Data. 2010;55:211–6.
24. Boonchom B, Kongtaweelert S. Study of kinetics and thermodynamics of the dehydration reaction of $AlPO_4{\bullet}H_2O$. J Therm Anal Calorim. 2010;99:531–8.
25. Boonchom B, Danvirutai C, Thongkam M. Non-isothermal decomposition kinetics of synthetic serrabrancaite ($MnPO_4{\bullet}H_2O$) precursor in N_2 atmosphere. J Therm Anal Calorim. 2010;99: 357–62.